Functional analysis of virulence genes in the rice blast fungus *Magnaporthe oryzae*

Rita Galhano

Supervised by Dr. Ane Sesma

PhD thesis

2010

Disease & Stress Biology Department

John Innes Centre

University of East Anglia

Norwich Research Park, Colney Lane, Norwich NR4 7UH

Abstract

The fungus *Magnaporthe oryzae* causes rice blast disease, one of the most devastating diseases of all cereals. This fungus infects rice, the essential staple crop for half of the world's population. *M. oryzae* attacks all parts of the rice plant, causing losses up to 30% of the annual rice harvest. Such losses have lead to rice shortages in many developing countries in recent years, making effective control of this devastating disease imperative to ensure global food security and economic and social stability. Fortunately, the availability of the genome sequences of both rice and *M. oryzae* has made this a model pathosystem for understanding the molecular basis of plant-fungal interactions.

In this study, I sought to identify novel genetic determinants for successful colonisation of plant tissue by *M. oryzae*, using two experimental approaches: 1) by screening a *M. oryzae* random insertional mutagenesis library; and 2) by targeted deletion of putatively secreted *M. oryzae* proteins. Unfortunately, these candidate effectors were not essential for successful colonisation of rice and barley cells and were not secreted into the plant host cells. The major outcome of this research project has been the identification of a new *M. oryzae* pathogenicity gene, *TPC1* (*Transcription factor for Polarity Control1*), which was identified as a pathogenicity-defective mutant M1422 generated by random insertional T-DNA mutagenesis. *TPC1* belongs to the strictly fungal group of $Zn(II)_2Cys_6$ binuclear cluster family. This transcriptional regulator appears to play an important role in vegetative fungal growth and in fungal colonisation *in planta*. The phenotypes observed during appressorium- and infection-associated developmental processes suggest that *TPC1* is a core polarity protein that is required for the correct development of apical-growing structures.

Acknowledgements

I would like to thank to my supervisor Dr. Ane Sesma for accepting me as a PhD student and for the opportunity to work in this project. Special thanks to Sara Tucker for her friendship and support during my time at JIC.

This work would not have been possible without the support and encouragement of Prof. Nick Talbot. His wide knowledge and his logical way of thinking have been of great value to me and my PhD project. I could not have completed it without your help. Thank you!!

My warm thanks are due to everyone in the lab, past and present, for making me feel at home in Exeter. It has been a real pleasure working with you!! I also add special thanks to Magdalena, Ignacio and Rafael… um beijo enorme!

I would also like to thank to the Portuguese Fundação para a Ciência e Tecnologia for providing me with the funding to carry out this research.

I cannot end without thanking my parents and Nuno for their unwavering encouragement throughout my studies. It is to them that I dedicate my work.
Aos meus pais… Amo-vos muito! Ao Nuno... obrigada por teres estado sempre ao meu lado, nos bons e nos maus momentos. A nossa caminhada só agora começou! Obrigada por tudo e por nunca deixarem de acreditar em mim.

Table of Contents

Abstract ii

Acknowledgements iii

Table of Contents iv

Table of Figures ix

Abbreviations xi

CHAPTER 1 – General Introduction 1

1.1. Rice blast disease 2

1.2. The infection cycle of the rice blast fungus *M. oryzae* 3

1.2.1. Attachment and germination of conidia 3

1.2.2. Cyclic AMP signaling during appressorium formation 6

1.2.3. The *PMK1* MAP kinase signaling pathway 10

1.2.4. Appressorium development and function 13

1.2.5. Appressorium-mediated plant infection regulated by cell cycle 16

1.2.6. Penetration peg formation 17

1.2.7. Biotrophic invasion *in planta* by *M. oryzae* 19

1.3. Effector biology of phytopathogens 19

1.3.1. *Pseudomonas* and *Xanthomonas* type III effectors 22

1.3.2. Oomycete effectors 22

1.3.3. Fungal effectors 23

Magnaporthe effectors 24

Translocation of *Magnaporthe* effectors into rice cells 29

1.4. Introduction to current study 32

CHAPTER 2 – Materials and Methods 34

2.1. Growth and maintenance of fungus stocks **35**

2.1.1. *Magnaporthe* strains 35

2.1.2. *Neurospora* strains 35

2.2. Pathogenicity and infection-related development assays **38**

2.2.1. Leaf infection assays 38

2.2.2. Root infection assays 38

2.2.3. Rice leaf sheath assay 39

2.2.4. Penetration assay 39

2.2.5. Assays for germination and appressorium formation rates 40

2.3. Nucleic acid analysis **40**

2.3.1. Fungal DNA extraction 40

Large-scale extraction of fungal genomic DNA 40

Small-scale extraction of fungal genomic DNA 41

2.3.2. DNA manipulations 42

Digestion of genomic or plasmid DNA with restriction enzymes 42

DNA gel electrophoresis 42

Gel purification of DNA fragments 43

Southern blotting 43

Radiolabelled DNA probe construction 44

Hybridisation conditions 45

2.3.3. DNA cloning procedures 46

Bacterial DNA mini preparations using Alkaline Lysis protocol 46

Midi-plasmid DNA preparations 47

DNA ligation and selection of recombinant clones 48

Preparation of competent cells 49

Transformation of competent bacterial hosts 50

2.3.4. DNA sequencing 50

2.4. Fungal transformation **50**

2.4.1. Generation of protoplasts 50

2.4.2. Transformation using hygromicin as a selectable marker 51

2.4.3. Transformation using sulfonylurea as a selectable marker 52

2.4.4. Generation of T-DNA insertional library by *Agrobacterium tumefaciens*-mediated transformation 52

2.5. Microscopy 54

2.5.1. Confocal microscopy 54

2.5.2. Olympus IX81-performed microscopy 54

2.5.3. Zeiss Axioskop 2-performed microscopy 54

CHAPTER 3 – Identification of pathogenicity-defective mutants of *M. oryzae* by screening a T-DNA insertional mutant library 55

3.1. Introduction 56

3.2. Materials and Methods 58

3.2.1. T-DNA localisation within the mutant fungal genome 58

3.2.2. Construction of Tpc1:GFP complementation vector 58

3.3. Results 61

3.3.1. Identification of M1422, a T-DNA *M. oryzae* mutant with defects in pathogenicity and vegetative growth 61

3.3.2. Localisation of T-DNA insertion within M1422 genome 62

3.3.3. Complementation of M1422 mutant with *Mo*Tpc1:GFP 67

3.4. Discussion 68

CHAPTER 4 – Functional characterisation of *MoTPC1* gene 70

4.1. Introduction 71

4.2. Materials and Methods 72

4.2.1. Cellular localisation of GFP:Atg8 and Fim:GFP in M1422 mutant background 72

4.3. Results **73**

4.3.1. The M1422 mutant is strongly affected on vegetative growth 73

4.3.2. *TPC1* is important in conidiogenesis 74

4.3.3. Appressorium development is impaired in the M1422 mutant 81

4.3.4. Polarity is coupled with autophagy and glycogen metabolism in *M. oryzae* 85

4.3.4. *TPC1* is required for re-establishing polarity in appressoria 92

4.4. Discussion **96**

CHAPTER 5 – Cellular localisation and site-directed mutagenesis of *Mo*Tpc1 **101**

5.1. Introduction **102**

5.2. Materials and Methods **107**

5.2.1. Cellular localisation of *Mo*Tpc1:GFP construct in wild-type Guy11 strain and different mutant backgrounds 107

5.2.2. PCR site-directed mutagenesis of *Mo*Tpc1:GFP construct 107

5.3. Results **109**

5.3.1. Expression and localisation of *Mo*Tpc1:GFP fusion proteins in wild-type Guy11 109

5.3.2. Expression and localisation of *Mo*Tpc1:GFP fusion proteins in different mutant backgrounds 109

5.3.3. Expression and localisation of mutated versions of *Mo*Tpc1:GFP fusion proteins 112

5.4. Discussion **116**

CHAPTER 6 – Phylogenetic analysis of Tpc1 protein **122**

6.1. Introduction **123**

6.2. Materials and Methods **126**

6.2.1. Phylogenetic analysis 126

6.3. Results **128**

6.3.1. Phylogenetic analysis of *Mo*Tpc1 within the *M. oryzae* genome and between fungal species 128

6.3.2. Characterisation of *N. crassa* Tpc1 protein 131

6.3.3. Characterisation of *N. crassa TPC1* KO 131

6.4. Discussion **137**

CHAPTER 7 – Identification of putatively secreted effectors delivered by *M. oryzae* during fungal-plant interaction **140**

7.1. Introduction **141**

7.2. Materials and Methods **144**

7.2.1. Bioinformatics analysis of *M. oryzae* predicted secretome 144

7.2.2. Targeted gene replacement of *FTF1*, *ZNC1* and *CPB1* 144

7.3. Results **148**

7.3.1. Analysis of *M. oryzae* predicted secretome 148

7.3.2. Targeted gene replacement of *FTF1*, *ZNC1* and *CPB1* 148

7.3.3. Vegetative growth of *Δftf, Δzncys* and *ΔcenpB* mutants 149

7.3.4. Cellular localisation of Ftf1:GFP, Znc1:GFP and Cpb1:GFP during infection-related development and in vegetative hyphae of *M. oryzae* 168

7.4. Discussion **175**

CHAPTER 8 – General Discussion **178**

APPENDIX **185**

Primer sequences **186**

REFERENCES **190**

Table of Figures

Figure 1.1.	Life cycle of the rice blast fungus *M. oryzae*.	**5**
Figure 1.2.	Model for signal transduction pathways that regulate appressorium morphogenesis.	**7**
Figure 1.3.	Zig-zag model of the plant immune system.	**21**
Figure 1.4.	Two-stage BIC development and preferential effector accumulation in successively invaded rice sheat cells.	**27**
Figure 3.1.	Schematic diagram showing the T-DNA fragment contained in the pKHt vector, which was used to generate the *M. oryzae* insertional library.	**59**
Figure 3.2.	Strategy for construction of the Tpc1:GFP translational protein fusion.	**60**
Figure 3.3.	The M1422 mutant is pathogenicity-defective on rice CO39 roots.	**63**
Figure 3.4.	The M1422 mutant is a T-DNA *M. oryzae* transformant with defects in leaf pathogenicity.	**64**
Figure 3.5.	Restoration of wild-type growth and virulence phenotypes by re-introduction of Tpc1:GFP into M1422.	**65**
Figure 3.6.	T-DNA was integrated in the coding region of *TPC1* gene within the M1422 mutant genome.	**66**
Figure 4.1.	Vegetative growth and colony morphology are severely affected on the M1422 T-DNA mutant.	**75**
Figure 4.2.	Vegetative growth and colony morphology are severely affected on the M1422 mutant.	**76**
Figure 4.3.	The M1422 mutant shows increased tolerance to hyperosmotic concentrations of sodium chloride (NaCl).	**77**
Figure 4.4.	Conidiogenesis is severely impaired in the M1422 T-DNA mutant.	**78**
Figure 4.5.	Conidia of the M1422 mutant show defects in the number of cells *per* conidium and morphology.	**79**
Figure 4.6.	Conidial size of the wild-type Guy11 and M1422 T-DNA mutant.	**80**
Figure 4.7.	Infection-related development is impaired in the M1422 mutant.	**82**
Figure 4.8.	The M1422 mutant showed an increased frequency of conidia germination from two cells.	**83**
Figure 4.9.	The M1422 conidia formed at least one appressorium during infection-related development.	**84**
Figure 4.10.	The M1422 mutant underwent conidial collapse during appressorium development.	**87**
Figure 4.11.	Cellular localisation of autophagosomes during infection-related development of wild-type Guy11 and M1422 mutant.	**88**
Figure 4.12.	Infection-associated autophagy was impaired in the M1422 mutant.	**89**
Figure 4.13.	Glycogen metabolism was delayed in the M1422 mutant during infection-related development.	**90**
Figure 4.14.	Glycogen metabolism was delayed in the M1422 mutant.	**91**
Figure 4.15.	The M1422 mutant was impaired in appressorium-mediated penetration.	**94**
Figure 4.16.	Cellular localisation of fimbrin, an actin-binding protein, during infection-related development of wild-type Guy11 and M1422 mutant.	**95**
Figure 5.1.	Cellular localisation of *Mo*Tpc1:GFP during infection-related development (A) and in vegetative hyphae (B) of *M. oryzae*.	**110**
Figure 5.2.	Cellular localisation *Mo*Tpc1:GFP in *Δpmk1*, *Δatg1*, *Δatg8*, *Δcpka*, *Δmps1*, *Δosm1* and *Δmst12* mutant backgrounds.	**111**
Figure 5.3.	The NLS and sumoylation site are crucial for the proper function of *Mo*Tpc1.	**113**
Figure 5.4.	The cysteine residues within the putative $Zn(II)_2Cys_6$ are crucial for the proper function of *Mo*Tpc1.	**114**
Figure 5.5.	The phosphorylation residues are crucial for the proper function of *Mo*Tpc1.	**115**
Figure 6.1.	HMM pattern for $Zn(II)_2Cys_6$ binuclear cluster (zn_clus) protein family.	**127**
Figure 6.2.	Maximum likelihood tree of *M. oryzae* $Zn(II)_2Cys_6$ cluster proteins.	**129**
Figure 6.3.	Maximum likelihood tree of *M. oryzae* Tpc1 protein (MGG_01285) with its closest fungal orthologous.	**130**
Figure 6.4.	Alignment of the *M. oryzae Mo*Tpc1 protein with its closest orthologous in *N. crassa*, *Nc*Tpc1.	**133**

Figure 6.5. Vegetative growth and colony morphology of *NcTPC1* deletion mutant. **134**

Figure 6.6. Vegetative growth and colony morphology of *NcTPC1* deletion mutant under NaCl osmotic stress. **135**

Figure 6.7. Vegetative growth phenotype of *NcTPC1* deletion mutant after exposure to increasing concentration of NaCl. **136**

Figure 7.1. Flow chart showing *M. oryzae* 70-15 predicted secreted proteins and its subcellular localisation within the cell. **146**

Figure 7.2. Split-marker strategy for gene deletion. **147**

Figure 7.3. Strategy for targeted gene deletion. **152**

Figure 7.4. The *Δftf1* mutants have wild-type phenotype with regard to leaf and root pathogenicity. **153**

Figure 7.5. The vegetative growth and colony morphology of *Δftf1* mutants. **154**

Figure 7.6. The vegetative growth and colony morphology of *Δftf1* mutants under osmotic stress (NaCl). **155**

Figure 7.7. The vegetative growth and colony morphology of *Δftf1* mutants in the presence of fungal cell wall inhibitors (CR and CFW), oxidative stress (H_2O_2) and membrane permeabilisant (Triton X-100). **156**

Figure 7.8. The *Δznc1* mutants have wild-type phenotype with regard to leaf and root pathogenicity. **158**

Figure 7.9. The vegetative growth and colony morphology of *Δznc1* mutants. **159**

Figure 7.10. The vegetative growth and colony morphology of *Δznc1* mutants under osmotic stress (NaCl). **160**

Figure 7.11. The vegetative growth and colony morphology of *Δznc1* mutants in the presence of fungal cell wall inhibitors (CR and CFW), oxidative stress (H_2O_2) and membrane permeabilisant (Triton X-100). **161**

Figure 7.12. The *Δcpb1* mutants have wild-type phenotype with regard to leaf and root pathogenicity. **163**

Figure 7.13. The vegetative growth and colony morphology of *Δcpb1* mutants. **164**

Figure 7.14. The vegetative growth and colony morphology of *Δcpb1* mutants under osmotic stress (NaCl). **165**

Figure 7.15. The vegetative growth and colony morphology of *Δcpb1* mutants in the presence of fungal cell wall inhibitors (CR and CFW), oxidative stress (H_2O_2) and membrane permeabilisant (Triton X-100). **166**

Figure 7.16. Cellular localisation of *Mo*Ftf1:GFP in vegetative (A) and invasive (B) hyphae and during infection-related development (C) of *M. oryzae*. **169**

Figure 7.17. Cellular localisation of *Mo*Znc1:GFP in vegetative (A) and invasive (B) hyphae and during infection-related development (C) of *M. oryzae*. **171**

Figure 7.18. Cellular localisation of *Mo*Cpb1:GFP in vegetative (A) and invasive (B) hyphae and during infection-related development (C) of *M. oryzae*. **173**

Abbreviations

%	percentage
% w/v	percentage weight by volume
% v/v	percentage volume by volume
ATMT	*Agrobacterium tumefaciens*-mediated transformation
ATP	adenosine triphosphate
AVR	avirulence
BAS	biotrophic-associated secreted
BIC	biotrophic interaction complex
BLAST	Basic Local Alignment Search Tool
bp	base pair
°C	degree Celsius
cAMP	cyclic 3',5' adenosine monophosphate
CFW	Calcofluor White
cm	centimeter
CM	complete medium
CR	Congo Red
DAG	diacylglycerol
DBD	DNA-binding domain
dH_2O	distilled water
DNA	deoxyribonucleic acid
dpi	days post-inoculation
EIHM	extra-invasive hyphal membrane
ER	endoplasmic reticulum
ETI	effector-triggered immunity
g	grams
$g\ L^{-1}$	grams per litre
GFP	green fluorescent protein
GPCR	G- protein-coupled receptor
GTP	guanosine triphosphate
H_2O_2	hydrogen peroxide
h	hour
H1	histone1
hpi	hours post-inoculation
HR	hypersensitive response

HYG	hygromycin
IBMX	isobutylmethylxanthine
IH	invasive hyphae
kb	kilobase
KO	knock-out
LRT	likelihood ratio test
µg	microgram
µL	microlitre
µm	micrometre
M	molar
MAPK	mitogen-activated protein kinase
MAPKK	mitogen-activated protein kinase kinase
MAPKKK	mitogen-activated protein kinase kinase kinase
mg	milligram
mL	millilitre
mm	millimetre
mM	millimolar
MM	minimal media
MM-C	minimal media without carbon source
MM-N	minimal media without nitrogen source
MPa	megapascal
mRNA	messenger RNA
NADPH	nicotinamide adenine dinucleotide phosphate
NBS-LRR	nucleotide binding site - leucine-rich repeat
NES	nuclear export signal
ng	nanogram
NLS	nuclear localisation signal
NRPS	non-ribosomal peptide synthetase
ORF	open reading frame
p	probability
PAMP	pathogen-associated molecular pattern
PCR	polymerase chain reaction
PFAM	Protein Family
PKS	polyketide synthase
PRR	PAMP-recognition receptor
PTI	PAMP-triggered immunity
R	resistance

RA	Ras-association
RNA	ribonucleic acid
RFP	red fluorescent protein
ROS	reactive oxygen species
rpm	revolutions per minute
SAM	sterile α-motif
SD	standard deviation
SUMO	small ubiquitin-related modifier
SUR	sulfonylurea
T-DNA	transfer DNA
T3SS	type III secretion system
TAL	transcription activator-like
TPC1	transcription factor for polarity control1
UPR	unfolded protein response
UBL	ubiquitin-like protein
UV	ultraviolet
WT	wild-type

CHAPTER 1

General Introduction

1.1. Rice blast disease

The filamentous ascomycete *Magnaporthe oryzae* (Hebert) Barr (anamorph *Pyricularia oryzae* Sacc.; class: Pyrenomycetes) is the causal agent of rice blast disease, one of the most devastating of all cereal diseases throughout the world. It is estimated that each year rice blast causes losses of 10% to 30% of the rice yield (Talbot, 2003; Skamnioti and Gurr, 2009). In addition to rice, *M. oryzae* also infects other agronomically important crops such as barley, wheat and millet (Valent and Chumley, 1991). *M. oryzae* is an important model organism for studying fungal infection-related development and pathogenicity due to the ease of culturing the fungus *in vitro* and its genetic tractability (Valent and Chumley, 1991; Talbot, 2003). The genomic sequences of both the fungus (Dean *et al.*, 2005) and rice (Goff *et al.*, 2002; Yu *et al.*, 2002) are available, providing a unique opportunity to study a host-pathogen interaction from both sides using functional genomics approaches.

In nature, the rice blast fungus attacks all above ground parts of rice plants and infections occur when conidia attach and germinate on the leaf surface (Hamer *et al.*, 1988). The germinating spore differentiates a melanised appressorium, which generates enormous turgor pressure that is required to penetrate the leaf cuticle and invade plant tissue (de Jong *et al.*, 1997; Dean, 1997). The fungus can also undergo a different series of developmental events and infect plant roots (Dufresne and Osbourn, 2001). Here, at infection sites, hyphal swellings resembling the hyphopodia of root-infecting fungi develop and invade the root tissue and the vascular system to cause systemic plant infection (Sesma and Osbourn, 2004). Subsequent invasive growth *in planta* is similar to that observed during foliar infection by *M. oryzae* (Kankanala *et al.*, 2007). For root infection, the fungus does not require the formation of a melanised appressorium or the cAMP signal transduction pathway (Sesma and Osbourn, 2004).

1.2. The infection cycle of the rice blast fungus *M. oryzae*

1.2.1. Attachment and germination of conidia

The disease cycle of *M. oryzae* is shown in Fig. 1.1 and it is initiated by asexual spores called conidia. Conidiophores emerge from infected tissues through stomata or by breaking out the host cuticle from underlying plant cells infected with the fungus and produce a sympodial arrangement of three-celled conidia. Conidia of *M. oryzae* are dispersed by wind and water splashes from plant to plant. Upon landing on a host leaf surface, the apical cell wall of the hydrated spore breaks open and the pre-formed spore tip mucilage is released, anchoring the conidium to the hydrophobic rice leaf surface. Once attached, even vigorous attempts to remove adherent conidia from surfaces are typically unsuccessful (Hamer *et al.*, 1988; Koga and Nakayachi, 2004). This attachment can be blocked by addition of concanavalin A, a lectin that binds to α-linked glucosyl and/ or mannosyl residues present in the spore tip mucilage (Hamer *et al.*, 1988; Xiao *et al.*, 1994*a*).

Conidia germinate by producing a polarised germ tube within 30 minutes after contact with a hard, hydrophobic substrate. Usually, a single germ tube emerges from the apical or basal cell of the three-celled conidia, but not from the middle cell (Bourett and Howard, 1990). The germ tube elongates by tip growth and extends for only a short distance (15 - 30μm) before swelling and bending at its tip. This process, involving germ tube tip deformation, is known as hooking and these changes may reflect a recognition phase toward appressorium morphogenesis, occurring 2 - 4h after germination of conidia (Mendgen *et al.*, 1988; Bourett and Howard, 1990). However, growth and differentiation of germ tubes also depend on environmental cues, such as surface hydrophobicity (Lee and Dean, 1993; Jelitto *et al.*, 1994; Lee and Dean, 1994), the hardness of the leaf surface (Xiao *et al.*, 1994*b*), light (Jelitto *et al.*, 1994), plant cutin monomers (Uchiyama and Okuyama, 1990;

Gilbert *et al.*, 1996), and nitrogen starvation (Talbot *et al.*, 1997). Therefore, the correct combination of these environmental cues will trigger signal transduction cascades and the formation of the mature appressorium (Xu *et al.*, 2007).

Fungal hydrophobins play a role in adhesion of the germ tube to the hydrophobic leaf surface and act as a signal for appressorium morphogenesis (Talbot, 1995). The highly expressed *MPG1* class I hydrophobin-encoding gene is necessary to secure germ tube attachment to the hydrophobic leaf cuticle. Mpg1 self-assembles into an amphipathic layer to increase the wettability of the hydrophobic leaf surface and ensure efficient surface attachment (Talbot *et al.*, 1996; Kershaw *et al.*, 1998). As a consequence, the Δ*mpg1* mutant is reduced in appressorium formation and pathogenicity (Talbot *et al.*, 1993; Beckerman and Ebbole, 1996). Kershaw *et al.* (2005) also showed that cysteine residues involved in intramolecular disulphide bonds are essential for Mpg1 protein secretion and subsequent virulence in *M. oryzae*. A class II hydrophobin *MHP1* was later characterised in *M. oryzae* and its targeted disruption reduces conidiation, conidial germination, appressorium development and plant infection (Kim *et al.*, 2005). However, it is still not clear if Mhp1 contributes to surface hydrophobicity. In the *M. oryzae* genome, at least 6 other genes encode putative hydrophobins (Xu *et al.*, 2007).

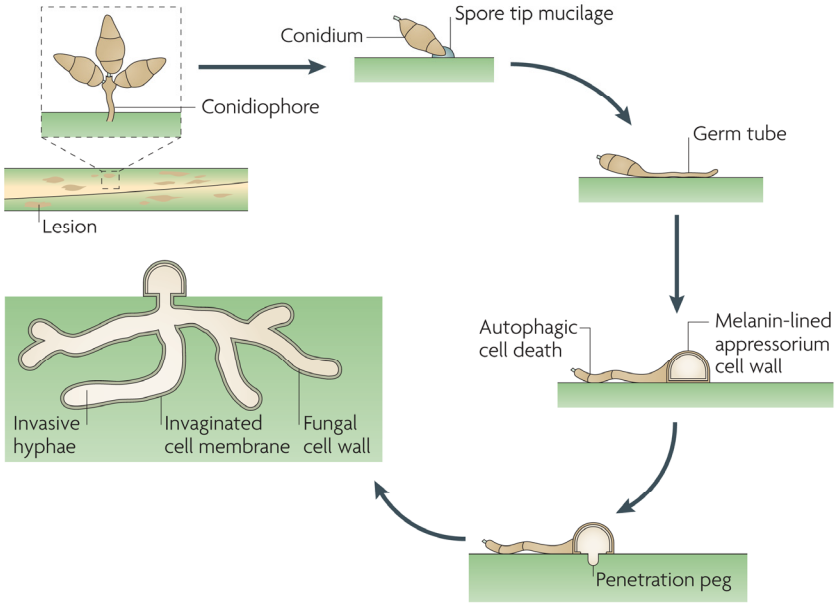

Figure 1.1. Life cycle of the rice blast fungus *M. oryzae.*

The rice blast fungus starts its infection cycle when a three-celled conidium lands on the rice leaf surface. The spore attaches to the hydrophobic cuticle and germinates, producing a germ tube, which subsequently hooks at its tip before differentiating into an appressorium. The appressorium becomes melanised and generates internal turgor pressure. Pressure force is generated and a penetration peg forms at the base, puncturing the cuticle and allowing entry into the rice epidermis. The appressorium matures and the conidium collapses and dies in a programmed process that requires autophagy. Plant invasion occurs by means of bulbous invasive hyphae that invaginate the rice plasma membrane and invade epidermal cells. Cell-to-cell movement occurs by plasmodesmata. Disease lesions occur between 72 – 96h after infection and sporulation occurs under humid conditions. Aerial conidiophores with sympodially-arrayed spores are carried to new host plants by wind or water splashes (Wilson and Talbot, 2009).

1.2.2. Cyclic AMP signaling during appressorium formation

The cyclic AMP (cAMP) response pathway is thought to be triggered at an early stage of *M. oryzae* germ tube elongation, with cAMP acting as a mediator of infection structure formation (Fig. 1.2). Appressorium formation can be induced on non-inductive surfaces by addition of exogenous cAMP or isobutylmethylxanthine (IBMX), an inhibitor of phosphodiesterase (Lee and Dean, 1993). In Δ*mac1* mutants, which lack the unique adenylate cyclase enzyme required for cAMP synthesis from ATP, there are pleiotropic defects on vegetative growth, sporulation and mating ability and mutants are unable to form appressoria and to infect susceptible rice leaves (Choi and Dean, 1997). Remarkably, on hydrophobic surfaces these mutants hook their germ tubes repeatedly and swell at their tips, but do not form appressoria. However, when Δ*mac1* mutants are grown on hydrophilic (non-inductive to appressorium formation) surfaces, the germ tubes are thinner, straight and undifferentiated, similar to germ tubes of the wild type strain Guy11 (Adachi and Hamer, 1998). These results demonstrate that Δ*mac1* mutants are impaired in their ability to discriminate between hydrophobic and hydrophilic surfaces, implying that cAMP signaling is involved in surface recognition in *M. oryzae*. Defects in Δ*mac1* mutants can be complemented by the presence of cAMP or suppressed by a spontaneous dominant active mutation in *SUM1*, which encodes the regulatory subunit of protein kinase A (PKA) (Choi and Dean, 1997; Adachi and Hamer, 1998). *SUM1* is an essential gene in *M. oryzae* and mutants with *SUM1* silenced by RNA interference are significantly reduced in the production of conidia and vegetative growth and are non-pathogenic (Xu *et al.*, 2007).

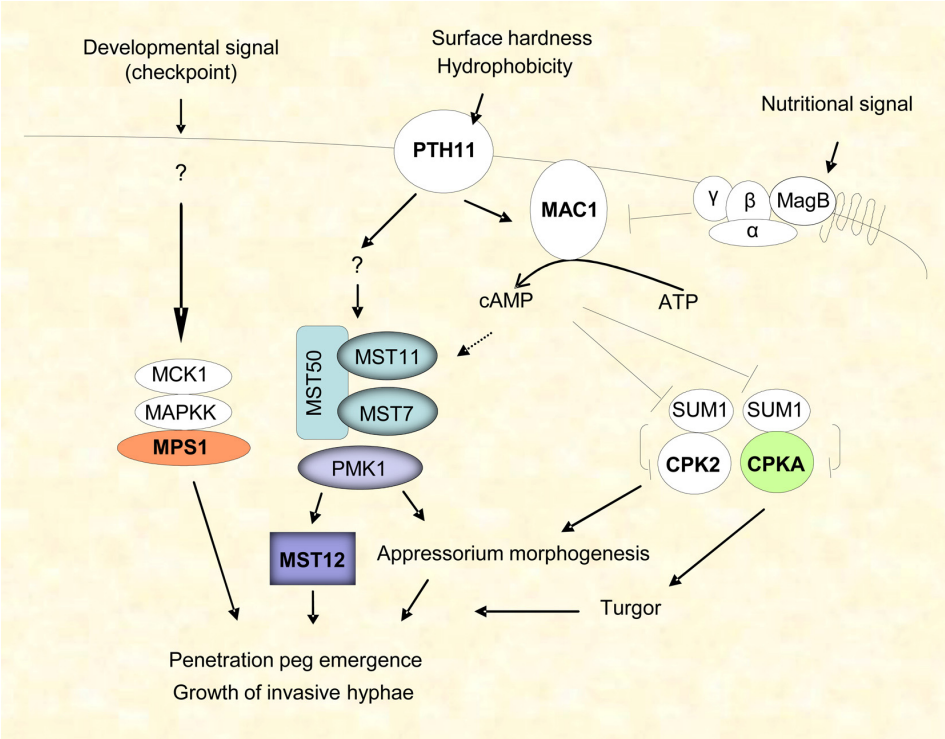

Figure 1.2. Model for signal transduction pathways that regulate appressorium morphogenesis. In this model, appressorium development is positively regulated by physical surface signals that are perceived by Pth11 receptor protein and activate Mac1 adenylate cyclase. Negative regulation of appressorium development in response to exogenous nutrients occurs via dissociation of the MagB-containing heterotrimeric G protein, releasing the βγ subunit, which acts as a repressor of Mac1. The *PMK1* MAPK signaling pathway regulates appressorium morphogenesis and later stages of invasive growth, acting via *MST12* transcription factor. The Pmk1 MAPK is regulated via interaction with Mst50, which acts as an adaptor protein for the Mst11 MAPKKK and Mst7 MAPKK. Mst7 is responsible for Pmk1 phosphorylation and associate with Pmk1 via a MAPK docking site. The cAMP pathway is also responsible for regulating carbohydrate and lipid metabolism during turgor generation. In this model, the *MPS1* regulatory pathway for penetration peg emergence is triggered by a developmental checkpoint, perhaps following completion of appressorium morphogenesis. Adapted from Talbot, 2003 and Caracuel-Rios and Talbot, 2007.

Gene replacement mutants of *CPKA*, a gene encoding a catalytic subunit of cAMP-dependent PKA, produce smaller melanised appressoria and are non-pathogenic (Mitchell and Dean, 1995; Xu *et al.*, 1997). However, Δ*cpka* mutants can infect abraded rice leaves, suggesting that CpkA is not essential for infectious growth after penetration. On non-inductive hydrophilic surfaces, Δ*cpka* mutants are still responsive to exogenous cAMP for appressorium formation (Xu *et al.*, 1997). Kulkarni and Dean (2004) identified several proteins that interact with Mac1 and Cpka, two regulators of appressorium development, using a yeast two-hybrid assay. The interactors of Mac1 include a MAP kinase kinase, a Ser/ Thr kinase and a membrane protein with a fungal-specific CFEM domain called Aci1 (Kulkarni *et al.*, 2003). Cpka also interacted with a putative transcriptional regulator and two different glycosyl hydrolases (Kulkarni and Dean, 2004). Further characterisation of these interacting partners will help to understand the protein interaction network involved in appressorium development and their roles in cAMP signaling.

Initial events in substrate sensing and transduction of extracellular cues into an intracellular signal to initiate appressorium formation are still poorly understood, but are likely to involve perception of signals through G-protein-coupled receptors (GPCRs). One of these components is the GPCR-like gene *PTH11*, which encodes a transmembrane protein with a cysteine-rich CFEM domain, and localises to the plasma membrane and vacuoles (DeZwaan *et al.*, 1999; Kulkarni *et al.*, 2005). Δ*pth11* mutants are non-pathogenic due to a defect in appressorium differentiation. However, Δ*pth11* mutants can form functional appressoria at a frequency 10-15% of the wild type and can infect wounded plant tissues, suggesting that Pth11 is not required for appressorium morphogenesis but is involved in host surface recognition. Defects in the Δ*pth11* mutants can be restored by addition of cAMP and diacylglycerol (DAG), which is consistent with Pth11 acting upstream of the cAMP pathway and mediating appressorium differentiation by activation of Mac1/ cAMP-

mediated intracellular signaling (DeZwaan *et al.*, 1999). To date, the *M. oryzae* genome appears to encode 76 GPCR-like proteins of which 61 represent a class related to Pth11. Interestingly, no Pth11 homologues are found in the model yeast species *Saccharomyces cerevisiae* and *Schizosaccharomyces pombe* or in the genomes of basidiomycetes, plants and animals (Kulkarni *et al.*, 2005).

In several fungi, activation of adenylate cyclase is mediated by heterotrimeric GTP-binding proteins and *M. oryzae* is no exception (Fig. 1.2). The fungus has three Gα (MagA, MagB, MagC), one Gβ (Mgb1) and one Gγ subunits. The Δ*magB* deletion mutant is reduced in appressorium formation and in the ability to infect rice leaves, whereas Δ*magA* and Δ*magC* mutants are still pathogenic, i.e. they act as virulence determinants (Liu and Dean, 1997). Deletion of *MAGC* reduces conidiation and both Δ*magA* and Δ*magC* mutants do not produce mature asci after sexual reproduction. In Δ*magB* mutants the defect in appressorium formation can be restored by addition of cAMP, IBMX and 1,16-hexadecanediol (a lipid monomer). The Δ*magB* mutants also fail to form perithecia and have reduced vegetative growth, conidiation and appressorium formation. Generation of a constitutively-active dominant $MAGB^{G42R}$ allele is predicted to abolish GTPase activity. The $MagB^{G42R}$ mutants are reduced in virulence but are able to produce appressoria on hydrophobic and hydrophilic surfaces (Fang and Dean, 2000). This dominant mutation also causes autolysis of aged colonies, mis-scheduled melanisation of hyphal tips and reduction in both sexual and asexual reproduction. These results suggest that Gα subunit genes are involved in multiple signal transduction pathways in *M. oryzae* that control vegetative growth, sporulation, mating, appressorium formation and pathogenicity. The G-protein β subunit is encoded by *MGB1* (Nishimura *et al.*, 2003). Mutants disrupted in *MGB1* are defective in vegetative growth, conidiation, appressorium formation and virulence, even on wounded plants. Exogenous cAMP induces the formation of abnormal and non-functional appressoria on hydrophobic or hydrophilic surfaces in

Δ*mgb1* mutants. Thus, *MGB1* may be involved in the cAMP signaling for regulating conidiation, surface recognition and appressorium formation. Although *MGB1* is not directly involved in regulating *PMK1* for appressorium formation, it may be involved in regulating *PMK1* for appressorium penetration and invasive growth.

1.2.3. The *PMK1* MAP kinase signaling pathway

Mitogen-activated protein kinases (MAPK) operate in association with upstream kinases to coordinate diverse cellular events in eukaryotic cells in response to environmental or developmental signals. *M. oryzae* expresses *PMK1*, which encodes a MAPK that is a functional homologue of yeast *FUS3*/ *KSS1* kinase genes, which play roles in the pheromone signaling pathway and the regulation of pseudohyphal growth (Xu and Hamer, 1996). *PMK1* is not essential for vegetative growth and sporulation in culture, although it can rescue the mating defect in a Δ*fus3* Δ*kss1* double mutant in yeast. The Δ*pmk1* deletion mutants fail to form appressoria and to grow invasively in rice plants, and are still non-pathogenic even when inoculated on wounded rice leaves. Pmk1 is distributed throughout the cytoplasm and nucleus during most stages of growth and may be translocated to the nucleus in developing appressoria as a response to inductive stimuli (Bruno *et al.*, 2004). In Δ*pmk1* mutants high extracellular concentrations of cAMP do not induce appressoria formation, but increase the level of germ tube hooking and swelling on non- and inductive surfaces (Xu and Hamer, 1996). These results demonstrate that Pmk1 acts downstream of a cAMP signal for appressorium morphogenesis (Fig 1.2). Studies in several other plant pathogenic fungi, including *Botrytis cinerea*, *Claviceps purpurea*, *Cochliobolus heterostrophus*, *Fusarium graminearum* and *Stagonospora nodorum*, have shown that the *PMK1* pathway is well conserved in many phytopathogenic fungi for regulating appressorium formation and other plant infection processes (Xu, 2000). Overall, the *PMK1* pathway regulates appressorium formation and infectious growth.

The MAP kinases (MAPK) are usually activated by MAPK kinases (MAPKK) that are, in turn, activated by MAPKK kinases (MAPKKK) and these MAPK cascades are conserved in eukaryotes (Schaeffer and Webber, 1999). In *M. oryzae*, *MST7* MAPKK and *MST11* MAPKKK genes are homologous to yeast *STE7* MAPKK and *STE11* MAPKKK genes, respectively. Similar to Δ*pmk1* mutant, mutants with *MST7* or *MST11* deleted fail to form appressoria and to colonise rice tissues even through wounds (Zhao *et al.*, 2005). Expression of a dominant active *MST7* allele restores appressorium formation in both Δ*mst7* and Δ*mst11* mutants, consistent with the idea that Mst7 is acting downstream of Mst11 (Fig. 1.2). However, appressoria formed by these mutants fail to penetrate and infect rice leaves. One explanation is that constitutively active *MST7* alleles in Δ*mst7* and Δ*mst11* mutants may have defects in the cAMP signaling pathway that regulates surface recognition and appressorial turgor generation (Zhao *et al.*, 2005; Park *et al.*, 2006). Mst7 is responsible for Pmk1 phosphorylation and these two proteins seem to interact physically during appressorium formation and require the intact MAPK-docking site of Mst7 (Zhao *et al.*, 2005). Activated Pmk1 can move to the nucleus and phosphorylate transcription factors (Zhao and Xu, 2007). The Mst11 MAPKKK contains an N-terminal sterile α-motif (SAM) domain, a Ras-association (RA) domain and a C-terminal protein kinase domain. The SAM domain is essential for Mst11 function and associates with the SAM-containing Mst50 protein (Zhao *et al.*, 2005). In *M. oryzae*, *MST50* gene is homologous to yeast *STE50* and has an N-terminal SAM and a C-terminal RA domain. Similar to Δ*mst11* mutant, the Δ*mst50* mutant was sensitive to osmotic stress and defective in appressorium formation and pathogenicity (Park *et al.*, 2006). Mst50 functions as an upstream component of the *PMK1* pathway and directly interacts with Mst11 via the SAM domain and Mst7. Therefore, it may function as the adaptor protein for the Mst11-Mst7-Pmk1 cascade (Fig. 1.2) (Zhao *et al.*, 2005; Park *et al.*, 2006). Mst50 also interacts with Ras1 and Ras2 via the RA domain, as well as

Cdc42 and Mgb1. These proteins may be responsible for transducing signals to activate the Mst11-Mst7-Pmk1 cascade, which regulates different plant infection processes via the Mst12 and other transcription factors.

There are numerous downstream targets of the Pmk1 MAPK signaling pathway and one likely target is the Mst12 transcription factor (Fig. 1.2) that weakly interacts with Pmk1 in a yeast two-hybrid assay (Park *et al.*, 2002, 2004). *MST12* from *M. oryzae* is homologous to yeast *STE12*, and *MST12* is dispensable for vegetative growth, sporulation and appressorium formation. However, the Δ*mst12* mutants are defective in appressorial penetration and plant infection and both the homeodomain and zinc finger domains of Mst12 are essential for these functions. Δ*mst12* mutants also fail to reorganise microtubules associated with penetration peg formation and to elicit localised plant defence responses, including papilla formation and autofluorescence (Park *et al.*, 2002, 2004). Thus, Mst12 seems to be involved on regulating appressorium maturation, penetration and invasive growth.

Another two genes regulated by *PMK1* during appressorium formation are *GAS1* and *GAS2* genes, which encode small proteins that are similar to *gEgh16* of the powdery mildew fungus (Xue *et al.*, 2002). Mutants deleted in *GAS1* and *GAS2* have normal vegetative growth, sporulation and appressorium formation, but are reduced in penetration and virulence on rice seedlings. Both are expressed only in appressoria, but Gas1 is localised preferentially in the vacuole, while Gas2 is throughout the cytoplasm. Interestingly, deletion of both *GAS1* and *GAS2* does not have an additive effect on appressorium-mediated penetration and lesion development, and *GAS1* and *GAS2* cannot complement each other (Xue *et al.*, 2002).

1.2.4. Appressorium development and function

Following germination and within 8h each germ tube forms a dome-shaped appressorium (Fig. 1.1). Its cell wall is rich in chitin and contains a homogeneous melanin layer (100nm thick) on the inner side of the wall. The layer also covers the septum that separates the appressorium and germ tube. The region in contact with the substratum will become the appressorium pore. This region will be the future site of penetration and is characterised for being thinner than the other areas of appressorium wall, single layered and lacking chitin and melanin (Bourett and Howard, 1990). Under the rim of the appressorium, a pore ring is clearly seen and it has been suggested a function in sealing the pore to the surface of the substrate (Bourett and Howard, 1990; Howard and Valent, 1996).

The appressorium attaches firmly to the leaf and then generates enormous turgor pressure estimated to be as high as 8MPa, which is used as mechanical force to rupture the plant cuticle (Howard *et al.*, 1991; Bechinger *et al.*, 1999). The turgor inside the appressorium is generated by a rapid increase in intracellular glycerol levels to greater than 3M, which is maintained by a melanin layer that effectively lowers the porosity of appressorial walls to < 1nm (Howard *et al.*, 1991; de Jong *et al.*, 1997). If melanin biosynthesis is blocked either by chemical inhibitors, such as tricyclazoles, or by mutation of biosynthetic genes, then the fungus is unable to penetrate the plant surface and cannot cause disease (Chumley and Valent, 1990).

Glycerol biosynthesis in the appressorium of *M. oryzae* is regulated in a distinct manner from that observed in *S. cerevisiae*. In yeast, glycerol is synthesised predominantly from carbohydrates and controlled by a conserved MAPK signaling system called the *HOG* (high osmolarity glycerol) pathway. Stimulation of the *HOG* pathway leads to accumulation of glycerol in yeast cells and maintenance of cellular turgor in response to hyperosmotic stress (Smith *et al.,* 2010). The *M. oryzae OSM1*

gene encodes an osmosensory MAPK that is functionally homologous to yeast *HOG1*. Although *OSM1* is required for mycelial growth under hyperosmotic stress conditions, it is dispensable for glycerol accumulation and turgor generation in appressoria and virulence (Dixon *et al.*, 1999). This suggests that *M. oryzae* has evolved specific signaling pathways for appressorium-mediated plant infection that operate independently of the conserved eukaryotic pathway mechanism for cellular turgor regulation. It seems likely that the cAMP and *PMK1* pathways coordinate the breakdown and transfer of storage carbohydrate and lipid reserves to the appressorium and consequently promote appressorium turgor generation (Thines *et al.*, 2000).

Conidial storage compounds such as glycogen, trehalose and lipids are trafficked to the developing appressorium and appear to be used in the synthesis of glycerol. Trehalose synthesis in *M. oryzae* is mediated by a trehalose-6-phosphate synthase, *TPS1*, which is also required for production of appressorial turgor, penetration hyphae and plant infection (Foster *et al.*, 2003; Wilson *et al.*, 2007). In the *M. oryzae* genome, two trehalases have been characterized, *NTH1* and *TRE1*, and shown to be involved in trehalose breakdown. Although Δ*nth1* mutants are able to penetrate the plant cuticle normally, their ability to proliferate effectively in plant tissue and induce disease symptoms is impaired. Conversely, *TRE1* gene is dispensable to pathogenicity (Foster *et al.*, 2003). Enzymatic activities of glycerol-3-phosphate dehydrogenase and glycerol dehydrogenase are expressed in appressoria but do not increase during appressorium development. So, glycerol synthesis from glycolytic intermediates is not the principal route for generating the glycerol required for turgor pressure (Thines *et al.*, 2000). In contrast, triacylglycerol lipase activity increases during appressorium formation and maturation. Lipid breakdown in appressoria is a complex process and an efficient way of producing glycerol rapidly and leads to production of fatty acids for oxidation and ATP generation (Thines *et*

al., 2000; Wang *et al.*, 2007). Deletion of *MFP1* gene, encoding the multifunctional β-oxidation enzyme, leads to attenuation of virulence (Wang *et al.*, 2007), while Δ*pex6* mutants are defective in β-oxidation of long chain fatty acids and functional peroxisomes and as a result are impaired in appressorium function and pathogenicity (Ramos-Pamplona and Naqvi, 2006). The major peroxisomal carnitine acetyl transferase in *M. oryzae* encoded by the *PTH2* gene plays a role in the transfer of acetyl-CoA molecules across intracellular membranes and subsequent generation of acetyl-CoA pools necessary for appressorium function and penetration hyphae during host invasion (Bhambra *et al.*, 2006). In summary, *M. oryzae* has a versatile capacity to synthesise glycerol in the appressorium for turgor generation.

In *M. oryzae*, the pigment melanin is synthesised from the polyketide precursor 1,8-dihydroxynaphthalene (DHN) and is essential for appressoria to accumulate turgor pressure (Chumley and Valent, 1990; Henson *et al.*, 1999). *ALB1*, *RSY1* and *BUF1* genes encode a polyketide synthase (PKS), a scytalone dehydratase and a polyhydroxynaphthalene reductase, respectively, and are 3 major genes involved in DHN melanin synthesis. These melanin-deficient mutants of *M. oryzae* fail to infect host plants, but the same mutants successfully infect plants that have wounded or abraded leaves (Chumley and Valent, 1990). Another gene identified to be involved in melanin biosynthesis is *PIG1*, which encodes a transcription factor that contains two types of DNA-binding motifs, Cys_2Hys_2 zinc finger and $Zn(II)_2Cys_6$ binuclear cluster motifs (Tsuji *et al.*, 2000). Mutants deleted for *PIG1* are defective in pathogenicity and mycelial melanisation but not in appressorial melanisation, indicating that melanin synthesis is regulated by different mechanisms in vegetative hyphae and appressoria of *M. oryzae*.

The potential role of extracellular enzymes to facilitate perforation of host surface is controversial. The infection process may be accelerated by the action of

extracellular enzymes, but the fact that *M. oryzae* can penetrate inert plastic surfaces shows that mechanical force is the primary means of infection (Howard *et al.*, 1991). Nonetheless, the *M. oryzae* genome is predicted to encode 16 putative cutinase and 20 putative xylanase genes and other hydrolytic enzymes that can erode the plant cuticle and degrade the plant cell wall (Dean *et al.*, 2005). Sweigard *et al.* (1992) identified a cutin-degrading enzyme encoded by *CUT1*, which was dispensable for pathogenicity. But *CUT1* was not among those cutinase genes that are significantly up-regulated during infection process. Recently, a second cutinase *CUT2*, the expression of which is up-regulated during appressorium maturation and penetration, was characterised (Skamnioti and Gurr, 2007). Contrary to the Δ*cut1* mutant, the Δ*cut2* mutant displays reduced conidiation, multiple elongated germ tubes, aberrant appressoria and is severely reduced in virulence. Morphological and pathogenicity defects can be restored by exogenous application of cAMP, IBMX and DAG. Therefore, Cut2 appears to play a pivotal role in surface sensing, leading to correct germling morphogenesis and successful plant penetration (Skamnioti and Gurr, 2007).

1.2.5. Appressorium-mediated plant infection regulated by cell cycle

Appressorium development by *M. oryzae* is cell cycle-regulated and requires autophagic programmed cell death in order to recycle the contents of the fungal spore before plant infection (Fig. 1.1) (Veneault-Fourrey *et al.*, 2006*a*; Kershaw and Talbot, 2009). During germination, one nucleus of the three-celled conidium migrates into the developing germ tube, where it undergoes mitosis (4 – 6h). Following mitosis, one of the daughter nuclei migrates into the nascent appressorium and the other returns to the cell of the conidium from which the mother nucleus originated (8h). Blocking mitosis in the germ tube prevents appressorium development (Veneault-Fourrey *et al.*, 2006*a*). Recently, Saunders *et al.* (2010) have shown that entry into mitosis is both necessary and sufficient to

initiate appressorium formation and maturation in *M. oryzae*, while exit from mitosis is an essential pre-requisite for plant infection.

Fungal autophagy is necessary for rice blast disease. A mutant lacking *ATG8* gene, which encodes an ubiquitin-like protein essential for autophagy, cannot undergo conidial collapse and is unable to produce functional appressoria, penetration hyphae and disease symptoms on the host leaves (Veneault-Fourrey *et al.*, 2006*a*). Furthermore, any of the 16 genes (*ATG1-10, 12-13, 15-18*) required for non-selective macroautophagy are indispensable for conidial programmed cell death and appressorium maturation. These deletion mutants are unable to cause rice blast disease (Kershaw and Talbot, 2009).

1.2.6. Penetration peg formation

Following appressorium melanisation, a narrow penetration peg (3 – 5μm in diameter) emerges from the appressorial pore to penetrate the host surface and conveys the contents of the appressorium into epidermal plant cells (Fig. 1.1). The peg wall is composed of a single cell wall layer which binds the lectins concanavalin A and wheat germ agglutinin (Bourett and Howard, 1990), although the presence of cell wall at the tip of penetration pegs remains controversial (Koga, 1994). The peg cytoplasm and the adjacent region in the appressorium are a zone-of-exclusion lacking organelles with only a few ribosomes present. However, an extensive cytoskeletal network is observed, containing actin and microtubules that might increase peg rigidity and act as an important factor of the mechanical penetration employed (Bourett and Howard, 1990). After piercing the plant cell wall, the narrow peg enlarges to form a primary infection hypha that differentiates into branched, vacuolated and bulbous secondary hyphae (> 5μm in diameter), which spread intracellularly (Heath *et al.*, 1990, 1992; Koga, 1994; Kankanala *et al.*, 2007). Within 3 to 5 days after initial inoculation, necrotic lesions appear developed on the surface of rice leaves.

Regulation of penetration peg formation requires *MPS1*, which encodes a MAPK essential for the maintenance of cell wall integrity and polarisation of the actin cytoskeleton (Fig. 1.2) (Xu *et al.*, 1998). *MPS1* is a functional homologue of the *S. cerevisiae SLT2* MAPK and is responsible for controlling cell wall growth in response to membrane stress. The Δ*mps1* mutants show hyper-sensitivity to cell wall digesting enzymes, reduced sporulation and fertility. Although Δ*mps1* mutants form melanised and functional appressoria, they fail to penetrate the plant surface and are non-pathogenic. Another surprising finding is that this mutant still activates plant defence responses, changes in the pattern of cytoplasmic streaming and rearrangement of the actin cytoskeleton *in planta* (Xu *et al.*, 1998).

Among the virulence factors that contribute for appressorial penetration is a tetraspanin-like protein encoded by the *PLS1* gene (Clergeot *et al.*, 2001). This fungal tetraspanin has a similar secondary structure to animal tetraspanin proteins, which are known to regulate cell morphology, motility, invasion, fusion and signaling events in animal systems (Hemler, 2005). In a similar way to the Δ*mps1* mutant, mutants lacking *PLS1* form melanised and functional appressoria but are unable to differentiate penetration pegs and are non-pathogenic. Pls1 protein is expressed only in appressoria and is localised in the appressorial plasma membrane and vacuoles (Clergeot *et al.*, 2001). The exact function of Pls1 is not clear, but it may be involved in re-establishing polarised growth and in the clustering or trafficking of membrane receptors involved in the generation of positional signals. Pls1 is the only tetraspanin in *M. oryzae* and a single copy of an orthologue tetraspanin gene is present in many filamentous ascomycetes (Veneault-Fourrey *et al.*, 2006*b*).

1.2.7. Biotrophic invasion *in planta* by *M. oryzae*

M. oryzae has been described as a hemibiotrophic pathogen, because the fungus can behave as either a biotroph or necrotroph, depending on the surrounding conditions or the stage of its life-cycle (Kankanala *et al.*, 2007). After appressorial penetration, thin filamentous primary hyphae grow in the first invaded rice plant cell. These hyphae differentiate into bulbous invasive hyphae (IH) and are sealed by a plant plasma membrane, termed the extra-invasive hyphal membrane (EIHM) (Kankanala *et al.*, 2007). These specialised invasive hyphal membranes contain multiple connections to peripheral rice cell membranes. Subsequently infected rice cells are invaded by filamentous IH. Successive cell invasions are biotrophic, although individual invaded cells are no longer viable when the fungus moves into the adjacent cells. Nothing is yet known regarding how, when and why biotrophic hyphae switch to necrotrophic growth. *M. oryzae* appears to manipulate the structure and function of plasmodesmata to mediate its cell-to-cell movement into live neighbour rice cells and for controlling plant cellular communication, suggesting that the fungus has outstanding means of perceiving plant cell structures and is capable of evading or suppressing plant defences during plant cell invasion (Kankanala *et al.*, 2007). Most likely, *M. oryzae* suppresses plant defence responses by delivering blast effector proteins during infectious hyphal growth *in planta*.

1.3. Effector biology of phytopathogens

Plant pathogens secrete proteins known as effectors, during colonisation of a plant host. Effector proteins are pathogen molecules that manipulate host cell structure and function, facilitating infection (virulence factors or toxins) and/ or triggering defence responses (avirulence factors or elicitors) (for definitions see Kamoun, 2006).

Flor (1971) stated the gene-for gene hypothesis in which for every avirulence (*AVR*) gene in the pathogen there is a corresponding resistance (*R*) gene. This interaction can be direct or indirect. Pathogen recognition triggers host resistance responses in order to block further growth of the pathogen. These defence responses include a rapid form of localised cell death termed the hypersensitive response (HR), production of antimicrobial compounds, lignin formation, an oxidative burst and increased expression of pathogenesis-related genes (Bent and Mackey, 2007). A newer "zig-zag" model (Fig. 1.3) has been proposed in which plants contain two lines of defence (Jones and Dangl, 2006). The first line of defence provides basal protection against all potential pathogens and is based on recognition of conserved microbial features (*e.g.* chitin), that are known as pathogen-associated molecular patterns (PAMPs) by PAMP-recognition receptors (PRRs). The PRRs activate PAMP-triggered immunity (PTI) that prevents further growth of the pathogen in the host. Successful pathogens deploy effectors that contribute to pathogen virulence. Plants respond with the development of a more specialised system based on effector recognition by R proteins (*e.g.* nucleotide binding site – leucine-rich repeat NBS-LRR receptors) and subsequent activation of effector-triggered immunity (ETI) that leads to fast and acute defence responses at infection sites (*e.g.* HR). This triggers a second wave of co-evolutionary arms race between pathogens and plants. Pathogens respond by mutating or losing effectors or by acquiring novel effectors that avoid or suppress ETI, whereas plants develop novel R proteins so that ETI can be triggered again (Jones and Dangl, 2006).

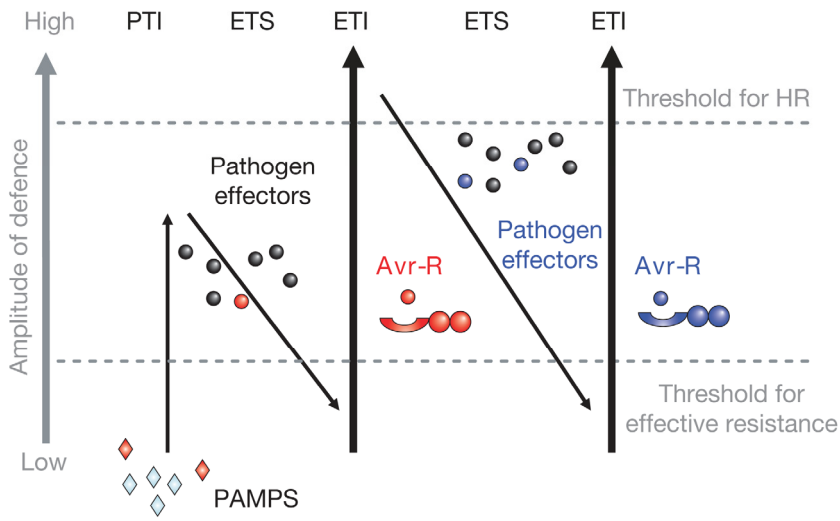

Figure 1.3. Zig-zag model of the plant immune system.

In a first phase, plants detect pathogen-associated molecular patterns (PAMPs, red diamonds) via PRRs to trigger PAMP-triggered immunity (PTI). In a second phase, successful pathogens deliver effectors that interfere with PTI, enabling pathogen nutrition and dispersal and resulting in effector-triggered susceptibility (ETS). In a third phase, one effector (indicated in red) is recognised by an NBS-LRR protein, activating effector-triggered immunity (ETI) and inducing hypersensitive cell death (HR). In a final phase, pathogen isolates that have lost the red effector are selected and perhaps gain novel effectors through horizontal gene flow (in blue). These proteins can help pathogens to suppress ETI. Selection favours new plant NBS-LRR alleles that can recognise one of the newly acquired effectors, resulting again in ETI (Jones and Dangl, 2006).

1.3.1. *Pseudomonas* and *Xanthomonas* type III effectors

The ability of *Pseudomonas*, *Xanthomonas* and most other Gram-negative phytopathogenic bacteria to grow and cause disease in plants is dependent on the injection of effector proteins directly into the cytoplasm of plant cells via the type III secretion system (T3SS) (Cornelis, 2006). Each bacterial strain has a set of 20-30 effectors, which are functionally redundant, interchangeable and apparently are not adapted for host specificity (reviewed by Cunnac *et al.*, 2009). Because effectors are individually dispensable for pathogenicity, they are easily missed in virulence mutant screens. However, the generalisations made above may be less true for X*anthomonas*, in which effectors of the transcription activator-like (TAL) genes are individually indispensable for pathogenicity and conserved between different strains (Kay and Bonas, 2009; Bogdanove *et al.*, 2010). Their specificity arises from the recognition of a target gene promoter motif named the *UPA* box, by the DNA binding domain of each TAL effector (Boch *et al.*, 2009).

Computational prediction programs and functional screens can be used to identify novel T3S effectors due to general features that these proteins present: (1) active effector genes are associated with *hypersensitive response and pathogenicity* (*Hrp*) box promoters; (2) the N-terminal region of effectors has characteristic amino-acid patterns; (3) several effectors are encoded in operons containing a chaperone gene; (4) generally effectors are located in regions harbouring signatures of horizontal acquisition (Cunnac *et al.*, 2009).

1.3.2. Oomycete effectors

Although oomycetes share morphological features with some filamentous fungal phytopathogens, they are heterokonts and more closely related to diatoms and brown algae (Birch *et al.,* 2006). During the early stages of infection, oomycetes form specialised feeding structures called haustoria as do biotrophic fungi. Haustoria play a key role in exploitation of water and nutrients and might be involved in the

delivery of effector molecules into the plant cell to suppress plant defences and enable parasitic colonisation (Mendgen and Hahn, 2002). The oomycete Avr proteins possess a conserved RXLR motif within the N-terminal signal peptide. Some of these effector proteins also have an EER motif right downstream of the RXLR motif. The RXLR-EER motifs are required for secretion from haustoria and translocation into the host plant cells (Whisson *et al.*, 2007). Interestingly, this RXLR motif resembles in both sequence and position the RXLX motif required for the translocation of malarial proteins from *Plasmodium falciparum* into the host erythrocytes (Hiller *et al.*, 2004) and is exchangeable with the *Plasmodium* host targeting signal (Bhattacharjee *et al.*, 2006). The occurrence of this conserved RXLR motif has enabled searches for candidate effectors from different oomycete genome sequences (Win *et al.*, 2007). Unfortunately, the RXLR motif is not detected in fungal Avr proteins and may be specific for oomycetes (Catanzariti *et al.*, 2007; Mosquera *et al.*, 2009).

1.3.3. Fungal effectors

In contrast to bacterial plant pathogens, little is known about effector function in fungi. Like Avr proteins from oomycetes, fungal Avr proteins are also detected intracellularly, suggesting that these plant pathogens must deliver effectors inside host cells (Catanzariti *et al.*, 2006; Ridout *et al.*, 2006; Mosquera *et al.*, 2009). However, the mechanism of translocation into the apoplast or cytoplasm of infected plant cells is unknown. Fungal effector proteins identified so far are predominantly small and cysteine-rich proteins: *e.g.* Avr2, Avr4, Avr9, Ecp1, Ecp2, Ecp4, Ecp5, Ecp6 and Ecp7 from fungal pathogen of tomato *Cladosporium fulvum* (van den Ackerveken *et al.*, 1993; Joosten *et al.*, 1994; Dixon *et al.*, 1996; Laugé *et al.*, 2000; Bolton *et al.*, 2008); Six1, Six2 and Six4 from vascular pathogen *Fusarium oxysporum* (Rep *et al.*, 2004; Houterman *et al.*, 2007); AvrLm6 and AvrLm4-7 from the causal agent of stem canker on oilseed rape *Leptosphaeria maculans* (Fudal *et*

al., 2007; Parlange *et al.*, 2009); AvrP123 and AvrP4 from flax rust fungus *Melampsora lini* (Catanzariti *et al.*, 2006); and Avra10 and Avrk1 from powdery mildew fungus *Blumeria graminis* f. sp. *hordei* (Ridout *et al.*, 2006).

The contribution of each fungal effector to virulence has also proven to be difficult to assess (reviewed by Stergiopoulos and de Wit, 2009). Many effectors seem to work in concert during colonisation *in planta* and their individual contribution to virulence is minor or undetectable, as their deletion has no apparent effect on pathogen fitness. Some effectors might have overlapping functions and therefore are redundant (*e.g.* Avr4 and Ecp6 of *C. fulvum*).

Some of the genes including *AVR2*, *AVR4*, *AVR9* and *ECP2* from *C. fulvum*, do not have orthologues in the *M. oryzae* genome. Similarly, *F. graminearum* lacks orthologues of known *M. oryzae AVR* genes *PWL2* and *AVR1-CO39* (Xu *et al.*, 2007). Hence, discovery of novel effector genes in sequenced genomes by comparative secretome analysis or BLAST sequence similarity search has been an unsuccessful process due to lack of common structural features or conserved domains among fungal *AVR* genes.

Magnaporthe effectors

The rice-*Magnaporthe* pathosystem is a classical gene-for-gene system (Flor, 1971) in which *AVR* genes in the pathogen show a functional correspondence with particular plant *R* genes. So far, over 80 blast *R* genes have been identified in the search for durable resistance to rice blast disease (Ballini *et al.*, 2008). However, few *AVR* genes (*e.g. AVR-Pita1*, *PWL2*, *AVR1-CO39*, *ACE1*) have been cloned and characterised in *M. oryzae*, suggesting that many effector genes remain to be identified (Skamnioti and Gurr, 2009; Liu *et al.*, 2010; Valent and Khang, 2010).

The *AVR-Pita1* gene encodes a putative neutral zinc metalloprotease that is likely to be secreted into the plant cytoplasm during penetration and further infection (Jia *et al.*, 2000; Orbach *et al.*, 2000). Interestingly, *AVR-Pita1* is located in the telomeric region and this situation may allow *M. oryzae* to adapt rapidly to its host by undergoing high rates of recombination at chromosome ends. The fungus can also escape recognition by NBS-LRR Pi-ta receptor through diverse mechanisms, including point mutations, insertion mutations and deletions of *AVR-Pita1* gene sequence (Orbach *et al.*, 2000; Takahashi *et al.*, 2010). Amino acid mutations in the Pi-ta LRR motif (Bryan *et al.*, 2000) or in the Avr-Pita1 protease motif (Jia *et al.*, 2000) result in loss of resistance responses in rice plants due to disruption of physical interaction between Pi-ta and Avr-Pita1 proteins. The Avr-Pita1/ Pi-ta interaction provides the first report of a direct intracellular Avr/ R protein interaction for a fungal avirulence protein.

The *PWL2* gene encodes a glycine-rich, hydrophilic protein with a putative secretion signal peptide (Kang *et al.*, 1995; Sweigard *et al.*, 1995). Distribution of several sequences homologous to *PWL2* with different levels of sequence homology and chromosome locations, such as *PWL1*, *PWL3* and *PWL4*, led to the discovery of a *PWL* multigene family in *M. oryzae*. The *PWL* genes are not avirulent toward any known rice cultivar but functional copies of *PWL* are recognised by weeping lovegrass plants. The *PWL* genes therefore act as avirulence factors at the host species level, rather than at the cultivar level.

The *AVR1-CO39* gene is responsible for conferring avirulence on the rice cultivars that contain the resistance gene *Pi-CO39* (*e.g.*, rice cultivar CO39) (Farman and Leong, 1998; Chauhan *et al.*, 2002). The *AVR1-CO39* was cloned from a weeping lovegrass pathogen and is not present in the genome of *M. oryzae* Guy11, 70-15, and most of the 45 rice-infecting isolates (Farman *et al.*, 2002; Tosa *et al.*, 2005). It is proposed that ancestral rearrangements at the *AVR1-CO39* locus may have

resulted in its non-functionality and loss during the early evolution of the *Oryza*-specific subgroup of *M. oryzae* (Tosa *et al.*, 2005).

The avirulence gene *ACE1* encodes a polyketide synthase/ non-ribosomal peptide synthetase (PKS/ NRPS) hybrid protein expected to produce a secondary metabolite (Bohnert *et al.*, 2004). Ace1 is specifically expressed in the cytoplasm of the appressorium but not in infectious hyphae and its expression is restricted to a specific stage of infection, during appressorium maturation and penetration. Although it behaves as a classical *AVR* gene, Ace1 is a non-secreted protein, unlike other fungal *AVR* genes. A single amino acid exchange in the catalytic site of the β-ketoacyl synthase domain of Ace1 abolishes recognition of the fungus by *Pi33*-containing resistant cultivars (Bohnert *et al.*, 2004). This fact suggests that the avirulence signal recognised by the *Pi33* resistance gene is not the Ace1 protein, but the secondary metabolite synthesised by *ACE1*. Such interaction between a fungal metabolite and a resistant gene is unique among known *AVR*/ *R* interactions in fungi. With the exception of *ACE1*, the blast effectors described above encode small IH-specific secreted proteins.

Novel *AVR* blast effectors have been described from *M. oryzae* by analysing the interaction of *Magnaporthe* - rice transcriptome (Mosquera *et al.*, 2009) and by combining a large-scale association genetics study with genome sequence (Yoshida *et al.*, 2009). Transcriptome analysis of biotrophic IH revealed that known blast effectors, such as *AVR-Pita1* and *PWL2* and predicted secreted effectors, are highly expressed during rice blast invasion *in planta* (Mosquera *et al.*, 2009). These fungal effectors are designated biotrophic-associated secreted (BAS) proteins. In general, the Bas proteins are small and cysteine rich and have no paralogues in *M. oryzae* or orthologues in other fungi. Secretion of four Bas proteins was observed into rice cells in a compatible, but not in an incompatible interaction (Mosquera *et al.*, 2009). Avr-Pita1, Pwl2, Bas1 and Bas2 proteins accumulate in a cap-like structure named

the biotrophic interaction complex (BIC) (Fig. 1.4). Bas3 localises in rice cell wall crossing points and Bas4 uniformly outlines growing IH. However, targeted deletion of *BAS1*, *BAS2* and *BAS3* did not impair the fungus pathogenicity, suggesting functional redundancy between effectors during biotrophic invasion (Mosquera *et al.*, 2009).

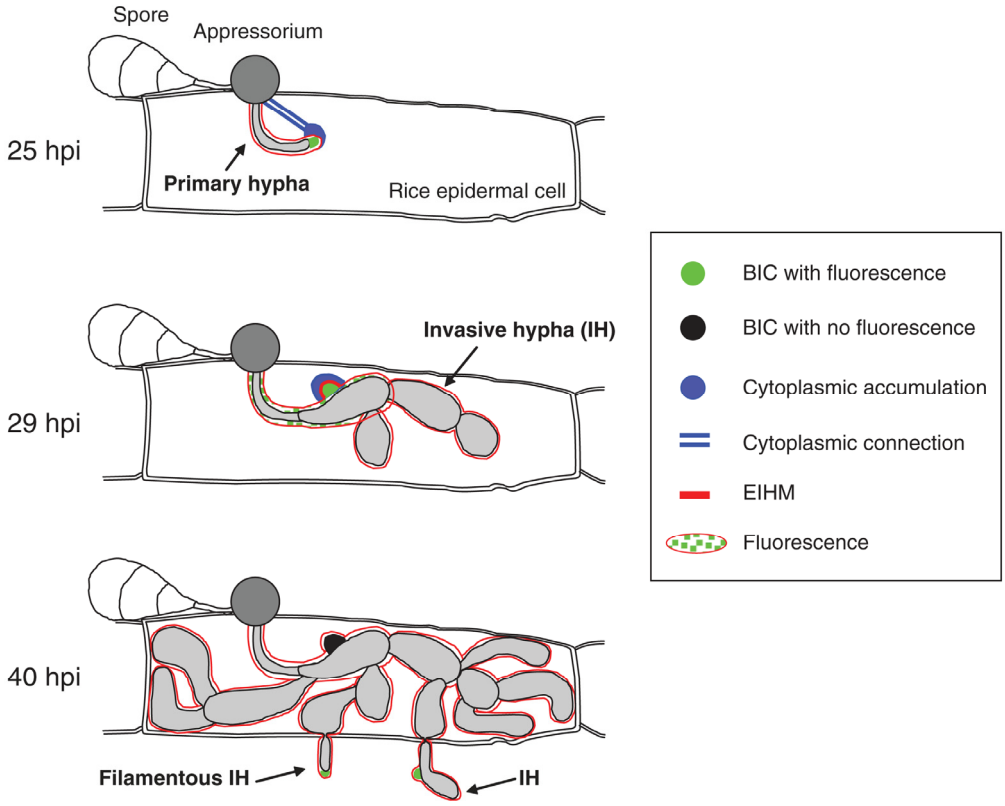

Figure 1.4. Two-stage BIC development and preferential effector accumulation in successively invaded rice sheat cells.

After appressorium-mediated penetration (25hpi), the fungus grows a filamentous primary hypha, which invaginates the rice plasma membrane. Effector:EGFP fusion proteins are secreted into the membranous cap (BIC) at the tips of primary hyphae. By 29hpi, primary hyphae have differentiated into bulbous IH, which are sealed in an EIHM compartment. The membranous cap (BIC) moves beside the differentiating IH and accumulates secreted effector:EGFP proteins as long as IH grow inside the cell. After filling first invaded cells, IH undergo extreme constriction to cross plant cell walls via plasmodesmata, immediately grow as filamentous IH, and then differentiate into bulbous IH (40hpi). This cycle is repeated for sequentially-invaded rice cells (Kankanala *et al.*, 2009).

Using the published *M. oryzae* 70-15 isolate genome sequence (Dean *et al.*, 2005), Yoshida and colleagues (2009) examined DNA polymorphisms of predicted secreted proteins that could be associated with *AVR* function on a panel of rice cultivars harbouring different *R* genes. However, no associations were found. Realising that a significant number of *AVR* genes might be missing from 70-15 isolate that is derived from a cross of *Magnaporthe* rice isolate with a *Magnaporthe* weeping lovegrass isolate (Chao and Ellingboe, 1991), they sequenced another *M. oryzae* isolate, Ina168. This Japanese *Magnaporthe* isolate carries 9 known *AVR* genes: *AVR-Pia*, *AVR-Pii*, *AVR-Pik*, *AVR-Pikm*, *AVR-Piz*, *AVR-Pita2*, *AVR-Pizt*, *AVR-Pib* and *AVR-Pit*. The Ina168 genome contains a region of 1.68Mb absent from the 70-15 isolate genome sequence, which comprises 316 putative secreted effectors (Yoshida *et al.*, 2009). Three of the open reading frames of these candidate effector genes, *PEX22*, *PEX31* and *PEX33*, showed polymorphisms that associated with three AVR phenotypes, *AVR-Pia*, *AVR-Pik/km/kp* and *AVR-Pii*, respectively. Furthermore, transformations of *M. oryzae* isolate lacking AVR function with Pex22, Pex31 and Pex33, conferred avirulence towards rice cultivars expressing *Pia*, *Pik/km/kp* and *Pii* resistance genes, respectively. These 3 novel AVR proteins are small, contain a signal peptide, and are recognised inside of rice cells carrying the cognate *R* genes, suggesting that they must be translocated into the plant cell during infection (Yoshida *et al.*, 2009).

Translocation of Magnaporthe effectors into rice cells

Bacterial pathogens secrete effector proteins directly into the plant cells via the T3SS, whereas oomycete effector proteins containing a RXLR sequence motif following the classical signal peptide are translocated inside host cells (Alfano, 2009). However, how the rice blast fungus delivers effector proteins during plant invasion is currently unknown. Bioinformatic identification for membrane translocation motifs and *cis*-elements in promoters mediating IH-specific

transcription of known and putative blast effectors has been unsuccessful (Mosquera *et al.*, 2009).

The plant-fungal interface has been analysed in an attempt to understand the mechanism of blast effector secretion and translocation from IH to the plant host cytoplasm. Khang *et al.* (2010) have presented a detailed analysis of the biotrophic interfacial complex (BIC) development (Fig. 1.4) and used sensitive techniques for tracking fluorescently tagged blast effector proteins and their delivery into infected rice cells. Expression of fluorescently tagged blast effector proteins (Avr-Pita1, Pwl2) under control of their native promoters showed that these proteins were secreted into the BIC soon after appressorium-mediated penetration of the first invaded rice cell. The first stage of BIC development corresponds to the EIHM membranous cap at the tip of primary or filamentous IH (Kankanala *et al.*, 2007). Then, the BIC is left behind beside the first infected cell when the fungus switches to bulbous IH growth. Fluorescent BIC development is also observed for IH that had invaded neighbour rice cells. Fluorescence recovery after photobleaching (FRAP) experiments revealed that blast effectors are continuously synthesised, delivered and accumulated in BICs, while the IH are growing somewhere else in the invaded cell (Khang *et al.*, 2010). Only BIC-localised proteins (*e.g.* Pwl2 and Bas1) are translocated into the cytoplasm of infected rice cells. This observation was facilitated by plasmolysing the rice cells or by targeting the blast effectors to the plant nucleus (Khang *et al.*, 2010). This elegant study confirms that the BIC is a novel structure that accumulates effectors and that proteins are delivered into the plant cytoplasm via BICs.

In *M. oryzae* there is evidence that translocation of effectors into the host plant cells might involve the endoplasmic reticulum (ER) classical secretion pathway of the pathogen from analysis of a P-type ATPase family (Balhadère and Talbot, 2001;

Gilbert *et al.*, 2006) and components of the unfolded protein response (UPR) machinery (Yi *et al.*, 2009).

M. oryzae genome carries four putative aminophospholipid translocases (APT)-encoding genes belonging to a P-type ATPase family. In *S. cerevisiae,* these enzymes maintain the asymmetrical distribution of aminophospholipids in cellular membranes and are required for efficient Golgi function and are involved in both endocytosis and exocytosis. One of these APT genes is *PDE1* and is expressed at low level during vegetative growth, conidial germination and appressorium formation (Balhadère and Talbot, 2001). The *Magnaporthe* Δ*pde1* mutant exhibits reduced appressorium-mediated penetration and produces few disease symptoms when inoculated onto a susceptible host. *APT2* gene encodes also an APT and Apt2 is a Golgi-localised protein (Gilbert *et al.*, 2006). Mutants lacking *APT2* have a functional appressorium but form abnormal infectious hyphae that arrest growth before invasion of the epidermal cell. Furthermore, these mutants are defective in secretion of extracellular enzymes and accumulate abnormal Golgi-like cisternae. Interestingly, the Δ*apt2* mutants also fail to elicit a hypersensitive response (HR) in the rice resistant cultivar IR-68 even on wounded leaves. This result suggests that the delivery of effector proteins was prevented, including the avirulence gene product necessary for HR induction in the Guy11/ IR-68 interaction (Gilbert *et al.*, 2006). Taken as a whole, Apt2 is required for both foliar and root infection and for rapid induction of host defence responses in an incompatible reaction.

Protein translocation in the secretory pathway is a highly complex and regulated process. Membrane trafficking and protein sorting is intimately connected with a number of cellular processes, such as quality control of ER and cytoskeletal dynamics (Derby and Gleeson, 2007). In *S. cerevisiae*, a member of the heat shock protein 70 (Hsp70) family, Lhs1, plays a role in the UPR pathway. This chaperone is involved in protein import into the ER and correct protein folding in the ER lumen (Tyson and Stirling, 2000). *Magnaporthe* Δ*lhs1* mutant is severely impaired in

conidiation, penetration, biotrophic invasion in susceptible rice plants, induction of HR mediated by the *Pi-ta* resistance gene and accumulation of secreted effector proteins in BICs (Yi *et al.*, 2009). This recent work gives evidence that chaperones via the ER secretory pathway play a key role in the proper processing of secreted proteins such as effectors and in the successful development of rice blast disease *in planta*.

1.4. Introduction to current study

Rice is one the most important staple food crops, feeding half of the world population. It is estimated that rice yield production will have to increase 30% over the next 20 years in order to sustain the nutritional needs of expanding global population (Khush and Jena, 2009). Although intensive breeding programmes have improved rice yield, rice blast disease causes losses of hundreds of millions of tons of rice grain annually. Such losses have led to rice shortages in many developing countries. Control of this devastating disease is vital for global food security, economic and social welfare. A deep understanding of the molecular events that occur during infection-related process of *M.oryzae* will illuminate the development of effective control methods for rice blast disease.

Here, the aim of this study was to identify genetic determinants of the successful colonisation of rice tissue by *M. oryzae*, using two different approaches. The first approach was the identification of pathogenicity-defective mutants of *M. oryzae* by screening a T-DNA insertional library. This led to the discovery of a mutant severely defective in both foliar and root virulence, M1422, and the functional characterisation of an 1422-associated gene called *Transcription factor for Polarity Control TPC1* (Chapters 3 to 6). The second approach was the generation of a catalogue of a set of secreted proteins for *M. oryzae* using bioinformatic analysis (Chapter 7). Targeted

deletion of three putative nuclear-localised secreted effectors was also carried out. Functional characterisation of Δ*ftf*, Δ*zncys* and Δ*cenpB* mutants showed that these genes are dispensable for the pathogenicity of *M. oryzae*, and are not secreted into the plant host cells.

CHAPTER 2

Materials and Methods

2.1. Growth and maintenance of fungus stocks

2.1.1. *Magnaporthe* strains

All isolates of *M. oryzae* used in this study are stored in the laboratory of N. J. Talbot (University of Exeter). Wild-type *M. oryzae* strain used was Guy11 and all knock-outs were performed in the same genetic background. For long-term storage, *M. oryzae* was grown through filter paper disks (3 mm, Whatman International), which were desiccated and stored at -20°C. The fungus was routinely incubated in a controlled temperature room at 25°C with a 12h light/ dark cycle. The fungus was grown in sterile complete medium (CM) (Table 2.1 and 2.2), minimal medium (MM), minimal medium without carbon (MM-C) or nitrogen (MM-N) sources (Table 2.3) (Talbot *et al.,* 1993). Diameter of colonies of wild-type and mutant *M. oryzae* strains were measured by performing 7 technical replicates per experiment and 3 biological replications on each media.

2.1.2. *Neurospora* strains

The wild-type *Neurospora crassa* strain *a* and isogenic deletion mutant NCU05996 strain *a* were obtained from the Fungal Genetics Stock Centre (FGSC, Kansas City, Missouri, USA). Vogels minimal medium (Table 2.4 and 2.5) was used for cultivation of *N. crassa* strains at 25ºC with a 12h light/ dark cycle and for stock-keeping at 4ºC (http://www.fgsc.net/Neurospora/NeurosporaProtocolGuide.htm). Diameter of colonies of wild-type and mutant *N. crassa* strains were measured by performing 7 technical replicates per experiment and 3 biological replications on each media.

Table 2.1. Composition of CM (1 L)

CM	
6 g	$NaNO_3$
0.52 g	KCl
0.52 g	$MgSO_4.7H_2O$
1.52 g	KH_2PO_4
10 g	Glucose
2 g	Peptone
1 g	Yeast Extract
1 g	Casamino Acids
1 mL	Trace elements (Table 2.2)
1 mL	Vitamin solution (Table 2.2)
15 g	Agar
pH 6.5 with NaOH	

Table 2.2. Composition of trace elements and vitamin solutions (100 ml)

Trace Elements		Vitamin Solution	
2.2 g	$ZnSO_4.7H_2O$	0.01 g	Biotin
1.1 g	H_3BO_3	0.01 g	Pyridoxin
0.5 g	$MnCl_2.4H_2O$	0.01 g	Thiamine
0.5 g	$FeSO_4.7H_2O$	0.01 g	Riboflavin
0.17 g	$CoCl_2.6H_2O$	0.01 g	p-aminobenzoic acid
0.16 g	$CuSO_4.2H_2O$	0.01 g	Nicotinic acid
0.15 g	$Na_2MoO_4.2H_2O$		
5 g	Na_4EDTA		
pH 6.5 with KOH			

Table 2.3. Composition of MM, MM-C and MM-N (1 L)

MM		MM-C	MM-N
6 g	$NaNO_3$		
0.52 g	KCl		
0.52 g	$MgSO_4.7H_2O$		
1.52 g	KH_2PO_4	As MM but omitting	As MM but omitting
10 g	Glucose	glucose.	$NaNO_3$.
1 mL	Thiamine 1%		
1 mL	Trace Elements		
50 µl	Biotin 0.05%		

Table 2.4. Composition of Vogels minimal Medium (1 L)

Vogels Medium	
20 mL	Vogels salts
15 g	Sucrose
15 g	Agar

Table 2.5. Composition of Vogels salts and trace element solutions

Vogels Salts (1 L)		Trace Element solution for VM (100 mL)	
150 g	Na_3 citrate	5 g	Citric acid
250 g	KH_2PO_4	5 g	$ZnSO_4.7H_2O$
100 g	NH_4NO_3	1 g	$Fe(NH_4)_2(SO_4)_2.6H_2O$
10 g	$MgSO_4.7H_2O$	0.25 g	$CuSO_4.5H_2O$
5 g	$CaCl_2.2H_2O$	0.05 g	$MnSO_4.1H_2O$
5 mL	Trace Element solution	0.05 g	H_3BO_3
5 mL	Biotin 0.05%	0.05 g	$Na_2MoO_4.2H_2O$

2.2. Pathogenicity and infection-related development assays

2.2.1. Leaf infection assays

Ten-day old cultures of *M. oryzae* grown on sterile CM agar were used for harvesting conidia in 3 mL of sterile deionised water. The resulting suspension was filtered through sterile miracloth (Calbiochem) and subjected to centrifugation at 5000 *g* (Beckman, JA-17) for 10 min at room temperature. The pellet was re-suspended in 0.2% gelatine (BDH) to a final concentration of 1 x 10^5 or 5 x 10^4 conidia mL^{-1}. This suspension was used in plant leaf infections by spray-inoculation using an artist's airbrush (Badger Airbrush, Franklin Park, Illinois, USA). Rice infections were carried out using a dwarf Indica rice (*Oryza sativa*) cultivar, CO-39, which is susceptible to rice blast (Valent *et al*., 1991). Barley (*Hordeum vulgare*) cultivar Golden Promise infections were also carried out (Balhadère and Talbot, 2001). Rice and barley plants were grown in 9 cm diameter pots (8 - 10 plants *per* pot), and inoculated at 14- and 8-days old (2-3 leaf stage), respectively. After spray-inoculation, plants were watered well and incubated in polythene bags for 48h and then grown for a further 3 days in a controlled environment room at 25°C with a 12h light/ dark cycle and 90% relative humidity, according to Valent *et al*. (1991). Lesion formation was monitored 5 days post-inoculation.

2.2.2. Root infection assays

Root infection assays were performed using sterile moist thick vermiculite as follows. The vermiculite was prepared by immersing it for 2h in distilled water and then draining it through a sieve. A 50 ml centrifuge tube (Corning) was filled with 30 cm of moist vermiculite, followed by a mycelial plug of the same diameter as the centrifuge tube, a further layer of 5 cm of moist vermiculite, and 5 seeds covered with another 5 cm layer of moist vermiculite. The tubes were sealed with parafilm to prevent loss of humidity. *M. oryzae* lesions on roots were scored after 15 days of

incubation at 22°C with a 16h light/ dark cycle. Lesions observed on roots were scored as 0 (non-pathogenic), 1 (strong symptom reduction), 2 (weak symptom reduction), or 3 (wild-type symptoms) based on colour intensity and lesion extension of disease symptoms (Tucker *et al.*, 2010).

2.2.3. Rice leaf sheath assay

Rice cultivar CO-39 plants were grown for 3- to 4- weeks and used for leaf sheath assays (Koga *et al.*, 2004; Kankanala *et al.*, 2007). Leaf sheaths from intermediate-aged leaves were cut into strips ~9 cm long. Fungal spores were harvested at a concentration of 1 x 10^5 conidia mL^{-1} in 0.2% gelatine (BDH). Inoculum was introduced into the hollow space enclosed by the sides of the leaf sheaths above the mid vein. Inoculated sheaths were incubated at 25°C with a 12 h light/ dark cycle and were supported horizontally in a closed moist chamber containing wet filter paper such that the spores settled on the mid vein regions. After 24h post-inoculation when the samples were ready for confocal microscopy, the sheaths were hand-trimmed to remove the sides and expose the epidermal layer above the mid-vein. Lower mid-vein cells were then removed to produce sections of 3 to 4 epidermal cell layers thick.

2.2.4. Penetration assay

Appressorium-mediated penetration of onion epidermal strips was assessed using a procedure based on Chida and Sisler (1987). A conidial suspension at a concentration of 1 x 10^5 conidia mL^{-1} was prepared and dropped onto the adaxial surface of epidermal layers taken from onion. The strips were incubated in a moist chamber at 25°C and penetration events scored 24h later by viewing with an Olympus IX81 inverted microscope.

2.2.5. Assays for germination and appressorium formation rates

Germination and development of appressoria was monitored over time on a borosilicate glass cover slip, using a method adapted from that of Hamer *et al*. (1988). A conidial suspension of 1 x 10^5 conidia mL^{-1} was prepared in distilled water and placed onto the surface of the cover slips. These were incubated in a moist chamber at 25°C. The percentage of conidia that had undergone germination was recorded over a 24h period.

2.3. Nucleic acid analysis

2.3.1. Fungal DNA extraction

Large-scale extraction of fungal genomic DNA

Liquid cultures of *M. oryzae* were generated by blending 5 – 10 cm^2 of mycelium into 200 mL of liquid CM in a commercial blender (Waring, Christison Scientific). The cultures were incubated for 48h at 25°C in an orbital incubator (New Brunswick Scientific) until a mat of white fungal mycelium had formed beneath the surface of the medium. The mycelium was harvested by filtration through sterile miracloth (Calbiochem) and blotted dry with paper towels (Kimberley Clark Corporation) in a class II microbiological cabinet. It was then placed in a chilled mortar and ground to a fine powder with liquid nitrogen. The powder was placed in sterile Oakridge tubes (Nalgene) containing 4 mL of CTAB buffer at 65°C (0.055 M CTAB [Hexadecyltrimethylammonium bromide] {H5882, Sigma}, 0.1 M Tris (Tris (hydroxymethyl)aminomethane, Trizma® Sigma), 0.0078 M Ethylenediaminetetraacetic acid EDTA, 0.7 M NaCl). Samples were incubated at 65°C for 20 minutes with occasional shaking. An equal volume of chloroform:pentanol (24:1) was added and the tubes shaken for 20 minutes at room temperature. Following centrifugation at 13,000 *g* for 10 minutes using a JA-17

fixed angle rotor in a Beckman J2-MC high speed centrifuge, the supernatants were transferred to new tubes containing an equal volume of chloroform:pentanol (24:1) (v/v). The suspensions were mixed rapidly and subjected to centrifugation at 13,000 *g* for a further 10 minutes. The supernatant was removed and an equal volume of isopropanol gently added to precipitate the nucleic acids. The tubes were incubated on ice for 5 minutes and the DNA recovered by centrifugation using a JS13.1 swinging bucket rotor (Beckman) at 13,000 *g* for 10 minutes. The supernatant was discarded and the tube inverted on paper towels for 15 minutes. The nucleic acid pellet was re-suspended in 500 μL of distilled water and then re-precipitated during 10 minutes of incubation at -20°C using 0.1 volumes of 3 M sodium acetate (pH 5.2) and 2 volumes of 95% (v/v) ethanol. The purified nucleic acid fraction was recovered by centrifugation for 20 minutes at 17,000 *g* (Micromax) and washed with 500 μL of 70% (v/v) ethanol. The nucleic acid pellet was dried for 20 minutes and re-suspended in 25 - 100 μL TE + 10 μg mL^{-1} RNase A. Genomic DNA samples were stored at -20°C.

Small-scale extraction of fungal genomic DNA

When screening putative fungal transformants for homologous recombination events, a smaller-scale DNA extraction protocol was followed. Agar cultures of *M. oryzae* were generated by placing a small plug of mycelium onto complete medium overlaid with a cellophane disc. The cultures were incubated at 25°C until a small mat of fungal mycelium had grown over the surface of the cellophane disc (6-8 days). The cellophane disc was then peeled from the agar plate along with the fungal mycelium, placed into a mortar and ground with a pestle to a fine powder in liquid nitrogen. The powder was placed in a 1.5 mL microcentrifuge tube containing 500 μL of CTAB buffer and incubated at 65 °C for 20 minutes with occasional shaking. An equal volume of chloroform:pentanol (24:1; ClA) (v/v) was added and

the tubes shaken vigorously for 20 minutes at room temperature. Centrifugation was carried out at 13,000 *g* for 10 minutes using a microcentrifuge (IEC, Micromax) and the supernatants were transferred to new tubes. The chloroform:pentanol (24:1) (v/v) extraction step was repeated twice, with the aqueous phase being removed to a new tube each time. The supernatant was removed and an equal volume of isopropanol added to precipitate the nucleic acids. The tubes were incubated at room temperature for 2 minutes and the DNA was recovered by centrifugation in a microcentrifuge at 13,000 *g* for 10 minutes. The nucleic acid pellet was dried and re-suspended in 200 µL of distilled water and then re-precipitated using 0.1 volumes of 3 M sodium acetate (pH 5.2) and two volumes of 100% (v/v) ethanol. The purified nucleic acid was recovered by centrifugation for 20 minutes at 17,000 *g* and washed with 200 µL of 70% (v/v) ethanol. The pellet was dried for 5 minutes in a vacuum rotary desiccator and re-suspended in 30 µL of distilled water. Genomic DNA samples were routinely stored at 4°C or at -20°C.

2.3.2. DNA manipulations

Digestion of genomic or plasmid DNA with restriction enzymes

Restriction endonucleases were routinely obtained from Promega UK Ltd. (Southampton, UK) or New England Biolabs (Hitchin, UK). DNA digestion was carried out using buffer solutions provided by the manufacturer in a total volume of 20 - 40 µl with 0.2-1 µg of DNA and 5-10 units of enzyme.

DNA gel electrophoresis

Digested DNA was fractionated by gel electrophoresis in 0.7% (w/v) – 1.0% (w/v) agarose gel matrices using a 1x Tris-borate EDTA buffer (TBE) (0.09 M Tris-borate, 0.002 M EDTA). These were visualised by the addition of ethidium bromide (final concentration 0.5 $\mu g\ mL^{-1}$). A 1kb size marker ladder (Promega) was used for determining the length of DNA fragments after fractionation using gel

electrophoresis. DNA was visualised using a gel documentation system (Image Master® VDS with a Fuji Film Thermal Imaging system FTI-500, Pharmacia Biotech).

Gel purification of DNA fragments

DNA fragments were purified from agarose gels using a commercial kit (QIAquick) according to manufacturers' instructions (Qiagen). Fragments were excised from the gel using a razor blade and placed in a pre-weighed microcentrifuge tube. The mass of agarose removed from the gel was determined and three volumes of Buffer QG (guanidine thiocyanate) added. Samples were incubated at 50°C and mixed by vortexing every 2-3 minutes until the gel slice had dissolved. One gel volume of isopropanol was added and mixed before the solution was placed in a QIAquick spin column held in a 2 mL collection tube. After centrifugation for 1 minute in centrifuge (13,000 *g*) the DNA is bound to the QIAquick column. The flow-through was discarded and the column placed back in the collection tube. To wash the column 0.75 mL of Buffer PE (ethanol-based) was added and centrifugation carried out for 1 minute (13,000 *g*). The flow-through was discarded and the column processed by centrifugation for an additional minute (13,000 *g*). The QIAquick column was placed in a clean microcentrifuge tube, 30 μL of sterile water added and after 1 minute there was a further centrifugation step for 1 minute, at 13,000 *g*. The DNA solution was removed to a fresh tube and stored at -20°C.

Southern blotting

Blotting of agarose DNA gels was performed according to Southern (1975). Each gel was submerged in 0.25 M HCl for 15 minutes to de-purinate the fractionated DNA and then denatured by immersing in 0.4 M NaOH, 0.6 M NaCl for 30 minutes. The gel was then transferred to Neutralisation buffer (1.5 M NaCl, 0.5 M Tris-HCl,

[pH 7.5]) for 30 minutes before capillary blotting onto Hybond-N (Amersham Biosciences). Gel blots were performed by placing the inverted gel onto a sheet of filter paper wick, which was supported on a perspex sheet with each end of the wick submerged in 20 x SSPE solution (3.6 M NaCl, 200 mM NaH_2PO_4, 22 mM EDTA). Hybond-N membrane was then placed onto the gel and overlaid with five layers of wet Whatman 3 mm paper and five layers of dry Whatman 3 mm paper onto which a 10 cm high pile of paper towels was placed (Kimberley Clark Corporation). Finally, a 500 g weight was placed on the stack and the blot was left to stand at room temperature overnight. The transferred DNA was cross-linked to the membrane using a BLX crosslinker (Bio-link®).

Radiolabelled DNA probe construction

DNA hybridisation probes were labelled by the random primer method (Feinberg and Vogelstein, 1983) using a Ready-To-Go kit (Amersham Biosciences) according to the manufacturer's instructions. A 25-50 ng aliquot of DNA was made to a final volume of 47 μL in water. The sample was boiled for 5 minutes to denature the DNA and then chilled on ice for 2 minutes. The tube was briefly subjected to centrifugation and its contents added to a Ready-To-Go reaction mix bead containing buffer, dATP, dGTP, dTTP, FLPC*pure*™ Klenow polymerase (7-12 units) and random oligonucleotides, primarily 9-mers. The reagents were mixed by gently pipetting and 3 μL of [α-^{32}P] dCTP (3,000 Ci/mmol) added. The labelling reaction was then incubated at 37°C for 10 minutes before being stopped by addition of 100 μl of labelling stop dye (0.1% SDS, 0.06 M EDTA, 0.5% bromophenol blue, 1.5% blue dextran). Unincorporated isotope was removed by passing the labelling reaction through a Biogel P60 (Bio-Rad) column, and collecting the dextran blue-labelled fraction. The probe was denatured by heating at 100°C for 5 minutes and quenched on ice for 2 minutes, before adding to the hybridisation mixture.

Hybridisation conditions

DNA gel blot hybridisations were performed using standard procedures (Sambrook *et al.*, 1989). Blots were incubated in hybridisation bottles (Hybaid Ltd.) in a hybridisation oven (Hybaid) for at least 4 hours at 65°C in 25-30 mL of pre-hybridisation solution 6 x SSPE (diluted from a 20x stock prepared by dissolving 175.3 g of NaCl, 27.6 g of NaH_2PO_4 and 7.4 g of EDTA in 800 mL of dH_2O, adjusting the pH to 7.4 with NaOH and making up to 1 litre with dH_2O), 5 x Denhardt's solution (diluted from a 50x stock prepared with 5 g Ficoll type 400, 5 g polyvinylpyrrolidone in 500 mL dH_20, 0.5 % SDS), with 100 μL denatured herring sperm DNA (1% [w/v] in 0.1 M NaCl) (Sigma) added. A denatured radio-labelled probe was then added and the mixture incubated overnight at 65°C.

Following hybridisation, the blot was washed at high stringency. The pre-hybridisation solution was removed along with any unbound probe and 25-30 mL of 2 x SSPE wash (0.1% SDS, 0.1% Sodium pyrophosphate [PPi], 2 x SSPE (diluted from the 20 x SSPE stock) [pH 7.4]) added. The mixture was then incubated for 30 minutes at 65°C. The wash solution was removed and replaced with 25-30 mL of 0.2 x SSPE wash (0.1% SDS, 0.1% Sodium pyrophosphate [PPi], 0.2 x SSPE, [pH 7.4]) and the blot again incubated for 30 minutes at 65°C. The 0.2 x SSPE wash was repeated and the membrane dried for 10 minutes.

Autoradiography was carried out by exposure of membranes to X-ray film (Fuji medical X-ray film, Fuji Photo Film (U.K.) Ltd.) at -80°C in the presence of an intensifying screen (Amersham). X-ray films were developed using Kodak chemicals.

2.3.3. DNA cloning procedures

Bacterial DNA mini preparations using Alkaline Lysis protocol

Small-scale preparations of plasmid DNA from bacterial colonies were made by modifying a larger scale method based on Sambrook *et al.* (1989). Single colonies were picked and used to inoculate 3 mL Luria-Bertani (LB) (10 g L^{-1} tryptone 5 g L^{-1} yeast extract, 86 mM NaCl, [pH to 7.5]) containing the appropriate antibiotic in a universal bottle. Cultures were grown overnight at 37°C, with vigorous aeration (200 rpm) in an Innova 4000 rotary incubator (New Brunswick Scientific). For long term storage of bacterial cells a fraction of the initial 3 mL culture was retained to make a glycerol stock. For this, an 800 μL aliquot of bacterial solution was added to 1.5 mL microcentrifuge tubes containing 200 μL sterile glycerol. The suspension was vortexed rapidly and stored at -80°C. The remainder of the culture was transferred to another 1.5 mL microcentrifuge tube and pelleted by centrifugation at 1,300 *g* (Micromax) for 1 minute. The supernatant was removed and the bacterial pellet re-suspended in 200 μL of ice-cold cell re-suspension solution (50 mM glucose, 25 mM Tris-HCl [pH 8.0], 10 mM EDTA [pH 8.0]) by vigorous vortexing using a Whirlimixer (Fisher Scientific). A 400 μL aliquot of freshly prepared lysis solution (0.2 M NaOH [freshly diluted from a 10 M stock], 1% SDS) was added to the cell suspension. The contents of the tube were mixed by inversion, ensuring that the entire surface of the tube came in contact with the solution. The tube was placed on ice for 5 minutes and then 300 μL of ice-cold neutralisation solution (3 M potassium acetate, 11.5 % (v/v) glacial acetic acid) was added and the contents mixed by inverting rapidly 5 times. The tube was stored on ice for 10 minutes, and processed by centrifugation at 13,000 *g* for 5 minutes in a microcentrifuge. The supernatant was transferred to a fresh tube and precipitated using an equal volume of isopropanol at room temperature. Centrifugation at 17,000 *g* for 15 minutes was performed in a

microcentrifuge and the resulting supernatant was removed and discarded. The pelleted nucleic acids were washed with 1 mL of 70% (v/v) ethanol and centrifugation carried out at 17,000 *g* for 5 minutes in a microcentrifuge. The supernatant was discarded and the pellet dried for 5 minutes in a vacuum rotary desiccator (microcentrifuge rotary concentrator 5301, Invitrogen). The pellet was re-suspended in 50 µL of sterile water containing DNase-free pancreatic RNase (20 µg mL^{-1}), vortexed briefly and incubated at 37ºC for 20 minutes. The preparations were stored at -20ºC.

Midi-plasmid DNA preparations

Midi-plasmid DNA preparations of high quality were prepared using a commercially available kit (Promega Wizard® *Plus* SV Mini-Prep DNA purification system Cat.#A1330), according to manufacturers' instructions. Bacterial cells were recovered by centrifugation at 10,000 *g*, re-suspended in 250 µL of cell resuspension solution (50 mM Tris [pH 7.5], 10 mM EDTA, 100 µg mL^{-1} RNase A) and transferred to a microcentrifuge tube. A 250 µL aliquot of cell lysis solution (0.2 M NaOH, 1% SDS) was then added and the contents mixed by gently inverting the tube four times. A 10 µL aliquot of alkaline protease solution was added and the tube inverted four times. After a 5 minute incubation at room temperature a 350 µL aliquot of neutralisation solution (4.1 M guanidine hydrochloride, 0.8 M potassium acetate, 2.1 M glacial acetic acid [final pH 4.2]) was added and the tube contents mixed by inversion. The samples were processed by centrifugation at 14,000 *g* in a microcentrifuge for 10 minutes. Meanwhile a spin column was inserted into its collection tube and the cleared lysate decanted into the column. This was processed by centrifugation at 14,000 *g* for 1 minute, the flow-through discarded and 750 µL wash solution (60 mM potassium acetate, 8.3 mM Tris-HCl [pH 7.5], 0.04 mM EDTA, 60% ethanol) added. The centrifugation step was repeated and the column washed again with a further 250 µL of column wash before centrifugation of

the empty column at 14,000 g for 2 minutes. The spin column was transferred to a sterile microcentrifuge tube and 100 µL of nuclease-free water added to the column followed by centrifugation at 14,000 *g* for 1 minute to elute the DNA which was then stored at -20°C.

DNA ligation and selection of recombinant clones

For routine cloning into standard vectors (pSC-A® [StrataClone] and the pGEM® series [Promega]) recombinant clones were selected using α-complementation of *lacZ* (Sambrook *et al*., 1989). To prevent re-circularisation of plasmid DNA vector when cut with a single restriction enzyme, treatment with Antarctic Phosphatase (NEB) was carried out. Vector (1 µg) is dephosphorylated in a reaction with 1 µl of Antarctic Phosphatase enzyme, 1 µl 10x Antarctic Phosphatase reaction buffer (50 mM Bis-Tris-propane-HCl, 1 mM $MgCl_2$, 0.1 mM $ZnCl_2$, pH 6.0) and nuclease-free water to give a total volume of 10 µl. This mix was incubated at 37 °C for 1h. Heat inactivation of the phosphatase enzyme was carried out at 65ºC for 30 minutes. The digested DNA was then gel purified and ligation reactions prepared. Routinely, vector and insert DNA were added to the ligation mixture at a 1:3 molar ratio and the reactions carried out in a total volume of 10 µL using the manufacturer's ligase buffer and 1 unit of T_4 DNA ligase (Promega). Ligation reactions were incubated overnight at 4°C for blunt ended ligations and for cohesive-ended ligation reactions. Directional cloning was carried out as detailed above.

DNA fragments amplified by the polymerase chain reaction (PCR) were routinely cloned by gel purification of the amplicons and ligated into pSC-A® or pGEM® series vectors, which allow T:A cloning of PCR fragments generated by certain thermostable DNA polymerases such as *Taq* polymerase (Mead *et al*., 1991). Ligation reactions were performed at 4ºC (Sambrook *et al*., 1989). DNA fragments amplified by polymerases not compatible with T:A cloning were heated to 70ºC for

30 minutes in the presence of 0.2 mM dATPs, 5 U *Taq* polymerase, 10 x *Taq* polymerase buffer and 2.5 mM $MgCl_2$ in a total volume of 10 μL before cloning in order to create a poly-A tail to facilitate cloning into the desired vector.

Preparation of competent cells

Stocks of laboratory-prepared transformation-competent cells were generated using a protocol adapted from Sambrook *et al.* (1989). Single bacterial colonies were obtained by streaking bacterial cells across a plate of LB containing the appropriate antibiotic and incubating at 37°C for 16 hours. A single colony was used to generate an overnight culture in 10 mL LB broth (37°C, 200 rpm). A 2.5 mL aliquot of this culture was inoculated into 250 mL of SOC (20 g L^{-1} tryptone, 5 g L^{-1} yeast extract, 8.6 mM NaCl, 10 mM $MgSO_4$, 10 mM $MgCl_2$) and this was allowed to grow until an OD_{600}= 0.6 had been reached (Sambrook *et al*., 1989). The culture was then transferred to a 50 mL Oakridge tube and incubated on ice for 10 minutes. Cells were recovered by centrifugation at 2,500 *g* (Beckman J2-MC, JS13.1 rotor) for 10 minutes (4°C). To each tube, 15 mL filter-sterilised FSB (10 mM potassium acetate [pH 7.5], 45 mM $MnCl_2{\cdot}4H_2O$, 10 mM $CaCl_2{\cdot}2H_2O$, 100 mM KCl, 3 mM hexamine-cobalt chloride, 10% glycerol [pH 6.4]) was added and the cells re-suspended by gentle pipetting. Samples were incubated on ice for 10 minutes and the centrifugation step repeated once. The cells were then re-suspended in 4 mL FSB and DMSO (dimethyl sulfoxide, Sigma) was added to a final concentration of 3.4% (v/v). The mixture was incubated on ice for 15 minutes. A further volume of DMSO was added such that the final concentration was 6.5% DMSO (v/v). The cells were then dispensed into 100 μl aliquots in pre-chilled microfuge tubes. Samples were immediately frozen by immersion in liquid nitrogen and stored at -80°C.

Transformation of competent bacterial hosts

Transformation was routinely carried out using *Escherichia coli* strain XL1 Blue (Stratagene). XL1 – Blue has a genotype *sup*E44 *hsd*R17 *rec*A1 *end*A1 *gyr*A46 *thi rel*A1 *lac*$^-$ [F′ *pro* AB$^+$ *lac*I^q *lac*ZΔM15 *Tn*10 (*tet* ^{r})]. A tube with 100 μl aliquot of competent cells was then incubated on ice for 10 minutes before 0.1-50 ng DNA was added and the mixture incubated on ice for a further 30 minutes. Cells were heat-shocked at 42°C for 45 seconds and then transferred to ice for 2 minutes. At this point, 500 μL of SOC was added to each tube and the recovering cells were incubated at 37°C for 1 hour with gentle shaking (150 rpm). Aliquots were plated on LB agar with the appropriate antibiotic. Where α-complementation selection was available (Sambrook *et al.,* 1989) the agar contained isopropyl-thiogalactoside (IPTG, 0.8 mg mL^{-1} per plate) (Calbiochem) and 5-bromo-4-chloro-3-indolyl-β-D-galactopyranoside (X-gal, 0.8 mg mL^{-1} per plate) (Calbiochem). Plates were inverted and incubated at 37^{o}C overnight.

2.3.4. DNA sequencing

Single colonies were pick up and plasmid DNA analysed by digestion with restriction enzymes. The constructs with the correct restriction profile were sequenced (Eurofins MWG Operon).

2.4. Fungal transformation

2.4.1. Generation of protoplasts

Half of a plate of *M. oryzae* mycelium was removed from a sterile culture on CM agar, blended in 200 mL sterile liquid CM and incubated at 26°C with shaking at 125 rpm in an orbital incubator for 48h in the dark. The mycelium was harvested by filtration through sterile miracloth (Calbiochem) and washed in sterile distilled water.

The mycelium was transferred to a Falcon tube (Corning) with 40 mL OM buffer (1.2M $MgSO_4$, 10mM Na-PO_4 pH 5.8) and 5% glucanex (Novo Industries, Copenhagen), and shaken gently at 75 rpm for 2-3 hours at 30°C in an orbital incubator. The resulting protoplasts were transferred to sterile polycarbonate Oakridge tubes (Nalgene) and overlaid with an equal volume of cold ST buffer (0.6M sucrose, 0.1M Tris-HCl pH 7). Protoplasts were recovered by centrifugation at 1,400 *g* and 4°C in a swinging bucket rotor (Beckman JS-13.1) in a Beckman J2.MC centrifuge. The protoplasts were recovered at the OM/ ST interface and transferred to new sterile Oakridge tube which was then filled with cold STC buffer (1.2M sucrose, 10 mM Tris-HCl pH 7.5, 10 mM $CaCl_2$). Protoplasts were pelleted at 1,400 *g* for 10 min at 4°C (Beckman JS-13.1 rotor), washed three or four times more with 10 mL STC, with complete re-suspension each time. After re-suspending in 1 mL of STC, the concentration of protoplasts was then determined by counting using a haemocytometer.

2.4.2. Transformation using hygromicin B as a selectable marker

DNA-mediated transformation was undertaken in 1.5 mL microcentrifuge tubes by combining an aliquot of purified protoplasts (10^7 mL^{-1}) with DNA (4-7 μg) in a total volume of 150 μl. The mixture was incubated at room temperature for 15-25 minutes and 1 ml of PTC (60% PEG 400, 10 mM Tris-HCl pH 7.5, 10 mM $CaCl_2$) added. Gentle mixing was performed after each addition of PTC. The mixture was incubated at room temperature for 15-20 minutes then added to 150 mL molten (45°C) OCM 1.5% agar (osmotically stabilised CM with 0.8M sucrose), mixed gently and poured into 5-6 sterile Petri dishes. For selection of transformants on hygromycin B (Calbiochem), plate cultures were incubated in the dark for at least 16 hours at 26°C and then overlaid with approximately 15 mL CM 1% agar containing

200 μg mL^{-1} hygromycin B freshly added to the medium from a stock solution of 50 mg mL^{-1}.

2.4.3. Transformation using sulfonylurea as a selectable marker

DNA-mediated transformation was undertaken in 1.5 mL microcentrifuge tubes by combining an aliquot of purified protoplasts (10^7 mL^{-1}) with DNA (4-7 μg) in a total volume of 150 μl. The mixture was incubated at room temperature for 15-25 minutes and 1 ml of PTC (60% PEG 400, 10 mM Tris-HCl pH 7.5, 10mM $CaCl_2$) added. Gentle mixing was performed after each addition of PTC. The mixture was incubated at room temperature for 15-20 minutes then added to 150 mL molten (45°C) 1.5% agar/BDCM Bottom (Table 2.6), mixed gently and poured into 5-6 sterile Petri dishes. For selection of transformants on sulfonylurea (Chlorimuron ethyl, Applichem Cat.#A7399), plate cultures were incubated in the dark for at least 16 hours at 26°C and then overlaid with approximately 15 mL BDCM Top 1% agar (Table 2.7) containing 300 μg mL^{-1} sulfonylurea freshly added to the medium from a stock solution of 100 mg mL^{-1}.

2.4.4. Generation of T-DNA insertional library by *Agrobacterium tumefaciens*-mediated transformation

Agrobacterium tumefaciens-mediated transformation was performed as previously described (Rho *et al.*, 2001), using the binary vector pKHt (Mullins *et al.*, 2001). The pKHt plasmid contains an autonomous origin of replication from *E. coli* and the chloramphenicol resistance gene within the T-DNA cassette to facilitate recovery of flanking DNA. T-DNA transformants were evaluated for leaf and root infection (Tucker *et al.*, 2010). Plant infection experiments with *M. oryzae* T-DNA transformants showing reduced virulence were performed 3 times.

Table 2.6. Composition of BDCM Bottom medium (1 L)

	BDCM Bottom
1.7 g	Yeast N base without amino acids and ammonium sulphate
2 g	Ammonium nitrate
1 g	Asparagine
273.84 g	Sucrose
10 g	Glucose
15 g	Agar
pH 6.0 with Na_2HPO_4	

Table 2.7. Composition of BDCM Top medium (1 L)

	BDCM Top
1.7 g	Yeast N base without amino acids and ammonium sulphate
2 g	Ammonium nitrate
1 g	Asparagine
10 g	Glucose
10 g	Agar
pH 6.0 with Na_2HPO_4	

2.5. Microscopy

2.5.1. Confocal microscopy

Images of conidial germination, appressorium development and rice leaf sheath assay were recorded using a Zeiss LSM510 Meta confocal laser scanning microscope system. Slides were prepared for processing by sealing cover slip preparations to a slide with petroleum jelly (Vaseline, Unilever). Argon (488nm) and helium-neon (543 nm) lasers were used to excite fluorochromes and all images were recorded under the x 63 oil objective. Offline image analysis was performed using the LSM image browser (Zeiss). At least three independent transformants were investigated for all experiments.

2.5.2. Olympus IX81-performed microscopy

Images of conidial germination, appressorium development and penetration assay on epidermal onion cells were recorded using an Olympus IX81 inverted microscope system. Slides were prepared for processing by sealing cover slip preparations to a slide with petroleum jelly (Vaseline, Unilever). Argon (488 nm) laser was used to excite GFP. All images were recorded under the x 60 or x 100 oil objectives. Offline image analysis was performed using the MetaMorph 7.5 (Molecular Devices). At least three independent transformants were investigated for all experiments.

2.5.3. Zeiss Axioskop 2-performed microscopy

Counting of conidial germination and appressorium formation were carried out using a Zeiss Axioskop 2 microscope. Images of conidial germination and appressorium development requiring light microscopy were recorded on this microscope. At least three independent biological repeats were made for all experiments.

CHAPTER 3

Identification of pathogenicity-defective mutants of *M. oryzae* by screening a T-DNA insertional mutant library

3.1. Introduction

The genomic sequences of *M. oryzae* (Dean *et al.*, 2005) and rice (Goff *et al.*, 2002; Yu *et al.*, 2002) provide a unique opportunity to study the function of individual genes during this host-pathogen interaction. Targeted gene disruption occurs at a low frequency in *M. oryzae* (Villalba *et al.*, 2008) and may lead to non-phenotypic alterations. An alternative approach to discover key genes for rice blast disease development is to perform a high throughput gene functional analysis in *M. oryzae* by screening random insertional mutagenesis libraries (Betts *et al.*, 2007; Jeon *et al.*, 2007). Several pathogenicity genes, such as *PDE1*, *RGS1*, *DES1*, *COS1* and *RIC8,* have been identified by using this method (Balhadère *et al.*, 1999; Liu *et al.*, 2007; Chi *et al.*, 2009; Zhou *et al*., 2009; Li *et al.*, 2010). Recently, Jeon and colleagues (2007) generated a set of 20,000 mutants of *M. oryzae* by T-DNA tagging via *Agrobacterium tumefaciens*-mediated transformation (ATMT). The T-DNA insertions covered 61% of the genome and led to the identification of ~200 novel genes required for rice blast disease. Genome wide analyses of fungal pathogenicity are important to unravel the functions of the ~112,841 genes that constitute the *M. oryzae* genome (Dean *et al.*, 2005).

In order to identify additional genes important for the ability of the fungus to cause disease, a total of 300 *M. oryzae* T-DNA transformants were selected from ATMT library based on defects of pathogenicity. Through this approach, any gene of interest can be recovered because they are each tagged by a T-DNA insertion. In this Chapter, I describe the identification and characterisation of one mutant, M1422, defective for root and leaf pathogenicity and vegetative growth. Within the M1422 mutant genome, the T-DNA fragment was found to disrupt the MGG_01285 gene. This gene encodes a putative transcription factor that belongs to a $Zn(II)_2Cys_6$

binuclear cluster family and it is termed *Transcription factor for Polarity Control1* (*TPC1*) throughout this study.

This Chapter also describes the construction of a gene replacement vector tagged with GFP, Tpc1:GFP, in order to complement the M1422 mutant and confirm that *TPC1* is the disrupted gene. The green fluorescent protein (GFP) is found naturally in the jellyfish *Aequorea victoria* (Prasher *et al*., 1992). Its main function is to act as an energy transfer acceptor in bioluminescence, fluorescing after receiving energy from either a luciferase-oxyluciferin-excited complex or by a Ca^{2+} activated phosphoprotein (Ward and Bokman, 1982; Prasher *et al*., 1992). The GFP gene has been cloned (Prasher *et al*., 1992) and subsequently expressed in many different cell types (Chalfie, 1995). The GFP protein is 238 amino acids in length with its biggest absorbance peak at 395 nm and a smaller peak at 475 nm. Excitation of the protein at 395 nm yields an emission maximum at 508 nm (Cubitt *et al*., 1995). To visualise GFP fluorescence, all that is needed is ultra-violet (UV) or blue light. GFP is extremely stable *in vivo* and has been fused to the C- or N- terminus of many cellular and extracellular proteins without a loss of activity, thereby permitting the tagging of proteins for gene regulation analysis, protein localisation, or specific organelle labelling (Reiser *et al*., 1999; Bruno *et al*., 2004). Various mutations have been used to make GFP a more sensitive and versatile tool for molecular and cell biology (Heim *et al*., 1995; Shaner *et al*., 2005). Modifications have, for instance, made the protein easier to detect and have reduced the gradual photobleaching effect of exposure to UV light (reviewed in Shaner *et al*., 2005). One such mutation, S65T, made the GFP lose the 395 nm absorption peak, shifting the remaining absorption peak to 490 nm and resulting in a six-fold increase in brightness and a reduced rate of photobleaching (Heim *et al*., 1995). It is this mutant allele, known as sGFP, which has been most successfully expressed in fungal backgrounds (Spellig *et al*., 1996; Rohel *et al*., 2001; Bruno *et al*., 2004) and is used in this study.

3.2. Materials and Methods

3.2.1. T-DNA localisation within the mutant fungal genome

Fungal genomic DNA was extracted, as previously described in Chapter 2, and digested with *Eco*RI and *Pst*I restriction enzymes in two independent reactions (Fig. 3.1). A ligation reaction using T4 DNA ligase (New England Biolabs) was performed, following purification using desalting agarose. The purified reaction mixture was used to transform *E. coli* DH10β cells (Invitrogen). For sequencing reactions, AT-RB and AT-LB2 primers were used to amplify the DNA sequence flanking the T-DNA on the right and left borders, respectively.

3.2.2. Construction of Tpc1:GFP complementation vector

Primers were designed in order to amplify the *TPC1* (MGG_01285) promoter region and ORF from genomic DNA of *M. oryzae* Guy11 (Fig. 3.2A). The TPC1_GFP_F forward primer was designed approximately 1.3 kb upstream from the *MoTPC*1 start codon to include a substantial component of the promoter sequence. The TPC1_GFP_R reverse primer spanned the stop codon and contained a complementary region to the GFP sequence. GFP primers were designed to amplify the 1.4 kb sGFP:*TrpC* construct cloned in pGEMT. Both fragments were joined together by fusion nested PCR (Fig. 3.2B). The amplicons were cloned into pGEMT-easy digested with *Eco*RI. The 4.3 kb Tpc1:GFP fragment was gel purified and cloned into pCB1532 that had previously been digested with *Eco*RI. The pCB1532 vector contains the 2.8 kb *ILV1* gene, which encodes the acetolactate synthase-encoding allele bestowing resistance to sulfonylurea (Sweigard *et al.*, 1997). The resulting plasmid pCB1532-Tpc1:GFP was used to transform protoplasts of M1422 mutant.

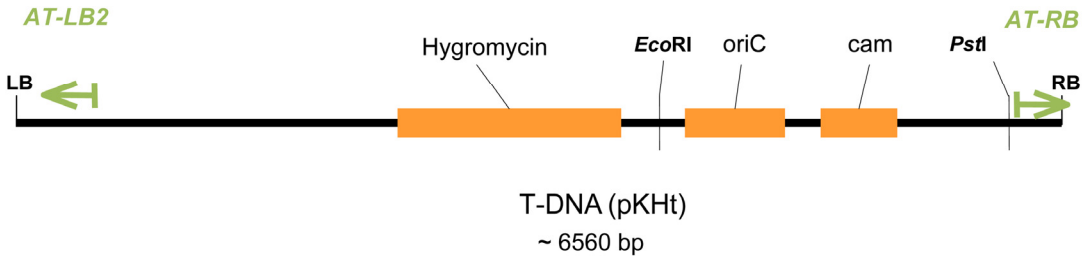

Figure 3.1. Schematic diagram showing the T-DNA fragment contained in the pKHt vector, which was used to generate the *M. oryzae* insertional library.

T-DNA *M. oryzae* transformants are hygromycin resistant. To identify the localisation of the T-DNA within the fungal genome, genomic DNA was digested with *Eco*RI and *Pst*I restriction enzymes in two independent reactions. Ligated products are transformed into *E. coli*. The T-DNA fragment has an autonomous origin of replication from *E. coli* (oriC) and the chloramphenicol (cam) resistance gene to facilitate recovery of flanking DNA. For sequencing reactions, AT-LB2 and AT-RB primers were used to identify the site of T-DNA insertion within *M. oryzae* genome.

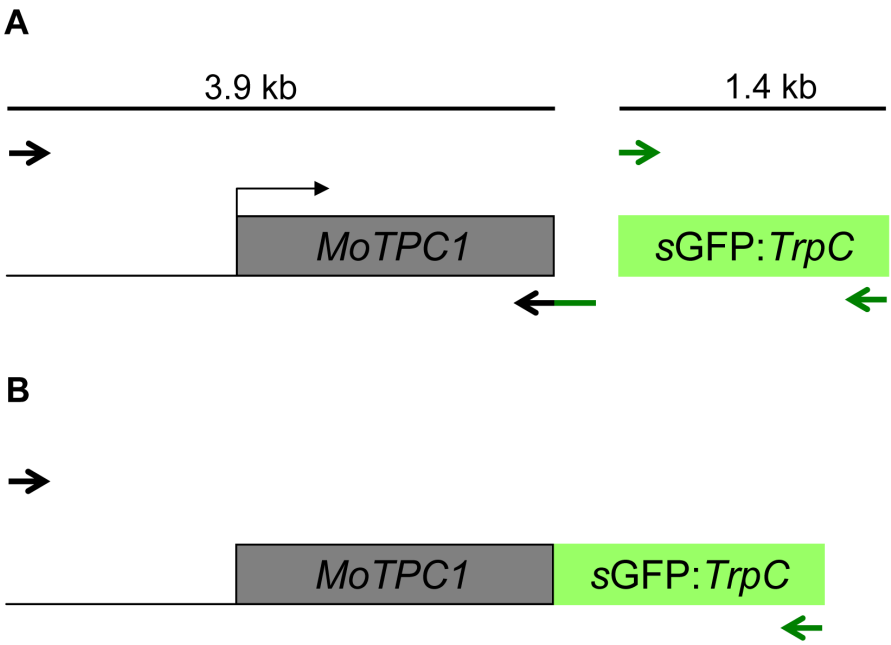

Figure 3.2. Strategy for construction of the Tpc1:GFP translational protein fusion.
(A) Primers were designed to amplify *TPC1* promoter region and ORF and *s*GFP:*TrpC* fragments. Note that the 5' end of *TPC1* reverse primer spans the *TPC1* stop codon and is complementary to the beginning of GFP sequence. **(B)** In a second round of PCR, the two fragments were fused together by overlapping the GFP region. The 4.3 kb final PCR product was gel purified and cloned into pGEMT-easy and then into the pCB1532 fungal transformation vector (Sweigard *et al.*, 1997).

3.3. Results

3.3.1. Identification of M1422, a T-DNA *M. oryzae* mutant with defects in pathogenicity and vegetative growth

A T-DNA insertion mutant, M1422, showing reduced virulence on roots and leaves was identified from the previously described *M. oryzae* ATMT mutant library (Tucker *et al.*, 2010). This mutant developed very restricted or no disease lesions on roots of rice cultivar CO-39 (Fig. 3.3). Most of the symptoms were scored as 0 (no lesions; 54%), and as 1 or 2 (very light-coloured lesions and constrained to the infection site; 23% for each score group). On the other hand, the wild-type strain Guy11 produced extensive dark lesions on roots of rice (score 3; 93%), not observed on roots infected with M1422 mutant (Fig. 3.3). Rice CO-39 leaves were also inoculated with a conidial suspension of Guy11 and M1422 (Fig. 3.4). After 5 days post-inoculation, leaves infected with Guy11 possessed a numerous number of rice blast lesions, characterised by a grey necrotic circle and pale yellowish chlorotic margins, indicating the advancing fungal infection (Fig. 3.4). However, M1422 mutant produced restricted resistant-type lesions (Talbot, 1995) and in a small number (Fig.3.4). The mean density of disease lesions on leaves inoculated with the wild-type *M. oryzae* strain Guy11 was 30.1 ± 4.1 lesions *per* 5 cm leaf tip compared with 5.3 ± 1.8 in seedlings inoculated with the M1422 mutant ($p < 0.01$). Similar results were observed on leaves of barley cultivar Golden Promise infected with M1422 mutant (Fig. 3.4).

The M1422 T-DNA mutant was also significantly defective in colonial morphology and vegetative growth (Fig 3.5A). Colonies of this mutant were compact and reduced in size (at 10 dpi, 2.80 ± 0.14 cm), compared with wild-type Guy11 (6.76 ± 0.13 cm) ($p < 0.01$). Strikingly, the M1422 colony grew in a convoluted mycelial form without invasion of the agar, compared with the normal flat more or less two-

dimensional growth of Guy11 (Fig. 3.5A). These phenotypes suggest that the T-DNA insertion in the M1422 mutant affects pathogenicity and mycelial growth of the fungus.

3.3.2. Localisation of T-DNA insertion within M1422 genome

The presence of a single hybridising restriction fragment of ~9 kb from *Mfe*I-digested M1422 genomic DNA and Southern blot hybridisation with hygromicin phosphotransferase gene cassette (Fig. 3.1) suggested that the M1422 mutant had a single insertion of T-DNA in its genome as shown in Fig. 3.6. The insertion locus was identified by sequencing the ligation products derived from M1422 *Eco*RI- and *Pst*I-digested DNA with T-DNA border primers, as described in a previous study (Tucker *et al.*, 2010). Sequences from the AT-LB2 and AT-RB primers revealed that the T-DNA was inserted 0.9 kb after the start codon of the MGG_01285 gene locus (Fig. 3.6). We named this gene *TPC1* for *Transcription factor for Polarity Control1*. The predicted coding region for *TPC1* is ~2.6 kb long, encoding 840 amino acids, and one intron on the C-terminus of the ORF. The *TPC1* amino acid sequence has also a putative nuclear localisation signal (NLS), $Zn(II)_2Cys_6$ binuclear cluster DNA binding domain, MAPK docking site, two putative phosphorylation sites (Thr residues at position 168 and 349) and a putative sumoylation site within the NLS. Neighbouring genes in the *M. oryzae* genome are located ~2.5 kb and 2.6 kb upstream and downstream of *TPC1*, respectively.

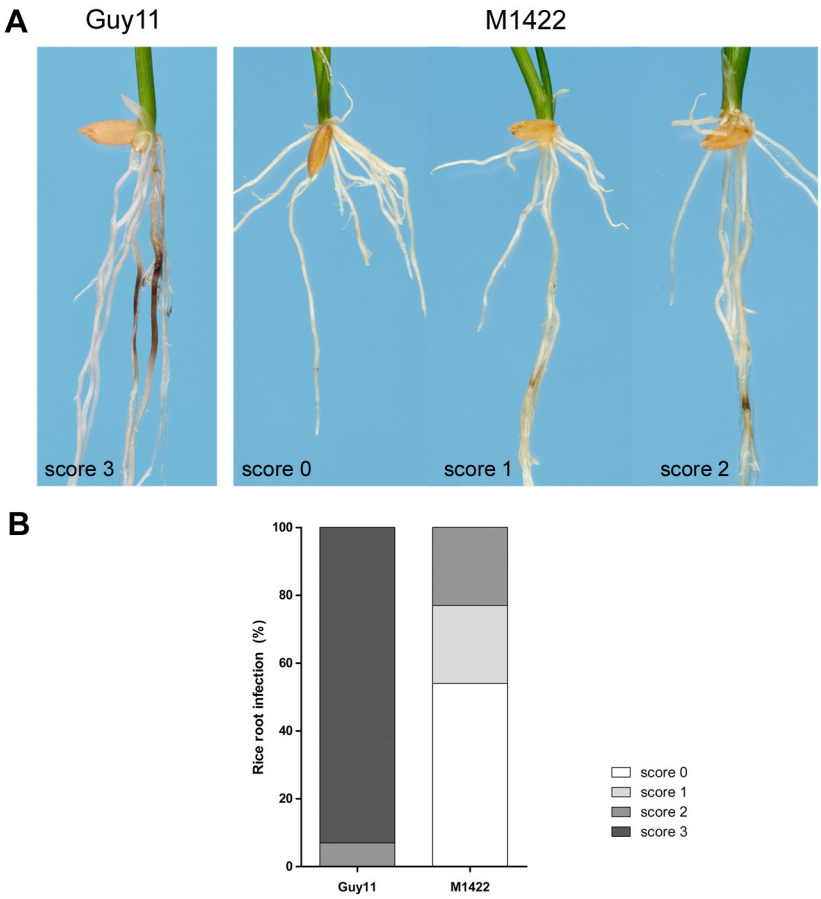

Figure 3.3. The M1422 mutant is pathogenicity-defective on rice CO39 roots.

(A) Root infection assays were performed as described by Tucker *et al.*, 2010. Photographs were taken 15 days after inoculation. **(B)** *M. oryzae* lesions on roots were scored on a scale 0 – 3, based on colour intensity and extension of the disease lesion (Tucker *et al.*, 2010) and compared with the wild-type strain Guy11 after 15 days of inoculation at 25ºC and 16h light/ 8h dark photoperiod.

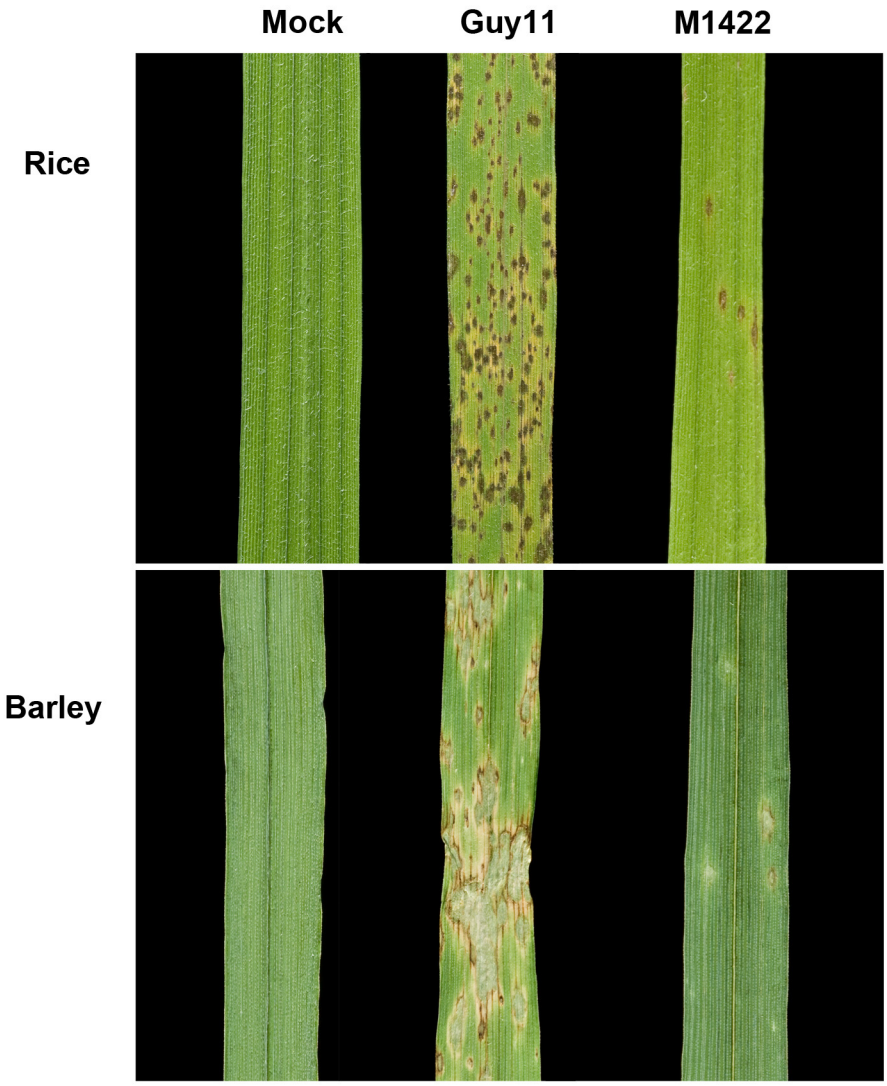

Figure 3.4. The M1422 mutant is a T-DNA *M. oryzae* transformant with defects in leaf pathogenicity.

Seedlings of rice cultivar CO-39 and barley cultivar Golden Promise were inoculated 0.20% gelatine (mock) and with *M. oryzae* conidial suspensions of identical concentration (10^5 conidia ml^{-1}) of Guy11 and M1422 mutant. Seedlings were incubated for 5 days for development of blast disease at 25ºC and 90% humidity.

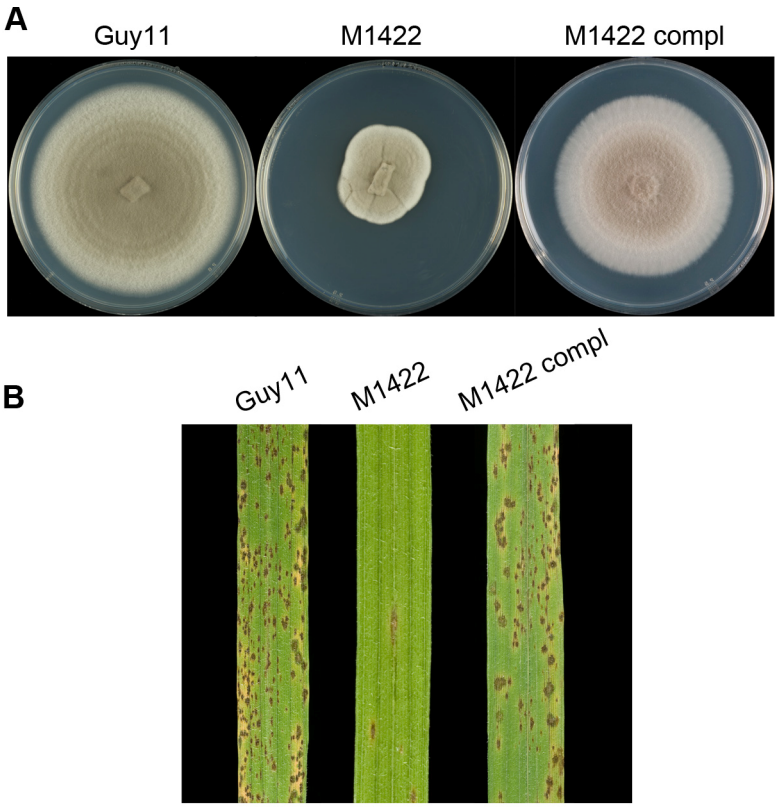

Figure 3.5. Restoration of wild-type growth and virulence phenotypes by re-introduction of Tpc1:GFP into M1422.

(A) Colonies of the wild-type strain Guy11, T-DNA insertional mutant M1422 and M1422 complemented with Tpc1:GFP (M1422 compl). Photographs were taken after incubating on CM at 25°C for 10 days. **(B)** Rice cultivar CO-39 leaves infected with a conidial suspension (10^5 conidia ml^{-1}) of Guy11, M1422 and M1422 complemented with Tpc1:GFP. Plants were incubated at 25ºC and 90% humidity. Photographs were taken 5 days after inoculation.

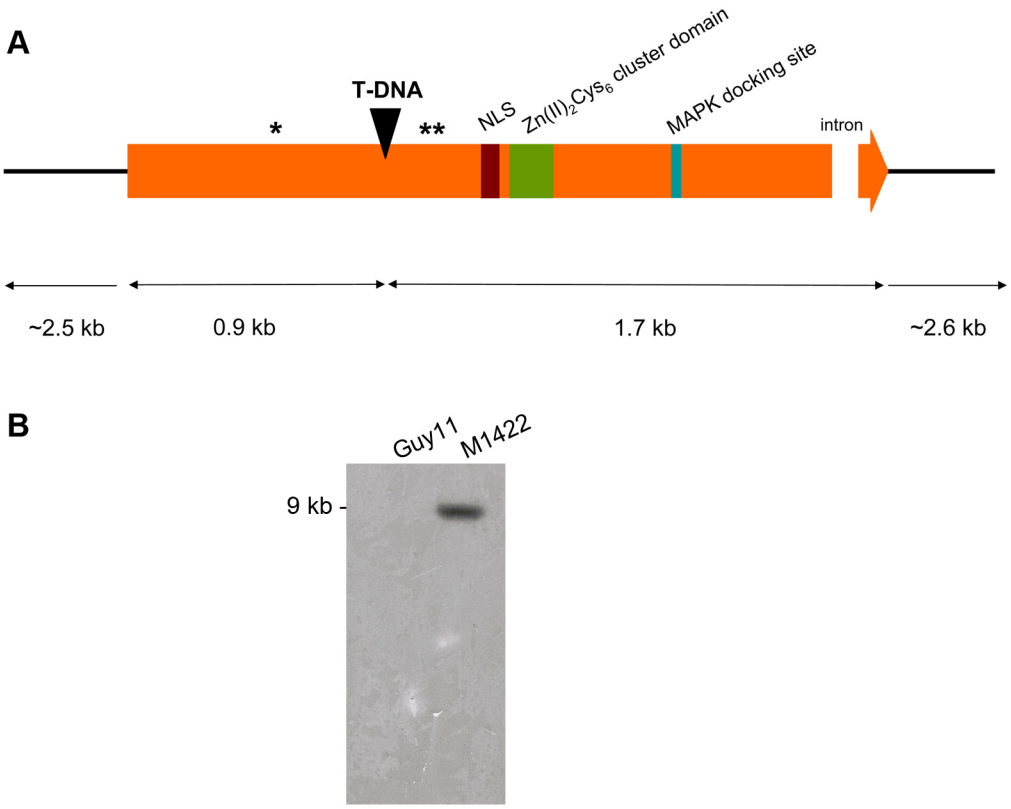

Figure 3.6. T-DNA was integrated in the coding region of *TPC1* gene within the M1422 mutant genome.

(A) The T-DNA was positioned 0.9 kb after the start codon of MGG_01285 gene. This gene was termed *TPC1* (*Transcription factor for Polarity Control1*). *TPC1* has a putative nuclear localisation signal (NLS) (brown box), $Zn(II)_2Cys_6$ binuclear cluster DNA binding domain (green box), MAPK docking site (blue box) and two phosphorylation sites (Thr residues at position 168 and 349 are indicated by one and two asterisks, respectively). **(B)** Southern hybridization to show single copy of T-DNA inserted in the M1422 genome. Total genomic DNA was digested with *Mfe*I and probed with hygromycin phosphotransferase gene cassette.

3.3.3. Complementation of M1422 mutant with *Mo*Tpc1:GFP

To confirm the single copy insertion and a correlation between the T-DNA insertion and M1422 mutant phenotypes, complementation of the mutant with the *TPC1* promoter region and coding region tagged with GFP (Tpc1:GFP) was made (Fig. 3.2). The complementation mutant was able to recover the wild-type rate of mycelial growth (at 10 dpi, 6.64 ± 0.55 cm), colonial morphology and full virulence on rice CO-39 leaves as shown in Fig. 3.5. The mean density of disease lesions on leaves inoculated with the wild-type *M. oryzae* strain Guy11 and the complementation mutant was 31.2 ± 4.6 and 28.8 ± 5.0 lesions *per* 5 cm leaf, respectively. This result is consistent with the T-DNA disrupting the *TPC1* gene within the M1422 genome and producing the associated defects in pathogenicity and vegetative growth.

3.4. Discussion

In this chapter, I have described a novel pathogenicity gene of *M. oryzae* that was named *TPC1* (*Transcription factor for Polarity Control*1), which plays an important role in vegetative fungal growth and in fungal colonisation *in planta*. *TPC1* was identified as a pathogenicity-defective mutant (M1422) generated by random insertional T-DNA mutagenesis of *M. oryzae* (Tucker *et al.*, 2010). Colonies of the M1422 T-DNA mutant were very compact, convoluted and reduced in size. This phenotype appeared to be due to a different hyphal branching pattern occurring in the mycelium of the mutant, rather than a slower vegetative growth rate. The mutant was also severely reduced in virulence on different plant tissues (root and leaf) and different host species (barley and rice). The mutant was still able to produce a small number of restricted disease lesions, characteristic of a resistant interaction between *M. oryzae* and rice (Bent and Mackey, 2007). The M1422 *M. oryzae* mutant was, however, able to penetrate the host plant. The most direct evidence of a role for *TPC1* in colony morphology and virulence was obtained by restoration of the wild-type phenotype upon re-transformation of the M1422 mutant with a functional copy of *TPC1.*

This putative transcription factor belongs to the strictly fungal $Zn(II)_2Cys_6$ cluster family (MacPherson *et al.*, 2006). Other features are the presence of a putative NLS, MAPK docking site, phosphorylation and sumoylation sites. Therefore, Tpc1 may be involved in many roles, including mediating protein-protein interactions, chromatin-remodelling, and regulating gene expression (Laity *et al.*, 2001). Tpc1 transcriptional activity may be controlled by a multitude of strategies such as nuclear-cytoplasmic shuffling, DNA binding and phosphorylation (Struhl, 1995; Sellick and Reece, 2005).

Other studies in fungi showing similar phenotypes on vegetative growth and pathogenesis have shown a misregulation of the polarisation process in apical-growing structures. Deletion of small GTPase *RAC* or the p21-activated kinase *CLA4* in *Claviceps purpurea*, for example, led to the formation of compact colonies, loss of polarity, sporulation and ability to colonise the plant host (Rolke and Tudzynski, 2008). Deletion mutants of the *CLA4* homologue, *CHM1* in *M. oryzae* displayed similar phenotypes such as reduced growth and conidiation, appressorium formation- and pathogenicity- defective (Li *et al.*, 2004). In *Aspergillus niger*, mutants in which the small GTPase *SRGA* was deleted, a homologue *S. cerevisiae SEC4*, were characterised by compact colonial morphology, reduced sporulation and defects in polarity (Punt *et al.*, 2001). Loss of Rrm4, a RNA-binding protein, in *Ustilago maydis* similarly resulted in reduced disease symptoms on maize (Becht *et al.*, 2005), polarity defects in filaments and colonies of reduced size (Becht *et al.*, 2006). When considered together, cell polarisation is a crucial process during a host-pathogen interaction and pivotal in the establishment of disease.

In order to dissect the function of this transcription factor, other defects such as conidiogenesis, conidial morphology, appressorium formation and a potential connexion with polarity were addressed and the results are described in the following chapters.

CHAPTER 4

Functional characterisation of *MoTPC1* gene

4.1. Introduction

The pathogenicity-defective M1422 mutant identified from screening the ATMT library has a single T-DNA insertion, disrupting the *TPC1* (MGG_01285) gene (see Chapter 3). *TPC1* encodes a putative transcription factor that belongs to the fungal $Zn(II)_2Cys_6$ binuclear cluster family. This mutant presents other phenotypes such as compact colonial growth that correlate with a loss of polarity (Punt *et al.*, 2001; Li *et al.*, 2004; Becht *et al.*, 2006; Rolke and Tudzynski, 2008). Polarity is a universal attribute of life and organisms can exhibit functional polarisation at a molecular, cell and structure level (Macara and Mili, 2008). The molecular and genetic control of cell polarity is understood best in the unicellular *S. cerevisiae* during budding (Drubin, 1991). In multicellular fungi, relatively little is known about the establishment of polarity and its effect on morphogenesis and developmental processes.

Here, I describe the characterisation of the M1422 mutant in order to determine the likely biological function of the *TPC1* gene. My aim was to investigate the effect of loss of *TPC1* function on conidiogenesis, conidiation, conidial germination, appressorial formation and conidial collapse and, in particular, to study the role of *TPC1* in polar-growing structures such as vegetative hyphae, germ tubes, penetration pegs and infectious hyphae. Actin and other cytoskeletal elements, as well as their motor proteins, are involved in the establishment and maintenance of polarity in apical-growing structures (Fischer *et al.*, 2008). Localisation of the actin-binding protein fimbrin tagged with GFP (Fim:GFP) was examined in both the wild-type strain Guy11 and M1422 mutant. I also analysed if *TPC1* is involved in other biological processes such as infection-associated autophagy (Veneault-Fourrey *et al.*, 2006*a*; Kershaw and Talbot, 2009) and glycogen metabolism (Thines *et al.*, 2000; Bhambra *et al.*, 2006; Ramos-Pamplona and Naqvi, 2006; Wang *et al.*, 2007), which have vital roles in virulence of *M. oryzae*.

4.2. Materials and Methods

4.2.1. Cellular localisation of GFP:Atg8 and Fim:GFP in M1422 mutant background

The GFP:Atg8 (Kershaw and Talbot, 2009) and the Fim:GFP (A.L. Martinez-Rocha and N.J. Talbot, unpublished data) protein fusion vectors were used to transform protoplasts of M1422 mutant. The GFP:Atg8 and the Fim:GFP protein fusion vectors were generated using the native *M. oryzae* Atg8-encoding gene (MGG_01062) and the native *M. oryzae* fimbrin-encoding gene (MGG_04478), respectively. Both fragments were cloned into pCB1532 vector that contains the 2.8 kb *ILV1* gene, which encodes the acetolactate synthase allele conferring sulfonylurea resistance (Sweigard *et al.*, 1997). Transformants showing identical growth and colony morphology to the background strain were selected for further examination using epifluorescence or confocal microscopy. At least three different transformants of each were analysed independently.

4.3. Results

4.3.1. The M1422 mutant is strongly affected on vegetative growth

One striking characteristic of the M1422 mutant is its impaired hyphal growth, which is associated with the formation of a compact colony of reduced diameter size (Chapter 3). In this study, I compared vegetative growth of Guy11 and M1422 mutant on complete (CM) and minimal (MM) medium without carbon (MM-C) and nitrogen (MM-N) sources (Fig. 4.1). In all these growth media, the wild-type Guy11 colony was ~2.5 times larger than the mutant M1422 colony. The vegetative growth of M1422 mutant was severely compromised in both growth media ($p < 0.01$) with the mutant showing a compact colony of reduced size (Fig. 4.1). Examining in detail the edge of each colony, it was evident that the branching pattern of vegetative hyphae of the mutant was different from the wild-type Guy11 (Fig. 4.1A).

I also tested mycelial growth on medium with Congo Red (CR) and Calcofluor White (CFW), which inhibit *in vivo* fungal cell wall assembly by binding β-1,4-glucans and chitin, respectively (Wood and Fulcher, 1983; Ram *et al.*, 1994). Compared with Guy11 wild-type *M. oryzae* colonies, the mycelial growth of M1422 was severely impaired ($p < 0.01$) (Fig. 4.2). It was not possible to conclude if these pharmacological agents had any additive effect on vegetative growth of the M1422 T-DNA mutant.

The colonial growth of wild-type Guy11 and M1422 mutant was studied under conditions of hyperosmotic stress. M1422 was grown on medium containing high concentrations of osmolytes such as 1M sorbitol (Fig. 4.2) and increasing concentrations of sodium chloride (NaCl) (Fig. 4.3). Under all conditions, M1422 colonies were smaller than the wild-type ($p < 0.01$). However, the 2.5:1 colonial growth ratio of Guy11 and M1422 did not change under conditions of sorbitol stress.

Interestingly, high concentrations of NaCl (0.4M – 1.0M) changed this ratio, eliminating the difference in colonial size between Guy11 and M1422 mutant. The M1422 colonies grew better with increasing concentrations of NaCl (Fig. 4.3). At 10 days post-inoculation (dpi), the colony size of wild-type Guy11 decreased sharply with increasing NaCl osmotic stress, whereas the growth of M1422 colonies was not affected as shown in Fig. 4.3B.

4.3.2. *TPC1* is important in conidiogenesis

In the previous Chapter, the M1422 T-DNA mutant was shown to be defective in pathogenicity in comparison with Guy11, even though rice plants were inoculated with the same concentration of conidia. The 1422-encoding gene is a virulence determinant. Conidiation was, however, severely impaired in the M1422 mutant (1.9 ± 0.6 x 10^4 conidia ml^{-1} cm^{-2}) compared with wild-type strain Guy11 (11.2 ± 3.3 x 10^4 conidia ml^{-1} cm^{-2}) ($p < 0.01$) as shown in Fig. 4.4.

Conidia from the M1422 mutant showed defects such as number of cell *per* conidia and in conidial morphology as shown in Fig. 4.5. Wild-type Guy11 conidia were pyriform cells and were uniformly 3-celled (99%) and only a very small percentage were 2-celled. In the M1422 mutant, the majority of the conidia were 3-celled (80%). However, a higher percentage of 2-celled conidia (17%) were generated by the mutant and single-celled (2%) and 4-celled conidia (1%) were also observed, that were not present in the wild-type. Some of the 3-celled M1422 conidia (26%) were misshapen showing abnormal morphology. By contrast, only 4% of the 3-celled Guy11 conidia were misshapen. The length and width of Guy11 conidia was 23.1 ± 1.8 µm and 8.9 ± 1.0 µm, respectively (Fig. 4.6). The M1422 conidia were slightly shorter (22.2 ± 2.6 µm) and thinner (7.4 ± 1.0 µm), but these values were not statistically significant different from the wild-type conidial length and width (Fig. 4.6).

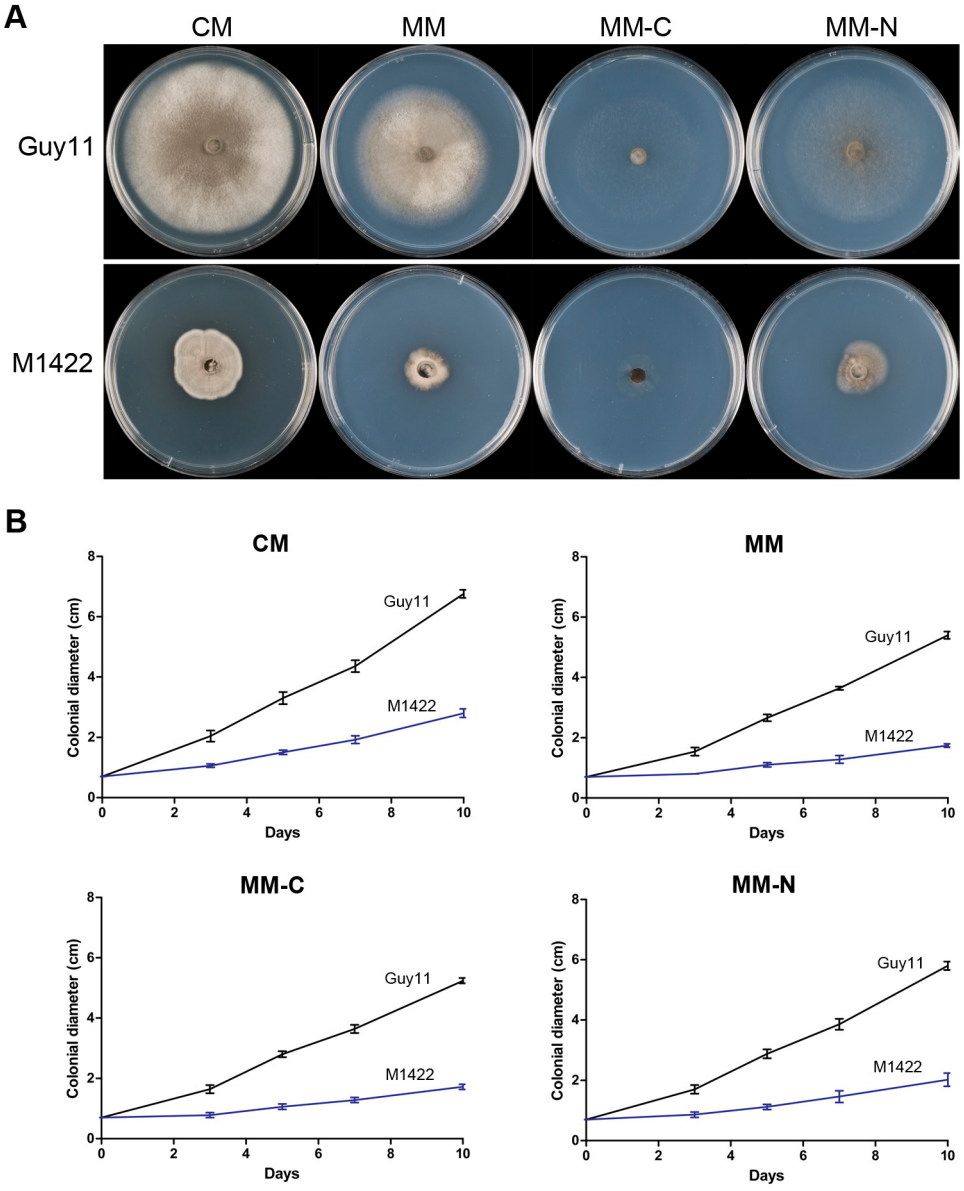

Figure 4.1. Vegetative growth and colony morphology are severely affected on the M1422 T-DNA mutant.

(A) CM, MM, MM-C and MM-N plates were inoculated with 7 mm plugs of mycelium from Guy11 and the M1422 mutant. Plates were incubated at 25ºC and the colony images captured 10 days after inoculation. **(B)** The diameter of subsequent colonies was measured at 3, 5, 7 and 10 days post-inoculation (dpi). Error bars represent the standard deviation of the three independent replications of the experiment.

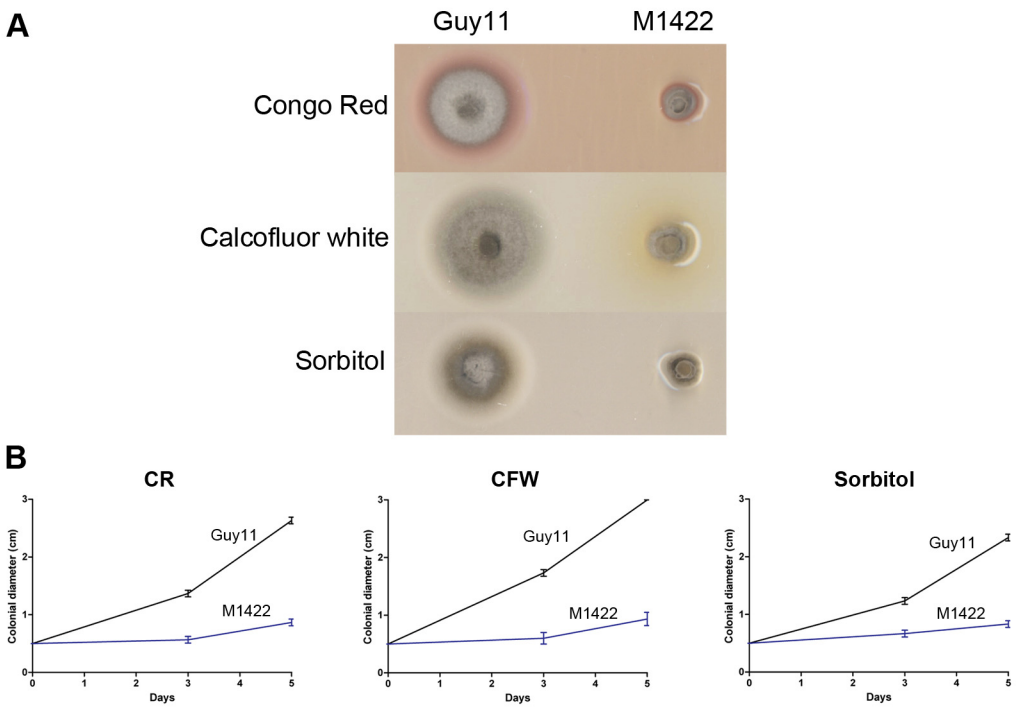

Figure 4.2. Vegetative growth and colony morphology are severely affected on the M1422 mutant.

(A) CM plates with 10 µg ml^{-1} Congo Red (CR), 10 µg ml^{-1} Calcofluor white (CFW) and 1M Sorbitol added to the media were inoculated with 5 mm plugs of mycelium from Guy11 and the M1422 mutant. Plates were incubated at 25ºC and the colony images captured at 5 dpi. **(B)** The diameter of subsequent colonies was measured at 3 and 5 dpi. Error bars represent the standard deviation of the three independent replications of the experiment.

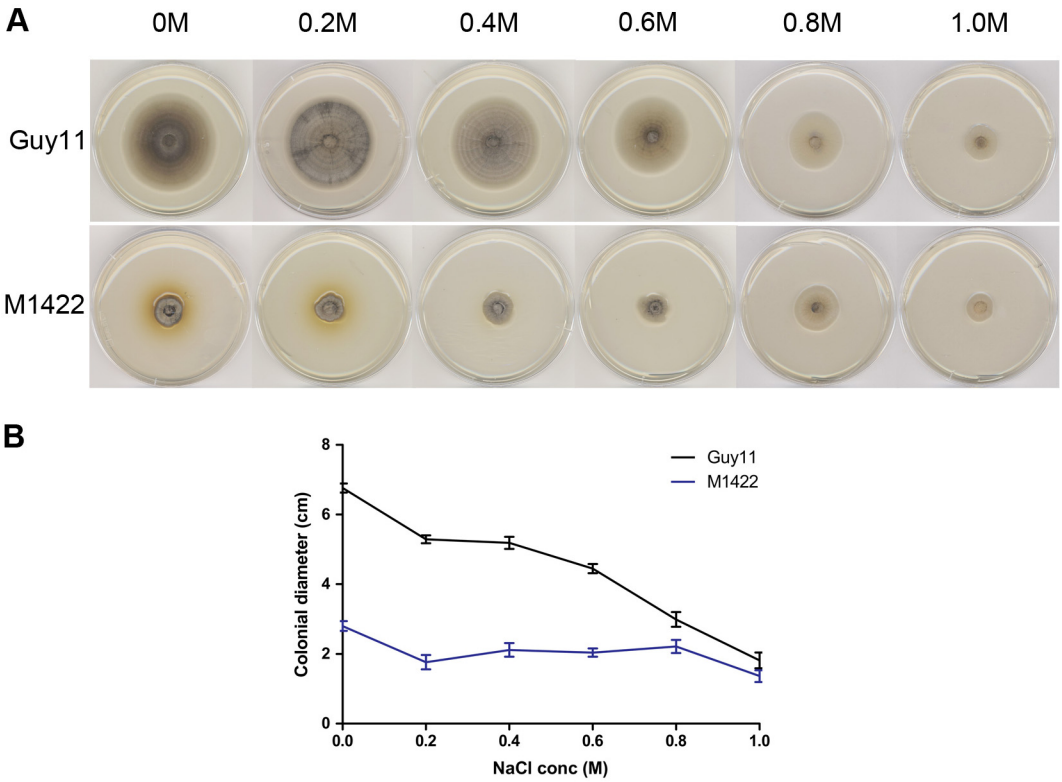

Figure 4.3. The M1422 mutant shows increased tolerance to hyperosmotic concentrations of sodium chloride (NaCl).

(A) CM plates with 0M, 0.2M, 0.4M, 0.6M, 0.8M and 1.0M NaCl added to the media were inoculated with 7 mm plugs of mycelium from Guy11 and the M1422 mutant. Plates were incubated at 25ºC and the colony images captured at 10 dpi. **(B)** The diameter of subsequent colonies was measured at 10 dpi. Error bars represent the standard deviation of the three independent replications of the experiment.

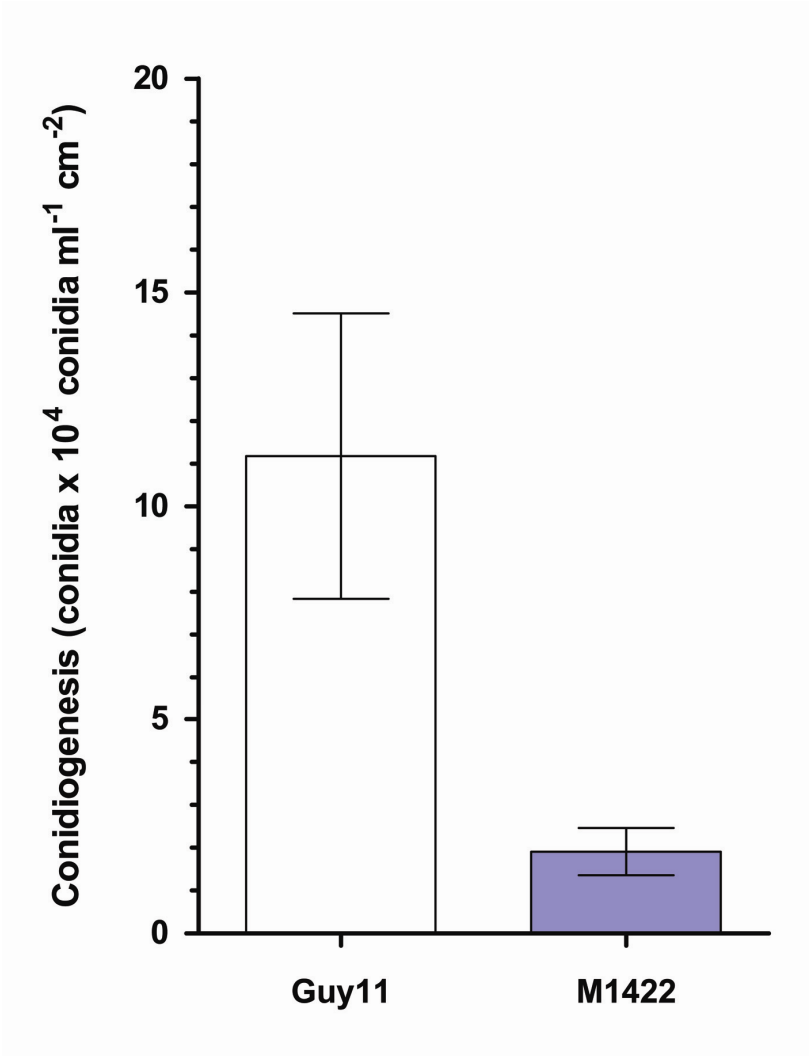

Figure 4.4. Conidiogenesis is severely impaired in the M1422 T-DNA mutant.
CM plates were inoculated with 7 mm plugs of mycelium from Guy11 and the M1422 mutant. Plates were incubated at 25ºC for a period of 10 days, after which plates were flooded with 4 mL dH_2O, and conidia were harvested, pelleted by centrifugation, re-suspended in 1 mL dH_2O and counted. Calculations were then carried out to determine the number of conidia generated *per* cm^2 of mycelium. Error bars represent the standard deviation of three independent replications of the experiment.

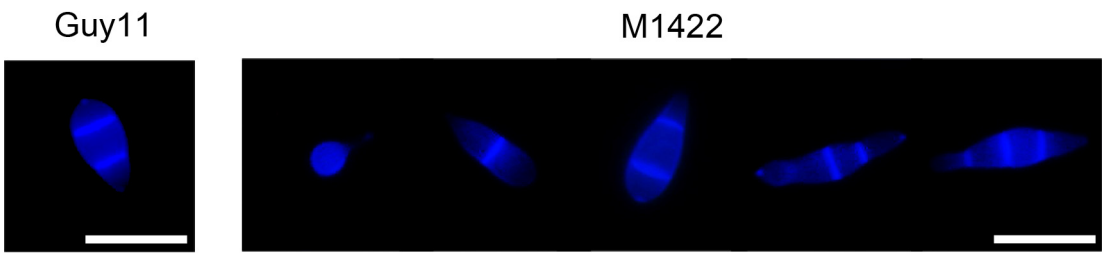

Figure 4.5. Conidia of the M1422 mutant show defects in the number of cells *per* conidium and morphology.

CFW was used to visualise septa in order to determine cell number *per* conidium. Conidia were stained with 5µl CFW solution (Fluka) and incubated at 25ºC for 30 minutes. Guy11 conidia are 3-celled. The M1422 mutant produces 1-, 2-, 3- (normal and abnormal morphology) and 4-celled conidia (same order in the panel). Photographs were taken using the Zeiss Axioskop 2 microscope camera. Scale = 20 µm.

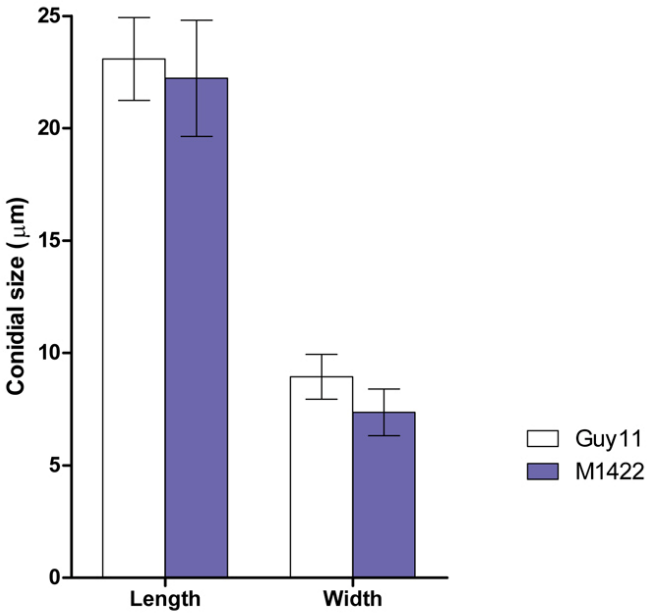

Figure 4.6. Conidial size of the wild-type Guy11 and M1422 T-DNA mutant.
Conidia were harvested and photographs were taken using the Zeiss Axioskop 2 microscope camera. Values are the mean ± SD from >300 conidia of each strain, which were measured using the ImageJ software (Collins, 2007). Conidial length is the distance from the base to apex of conidia. Conidial width is the size of the longest septum.

4.3.3. Appressorium development is impaired in the M1422 mutant

Since conidiogenesis is affected in the M1422 mutant, I investigated whether the appressorium-related development was also impaired in this mutant (Fig. 4.7). The majority of the three-celled wild-type conidia germinated (>90%) as shown in Fig. 4.8. Conidia germinated by forming a germ tube that emerged from the basal or apical cell. The germ tube only extended for a short distance at its tip and an appressorium formed within 4h – 8h (Fig. 4.7). A long period (6h – 8h) after the inoculation of conidia on the coverslip, some conidia started to germinate germ tubes from both apical and basal cells (< 3%) (Fig. 4.8). One of the germ tubes then differentiated an appressorium (Fig. 4.9). The emergence of a second germ tube may have occurred due to a lack of surface recognition of the germ tube to trigger appressorium morphogenesis in one of cells of the conidium.

Even though there were a higher percentage of abnormal conidia, most of the three-celled conidia of the M1422 mutant germinated (89%) (Fig. 4.8). Surprisingly, only 2h after inoculation, 40% of the M1422 conidia had germinated from two cells (Fig. 4.9). This percentage increased to 50% - 60% with incubation time (4h – 8h) on an inductive surface. During appressorium formation, the M1422 mutant conidia showed multiple phenotypes, including formation of two germ tubes, two appressoria or one germ tube germinated from one cell and an appressorium forming from another cell (Fig. 4.7 and Fig. 4.9). The formation of two appressoria observed in M1422 was not observed in conidia of Guy11. Although, the pattern of appressorium-related development was affected, the M1422 conidia did not lose the ability to form at least one appressorium (97%) (Fig. 4.9). Very rarely the middle cell of the M1422 conidia also germinated a germ tube (0.01%) (Fig. 4.7). This situation was not observed during appressorium-mediated process in wild-type Guy11.

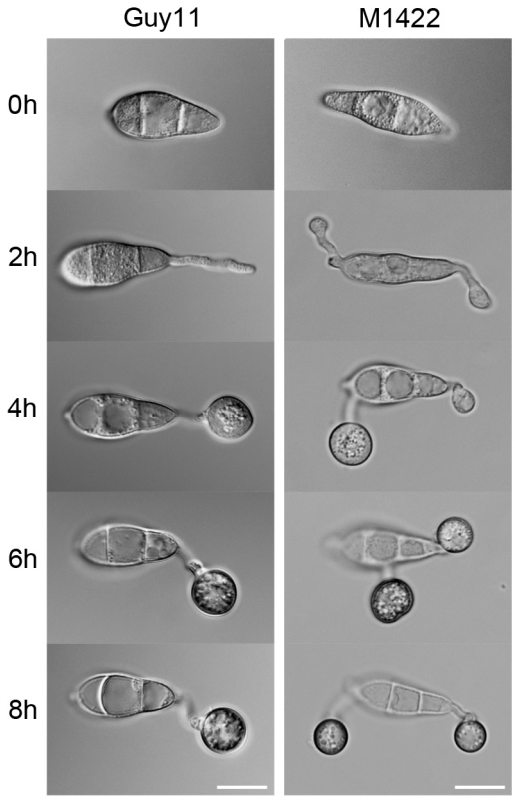

Figure 4.7. Infection-related development is impaired in the M1422 mutant.
Conidia were harvested from wild-type Guy11 and M1422 mutant, inoculated onto glass coverslips, and observed by differential interference contrast (DIC) microscopy at the times indicated 0h, 2h, 4h, 6h and 8h. Scale bar = 10μm.

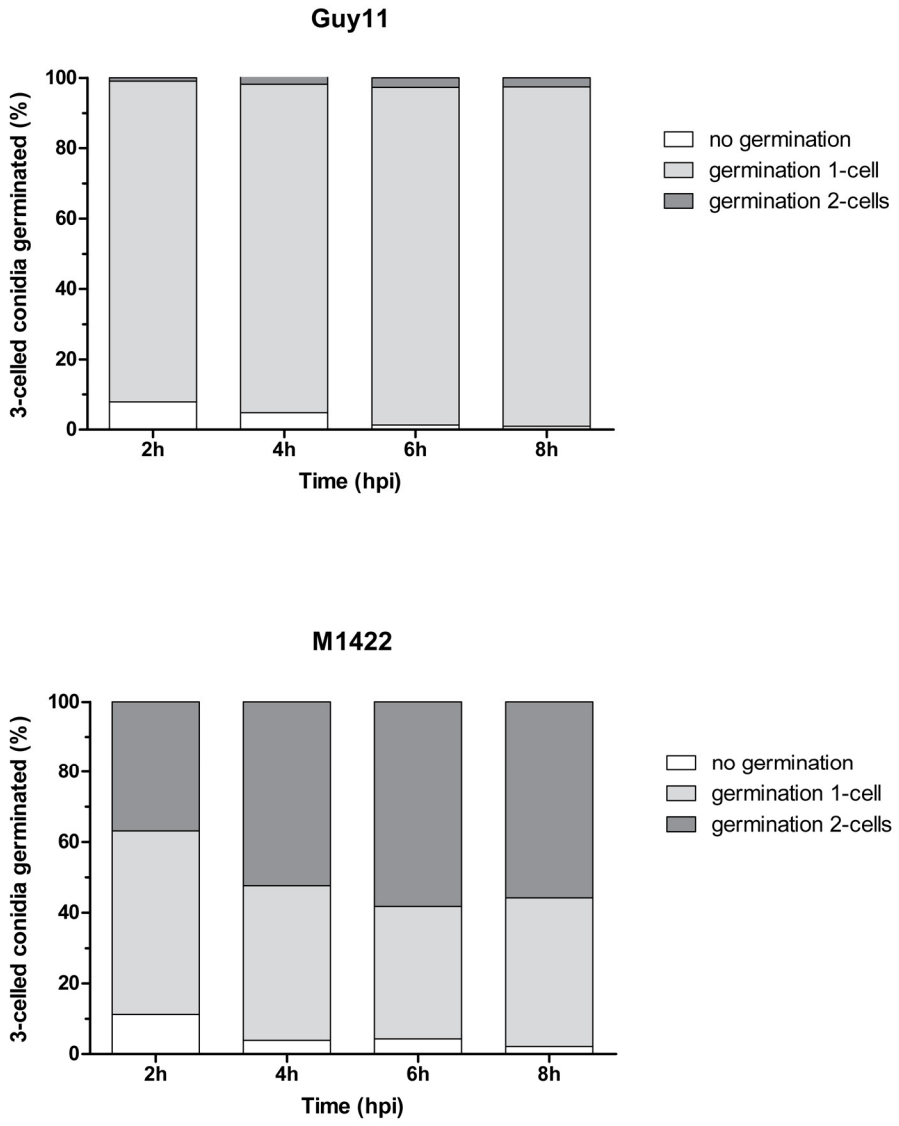

Figure 4.8. The M1422 mutant showed an increased frequency of conidia germination from two cells.

Conidia were harvested from wild-type Guy11 and M1422 mutant, inoculated onto glass coverslips, and observed and counted at 2h, 4h, 6h and 8h after inoculation. Bar charts showing the relative percentage of non-germinated conidia and conidia that germinate from 1-cell and 2-cells at each time point indicated. Data from three biological repeats.

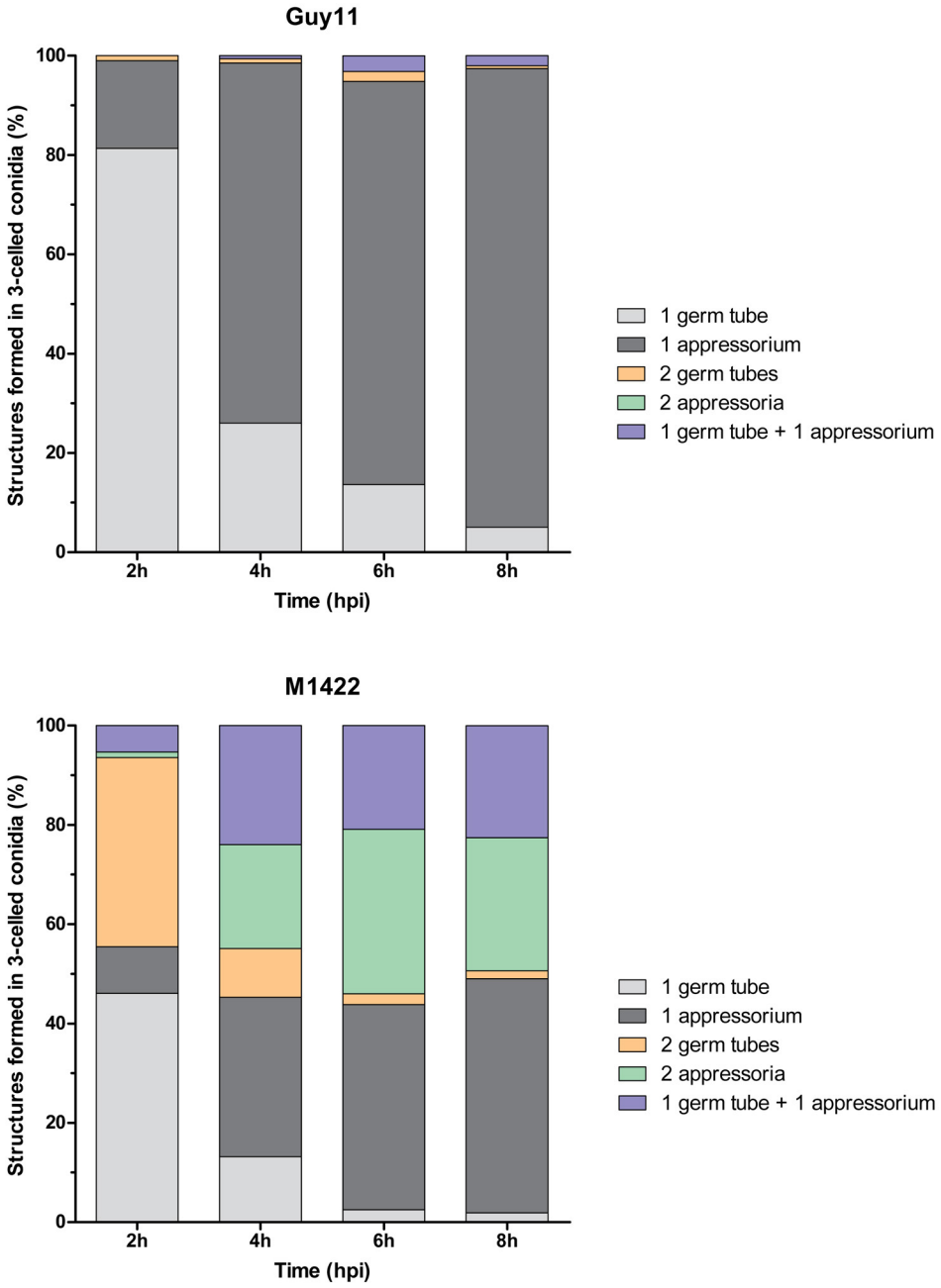

Figure 4.9. The M1422 conidia formed at least one appressorium during infection-related development.

Conidia were harvested from wild-type Guy11 and M1422 mutant, inoculated onto glass coverslips, and observed and counted at 2h, 4h, 6h and 8h after inoculation. Bar charts showing the relative percentage of the different infection structures formed at each time point are shown. Data from three biological repeats.

4.3.4. Polarity is coupled with autophagy and glycogen metabolism in *M. oryzae*

The impairment in appressorium-mediated development in the M1422 mutant suggested that the morphogenetic pathway might be affected (Saunders *et al.*, 2010). I therefore investigated whether infection-associated autophagy proceeds normally and if conidia underdo autophagic cell death. After 24h, the conidia of both Guy11 (97%) and M1422 (93%) strains were no longer viable and conidial cells and germ tube collapsed (Fig. 4.10). A GFP:Atg8 construct was introduced into the M1422 mutant in order to determine the spatial and temporal dynamics of autophagy in the mutant (Fig. 4.11). Atg8 encodes an autophagic ubiquitin-like protein and has been shown to be a reliable marker for autophagy (Kershaw and Talbot, 2009). The first clear observation was that the GFP:Atg8-labeled autophagosomes accumulated in conidia in significantly smaller numbers in the M1422 mutant (21.6 ± 5.5) when compared with the wild-type Guy11 (33.5 ± 4.4) ($p < 0.01$; Fig. 4.12). The number of autophagosomes decreased during germination, appressorium maturation and the onset of conidial cell death (Fig. 4.12) in both WT and M1422 mutant. However, the occurrence of this decrease was more pronounced in Guy11 conidia. Even at 24h, the M1422 conidia (3.8 ± 2.9) contained slightly more autophagic vesicles than the wild-type (0.8 ± 1.8). Germ tubes germinated from Guy11 conidia tend to not have autophagosomes during appressorium-mediated development (Fig. 4.12). Conversely, germ tubes from M1422 conidia contained a few autophagosomes throughout the developmental process (Fig. 4.12). Within developing appressoria of Guy11, autophagosome numbers increased during appressorium maturation and intense autophagic activity was associated with mature appressoria (8h; 16.1 ± 4.9). The number of autophagic vesicles within the appressoria dropped considerably after conidial death (24h; 5.0 ± 1.8). By contrast, the number of autophagosomes within appressoria of M1422 was

steady during appressorium maturation (8.4 ± 4.1), even after conidial cell death (7.5 ± 3.3) (Fig. 4.12).

Recently, a link between autophagy and glycogen metabolism has been studied in *M. oryzae* (Deng and Naqvi, 2010). Glycogen levels during appressorium-mediated development were therefore determined using potassium iodide (KI) staining (Fig. 4.13). During the initial stages of conidial germination, glycogen metabolism was similar in both Guy11 and M1422. The two ungerminated conidial cells showed increased levels of glycogen (confirmed by more intense staining), whereas the germinated cell and germ tube remained unstained (Fig. 4.13). During appressorium formation and maturation, glycogen levels increased within the appressorium while its levels decreased within the two cells of the conidium (Fig. 4.13). However, comparative analysis of KI staining between wild-type Guy11 and the M1422 mutant showed differences during the onset and later stages of conidial cell death (8h and 24h) (Fig. 4.13). Wild-type conidia were depleted of glycogen (no staining) within the conidial cells and appressorium (Fig. 4.13 and Fig. 4.14). Interestingly, although conidial cells of M1422 mutant were also depleted of glycogen, the appressorium remained with high levels of glycogen (concomitant with strong staining with iodide solution). At 24h, 95% of the mutant appressoria were still stained with iodide (Fig. 4.13 and Fig. 4.14).

When considered together, these observations suggest that autophagy and glycogen metabolism appear to be delayed during appressorium-mediated development in the M1422 mutant.

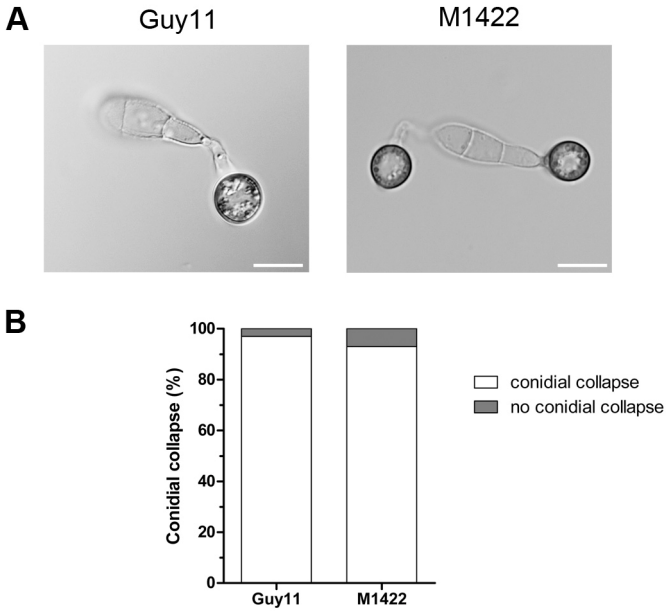

Figure 4.10. The M1422 mutant underwent conidial collapse during appressorium development. **(A)** Conidia were germinated on hydrophobic glass coverslips and incubated for 24 h to form appressoria. Micrograph shows conidial cell death in Guy11 and in the M1422 mutant. Scale bar = 10 µm. **(B)** Guy11 and M1422 both showed equivalent frequencies of spore collapse during appressorium development. Bar charts showing the relative percentage of conidia that collapsed and did not collapse for each strain at 24h after inoculation. Data from three biological replications.

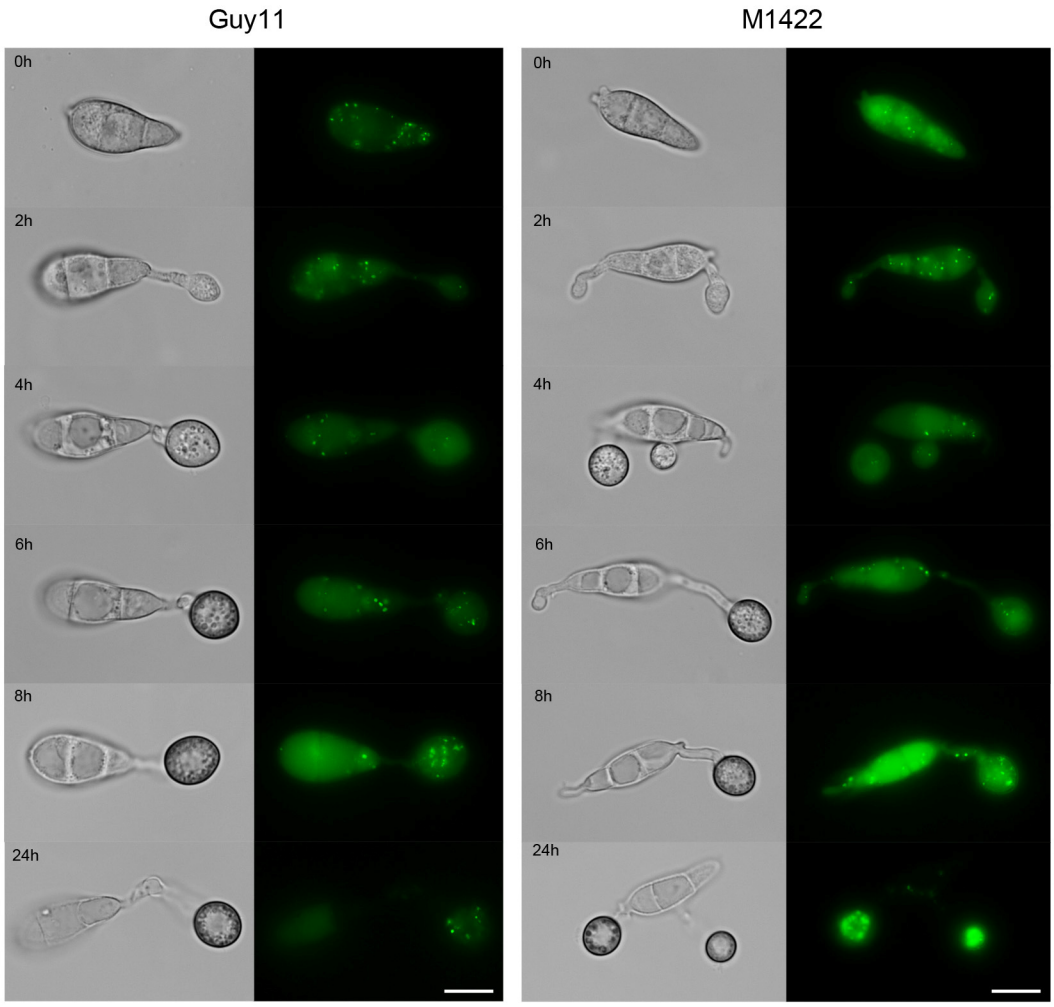

Figure 4.11. Cellular localisation of autophagosomes during infection-related development of wild-type Guy11 and M1422 mutant.

Conidia were harvested from Guy11 and M1422 transformants expressing GFP:Atg8, inoculated onto borosilicate glass coverslips and observed by epifluorescence microscopy at the times indicated. Scale bar = 10 µm.

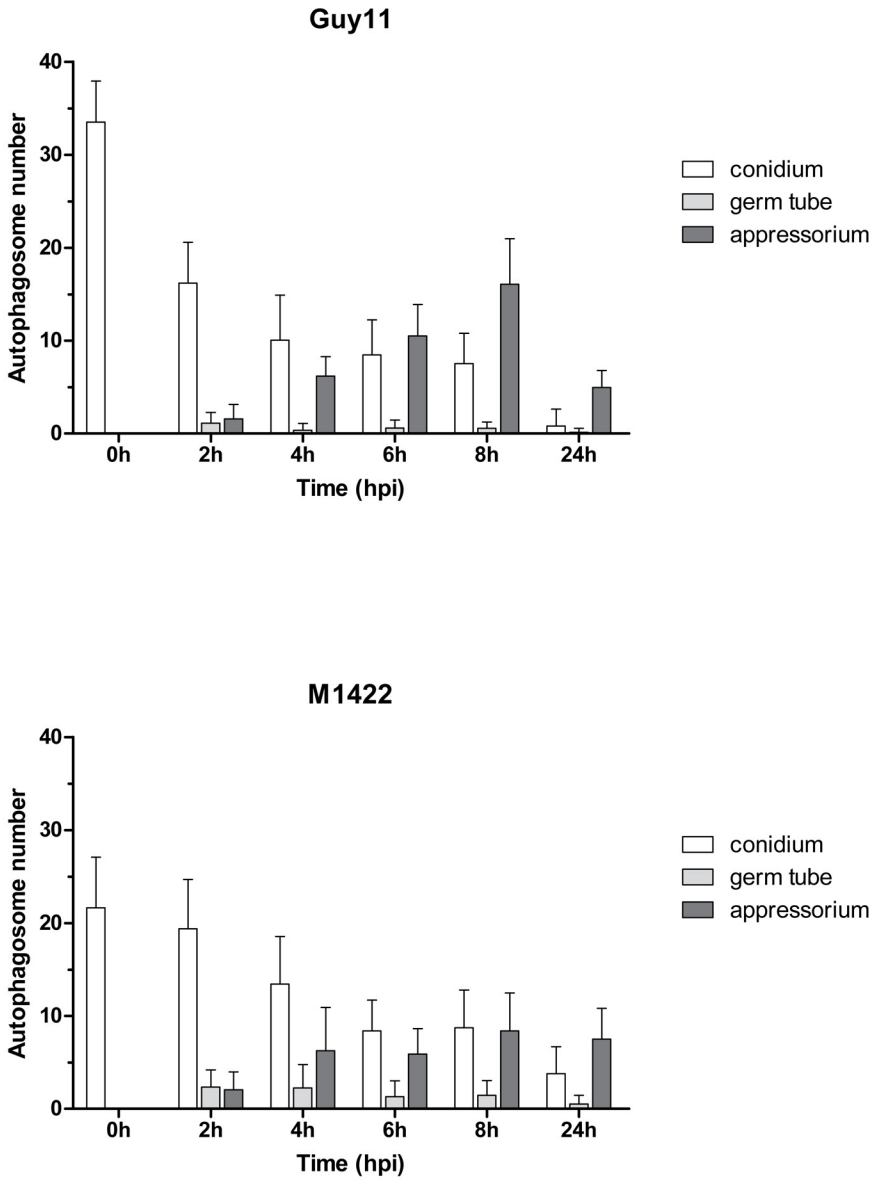

Figure 4.12. Infection-associated autophagy was impaired in the M1422 mutant.
Bar charts showing mean autophagosome numbers present in conidium, germ tube, and appressorium at the time points indicated with Guy11 and M1422 transformants expressing GFP:Atg8. Error bars represent the standard deviation of three independent replications of the experiment.

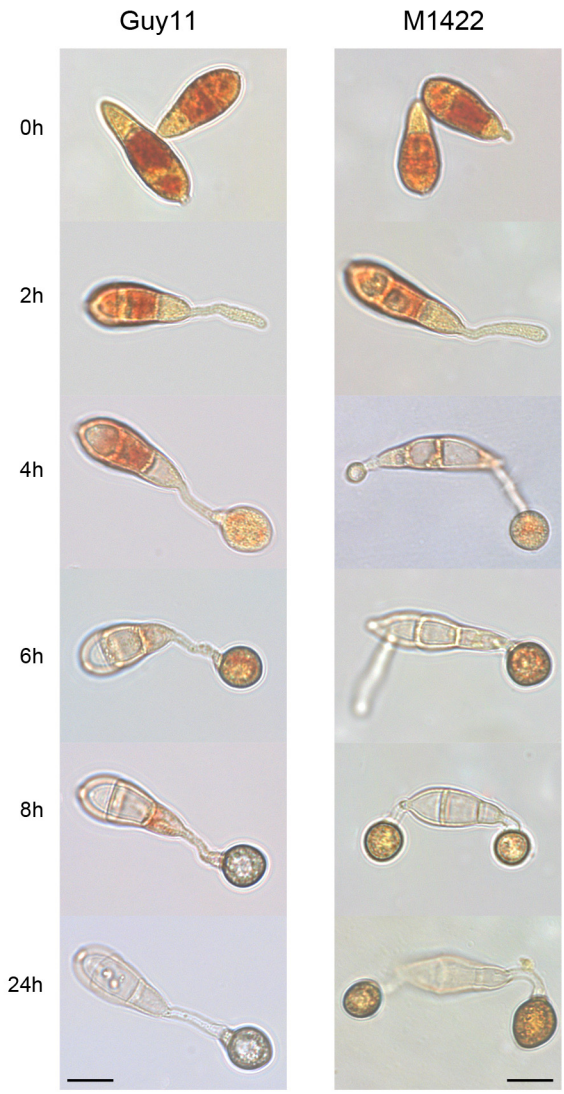

Figure 4.13. Glycogen metabolism was delayed in the M1422 mutant during infection-related development.

Conidia were harvested from Guy11 and the M1422 mutant, inoculated onto borosilicate glass coverslips and exposed to potassium iodide (KI) solution, and observed at 0h, 2h, 4h, 6h, 8h and 24h after inoculation. The KI solution stains glycogen within the conidia, but not simple sugars such as glucose and fructose. Scale bar = 10 μm.

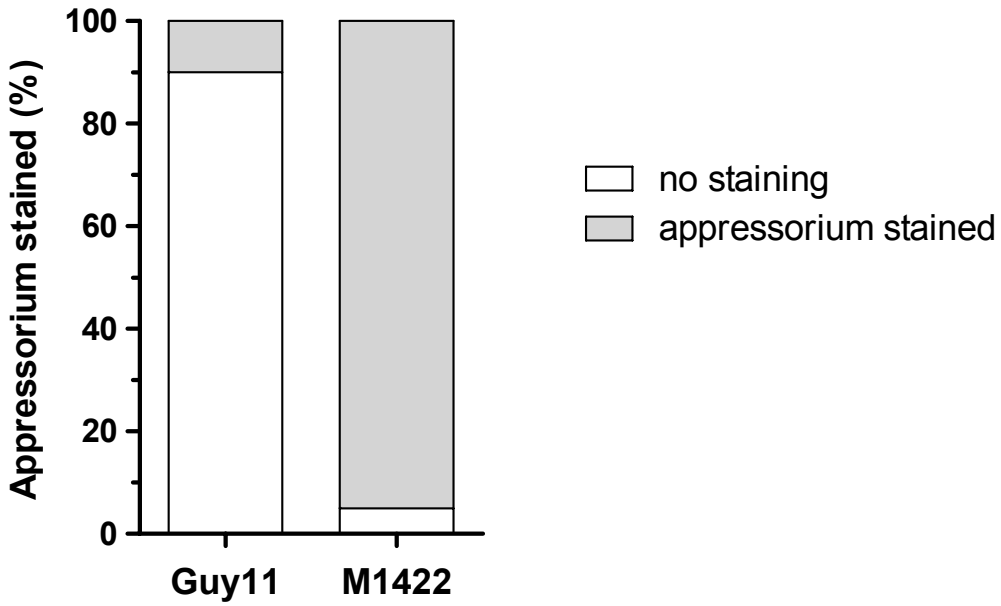

Figure 4.14. Glycogen metabolism was delayed in the M1422 mutant.

Conidia were harvested from wild-type Guy11 and M1422 mutant, inoculated onto borosilicate glass coverslips with potassium iodide (KI) solution. Bar charts showing the relative percentage of stained appressoria with KI solution for each strain at 24h after inoculation. Data from three biological replicas.

4.3.4. *TPC1* is required for re-establishing polarity in appressoria

Following appressorium maturation, a penetration peg emerges from the appressorial pore to penetrate the plant cuticle and successfully colonise the plant host. To assess if this re-polarisation within the appressorium was impaired in the M1422 mutant, a penetration assay was performed on onion epidermis (Fig. 4.15). After 24h of incubation, 91% of the wild-type Guy11 conidia that formed an appressorium had effectively penetrated and invaded the epidermal cells (Fig. 4.15). By contrast, only 40% of the M1422 appressoria had formed a penetration peg (Fig. 4.15). Even those that were able to invade the onion epidermal cells did not grow further from the point of penetration. The majority of the M1422 conidia (60%) germinated and produced an appressorium, but failed to penetrate and invade onion cells (Fig. 4.15).

High concentrations of actin filaments are necessary to stabilise the tip of penetration peg (Howard and Valent, 1996). To examine how the formation of the germ tube and penetration peg was compromised, I investigated the dynamics of actin-binding protein fimbrin (Fim:GFP) during infection-related development (Fig. 4.16). Once wild-type conidia attached to borosilicate glass coverslip, a concentration of Fim:GFP was observed at the periphery of conidial cell that germinated. Conidia harvested from the M1422 mutant, however did not show this characteristic. Fimbrin instead localised randomly at the periphery of the three cells of the conidia, and not preferentially in the germinating cell. During germ tube formation (2h), differences in fimbrin organisation between Guy11 and M1422 mutant were obvious. The wild-type conidia showed strong expression of fimbrin at the periphery of the germ tube tip. Although the mutant also showed strong fimbrin expression at the tip of the germ tubes, this localisation was not defined only at the periphery. Fimbrin was dispersed and localised within the cytoplasm of the germ tube of the M1422 conidia. During appressorium formation (4h-6h), fimbrin was

localised in discrete puncta at the periphery of the Guy11 appressorium. However, fimbrin mislocalisation was observed in the M1422 mutant. Fim:GFP was dispersed within the appressorium. At the onset of conidial cell death (8h – 24h), formation of one central appressorial pore within the appressoria was seen in Guy11. The appressorium pore determines the site of emergence of the penetration peg (Bourett and Howard, 1992). At 8h, an appressorial pore could not be observed on the M1422 mutant. Appressorium pore development was delayed in the mutant (Fig. 4.16). However, after conidial cell death, several non-central appressorial pores were formed within the mutant appressorium. This indicates that the re-polarisation process is adversely affected in the M1422 mutant and that *TPC1* is required for the correct polarised penetration peg emergence in *M. oryzae*.

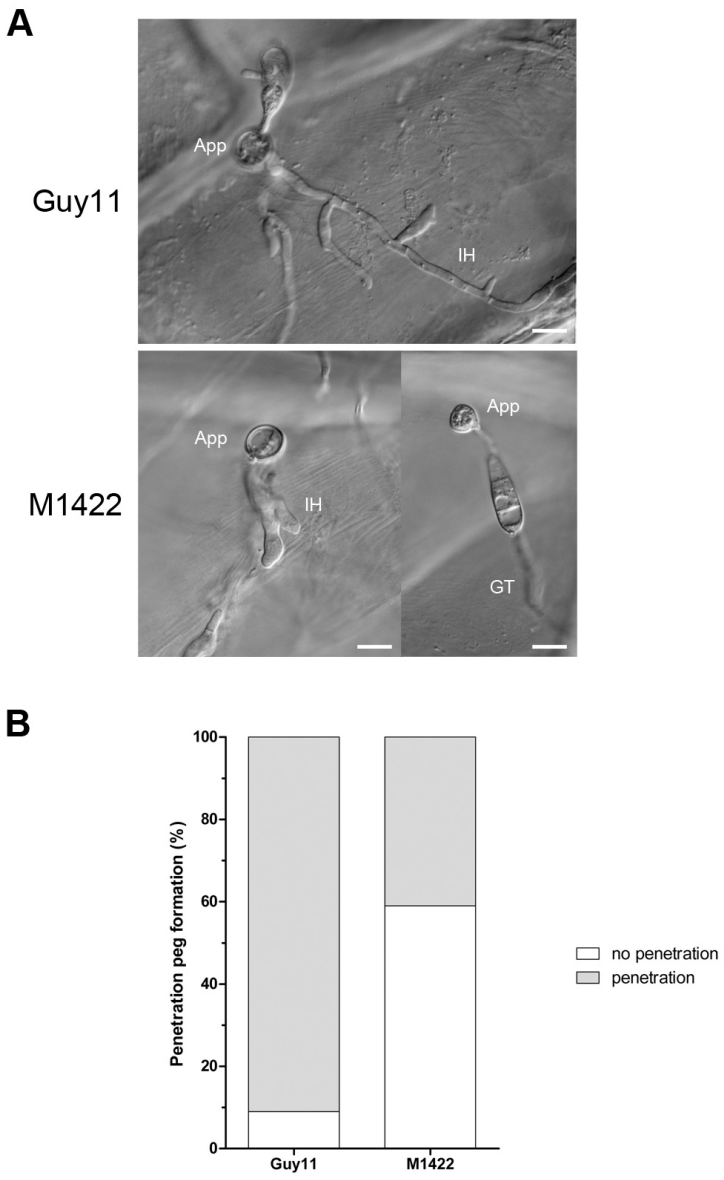

Figure 4.15. The M1422 mutant was impaired in appressorium-mediated penetration.
(A) Onion penetration assay by wild-type Guy11 and M1422 mutant after 24hpi. Appressorium formed on surface of the onion strip has penetrated the underlying epidermal cell and formed invasive hyphae (Guy11 and M1422 - left panel). Left panel of M1422 mutant shows a defective penetration of onion epidermis by this mutant. Right panel of M1422 mutant shows a germinated conidia which did not form penetration peg after 24 hpi. Scale bar = 10 µm. **(B)** Bar charts showing the relative percentage of appressorial-penetration of onion epidermis for each strain at 24hpi. Data from three biological replicas.

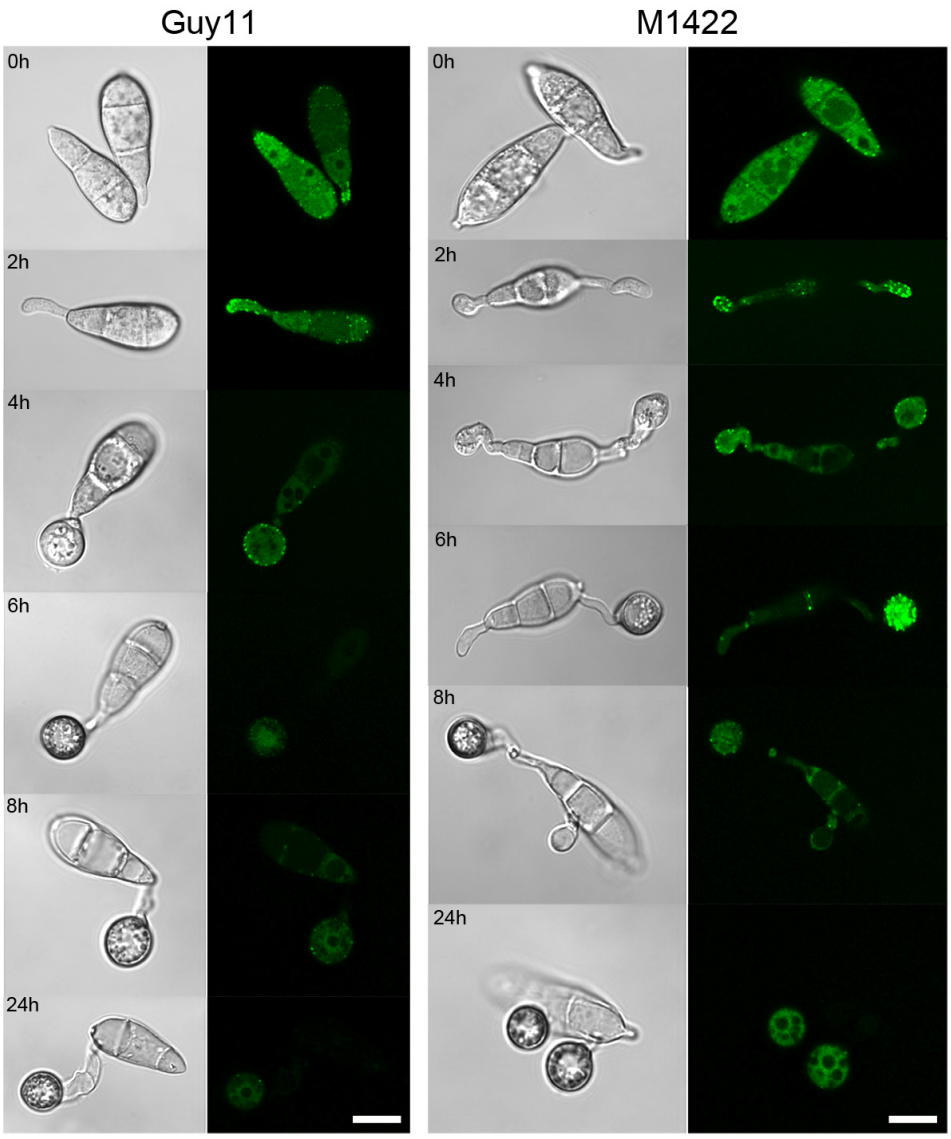

Figure 4.16. Cellular localisation of fimbrin, an actin-binding protein, during infection-related development of wild-type Guy11 and M1422 mutant.

Conidia were harvested from Guy11 and M1422 transformants expressing Fim:GFP, inoculated onto borosilicate glass coverslips and observed by epifluorescence microscopy at the times indicated. Scale bar = 10 µm.

4.4. Discussion

The establishment of polarity is a crucial process in every living organism and functional polarity can be observed at a molecular, cell and structure level. Polarisation implies several steps: 1) a spatial clue that must demarcate a unique zone of the cell to undergo polarised growth or modification; 2) signals which must transmit spatial information to drive asymmetric organisation of the cytoskeleton (*e.g.* actin); 3) polarised transport of RNAs or proteins to the marked region, which must occur along the cytoskeleton to the polarising zone (Macara and Mili, 2008). Polarised growth enables the fungus to grow (vegetative growth and branching) and to progress along the plant surface (by formation of germ tube) and inside infected rice cells (by formation of penetration pegs and invasive growth) (Xu *et al.*, 2007; Harris, 2008; Brand and Gow, 2009). Sensing the correct surface stimulus is therefore critical for plant infection in *M. oryzae*. The M1422 T-DNA mutant, defective in *TPC1* (*Transcription factor for Polarity Control1*), demonstrates the importance of polarity establishment in both general developmental processes in the fungus and in the virulence of *M. oryzae*.

Vegetative growth and branching of vegetative hyphae were severely impaired in the M1422 mutant when grown on complete (CM), minimal medium (MM) or minimal medium without carbon (MM-C) and nitrogen source (MM-N) (Fig. 4.1). The mutant colonies were very reduced in size and showed a compact phenotype. This phenotype suggests defects in polarity establishment in apical-growing hyphae and branch formation. These two processes are intimately interlinked (Harris, 2008; Brand and Gow, 2009). The ability of rapidly apical-growing hyphae to generate new polarity axes results in the formation of a branch and hyphal branching is vital to the development of mycelial colonies (Harris, 2008). Hyphal branching permits an increase of the surface area of a colony, enhancing space occupancy and substrate

acquisition by the fungus, and the exchange of nutrients and signals between different cells in the same colony (Harris, 2008; Brand and Gow, 2009). It also appears to play a pivotal role in fungal interactions with other organisms (Harris, 2008). The M1422 mutant was clearly affected in normal hyphal growth rate and in the establishment of normal patterns of hyphal branching and mycelial organisation perhaps due to the lack of polarisation of temporal and spatial regulatory mechanisms that ensure these processes.

Vegetative growth was not affected by the presence of CR and CFW (Fig. 4.2), which implies that chitin deposition was not affected by the absence of *TPC1*. By contrast, hyperosmotic stress conditions (Fig. 4.3) led to an increase in the relative growth rate of M1422 compared to the wild-type, consistent with an effect of cell wall integrity or hyperosmotic stress adaptation processes such as compatible solute generation or membrane function (Quinn, 2008; Fuchs and Mylonakis, 2009; Smith *et al.*, 2010). In *M. oryzae*, the *MPS1* MAPK regulates nutrient sensing and the cell wall integrity pathway (Xu *et al.*, 1998). *MPS1* gene is also required to re-establish polarised growth and the elaboration of a penetration peg by the mature appressorium (Xu *et al.*, 1998). A similar phenotype was observed in the M1422 mutant throughout this study (Fig. 4.15 and Fig. 4.16), consistent with such a relationship.

In *M. oryzae,* conidia are produced in sympodially arrays at the tips of aerial hyphae that emerge from the necrotic lesions of rice blast infected plants. Mitotic divisions of a single progenitor nucleus occur in the conidiophore, leading to the production of the first three-celled conidium. Then, the hyphal tip moves to the side of the conidium and produces a second spore until three to five conidia are produced in a whorl at the conidiophore tip (Lau and Hamer, 1998). However, the developmental process of conidiogenesis was affected in the M1422 mutant. Conidiation was severely reduced in the mutant compared with wild-type ($p < 0.01$) as shown in Fig.

4.4. Despite the changes in conidial morphology, conidial cell number and germination of conidial cells (Fig. 4.5 and Fig. 4.8), M1422 conidia were able to germinate normally to form appressoria (Fig. 4.7 and 4.9). The germinated M1422 conidia showed multiple phenotypes such as formation of two germ tubes, two appressoria or one germ tube from one cell and an appressorium forming from another cell (Fig. 4.7 and 4.9). The formation of two appressoria and germination from the middle cell (Fig. 4.9) in the M1422 conidia, were phenotypes not observed in Guy11 conidia. Other mutants affected in conidiation in *M. oryzae* have pleiotropic effects on appressorium formation and pathogenicity (*e.g. Δsmo, Δcon* and *Δacr1* mutants (Hamer *et al.*, 1989; Shi and Leung, 1995; Lau and Hamer, 1998), which highlight the developmental parallels between conidiation and appressorium morphogenesis.

When appressoria mature, the conidial and germ tube cells usually collapse and are no longer viable after 24 h (Veneault-Fourrey *et al.,* 2006*a*). Although M1422 conidia appeared able to undergo cell death (Fig. 4.10), cellular localisation of autophagosomes (Fig. 4.11 and Fig. 4.12) and glycogen metabolism (Fig. 4.13 and Fig. 4.14) suggested that this process is impaired. Autophagy targets portions of cytoplasm, damaged organelles and proteins for lysosomal degradation and has crucial roles in development and disease (He and Klionsky, 2009; Talbot and Kershaw, 2009; Wang and Levine, 2010). The association of Atg8 with mature autophagosomes has made this a marker for autophagy (Kershaw and Talbot, 2009). Generation and expression of a GFP:Atg8 fusion protein provides the means to determine spatial regulation of autophagy by measuring the distribution of punctate GFP:Atg8 autophagosome-associated signal within cells (Kershaw and Talbot, 2009). Interestingly, autophagy was affected in the M1422 mutant (Fig. 4.11 and Fig. 4.12). The most striking observations made during infection-related development were: 1) M1422 conidia had a smaller number of autophagic vesicles;

2) the number of autophagosomes within M1422 appressorium did not significantly alter throughout this process; 3) at 24h, the M1422 conidia still maintained a considerable number of autophagosomes. Absence of *TPC1* transcription factor therefore affects and delays the autophagic pathway within the M1422 conidia. Recently, a close relationship between glycogen homeostasis and autophagy has been reported (Deng *et al.*, 2009). Loss of autophagy leads to an increase of glycogen levels within fungal cells (Deng *et al.*, 2009). Glycogen metabolism was followed during appressorium formation and maturation in Guy11 and M1422 mutant (Fig. 4.13). At 24h, wild-type conidial cells and appressorium were depleted of glycogen, whereas M1422 appressoria still had a considerable amount of glycogen levels concomitant with staining within the appressoria (Fig. 4.13 and Fig. 4.14). Glycogen metabolism and autophagy are delayed in the M1422 mutant. These results link control of polarised growth with autophagy and other developmental processes and demonstrate that *TPC1* is a core developmental regulator, capable of coupling different signalling pathways in a context-dependent manner.

Autophagic cell death has been also linked with appressorium formation and penetration in *M. oryzae* (Veneault-Fourrey *et al.*, 2006*a*). Mature appressoria develop a thin-walled appressorium pore area at the contact site to the plant surface and a penetration peg will emerge from the appressorial pore (Bourett and Howard, 1992). Although the majority of wild-type appressoria penetrated onion epidermal cells, the M1422 mutant was shown to be penetration defective (Fig. 4.15). The penetration peg emerging from the appressorial pore contains high concentrations of actin filaments that may be necessary to stabilise the tip of penetration peg (Howard and Valent, 1996). To investigate cytoskeletal dynamics GFP was fused with fimbrin (Matsudaira, 1994; A.L. Martinez-Rocha and N.J. Talbot, unpublished data), an actin cross-linking protein, and used in live cell imaging in *M. oryzae* (Fig. 4.16). The introduction of Fim:GFP has also been used successfully to study cell

polarity in *A. nidulans* (Upadhyay and Shaw, 2008). The network of fimbrin observed in mature appressoria (8h – 24h) of the wild-type strain to delineate the appressorial pore was strikingly absent in the M1422 mutant (Fig. 4.16). This result indicates that actin involved in the selection of the penetration emergence site and re-establishment of polarised growth is disturbed in the M1422 mutant. In pollen tubes and root hairs, it has been also shown that actin microfilaments are involved in organellar movements, cellular morphogenesis and the regulation of apical growth (Hepler *et al.*, 2001).

Taken together, these results provide evidence that Tpc1 has a broad involvement in polarised growth potential and differential inheritance of cellular components occurring in different developmental processes. The differential inheritance of cell fate determinants is used to generate diverse cell types during development of multicellular organisms. These determinants can be RNAs or proteins and have diverse functions that ultimately control programs of gene expression to either suppress or drive cell fate differentiation and control axis formation (Macara and Mili, 2008). *MoTPC1*-deleted mutant may therefore provide a means to dissect how polarity is established and regulated in *M. oryzae*, and also allow the organisation of cytoskeletal elements, and how assimetrically localised RNAs/ proteins determine morphogenesis and cell fate in *M. oryzae*.

Based on the initial characterization of Tpc1, I decided to investigate the expression of Tpc1 during infection-related development and also to characterise structure-function relationships in the Tpc1 protein using directed mutagenesis.

CHAPTER 5

Cellular localisation and site-directed mutagenesis of *Mo*Tpc1

5.1. Introduction

Members of the $Zn(II)_2Cys_6$ binuclear cluster protein family are exclusively fungal. The six cysteine residues bind to two zinc atoms, which coordinate folding of the domain involved in DNA-binding (Pan and Coleman, 1990, 1991). The first and fourth cysteine residues act as bridging ligands by ligating both zinc metal ions, whereas the other cysteine residues act as terminal ligands (Gardner *et al.*, 1991; Pan and Coleman, 1991). Zinc cluster proteins are found predominantly in ascomycetes such as the saprotrophs *S. pombe*, *Kluyveromyces lactis*, *Neurospora crassa*, *Trichoderma reesei*, in the plant pathogens *M. oryzae* and *Ustilago maydis*, and the human pathogen *Candida albicans*; and only one zinc cluster protein is known in the basidiomycete *Lentinus edodes* (reviewed in Todd and Andrionopoulos, 1997). However, this family is best characterised in the budding yeast *S. cerevisiae* genome, with over 50 putative zinc cluster proteins (Cornell *et al.*, 2007). The first discovered zinc cluster protein was the *S. cerevisiae* Gal4 protein, a transcriptional activator of genes involved in the catabolism of galactose (Klar and Halvorson, 1974; Laughon and Gesteland, 1982), which became the driving force behind further studies in other members within this fungal family of transcription factors.

The $Zn(II)_2Cys_6$ binuclear cluster proteins contain several functional domains: the cysteine-rich DNA-binding domain (DBD), the regulatory domain, and the acidic region. The DBD domain is commonly located at the N-terminus of the other domains and is divided into three sub-regions: the zinc finger, the linker, and the dimerization domain (MacPherson *et al.*, 2006). Several site-mutagenesis studies have shown the importance of cysteine residues contained within the DBD in DNA binding and protein function (Johnston and Dover, 1987; Pfeifer *et al.*, 1989; Bai and Kohlhaw, 1991; Yuan *et al.*, 1991; Parsons *et al.*, 1992). However, two zinc cluster

proteins are known for not requiring the cysteine-rich DBD to be functional. The *S. cerevisiae* Dal81 and the *A. nidulans* TamA proteins appear to be fully functional when their zinc cluster domain is either deleted or disrupted (Bricmont *et al.*, 1991; Davis *et al.*, 1996). In general, zinc ions are required for stabilising protein folding and function of $Zn(II)_2Cys_6$ cluster proteins. However, zinc cluster proteins can still be functional and bind to DNA in a metal ion-dependent manner when zinc is replaced by other metal ions like Cd(II) (Marmorstein *et al.*, 1992). The linker sub-region is located right after the zinc cluster motif within the DBD region. It provides a structure for mediating DNA-binding to a specific sequence and prevents binding to non-specific sites (Mamane *et al.*, 1998). Moreover, replacing the zinc cluster motif of one protein with another does not affect DNA targeting, whereas switching the linker sub-region does (Reece and Patshne, 1993; Mamane *et al.*, 1998). Within the DBD the dimerization sub-region is the last component to be described. Although not present in all $Zn(II)_2Cys_6$ cluster proteins, the dimerization sub-region consists of heptad repeats that form a highly conserved coiled-coiled structure (Schjerling and Holmberg, 1996). It is proposed that this sub-region is responsible for dimerization and protein-protein interactions. The other two functional domains in zinc cluster proteins (regulatory and acidic domains) are not conserved or present in all proteins of this family (Schjerling and Holmberg, 1996). Most likely, the regulatory domain plays a role in regulating the transcriptional activity of the zinc cluster proteins. The function of the acidic domain is diverse and it is thought to play an important function in each zinc cluster protein.

The transcriptional activity of the $Zn(II)_2Cys_6$ cluster proteins can be modulated by numerous strategies such as nuclear-cytoplasmic shuffling, DNA binding, phosphorylation, and unmasking of the activation domain (Struhl, 1995; Sellick and Reece, 2005). These transcription factors are found to regulate target genes as monomers, homodimers or heterodimers (Cahuzac *et al.*, 2001; Mamnun *et al.*,

2002). They can also regulate transcription of target genes alone or in coordinated networks with other members of this class by binding to one or more DNA recognition sites (Kim *et al.*, 2003). Several members of this family can regulate the expression of other zinc cluster proteins or these proteins can have a self-regulation mechanism, forming a positive feedback loop (Lucau-Danila *et al.*, 2003). In order to act as transcriptional regulators, members within the $Zn(II)_2Cys_6$ family must be localised to the nucleus. They can be constitutively present in the nucleus or be initially localised in the cytoplasm and then translocated into the nucleus (MacPherson *et al.*, 2006). In general, the translocation of proteins across the nuclear membrane is mediated through binding of transport receptors to the nuclear localisation signal (NLS) present in the zinc cluster proteins (Nakielny and Dreyfuss, 1999). Usually the NLS is located within or very close to the DBD region (Nikolaev *et al.*, 2003). However, non-classical nuclear import pathways have also been described for some of these transcription factors (Nikolaev *et al.*, 2003). Activation of several zinc cluster proteins can, for instance, occur by phosphorylation or dephosphorylation event. For example, Gal4 is activated upon phosphorylation at a single serine residue (S699) (Sadwoski *et al.*, 1996). Although this phosphorylation event is required for activation, it is dispensable for Gal4 activity (Rohde *et al.*, 2000).

Most of the $Zn(II)_2Cys_6$ cluster protein studies have been carried out in *S. cerevisiae* and have provided a better understanding of these fungal transcription factors and their functions within the cell. These transcriptional regulators are known to act as repressors, activators, or as both repressors and activators for certain genes (reviewed in Turcotte *et al.*, 2004). In order to make DNA accessible and facilitate gene transcription, several zinc cluster proteins have been described that require the support of chromatin-remodelling complexes, histone-modifying enzymes, and transcriptional co-factors (MacPherson *et al.*, 2006). The zinc cluster proteins are

involved in a plethora of cellular processes: glucose/ galactose metabolism, gluconeogenesis and respiration, nitrogen metabolism, secondary metabolism, mitosis, meiosis, chromatin remodelling, stress responses, pleiotropic drug resistance (PDR), and morphogenesis (for review see MacPherson *et al.*, 2006). The majority of the $Zn(II)_2Cys_6$ transcription factors have more than one distinct role and can have overlapping functions regarding gene regulation of different subset of genes being coordinated together or at different times (Strich *et al.*, 1994; Jackson and Lopes, 1996; Cohen *et al.*, 2001; Hallstrom *et al.*, 2001).

In this Chapter, I report the temporal and spatial localisation of Tpc1 during vegetative growth and during the infection-related development of *M. oryzae*, using the Tpc1:GFP fusion vector described in Chapter 3. In *M. oryzae*, infection-related development is characterised by a series of morphogenetic stages (Dean *et al.*, 2005): germination of a polarised-growing germ tube from the conidium, appressorium formation, appressorium maturation and conidial collapse, followed by polarised growth from the base of appressorium to form a penetration peg and enter the plant. Together with hyphal extension, during these different developmental stages the expression of Tpc1 was observed in order to determine whether there is a correlation between the expression of the transcription factor and the developmental changes involving the establishment of polarity. To gain insight into whether Tpc1 transcription factor is involved in a specific or several regulatory networks such as the Pmk1 (Xu and Hamer, 1996; Park *et al.*, 2002), Mps1 (Xu et al., 1998) and Osm1 MAPK pathways (Dixon *et al.*, 1999), or the Cpka response pathway (Lee and Dean, 1993) and autophagy–related pathways (Kershaw and Talbot, 2009), Tpc1:GFP expression was analysed in these different mutant backgrounds.

PCR site-directed mutagenesis was also used to create a mutation at a defined site in a DNA molecule (Hutchison *et al.*, 1978; Storici and Resnick, 2003). A functional analysis of Tpc1 was also reported using directed mutagenesis to investigate the importance of the NLS (plus two other types of constructs with the NLS disrupted: ΔRR and ΔKK), the putative sumoylation site within the NLS, the putative phosphorylation sites (T168 and T349) and the cysteine residues within the DBD, in the function and spatial localisation of *Mo*Tpc1 in vegetative hyphae and in conidia of *M. oryzae*.

5.2. Materials and Methods

5.2.1. Cellular localisation of *Mo*Tpc1:GFP construct in wild-type Guy11 strain and different mutant backgrounds

The *Mo*Tpc1:GFP construct was cloned into pCB1532 vector (SUR^R), as described previously in Chapter 3, and then used to transform protoplasts of the wild-type strain Guy11 expressing histone1 fused with red fluorescent protein (H1:RFP) (Saunders *et al.*, 2010), *Δpmk1, Δatg1, Δatg8, Δcpka, Δmps1, Δmst12* and *Δosm1* mutants. Transformants showing identical growth and colony morphology to the background strain were selected for further examination using confocal microscopy. At least three different transformants of each were used.

5.2.2. PCR site-directed mutagenesis of *Mo*Tpc1:GFP construct

To create a mutation or deletion of a specific region of *Mo*Tpc1:GFP construct, primers were designed to contain a desired mutation or deletion (Hutchison *et al.*, 1978; Storici and Resnick, 2003). A first PCR round was used to amplify two parts of *Mo*Tpc1:GFP. To amplify *Mo*Tpc1:GFP part 1, a reverse primer was used containing the mutation or deletion desired, whereas to amplify *Mo*Tpc1:GFP part 2 the forward primer containing the specific mutation or deletion was used. A second PCR round was then used to join both fragments together using flanking primers. To obtain *Mo*Tpc1ΔNLS:GFP, *Mo*Tpc1ΔRR:GFP and *Mo*Tpc1ΔKK:GFP, primers were engineered to delete the NLS, and the two basic arginine (RR) and lysine (KK) amino acids present within the NLS. The other constructs were made in order to mutate a specific amino acid without changing the reading frame. *Mo*Tpc1_T168G:GFP, *Mo*Tpc1_T349G:GFP, *Mo*Tpc1noSUMOylation:GFP and *Mo*Tpc1noCys1/2:GFP in which the putative phosphorylation sites (Thr at position 168 and 349) changed to a Gly residue, putative sumoylation site (Lys) changed to an Ala residue and two first Cys residues of $Zn(II)_2Cys_6$ cluster domain changed to

Gly residues, respectively. Fragments were gel purified and cloned into pGEMT-easy vector and mutations confirmed by DNA sequencing. The constructs with the mutation or deletion introduced correctly were then cloned into pCB1532 (SUR^R) (Sweigard *et al.*, 1997). The resulting plasmids were used to transform protoplasts of the wild-type strain Guy11 and the M1422 mutant background. At least three transformants were selected for further examination using confocal microscopy.

5.3. Results

5.3.1. Expression and localisation of *Mo*Tpc1:GFP fusion proteins in wild-type Guy11

To determine whether Tpc1:GFP expression was restricted to specific developmental stages and specific organelles within the cell, I performed live-cell imaging of *M. oryzae* Guy11 expressing a histone H1-enhanced red fluorescent protein (H1:RFP) fusion in order to identify nuclei (Saunders *et al.*, 2010) (Fig. 5.1). The nuclei of vegetative hyphae, attached (30 min), germinated (2h) and collapsed (24h) conidia expressed *Mo*Tpc1:GFP fusion protein, co-localised with H1:RFP expression. The only developmental stage where *Mo*Tpc1:GFP was not detected in the nuclei occurred during appressorium formation and maturation (4h – 6h). Whenever Tpc1 was expressed in the nuclei, it was at a relatively low level. GFP fluorescence was never observed in the cytoplasm or other organelles within conidia.

5.3.2. Expression and localisation of *Mo*Tpc1:GFP fusion proteins in different mutant backgrounds

To investigate whether the Tpc1 transcription factor is involved in specific or multiple regulatory networks, *Mo*Tpc1:GFP expression was observed in conidia of different mutants (Fig. 5.2). In the Δ*pmk1* MAPK mutant background, *Mo*Tpc1:GFP fusion proteins were mislocalised within the conidia. Expression was detected in the cytoplasm, but not in nuclei. Interestingly, GFP fluorescence was still visible but was enhanced in the nuclei of conidia and in the cytoplasm of Δ*atg1* and Δ*atg8* autophagy-defective mutants, compared with the fluorescence observed in the wild-type Guy11. In the other mutants analysed (Δ*cpka*, Δ*mst12*, Δ*mps1* and Δ*osm1*), *Mo*Tpc1:GFP expression was not detected within conidia.

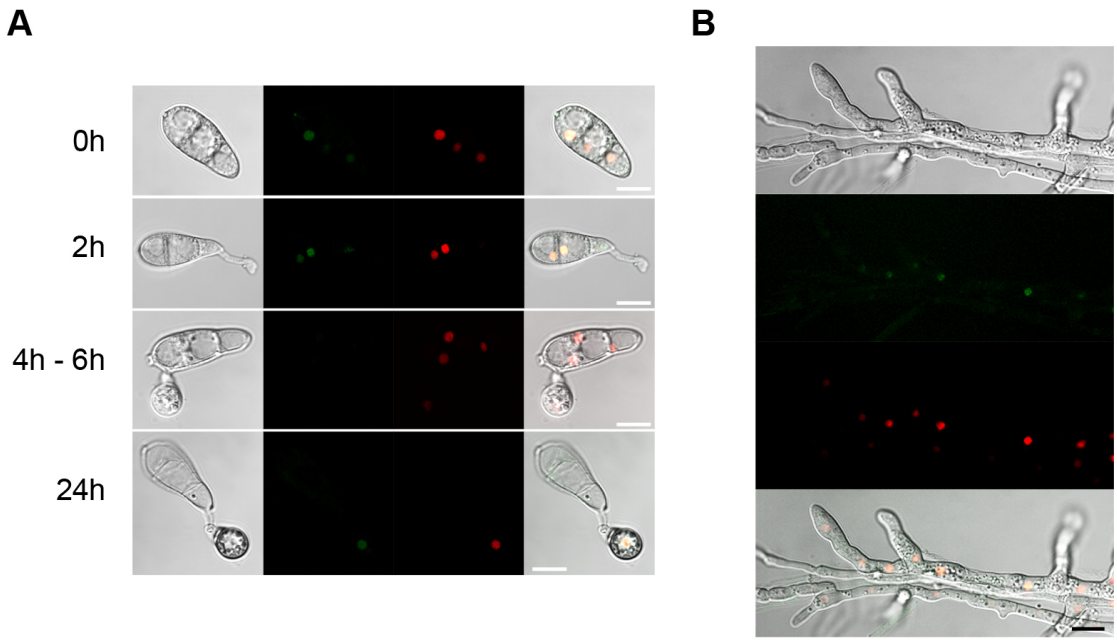

Figure 5.1. Cellular localisation of MoTpc1:GFP during infection-related development (A) and in vegetative hyphae (B) of *M. oryzae*.

(A) Conidia were harvested from a Guy11 transformant expressing H1:RFP and *Mo*Tpc1:GFP protein fusion, inoculated onto glass coverslips at 25ºC, and observed by confocal microscopy at the times indicated (Scale bar = 10 µm). **(B)** A plug of mycelium from a Guy11 transformant expressing H1:RFP and *Mo*Tpc1:GFP was inoculated onto slide covered with CM and incubated at 25ºC. Observations were made 24hpi by confocal microscopy (Scale bar = 10 µm).

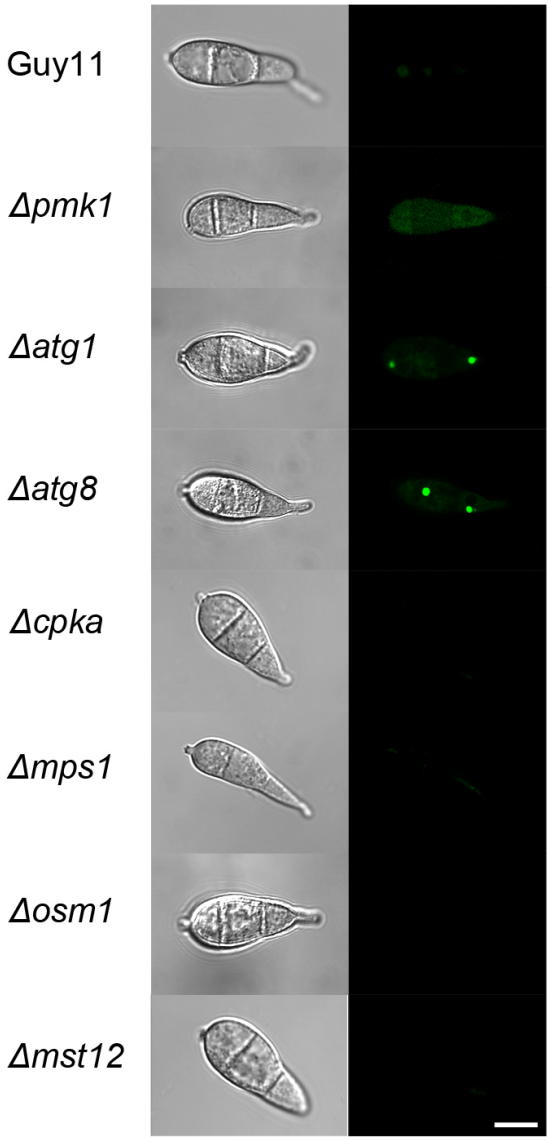

Figure 5.2. Cellular localisation *Mo*Tpc1:GFP in *Δpmk1, Δatg1, Δatg8, Δcpka, Δmps1, Δosm1* and *Δmst12* mutant backgrounds.

Conidia were harvested from the different strains expressing *Mo*Tpc1:GFP, inoculated onto borosilicate glass coverslips and observed by confocal microscopy (30 minutes). Scale bar = 10 µm.

5.3.3. Expression and localisation of mutated versions of *Mo*Tpc1:GFP fusion proteins

To explore the importance of certain regions in the expression and function of *Mo*Tpc1 protein, PCR site-directed mutagenesis technique (Hutchison *et al.*, 1978; Storici and Resnick, 2003) was applied to obtain mutated versions of the *Mo*Tpc1:GFP fusion proteins. Deletion of the entire NLS (*Mo*Tpc1ΔNLS:GFP) and two basic amino acids within the NLS (*Mo*Tpc1ΔRR:GFP and *Mo*Tpc1ΔKK:GFP) caused mislocation of the *Mo*Tpc1 protein into the cytoplasm of conidia (Fig. 5.3C). Furthermore, the *Mo*Tpc1ΔNLS:GFP and *Mo*Tpc1ΔRR:GFP protein fusion constructs did not complement the M1422 mutant (Fig. 5.3B). The ΔKK mutated version only partially complemented M1422 background to wild-type in terms of vegetative growth on CM (Fig. 5.3B). The *Mo*Tpc1noCys1/2:GFP protein fusion contains a substitution of cysteine residues into glycine residues within the DBD of $Zn(II)_2Cys_6$ domain (Fig. 5.4A). No GFP fluorescence was observed in conidia and no complementation occurred using the M1422 mutant (Fig. 5.4B and Fig. 5.4C). Post-translational modifications fine-tune the function of transcription regulators by affecting their localisation, conformation or stability (Stein *et al.*, 2009; Miura and Hasegawa, 2010). Therefore, modification of putative phosphorylation sites (*Mo*Tpc1_T168G:GFP and *Mo*Tpc1_T349G:GFP) (Fig. 5.5A) and sumoylation site within the NLS (*Mo*Tpc1noSUMOylation:GFP) (Fig. 5.3A) was performed. GFP expression of these mutated protein fusion constructs was detectable in the cytoplasm and not the nuclei of conidia (Fig. 5.3C and Fig. 5.5C). These constructs can also revert partially the reduced growth phenotype of the M1422 mutant on CM, when used to complement M1422 T-DNA background (Fig. 5.3B and Fig. 5.5B).

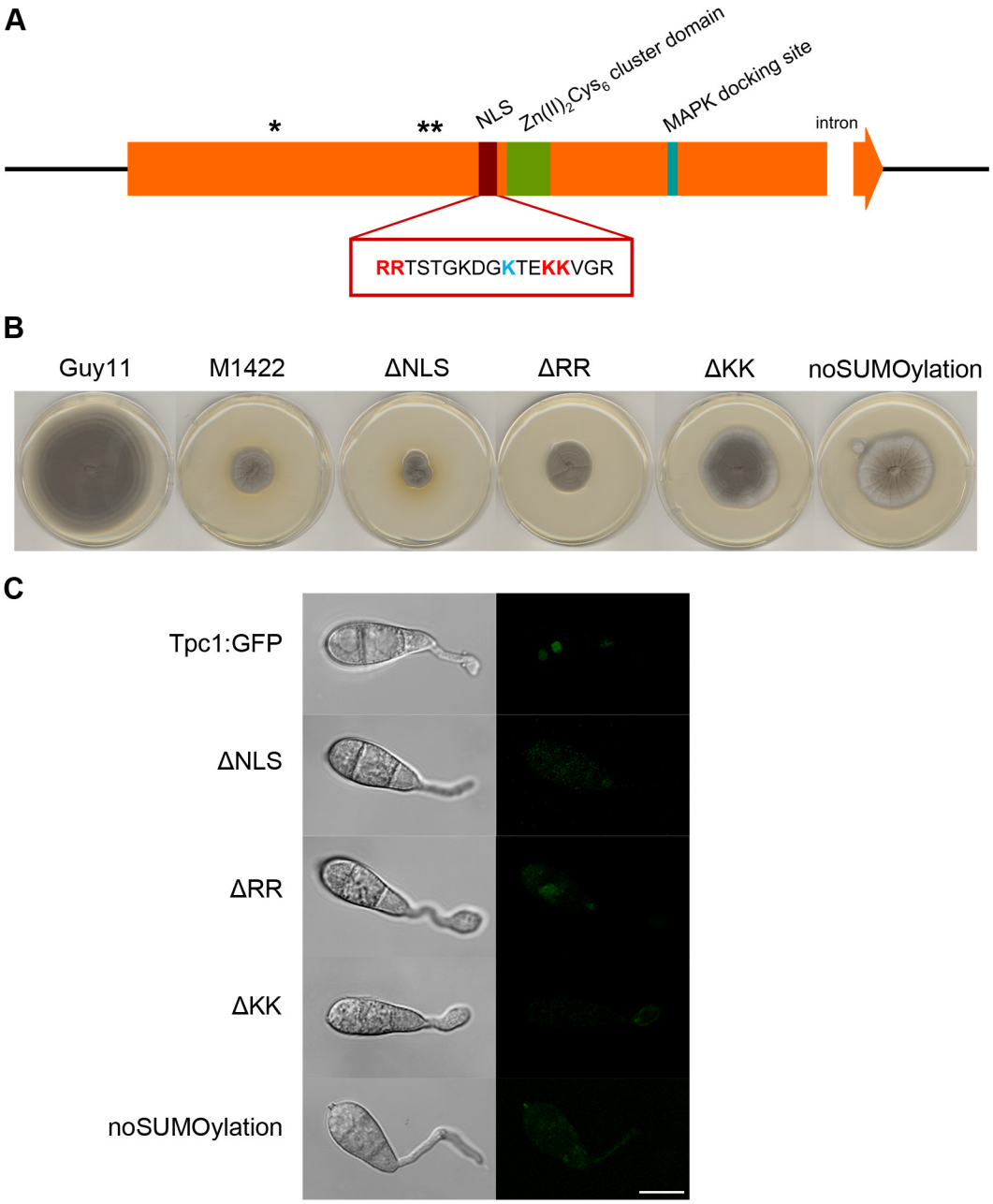

Figure 5.3. The NLS and sumoylation site are crucial for the proper function of *Mo*Tpc1.
(A) Schematic diagram showing the localisation of the NLS within *MoTPC1*. The sequence within the red box contains the NLS sequence deleted. The amino acids in red were deleted to obtain Tpc1ΔRR:GFP and Tpc1ΔKK:GFP constructs. The lysine residue in blue corresponds to the sumoylation site that was changed to an alanine residue (Tpc1noSUMOylation:GFP). **(B)** Tpc1ΔNLS:GFP, Tpc1ΔRR:GFP, Tpc1ΔKK:GFP and Tpc1noSUMOylation:GFP constructs were used to transform M1422 protoplasts. CM plates were inoculated with Guy11, M1422 and M1422 transformants complemented with different constructs. Plates were incubated at 25ºC and the colony images captured at 10 dpi. **(C)** Tpc1ΔNLS:GFP, Tpc1ΔRR:GFP, Tpc1ΔKK:GFP and Tpc1noSUMOylation:GFP constructs were used to transform Guy11 protoplasts. Conidia were harvested from the different strains expressing different constructs, inoculated onto borosilicate glass coverslips and observed by confocal microscopy (2 hpi). Scale bar = 10 µm.

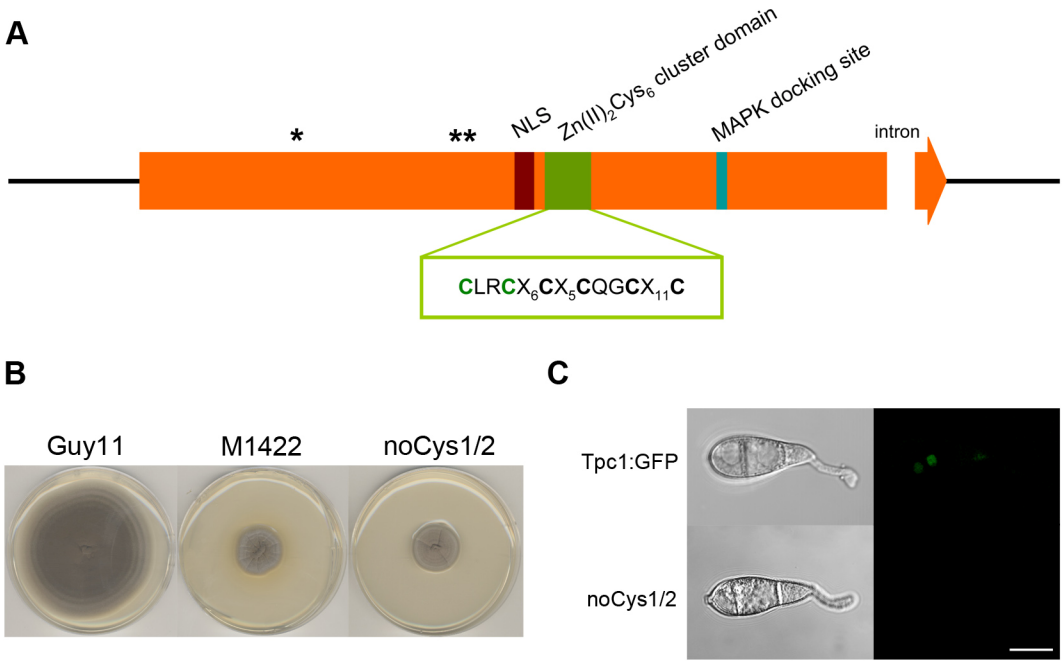

Figure 5.4. The cysteine residues within the putative $Zn(II)_2Cys_6$ are crucial for the proper function of *Mo*Tpc1.

(A) Schematic diagram showing the localisation of the $Zn(II)_2Cys_6$ cluster domain within *MoTPC1*. The amino acids in green correspond to the 2 cysteine residues that were changed to glycine residues (Tpc1noCys1/2:GFP). **(B)** Tpc1noCys1/2:GFP construct was used to transform M1422 protoplasts. CM plates were inoculated with Guy11, M1422 and M1422 transformants complemented with Tpc1noCys1/2:GFP construct. Plates were incubated at 25ºC and the colony images captured at 10 dpi. **(C)** Tpc1noCys1/2:GFP construct was used to transform Guy11 protoplasts. Conidia were harvested from the different strains, inoculated onto borosilicate glass coverslips and observed by confocal microscopy (2 hpi). Scale bar = 10 µm.

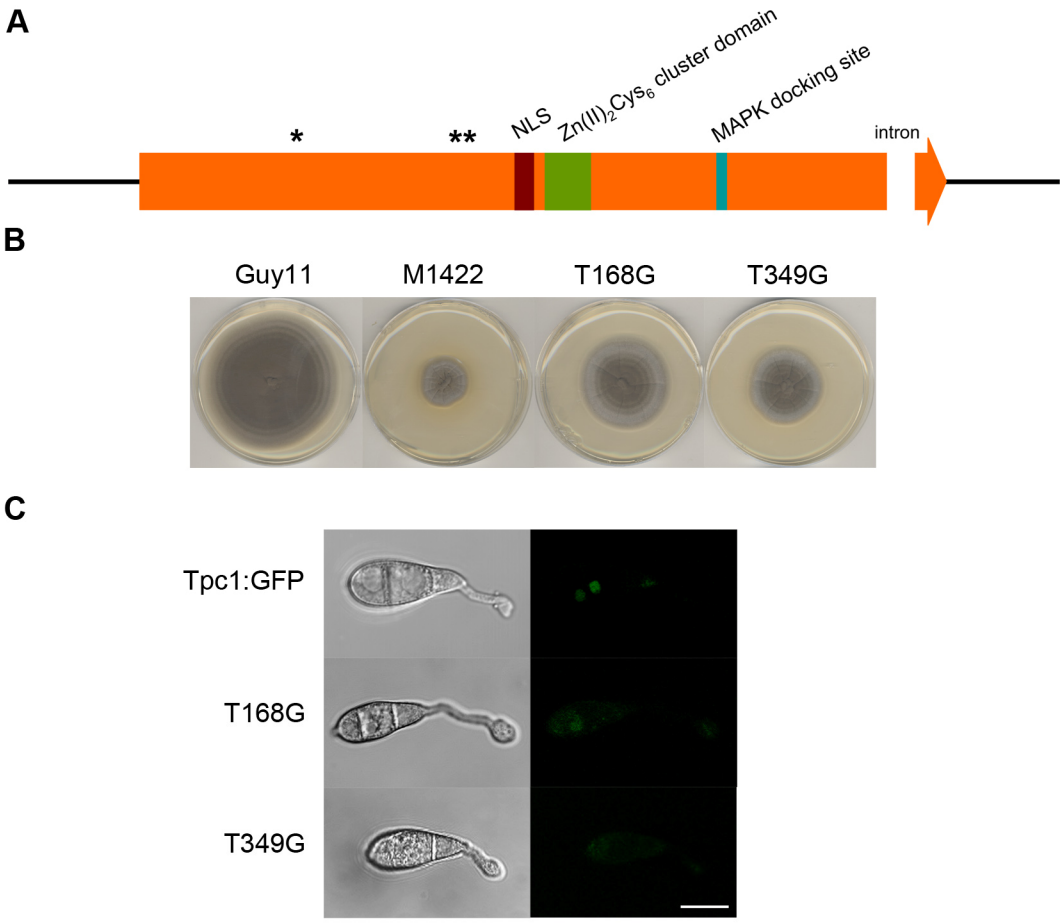

Figure 5.5. The phosphorylation residues are crucial for the proper function of *Mo*Tpc1.
(A) Schematic diagram showing the localisation of the putative phosphorylation sites within *MoTPC1*. T168 and T349 residues correspond to one and two asterisks, respectively. These threonine residues were changed to glycine residues to obtain Tpc1_T168G:GFP and Tpc1_T349G:GFP constructs. **(B)** Tpc1_T168G:GFP and Tpc1_T349G:GFP constructs were used to transform M1422 protoplasts. CM plates were inoculated with Guy11, M1422 and M1422 transformants complemented with Tpc1_T168G:GFP and Tpc1_T349G:GFP. Plates were incubated at 25ºC and the colony images captured at 10 dpi. **(C)** Tpc1_T168G:GFP and Tpc1_T349G:GFP constructs were used to transform Guy11 protoplasts. Conidia were harvested from the different strains, inoculated onto borosilicate glass coverslips and observed by confocal microscopy (2 hpi). Scale bar = 10 µm.

5.4. Discussion

To examine the expression and localisation of Tpc1 in *M. oryzae* wild-type strain Guy11, a *Mo*Tpc1:GFP fusion was generated and expressed under the control of the native Tpc1 promoter sequence. Since the M1422 T-DNA mutant expressing this fusion construct fully complemented and was able to infect rice plants and grow normally on CM, the fusion of GFP had no obvious detrimental effect on the function of Tpc1 transcription factor *in vivo* (see Chapter 3). A weak GFP signal is detectable in the nuclei of vegetative hyphae and conidia (Fig. 5.1). During germination of germ tube, the fluorescence of Tpc1:GFP fusion protein is observed in the three nuclei of the developing conidium. During appressorium formation, when one nucleus migrates into the developing germ tube and undergoes mitosis (4-nuclei stage), no expression of Tpc1:GFP was observed. However, the expression of Tpc1:GFP was observed in the single nucleus present in the appressorium, after conidial collapse. The Tpc1:GFP expression pattern seems therefore to be correlated with establishment of polarity. Vegetative hyphae, attached and germinated conidia display apical dominance, whereby the growing tip of these structures expands apically and suppresses growth in its vicinity (Bourett and Howard, 1990; Harris *et al.*, 2005, Harris, 2008). The formation and maturation of appressorium is under isotropic growth, where enormous turgor pressure is generated in all directions of the appressorium by an increase in intracellular glycerol levels (Howard *et al.*, 1991). During isotropic appressorial growth stage, no expression of Tpc1:GFP is observed within the nuclei (Fig. 5.1). After conidial collapse, polarised growth is initiated to form a penetration peg at the base of appressorium (Bourett and Howard, 1990). This result is concomitant with the re-expression of Tpc1 within the appressorial nucleus (Fig. 5.1). Therefore, Tpc1 may be involved in re-establishing polarised growth and in the clustering or trafficking of polarity factors involved in the generation of positional signals.

To determine if Tpc1 transcription factor is involved in one specific or several regulatory networks, the cellular localisation of this protein was observed in different mutant backgrounds. Analysis of the cellular localisation pattern of Tpc1:GFP in *Δpmk1* mutants shows that Tpc1 zinc cluster protein is mislocalised in the cytoplasm of conidia (Fig. 5.2). The lack of nuclear localisation of Tpc1:GFP fusion protein in *Δpmk1* mutant background indicates that translocation of Tpc1 into the nucleus must occur through Pmk1 MAPK. Several activated MAPKs are known to phosphorylate transcription factors and other signaling components and can induce their relocalisation within the cell, triggering an appropriate cellular response to the stimulus. (Qi and Elion, 2005). *ATG1* and *ATG8* genes are involved in fungal autophagy and encode a Ser/Thr kinase protein and ubiquitin-like protein involved in the autophagosome expansion, respectively (Veneault-Fourrey *et al.*, 2006*a*; Liu *et al.*, 2007; Kershaw and Talbot, 2009). Although Tpc1:GFP localises in the cytoplasm and in the nuclei of *Δatg1* and *Δatg8* conidia, its expression is strong (Fig. 5.2). By contrast, Tpc1 is expressed at a relatively low level in the nuclei of wild-type strain Guy11. Autophagy is a process responsible for the turnover of damaged proteins and organelles and is crucial for differentiation, development, pathogenesis and other fundamental biological processes (Nakatogawa *et al.*, 2009; Talbot and Kershaw, 2009). Results indicate that Tpc1 is a target protein substrate for proteasomal degradation, probably regulated by a feedback loop between Tpc1 expression levels and autophagy-related proteins (see also Chapter 4). GFP signals were not observed in the conidia of *Δcpka*, *Δmst12* transcription factor regulated by *PMK1*, *Δmps1* and *Δosm1* MAPKs deleted mutants (Fig. 5.2). These data indicate that Tpc1:GFP is not expressed or is expressed at lower levels in these mutant backgrounds. To investigate this further, reverse transcription quantitative polymerase chain reaction (qRT-PCR) analysis of *TPC1* in *Δcpka*, *Δmst12*, *Δmps1* and *Δosm1* mutants should be carried out in future. This technique is extremely sensitive and reliable for quantifying gene transcripts (Nolan *et al.*, 2005).

The Tpc1 transcription factor is therefore highly connected to a plethora of cellular signalling pathways, being involved in different regulatory networks and regulating the expression of different genes.

All proteins found in the nucleus are synthesised in the cytoplasm and then actively imported into the nucleus through the nuclear pore complex (NPC). Therefore, these proteins must have a nuclear localisation signal (NLS) (Cole and Hammell, 1998). These include nucleus-restricted proteins such as histones and transcription factors. Experiments suggested that *Mo*Tpc1 zinc cluster transcription factor is actively imported into the nucleus. Two lines of evidence supported this: 1) Tpc1 is expressed in the nuclei of vegetative hyphae, conidia during germination, and after conidial collapse (Fig. 5.1); 2) mutated versions of the NLS of Tpc1 (ΔNLS, ΔRR and ΔKK) result in accumulation of Tpc1 protein in the cytoplasm (Fig. 5.3C). Similar studies were carried out to analyse the nuclear localisation of the simian virus 40 (SV40) large T-antigen proteins and the importance of NLS in the translocation of these proteins into the nucleus (reviewed in Lodish *et al.*, 2000). The *Mo*Tpc1ΔNLS:GFP, *Mo*Tpc1ΔRR:GFP constructs were not able to restore normal vegetative growth and colonial morphology in M1422 background (Fig. 5.3B). The other mutated version of NLS, *Mo*Tpc1ΔKK:GFP, complemented the reduced colonial morphology phenotype present in the M1422 mutant partially (Fig. 5.3B). Although *Mo*Tpc1ΔKK:GFP was expressed in the cytoplasm of the conidia, most probably leaking and import of these mutated proteins was occurring into the nucleus. This may explain the less dramatic colonial phenotype, and the fact that the normal wild-type vegetative growth was not fully restored when complemented with *Mo*Tpc1ΔKK:GFP. When considered together, these results suggest that for the proper function of Tpc1 protein, its nuclear localisation is essential. Other studies demonstrated the same principle (Hahn *et al.*, 2008). It can also be assumed that

Tpc1 is not acting as a shuttling protein like ribonucleoproteins, due to the lack of a clear nuclear export signal (NES) within its sequence (Lodish *et al.*, 2000).

As other members of the $Zn(II)_2Cys_6$ cluster family, Tpc1 contains a cysteine rich-DBD region (Schjerling and Holmberg, 1996). Modification of two of the six cysteine residues within the zinc finger had dramatic effects on the structure and activity of Tpc1 (Fig. 5.4). No expression of Tpc1:GFP was observed within conidia examined and this mutated version of Tpc1 (*Mo*Tpc1noCys1/2:GFP) did not complement the M1422 T-DNA mutant. The wild-type phenotype was not restored after complementation, with the colonies displaying the compact colony growth phenotype. Mutagenic studies of the cysteine residues in other fungal $Zn(II)_2Cys_6$ proteins (Leu3, Hap1, AmdR, Ume6, Nit-4, Gal4 and FacB) also demonstrated the significance of these residues in DNA-binding and protein function (Johnston and Dover, 1987; Pfeifer *et al.*, 1989; Bai and Kohlhaw, 1991; Yuan *et al.*, 1991; Parsons *et al.*, 1992; Defranoux *et al.*, 1994; Strich *et al.*, 1994; Todd *et al.*, 1997). In addition, by changing cysteines to glycine residues, the zinc ions are not able to be bound and bridge the structure induced by the six cysteine residues (Pan and Coleman, 1990; Gardner *et al.*, 1991). The requirement of zinc ions is evident by the stabilisation of protein folding and function of these transcription factors (MacPherson *et al.*, 2006).

Post-translational modifications such as sumoylation and phosphorylation are crucial to alter the activity, life-span, or cellular location of proteins (Stein *et al.*, 2009; Miura and Hasegawa, 2010). These modifications allow the mediation of complex hierarchical regulatory networks and are involved in numerous cellular and developmental processes (Stein *et al.*, 2009; Miura and Hasegawa, 2010). Sumoylation is an ubiquitin-like protein (UBL) conjugation process, where small ubiquitin-related modifier (SUMO) conjugates reversibly through linkage to the lysine residue in the conserved sumoylation motif of the target protein (Kerscher *et al.*,

2006). Remarkably, the *Mo*Tpc1 protein has a putative sumoylation site within the NLS (Fig. 5.3A). Changing the acceptor lysine residue into an alanine residue resulted in an altered cellular localisation of Tpc1. The protein accumulated in the cytoplasm, instead of the nuclei of the conidia (Fig. 5.3C). The *Mo*Tpc1noSUMOylation:GFP construct did not fully complemented the colonial morphology observed in the M1422 T-DNA mutant to the wild-type parameters (Fig. 5.3B). Two questions can be raised by these results: 1) the lysine/ alanine substitution has an effect in the function of the NLS, as seen with ΔNLS, ΔRR and ΔKK construct versions; or, 2) the lysine mutated is a genuine sumoylation site. Recently, sumoylation sites within the NLS of several proteins such as Daxx, Rad52, Pap have been characterised, showing its significance in the protein function and translocation into the nucleus (Chen *et al.*, 2006; Ohuchi *et al.*, 2008; Vethantham *et al.*, 2008). Current models assume that sumoylation regulates gene expression through chromatin remodelling, interfering positively or negatively between the target and partner proteins interaction, and/or through sub-nuclear compartmentalisation of transcriptional co-regulators (Miura and Hasegawa, 2010). Whether the Tpc1 zinc cluster protein is involved in transcriptional regulation through one or more of the mechanisms described above is unknown. However, considering the diverse expression data of *Mo*Tpc1 in different mutant backgrounds and the pleiotropic phenotypes that M1422 mutant displays, this issue needs to be further investigated to understand the function of this transcription factor in these regulatory networks.

The internal threonine, serine and tyrosine residues in proteins can be modified by attachment of phosphate groups to their side chains (Stein *et al.*, 2009). In *Mo*Tpc1 case, two putative phosphorylation sites (T168 and T349) were identified (Fig. 5.5A). Modification of these threonine residues to glycine residues resulted also in the accumulation of Tpc1 in the cytoplasm (Fig. 5.5C). The M1422 mutant complemented with *Mo*Tpc1_T168G:GFP or *Mo*Tpc1_T349G:GFP fusion proteins

were still slightly impaired in colonial growth (Fig. 5.5B). These threonine residues may therefore be functional phosphorylation sites recognised by protein kinases (*eg.* Pmk1). It is known that reversible phosphorylation and dephosphorylation processes can regulate the activity of many proteins and play a crucial role in signal transduction pathways and control other biological processes such as cell growth and differentiation (Stein *et al.*, 2009). Further identification of which protein kinases are involved in the phosphorylation of these residues could give more support to the data examined so far.

CHAPTER 6

Phylogenetic analysis of Tpc1 protein

6.1. Introduction

The $Zn(II)_2Cys_6$ binuclear cluster DNA binding domain is exclusively found in fungal proteins (MacPherson *et al.*, 2006). In general, the 6 cysteine residues are arranged in a $CX_2CX_6CX_{5-12}CX_2CX_{6-8}C$ manner. The cysteine residues bond to 2 zinc atoms, which coordinate correct folding of the domain involved in DNA binding and function of the protein (Gardner *et al.*, 1991). The first zinc cluster protein characterised was the *S. cerevisiae* Gal4 protein (Johnston, 1987). The $Zn(II)_2Cys_6$ cluster proteins are also found in many other ascomycetes: *Schizosaccharomyces*, *Aspergillus*, *Kluyveromyces*, *Neurospora*, *Candida*, *Pichia*, *Cochliobolus* and *Magnaporthe* species, suggesting that this motif is probably used throughout the *Ascomycota* phylum (MacPherson *et al.*, 2006). So far, only one $Zn(II)_2Cys_6$ protein has been identified in the basidiomycete *Lentinus edodes* (Endo *et al.*, 1994). This fact implies that the $Zn(II)_2Cys_6$ zinc cluster motif may have arisen prior to the divergence of these two major groups, *Ascomycota* and *Basidiomycota*. However, the list of zinc cluster proteins will grow with the sequencing of other fungal genomes, which will allow the identification and characterisation of more transcription factors within this family.

DNA-binding domains of a particular class generally bind similar DNA target sequences (Suzuki *et al.*, 1994). To date, only one zinc cluster protein, Pig1 (MGG_07215), has been characterised in *M. oryzae* (Tsuji *et al.*, 2000). This protein is a transcription factor involved in melanin biosynthesis. The pathogenicity-defective Δ*pig1* mutant produces melanin in the appressorium, but not in vegetative hyphae (Tsuji *et al.*, 2000). However, phylogenetic analyses of the $Zn(II)_2Cys_6$ region from known proteins of *Saccharomyces*, *Aspergillus*, *Kluyveromyces* and *Neurospora,* show that $Zn(II)_2Cys_6$ proteins with similar functions cluster together and are more closely related, even from different species

(Todd and Andrianopoulos, 1997) . Thus, comparison of previous characterised zinc cluster transcription factors in one species with unknown zinc cluster proteins in another species can help in the identification of potential targets and function.

Even though the filamentous ascomycete *N. crassa* is a free living saprotroph, it is a close relative of *M. oryzae*. These two fungal species are estimated to have evolved from a common ancestor 50 to 150 million years ago and share about 60% of their genes (Borkovich *et al.*, 2004). An open question regarding their common ancestor persists. Whether it was a plant pathogen, a saprophyte or a non-pathogenic symbiont is still uncertain (Berbee, 2001), but the availability of additional fungal genome sequences may allow this question to be addressed. The presence of gene homologues in *N. crassa* encoding secondary metabolites and virulence factors in common with those of plant pathogens suggests that the lineage leading to *Neurospora* is likely to have lost its ancestral ability to infect plants, as the lineage leading to *Magnaporthe* has gained parasitism (Galagan *et al.*, 2003). The genome sequence of *N. crassa* also reveals that there are a very large number of shared genes with no homologues in the yeast *S. cerevisiae*, making *Neurospora* a better model for understanding the biology of filamentous fungi.

Previous analysis of the *N. crassa* genome has provided evidence that the $Zn(II)_2Cys_6$ binuclear cluster family is the largest class of transcription factors present (Borkovich *et al.*, 2004; Cornell *et al.*, 2007). We were intrigued by the fact that the zinc cluster family is strictly fungal in distribution and diverse, but that little is known about the members and function of these transcription factors in *Magnaporthe*. In this chapter, I dissect the $Zn(II)_2Cys_6$ binuclear cluster family in *Magnaporthe* and the phylogenetic relationship of *Mo*Tpc1 with other *Magnaporthe* proteins. To gain insight into putative functions for *Mo*Tpc1 protein, I have analysed whether there has been evolutionary recruitment of this gene by other fungi. I

decided to explore the conservation of *Mo*Tpc1 function by characterising the homologous gene in *N. crassa*. In this way, I aimed to be able to define the broader biological function of this clan of transcription factors in developmental biology of fungi.

6.2. Materials and Methods

6.2.1. Phylogenetic analysis

The *M. oryzae* protein sequences containing a fungal $Zn(II)_2Cys_6$ binuclear cluster domain (PF00172) were identified from the *Magnaporthe* sequence database at the BROAD Institute (http://www.broadinstitute.org/annotation/fungi/magnaporthe). HMMsearch (Eddy, 1998) was used to screen the genome assembly of *M. oryzae* proteins with the PFAM (Finn *et al.*, 2010) profile hidden Markov model (pHMM) zn_clus_ls.hmm (http://pfam.sanger.ac.uk/). Basic Local Alignment Search Tool (BLAST) was used to find orthologous proteins of MGG_01285 (http://blast.ncbi.nlm.nih.gov/Blast.cgi). Protein sequences were pre-aligned using HMMalign and the pHMM zn_clus_ls.hmm (Fig. 6.1) from PFAM. The $Zn(II)_2Cys_6$ binuclear cluster domain region was extensively manually aligned in BioEdit (http://www.mbio.ncsu.edu/BioEdit/BioEdit.html). Unambiguous aligned positions were used for the subsequent phylogenetic analyses. The maximum likelihood (ML) analyses were performed with the program PhyML version 3.0.1 (Guindon and Gascuel, 2003). All trees were visualised using the program Figtree (http://tree.bio.ed.ac.uk/software/figtree/).

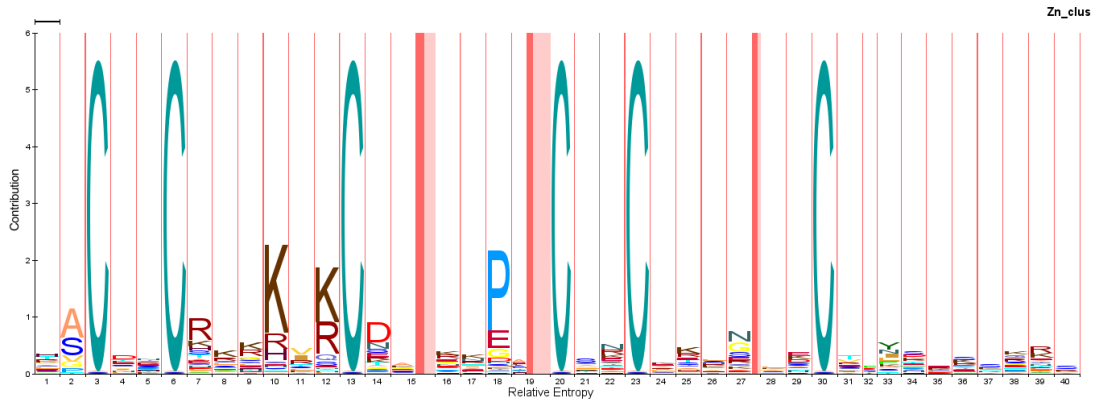

Figure 6.1. HMM pattern for $Zn(II)_2Cys_6$ binuclear cluster (zn_clus) protein family.

The HMM pattern is a graphical representation of a probabilistic model to represent sequence families (Schuster-Böckler *et al.*, 2004). The $Zn(II)_2Cys_6$ cluster protein family is characterised by 6 cysteine residues arranged as the motif $CX_2CX_6CX_{5-12}CX_2CX_{6-8}C$ that bind to 2 zinc atoms.

6.3. Results

6.3.1. Phylogenetic analysis of *Mo*Tpc1 within the *M. oryzae* genome and between fungal species

Understanding how in evolutionary terms the zinc cluster family has evolved within the *M. oryzae* genome and in other fungal genomes can provide insight into the potential function and targets of the *Mo*Tpc1 protein. For that purpose I analysed the *M. oryzae* protein sequences containing a fungal $Zn(II)_2Cys_6$ binuclear cluster domain (Fig. 6.2) and the closest orthologues of *Mo*Tpc1 in other fungal species (Fig. 6.3).

In *M. oryzae*, the $Zn(II)_2Cys_6$ binuclear cluster family is very diverse and is composed by 119 members (Fig. 6.2). The *Mo*Tpc1 protein (MGG_01285) is a single copy gene and has no paralogues in the *M. oryzae* genome.

The 22 closest orthologous proteins of *Mo*Tpc1 protein clustered in a group with other fungal Tpc1-like proteins that belong to the same phylogenetic class (Sordariomycetes, Dothideomycetes, Leotiomycetes and Eurotiomycetes) (Fig. 6.3). Therefore, *Mo*Tpc1 clustered in a group with other Sordariomycetes such as *Fusarium graminearum, N. crassa, Chaetomium globosum* and *Podospora anserina*. There was no relationship between these orthologous groups and lifestyle of the fungi analysed. For example, *Nc*Tpc1 and *Mo*Tpc1 proteins were clustered within the same group, even though *N. crassa* is a saprophyte and *M. oryzae* a plant pathogen. As observed in *Magnaporthe* genome, there was only a single copy of Tpc1-like protein in each fungal genome analysed. Interestingly, there was no putative *S. cerevisiae* or *S. pombe* orthologue of *Mo*Tpc1.

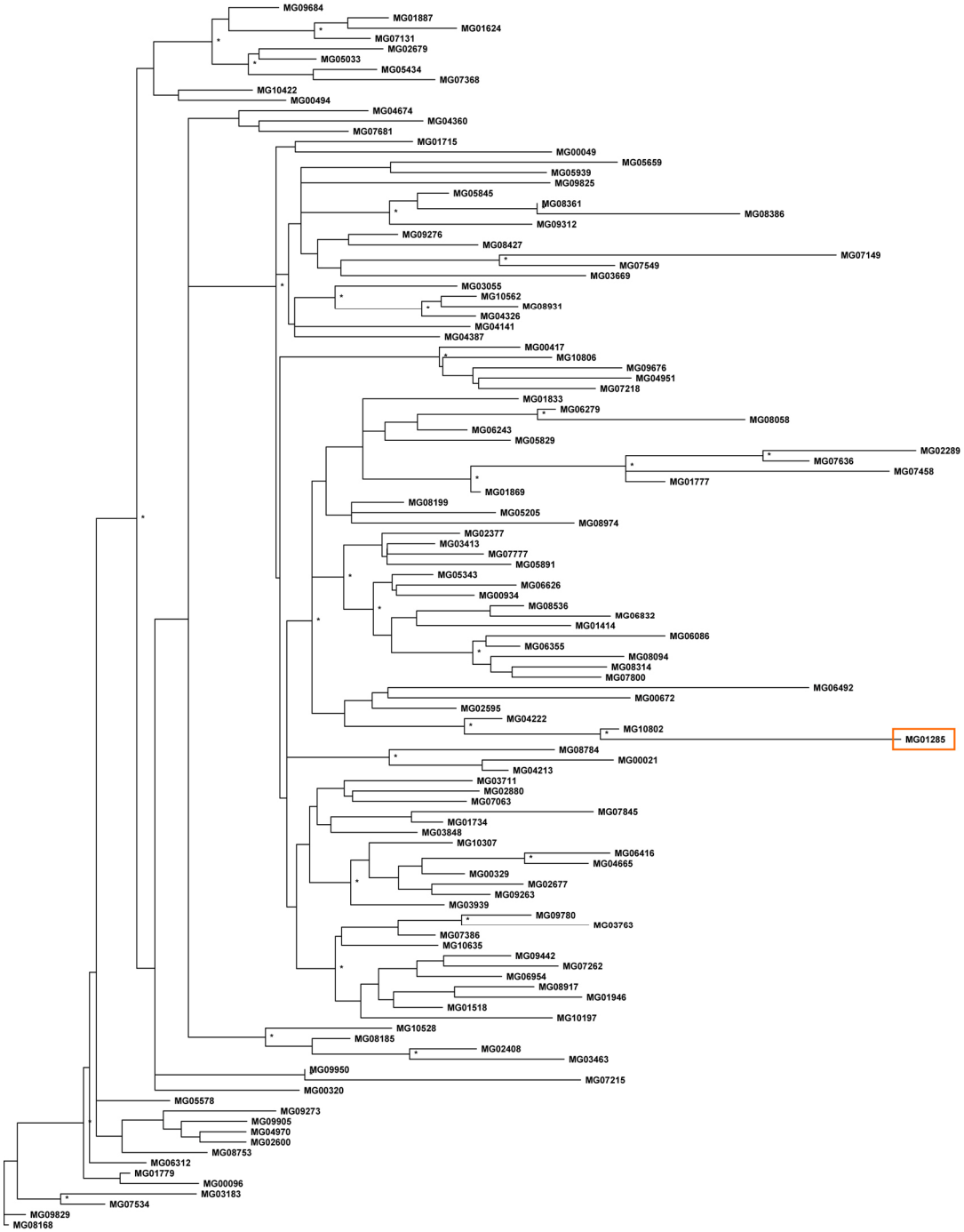

Figure 6.2. Maximum likelihood tree of *M. oryzae* Zn(II)$_2$Cys$_6$ cluster proteins.

Proteins containing Zn(II)$_2$Cys$_6$ domain were identified in the *Magnaporthe* database using PFAM pHMM zn_clus_ls.hmm. The unrooted phylogenetic tree was constructed using an aligment of 119 zinc cluster *M. oryzae* sequences. The orange box indicates *Mo*Tpc1 protein (MGG_01285). Asterisks in the clades denote high LRT support values (* LRT > 80%).

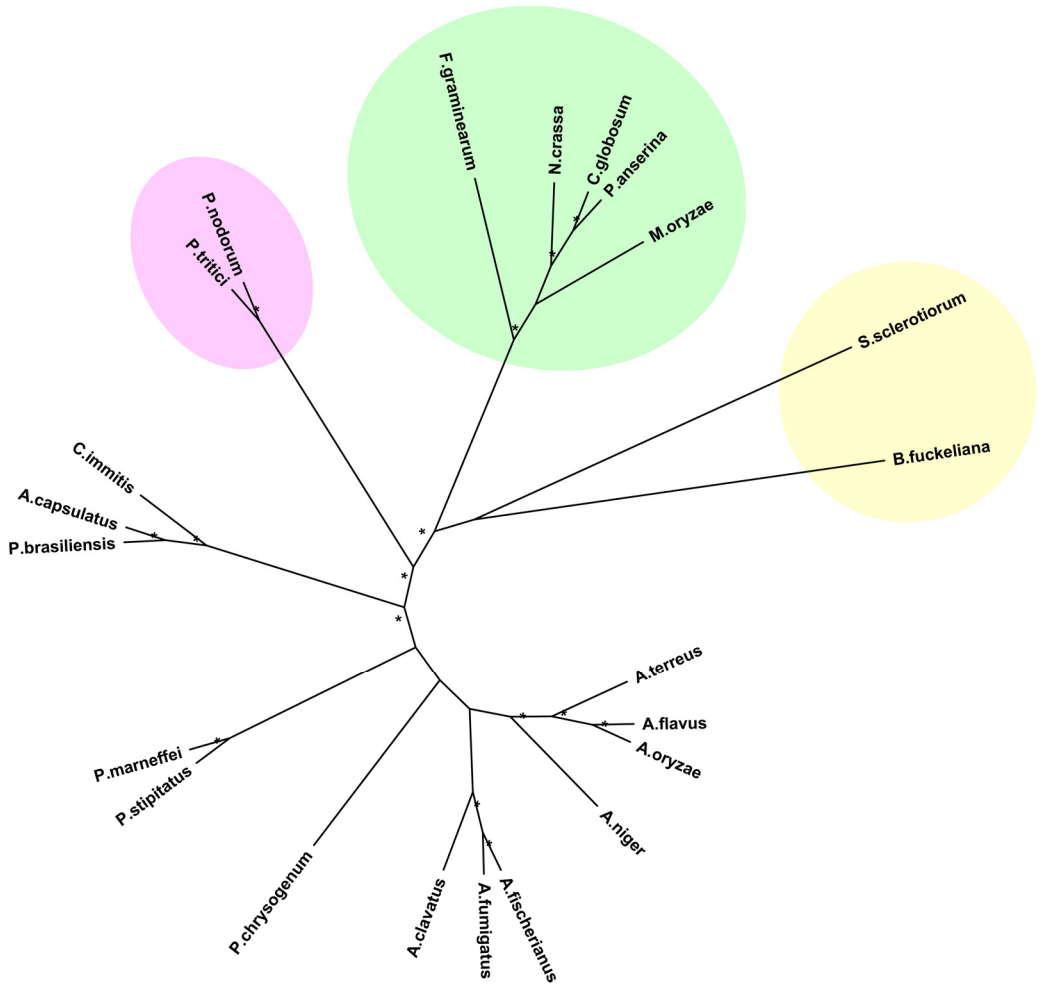

Figure 6.3. Maximum likelihood tree of *M. oryzae* Tpc1 protein (MGG_01285) with its closest fungal orthologues.

Orthologous proteins of MGG_01285 were identified using BLAST and aligned manually in BioEdit program. This unrooted phylogenetic tree was constructed using an aligment of 22 fungal sequences from different fungal species: *Ajellomyces capsulatus* (EH07230.1), *Aspergillus clavatus* (XP_001271908.1), *Aspergillus fischerianus* (XP_001266982.1), *Aspergillus flavus* (EED55362.1), *Aspergillus fumigatus* (XP_751792.1), *Aspergillus niger* (An04g06640), *Aspergillus oryzae* (XP_001820273.1), *Aspergillus terreus* (XP_001210781.1), *Botryotinia fuckeliana* (BC1G_06121), *Chaetomium globosum* (CHGG_09110), *Coccidioides immitis* (CIMG_00566), *Fusarium graminearum* (FG08769.1), *Neurospora crassa* (NCU05996), *Magnaporthe oryzae* (MGG_01285), *Podospora anserina* (XP_001906056.1), *Paracoccidioides brasiliensis* (EEH45457.1), *Penicillium chrysogenum* (Pc22g12400), *Penicillium marneffei* (XP_002151174.1), *Phaeosphaeria nodorum* (SNOG_06665), *Penicillium stipitatus* (EED24478.1), *Pyrenophora tritici* (XP_001931826.1), *Sclerotinia sclerotiorum* (SS1G_00170). Fungal species within a pink, green and yellow balloon belong to the Dothideomycetes, Sordariomycetes and Leotiomycetes classes, respectively. The other species belong to Eurotiomycetes (*Ajellomyces*, *Aspergillus, Paracoccidioides* and *Penicillium* species) and Euascomycetes (*Coccidioides*) classes. Asterisks in the clades denote high LRT support values (* LRT > 80%).

6.3.2. Characterisation of *N. crassa* Tpc1 protein

The analysis of the alignment of *Mo*Tpc1 (MGG_01285) and *Nc*Tpc1 (NCU05996) proteins showed that they share 67% amino acid identity (Fig. 6.4). The N-terminus of these proteins presented a lower degree of similarity (46%), whereas the C-terminus (between 423 – 878 amino acid positions in the alignment) was 86% similar. This region included a putative nuclear localisation signal (NLS), a $Zn(II)_2Cys_6$ binuclear cluster DNA binding domain and a MAPK docking site. The two putative phosphorylation sites and the sumoylation site within the NLS present in *Mo*Tpc1 protein were absent in the *Nc*Tpc1 protein.

6.3.3. Characterisation of *N. crassa TPC1* KO

In order to gain insight regarding the putative function and targets of *Mo*Tpc1, a *N. crassa TPC1* KO mutant strain was ordered from the FGSC for further characterisation. This *N. crassa* mutant has no been described in the literature. *NcTPC1* KO mutant was severely reduced in vegetative growth compared with WT ($p < 0.01$) (Fig. 6.5 and Fig. 6.6). After 24 hpi in Vogel's media, the colony diameter of the *N. crassa* WT and *NcTPC1* KO mutant were 8.46 ± 0.11 cm and 2.23 ± -.30 cm (ratio 4:1), respectively (Fig. 6.6 and Fig. 6.7). The vegetative hyphae of the mutant also branched in a different manner. In the *N. crassa* WT, the branching occurred in the sub-apical region of the vegetative hyphae. However, vegetative hyphae of *NcTPC1* KO mutant branched randomly along the vegetative hyphae and the spacing between these branching points did not match the spacing observed in the WT.

In Chapter 4, it was observed that the *M. oryzae* M1422 mutant was resistant to high concentrations of NaCl (0.2M and 0.8M). However, in the Δ*tpc1* mutant of *N. crassa* an osmotic-resistance *plateau* of growth did not occur in high concentrations of NaCl (Fig. 6.7). The vegetative growth of *NcTPC1* KO was also severely affected when

exposed to increasing osmotic stress, compared with *N. crassa* wild-type ($p < 0.01$) (Fig. 6.6 and Fig. 6.7).

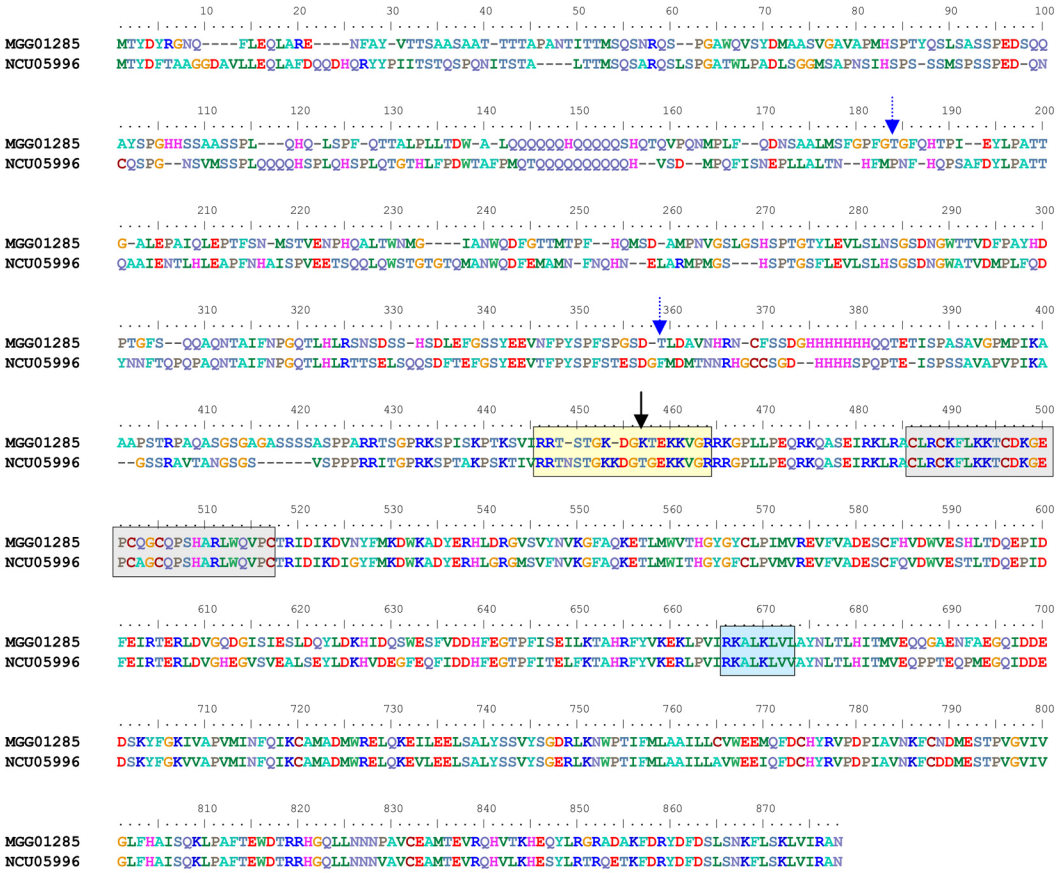

Figure 6.4. Alignment of the *M. oryzae Mo*Tpc1 protein with its closest orthologous in *N. crassa, Nc*Tpc1.

The sequenced *M. oryzae Mo*Tpc1 (MGG_01285) gene product was aligned with *Nc*Tpc1-like protein (NCU05996) from *N. crassa* genome. Sequences were aligned using BioEdit program. Amino acid residues within an yellow, grey and blue boxes correspond to the nuclear localisation signal (NLS), $Zn(II)_2Cys_6$ cluster domain and MAPK docking site, respectively. The blue dashed arrows indicate the putative phosphorylation sites (threonine residues), while the black arrow indicates the putative sumoylation site (lysine residue) present in the *Mo*Tpc1.

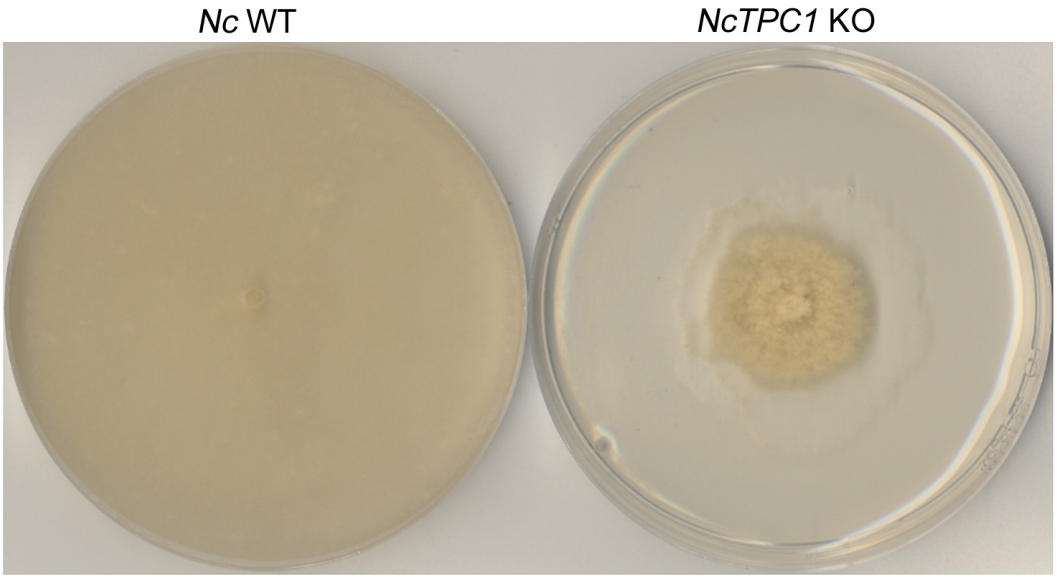

Figure 6.5. Vegetative growth and colony morphology of *NcTPC1* deletion mutant.
Vogel plates were inoculated with 5 mm plugs of mycelium from *N. crassa* WT and *NcTPC1* KO strains. Plates were incubated at 25ºC for 2 days. The *NcTPC1* KO mutant colony was severely reduced in vegetative growth and the branching of the vegetative hyphae was different to that observed for the isogenic *N. crassa* WT strain.

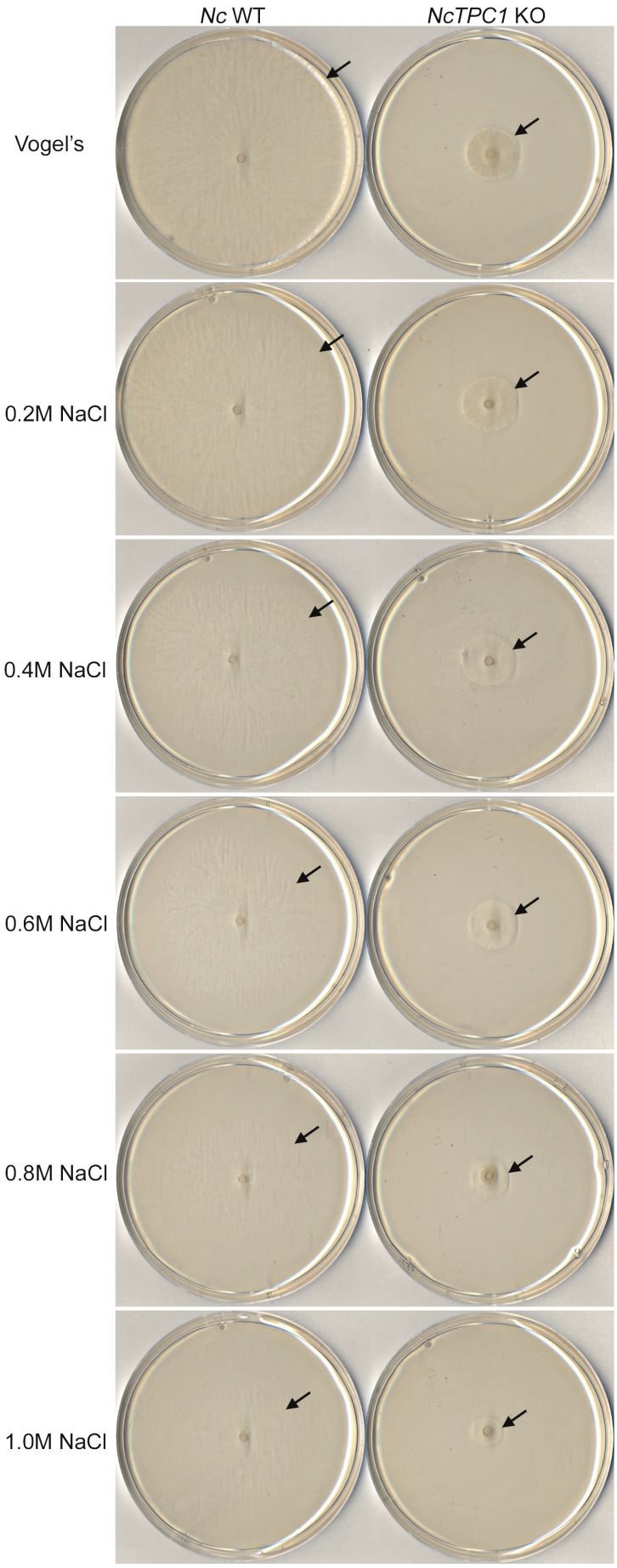
Nc WT
NcTPC1 KO
Vogel's
0.2M NaCl
0.4M NaCl
0.6M NaCl
0.8M NaCl
1.0M NaCl

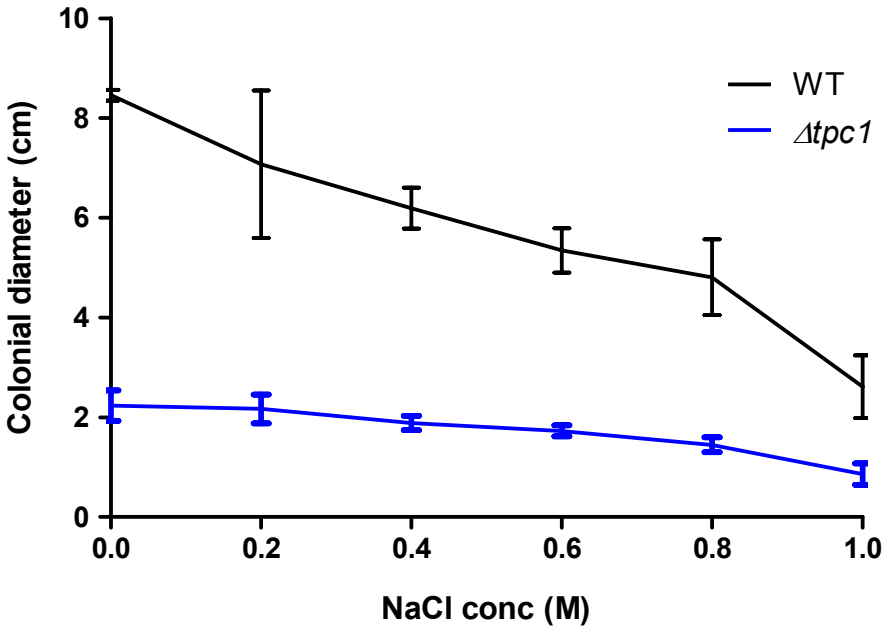

Figure 6.7. Vegetative growth phenotype of *NcTPC1* deletion mutant after exposure to increasing concentration of NaCl.

Vogel plates were inoculated with 5 mm plugs of mycelium from *N. crassa* WT and *NcTPC1* KO strains. Plates were incubated at 25ºC and the diameter of the subsequent colonies measured after 24h. Error bars represent standard deviation of three independent replications of the experiment.

(previous page)

Figure 6.6. Vegetative growth and colony morphology of *NcTPC1* deletion mutant under NaCl osmotic stress.

Vogel plates were inoculated with 5 mm plugs of mycelium from *N. crassa* WT and *NcTPC1* KO strains. Plates were incubated at 25ºC for 1 day. The *NcTPC1* KO mutant and WT colonies grew slower with increasing NaCl concentrations. The branching of the vegetative hyphae of *NcTPC1* mutant was different than that observed for the WT. Arrows indicate the edge of the colony.

6.4. Discussion

The $Zn(II)_2Cys_6$ binuclear cluster proteins are a class of transcription factors unique to fungi (Todd and Andrianopoulos, 1997). A better understanding of the function and targets of Tpc1 transcription factor was attempted by investigating the evolutionary relationships of Tpc1 homologues in different fungi. The *NcTPC1* KO mutant was also characterised during this study. The choice of the multicellular filamentous fungus *N. crassa* relied on the fact that it possesses a large number of genes without homologues in *S. cerevisiae*, suggesting that *N. crassa* is a better model to study fundamental biological processes in higher eukaryotes (Borkovich *et al.*, 2004; Cornell *et al.*, 2007). The presence of homologues within the *Neurospora* genome with highly diversified plant pathogens and other specialised fungi of narrow habitat, also offers a starting point for comparison with these pathogens such as *Magnaporthe* (Borkovich *et al.*, 2004).

Interestingly, one of the largest classes of transcription factors in *Neurospora* (90 proteins) and *Magnaporthe* (119 proteins) belongs to the $Zn(II)_2Cys_6$ fungal binuclear cluster family (Cornell *et al.*, 2007). Compared with *Saccharomyces* species (52 proteins), *N. crassa* and *M. oryzae* possess almost twice as many proteins that contain this motif and some of them have no match with yeast zinc cluster proteins seen in Tpc1. Being that this family is closely associated with regulation of gene expression, it has probably expanded along with the evolution of multicellularity and adaptation to environment/ lifestyle (Cornell *et al.*, 2007). Additionally, the $Zn(II)_2Cys_6$ binuclear cluster family has been linked to the regulation of secondary metabolism clusters. Production of aflatoxin (Flaherty and Payne, 1997), fumonisin (Brown *et al.*, 2007), and the *ACE1* cluster-derived secondary metabolites (Collemare *et al.*, 2008) is regulated by $Zn(II)_2Cys_6$ genes located within these clusters in *Aspergillus*, *Fusarium* and *Magnaporthe*, respectively. Functioning

as virulence factors, this family of transcription factors is under selective pressure to evolve more rapidly in order to overcome the evolution of plant defences (Berbee, 2001). Within the *Ascomycota* group, Tpc1-like proteins were present in several multicellular fungal species, which cluster into groups relating to the taxonomic class to which they belong, and not with their ecological role. This may reflect the fact that Tpc1 is involved in the establishment of polarity, a fundamental process that affects largely all the other developmental processes such as sporulation, vegetative and invasive growth *in planta*.

Comparative genomics is a powerful technique for identifying orthologous genes in different species (Tatusov *et al.*, 1997) and for inferring putative functions for unknown proteins (Burger *et al.*, 1991). Although *N. crassa* has a close orthologue of *Mo*Tpc1, *NcTPC1* KO has never been characterised before. Both proteins are incredibly similar (86%) in their C-terminus, which probably contains most of the regulatory regions, the NLS, the zinc cluster DNA binding domain and the MAPK docking site; suggesting that they are functional orthologues (Burger *et al*. 1991). However, putative phosphorylation and sumoylation sites are present in *Mo*Tpc1, but absent in the *Nc*Tpc1 protein. Phosphorylation and sumoylation are post-translational modifications that mediate molecular interaction with specific substrates and regulate physiological processes such as cell-cycle, development and biotic and abiotic stress responses (Bhattacharyya *et al.*, 2006; Miura and Hasegawa, 2010). Whether these gained putative regulating motifs in *Mo*Tpc1 (or lost in *Nc*Tpc1 protein) have a biological function is not known. These regulatory elements may, however, have contributed to expression divergence, a quantitative measure of the differences in expression of a pair of orthologues between two species (Tirosh *et al.*, 2006). Expression divergence can occur within relatively short time scales (5 – 20 Mya), both within and between species (Tuch *et al.*, 2008; Tirosh *et al.*, 2009). These regulatory changes can drive gain or loss of gene targets or simply operate

by remodulating regulatory patterns, allowing the fine-tuning of complex regulatory networks (Thompson and Regev, 2009), which might be the case for the Tpc1 regulatory network. The *NcTPC1* deletion mutant showed defects in general developmental processes (vegetative growth and branching). However, *NcTPC1* KO mutant did not show an osmotic-resistant phenotype to high concentrations of NaCl as observed with the M1422 T-DNA mutant (see Chapter 4). This could be explained by the expression divergence model described above (Tirosh *et al.*, 2006), where *Mo*Tpc1 may have gain a novel target, *e.g. MPS1,* to coordinate within this regulatory network.

When considered together, it suggests that the Tpc1 group of transcription factors may serve important roles in hyphal polarisation and the maintenance of polarity, hyphal branching and the cell wall biogenesis underpinning such morphogenetic transitions.

CHAPTER 7

Identification of putatively secreted effectors delivered by *M. oryzae* during fungal-plant interaction

7.1. Introduction

The penetration peg acts as a channel for moving the nucleus and cytoplasmic contents from the appressorium into the growing primary hypha. In the compatible interaction, primary hyphae differentiate into thicker bulbous invasive hyphae (IH) that fill the first-invaded rice cells and then move into neighbouring cells through pit field sites-containing plasmodesmata (Heath *et al.*, 1990; Kankanala *et al.*, 2007). During an incompatible interaction, avirulence (AVR) effectors are recognised by the corresponding resistance gene products and the invaded plant cells lose membrane integrity and induce a hypersensitive response (HR), callose deposition and oxidative burst to block spreading of blast disease (Peng and Shishiyama, 1989; Koga, 1994; Koga *et al.*, 2004).

Many studies have focused on genes with a role in appressorium development and function (Talbot, 2003). Less is known about the genes that are necessary for biotrophic growth of the blast fungus within rice cells. However, recent cellular studies have led to a better understanding of the biotrophic invasion strategy used by *M. oryzae* in susceptible rice cultivars (Koga *et al.*, 2004; Kankanala *et al.*, 2007). Thin filamentous primary hyphae grow in the rice cell lumen after appressorial penetration and invaginate the plant plasma membrane. These hyphae differentiate into bulbous invasive hyphae (IH), sealed in an extra-invasive hyphal membrane (EIHM) compartment and they exhibit pseudohyphal growth as they fill the invaded cell. The IH constrict and cross into live neighbouring rice cells apparently through plasmodesmata (Kankanala *et al.*, 2007). To counteract plant defences and successively invade live cells, IH must transport specialised effector proteins into the host cytoplasm (Kamoun, 2006). Recently, Khang *et al.* (2010) have shown that blast effector proteins (*e.g.* Avr-Pita1 and Pwl2) accumulate in a novel pathogen-induced structure called the biotrophic interfacial complex (BIC) at specific locations

inside the EIHM compartment, and are secreted by IH growing within rice cells. The BIC first appears as an EIHM membranous cap at the hyphal tip of filamentous primary hyphae (Kankanala *et al.*, 2007). When each filamentous hypha differentiates into bulbous IH, the BIC moves beside the first IH cell and remains there as IH continue to grow in the rice cell (Khang *et al.*, 2010). Due to the accumulation of fluorescent effectors in BICs, it has been assumed that BIC localisation is diagnostic of the secretion of blast effectors and may therefore play a role in the translocation of effectors to the rice cell cytoplasm (Kankanala *et al.*, 2007; Mosquera *et al.*, 2009; Khang *et al.*, 2010).

Several genes encoding secreted effectors such as Avr-Pita1 (Jia *et al.*, 2000; Orbach *et al.*, 2000), Pwl2 (Sweigard *et al.*, 1995), and Avr-CO39 (Peyyala and Farman, 2006) have been described in the rice blast fungus. Although these are *in planta*-specific secreted proteins, no motif has been described for identification of additional effectors in the *M. oryzae* genome (Dean *et al.*, 2005; Mosquera *et al.*, 2009). By contrast, the RXLR sequence motif has been defined as a host translocation domain in the RXLR family of oomycete effectors (Whisson *et al.*, 2007; Birch *et al.*, 2008). The presence of the RXLR motif has enabled computational development of catalogues of candidate RXLR effectors from the genome sequence of several oomycete pathogens (Tyler *et al.*, 2006; Win *et al.*, 2007; Jiang *et al.*, 2008; Haas *et al.*, 2009). This method accelerates discovery and functional profiling of effector proteins from filamentous phytopathogens (Vleeshouwers *et al.*, 2008; Oh *et al.*, 2009; Kale *et al.*, 2010; Schornack *et al.*, 2010).

In this Chapter, I report an investigation in which I set out to identify novel effectors from *M. oryzae* using bioinformatics based initially on the published genome sequence of isolate 70-15 (Dean *et al.*, 2005). Assuming the concept that *M. oryzae* secretes effector proteins to modulate plant innate immunity and enable infection,

we predicted the secretome for the blast fungus using SignalP3.0 (Bendtsen *et al.*, 2004) and Phobius (Kall *et al.*, 2004) programmes (Chou, 2007). These bioinformatics tools detect the presence of a signal peptide in a protein. According to the results, there were 1731 putative secreted proteins without transmembrane domains. WoLF PSORT program (Horton *et al.*, 2007) was used to predict the subcellular localisation of these putative secreted proteins within the cell. PFAM domain (Finn *et al.*, 2010) search was also carried out to understand the possible functions of these candidate blast effectors. Here, I described the functional characterisation of three putative nuclear-localised effector proteins (MGG_03438, MGG_04326 and MGG_13165) that contain a DNA-binding domain. MGG_03438, MGG_04326 and MGG_13165 genes encode a putative fungal specific transcription factor, a putative fungal $Zn(II)_2Cys_6$ binuclear transcription factor, and a putative centromere binding protein B, respectively. Throughout this study, these putative effectors are termed Ftf1, Znc1 and Cpb1, respectively. Targeted deletion of *FTF1*, *ZNC1* and *CPB1* by split-marker strategy (Catlett *et al.*, 2002) is attempted in *M. oryzae* Guy11 isolate. I reported the phenotypic analysis of three independent mutants for *Δftf1* (T19, T27 and T33), and two independent mutants for *Δznc1* (T7 and T8) and *Δcpb1* (T2 and T3) to elucidate the biological function of Ftf1, Znc1 and Cpb1 in rice blast disease.

7.2. Materials and Methods

7.2.1. Bioinformatics analysis of *M. oryzae* predicted secretome

The *M. oryzae* wild-type isolate 70-15 protein sequences were retrieved from the *Magnaporthe* sequence database at the BROAD Institute (http://www.broadinstitute.org/annotation/fungi/magnaporthe). The secretome of *M. oryzae* was predicted by analysing the set of translated gene sequences using bioinformatics (Chou, 2007): 1) SignalP3.0 (Bendtsen *et al.*, 2004), which detects the presence of a signal peptide in the amino terminus of a protein; 2) Phobius (Kall *et al.*, 2004), a combined transmembrane (TM) topology and signal peptide predictor (Fig. 7.1). WoLF PSORT program (Horton *et al.*, 2007) was then used to predict the subcellular localisation of 1731 putative secreted proteins without transmembrane domains within the cells (Fig. 7.1). To gain insight into their function, these protein sequences were analysed for PFAM (Finn *et al.*, 2010) domain matches.

7.2.2. Targeted gene replacement of *FTF1*, *ZNC1* and *CPB1*

From the 1731 candidate effector proteins, three putative nuclear-localised secreted proteins (MGG_03438, MGG_04326 and MGG_13165) were selected for functional characterisation. For targeted deletion of these three genes in *M. oryzae* Guy11, the split-marker deletion method based on PCR fusion was used (Catlett *et al.*, 2002) (Fig.7.2 and Fig 7.3). The PCR-based strategy required four selectable marker primers (M13F, M13R, HY and YG primers) and four gene-specific primers (F1, F2, F3 and F4 primers) as shown in Fig. 7.2.

In PCR round 1 (Fig. 7.2A), the flanks and the selectable marker hygromycin phosphotransferase (*HYG*) were amplified. Primers F1 and F2 amplified the 5' flank of the gene of interest to be deleted; F3 and F4 amplified the 3' flank. The overlapping marker fragments *HY* and *YG* of the hygromycin cassette (*HYG*) were amplified from plasmid pCB1004 (Carroll *et al.*, 1994) using M13R/ HY and M13F/

YG primers, respectively. To facilitate fusion of the flanks and the marker sequences, the 5' ends of F2 and F3 primers were complementary to the M13F and M13R primer sequences, respectively. In PCR round 2 (Fig. 7.2B), each flank from round 1 was fused to the *HYG* selectable marker through PCR by overlap extension (Ho *et al*., 1989). For the 5' construct, templates were the M13F/ YG amplified fragment (*YG*) and F1/ F2 flank from PCR round 1; primers were F1 and YG. For the 3' construct, templates were the M13R/ HY amplified fragment (*HY*) and F3/ F4 flank from PCR round 1; primers were F4 and HY. In PCR round 3 (Fig. 7.2C), both fragments amplified from previously PCR round were fused together. The final product should be the *HYG* selectable marker flanked with 3' and 5' flanking sequences of the target gene to be deleted.

For all rounds of PCR amplification, Phusion® High-Fidelity DNA polymerase (Finnzymes, Thermo Fischer Scientific Inc.) was used, following the manufacters' guidelines for PCR conditions. The final PCR product of PCR round 3 was concentrated using the QIAquick PCR purification kit (Qiagen) and used for protoplast transformation (see Chapter 2).

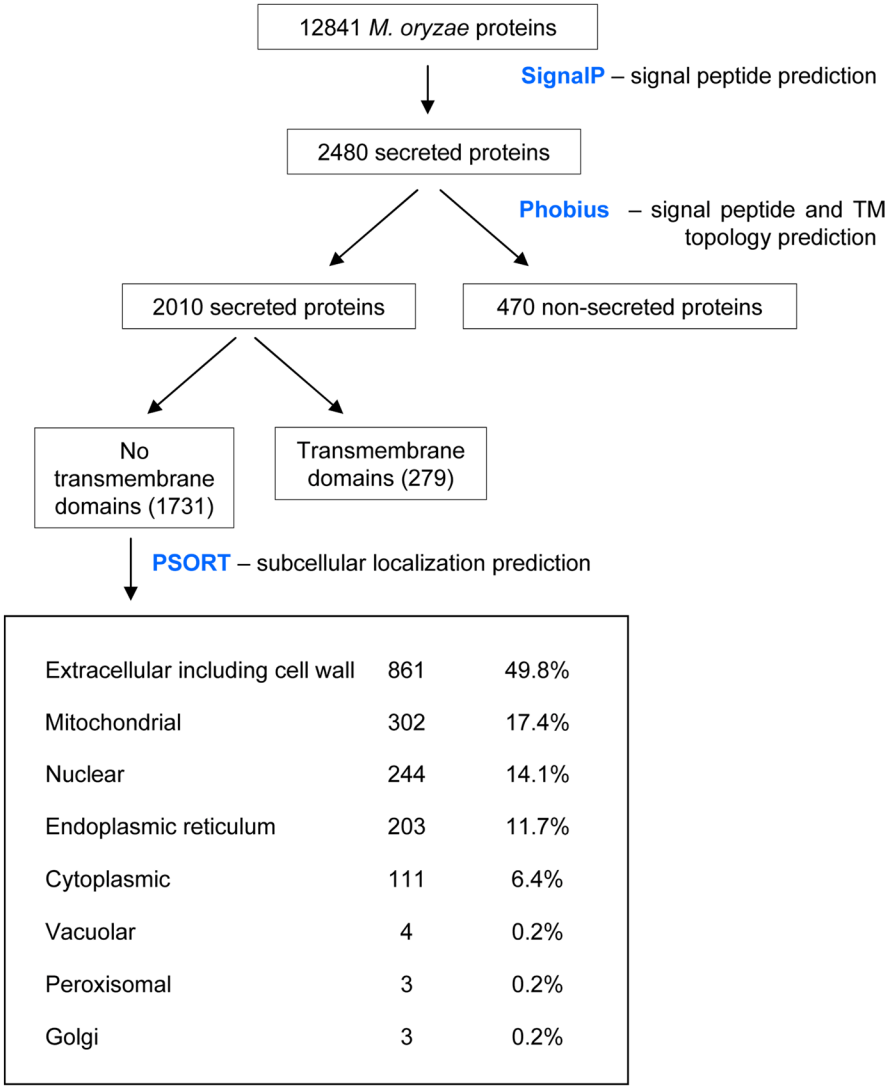

Figure 7.1. Flow chart showing *M. oryzae* 70-15 predicted secreted proteins and its subcellular localisation within the cell.

M. oryzae 70-15 protein sequences were retrieved from the BROAD institute (http://www.broadinstitute.org/annotation/fungi/magnaporthe). The secretome of *M. oryzae* was predicted by analysing the set of translated gene sequences using SignalP3.0 and Phobius bioinformatics tools. WoLF PSORT was used to predict the subcellular localisation of the 1731 *M. oryzae* secreted proteins without transmembrane domains within the cells.

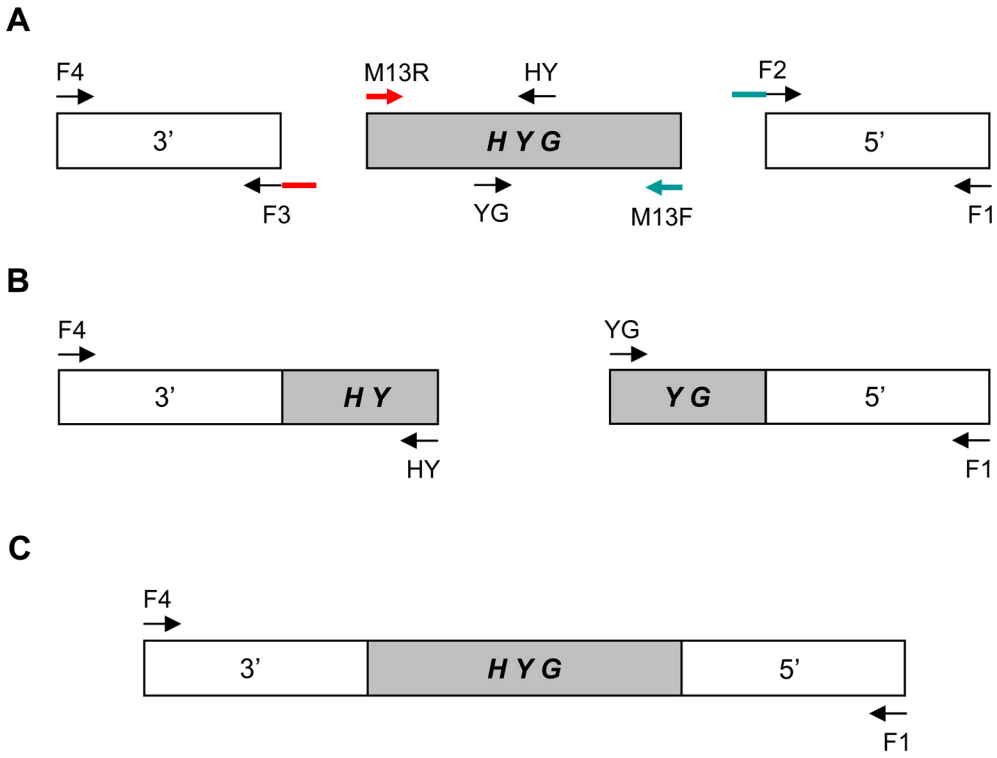

Figure 7.2. Split-marker strategy for gene deletion.

(A) Primers F1/ F2 and F3/ F4 amplify target gene flanking sequences. Primers M13R/ HY and M13F/ YG amplify *HY* and *YG* marker fragments, respectively. Note that the 5' ends of primers F2 and F3 are complementary to the M13F and M13R sequences, respectively. **(B)** Two separate PCR reactions (F1/ YG and HY/ F4) fuse the flank sequences to the 3' *YG* or 5' *HY* portions of *HYG*, respectively. **(C)** A final PCR reaction (F1/ F4 primers) fuse the two PCR fragments from (B) and the targeting deletion construct is obtained with *HYG* selectable marker flanked on both sides by short DNA sequences that target a gene of interest.

7.3. Results

7.3.1. Analysis of *M. oryzae* predicted secretome

The secretome of *M. oryzae* was predicted by first analysing the set of translated gene sequences (12841 putative proteins) using the bioinformatics tools SignalP3.0 (Bendtsen *et al.*, 2004) and Phobius (Kall *et al.*, 2004). From the *M. oryzae* genome, 1731 proteins without transmembrane domains were expected to be secreted (Fig. 7.1). WoLF PSORT (Horton *et al.*, 2007) was then used to predict the subcellular localisation of these proteins within the cell. The majority of these putative secreted proteins were expected to be extracellular or secreted to the cell wall (861 proteins; 49.8%) as shown in Fig. 7.1. The remaining proteins were predicted to be secreted into the different organelles within the cell: mitochondria (17.4%), nucleus (14.1%), endoplasmic reticulum (11.7%), cytoplasm (6.4%), Golgi (0.2%), and peroxisome (0.2%) as shown in Fig. 7.1. The search was therefore refined to select proteins expected to be delivered outside of fungal cells but which unexpectedly still had an organellar localisation signal. This might signify that or is a putatively delivered effector protein being targeted to the cells during infection.

7.3.2. Targeted gene replacement of *FTF1*, *ZNC1* and *CPB1*

Three putative nuclear localised-effector proteins in *M. oryzae* were selected for functional characterisation. These proteins are predicted to have a DNA binding domain: 1) MGG_03438 with a fungal specific transcription factor domain (PF04082); 2) MGG_04326 with a fungal $Zn(II)_2Cys_6$ binuclear domain (PF00172); 3) MGG_13165 with a centromere binding protein B domain (PF09091). In this study, these putative effectors were renamed Ftf1, Znc1 and Cpb1, respectively.

To test the role of these putative effectors during rice blast disease, targeted gene replacements (Fig. 7.2) were performed in which ~3 kilobase (kb) of each coding sequence was removed and replaced with a gene cassette conferring hygromycin resistance (Fig. 7.3A). All candidate genes were deleted in wild-type Guy11 background (Fig. 7.3B, C, D). Growth of three independent *Δftf1* (T19, T27 and T33; Fig. 7.3B) mutants and two independent *Δznc1* (T7 and T8; Fig. 7.3C) and *Δcpb1* (T2 and T3; Fig. 7.3C) mutants were selected for further functional characterisation of the corresponding genes.

7.3.3. Vegetative growth of *Δftf1, Δznc1* and *Δcpb1* mutants

The targeted deletion putative effector strains were assayed for pathogenicity in roots and leaf of rice and barley. We predicted that deletion of these candidate effector genes might result in loss of virulence as shown in other filamentous fungi (van den Ackerveken *et al.*, 1993; Bolton *et al.*, 2008; Doehlemann *et al.*, 2009). If not, they could be functionally redundant during colonisation *in planta* or not required for virulence (reviewed in Stergiopoulos and de Wit, 2009; Oliva *et al.*, 2010). To elucidate whether the candidate blast effectors were also needed for growth of *M. oryzae*, targeted deleted effector strains (*Δftf1*, *Δznc1* and *Δcpb1*) were also grown under conditions of nutrient deprivation, cell wall stress or oxidative stress. If the genes have plant colonisation-specific roles, then they would be predicted not to have various growth defects in axenic culture, as it was illustrated with *Δpep1* in *U. maydis* (Doehlemann *et al.*, 2009).

Growth of three independent *Δftf1* mutants revealed that they each displayed wild-type phenotypes with regard to leaf and root pathogenicity in both rice (Fig. 7.4A, C) and barley (Fig. 7.4B). However, the lesions of rice infected with *Δftf1_T19*, *Δftf1_T27* and *Δftf1_T33* mutants were smaller (0.6 ± 0.3 cm, 0.6 ± 0.3 cm and 0.6 ± 0.3 cm, respectively) when compared to roots infected with Guy11 (1.0 ± 0.5 cm ; p

< 0.01) (Fig. 7.4D and Table 7.1). On complete and minimal medium without carbon and nitrogen sources, *Δftf1* mutants grew faster that the wild-type strain ($p < 0.01$) (Fig. 7.5A, B and Table 7.1). These mutants tended to branch more, especially on minimal media and on media lacking glucose (Fig. 7.5A). Another morphological difference was that *Δftf1* mutants were lighter than the grey colonies of Guy11 (Fig. 7.5A). Conidiation was not affected in the *Δftf1* mutants. The *Δftf1* mutants showed hypersensitivity to high concentrations of external solutes, particularly between 0.4M and 1M NaCl, compared with Guy11 ($p < 0.01$) as shown in Fig. 7.6A, B. The colonial growth of *Δftf1* was also severely affected under oxidative stress (0.1% H_2O_2) conditions ($p < 0.01$) (Fig. 7.7 and Table 7.1). The hypersensitivity to osmotic and oxidative stresses and "reduced" virulence may be due to defects in cell wall composition. To investigate this possibility, Congo Red (CR) and Calcofluor white (CFW) were added to the medium, which inhibit fungal cell wall assembly by binding β-1,4-glucans and chitin, respectively (Wood and Fulcher, 1983; Ram *et al.*, 1994). Mycelial growth of the *Δftf1* mutants on 50μg/ml CR media (Fig. 7.7) and 100μg/ml CFW (Fig. 7.7) was enhanced when compared with wild-type Guy11 strain ($p < 0.01$) (Table 7.1). On CR medium, a clear degradation halo was observed around the wild-type colonies, whereas no degradation halo was present around the *Δftf1* colonies, as shown in Fig. 7.7. These defects on CR media were probably due to the absence of CR-degrading activity also defects in cell wall composition. The *Δftf1* mutants were also more resistant to detergents (0.1% Triton-X) that permeabilise eukaryotic cell membranes than Guy11 ($p < 0.01$) (Fig. 7.7 and Table 7.1).

The *Δznc1* deletion strains were able to infect leaves and roots of rice cultivar CO-39 (Fig. 7.8A, C, D) and barley cultivar Golden Promise (Fig. 7.8B). They were fully pathogenic. The vegetative growth of these mutants was not affected on complete and minimal medium without carbon and nitrogen sources (Fig. 7.9A, B and Table 7.2). High concentration of osmolytes (Fig. 7.10A, B), oxidative stress

(H_2O_2) (Fig. 7.11 and Table 7.2) and inhibitors of fungal cell wall (CR and CFW) (Fig. 7.11 and Table 7.2) added to the medium had no effect on the growth of the colonies of *Δznc1_T7* and *Δznc1_T8* mutants. However, colonial growth was impaired in *Δznc1* mutants compared to wild-type strain Guy11 in the presence of detergents (Triton-X) on the medium ($p < 0.01$) (Fig. 7.11 and Table 7.2).

Knocking-out of the *CPB1* gene had no effect on leaf and root pathogenicity of rice and barley (Fig. 7.12A, B, C, D), vegetative growth in complete and minimal medium (Fig. 7.13A, B and Table 7.3) and under osmotic (Fig. 7.14), oxidative (Fig. 7.15 and Table 7.3), cell wall (Fig. 7.15 and Table 7.3) stresses or sporulation.

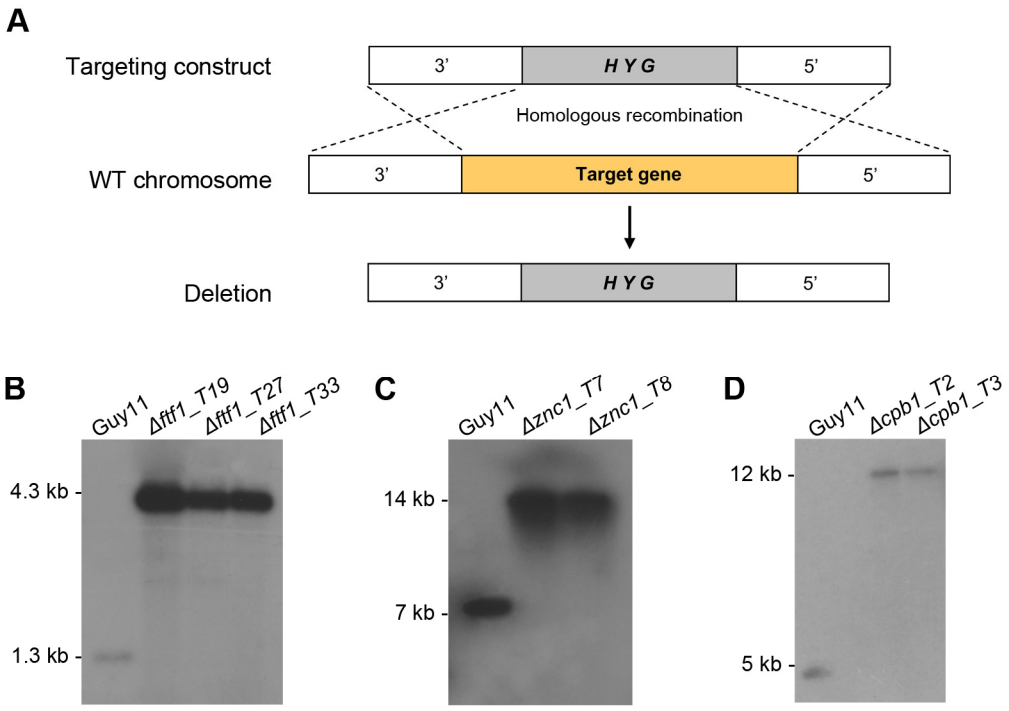

Figure 7.3. Strategy for targeted gene deletion.

(A) The targeting KO construct was used directly for protoplast transformation. Homologous recombination between the overlapping regions of the selectable marker *HYG* and between the flank regions and chromosomal *M. oryzae* Guy11 DNA results in a directed deletion of the gene of interest. **(B)** Southern hybridization to show single copy of FTF1 KO construct inserted correctly in the Guy11 genome. Total genomic DNA was digested with *Pvu*II and probed with flanking region fragment of *FTF1* gene (see Appendix). **(C)** Southern hybridization to show single copy of ZNC1 KO construct inserted correctly in the Guy11 genome. Total genomic DNA was digested with *Mfe*I and probed with flanking region fragment of *ZNC1* gene (see Appendix). **(D)** Southern hybridization to show single copy of CPB1 KO construct inserted correctly in the Guy11 genome. Total genomic DNA was digested with *Hind*III and probed with flanking region fragment of *CPB1* gene (see Appendix).

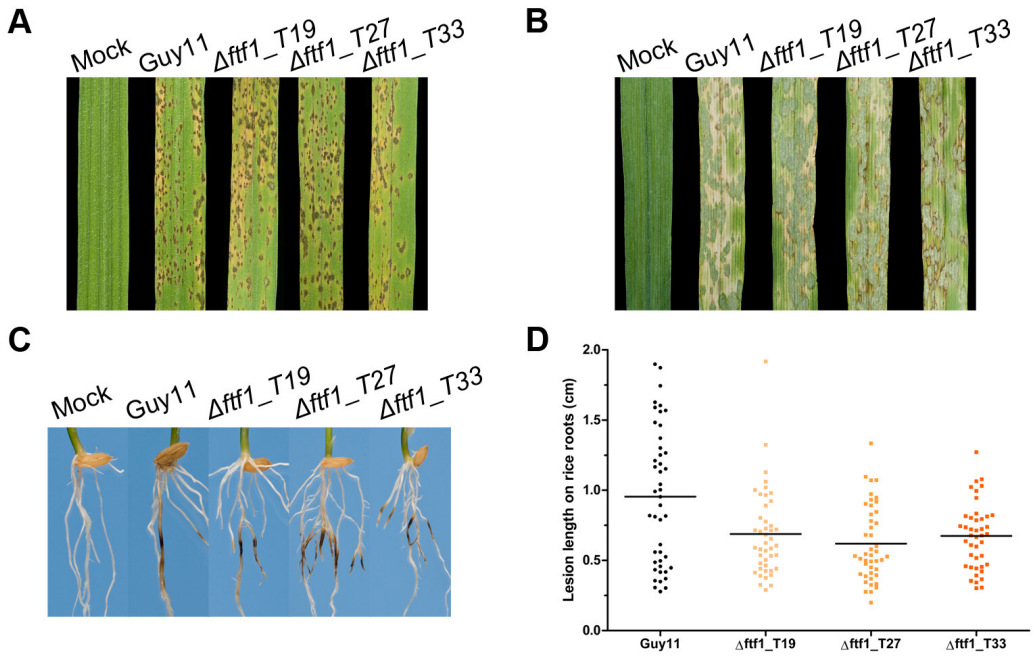

Figure 7.4. The *Δftf1* mutants have wild-type phenotype with regard to leaf and root pathogenicity.

Seedlings of rice cultivar CO-39 **(A)** and barley cultivar Golden Promise **(B)** were inoculated with 0.20% gelatine (mock) and with *M. oryzae* conidial suspensions of identical concentration (10^5 conidia ml^{-1}) of Guy11 and *Δftf1* mutants (transformants T19, T27 and T33). Plants were incubated at 25ºC and 90% humidity. Photographs were taken at 5 dpi. **(C)** Seedlings of rice cultivar CO-39 were inoculated with a plug of agar (mock) and mycelium from Guy11 and *Δftf1* mutants (transformants T19, T27 and T33) and were incubated at 25ºC for 15 dpi. Photographs were taken at 15 dpi. **(D)** Rice blast root lesions were measured at 15 dpi. Horizontal lines indicate the mean. *Δftf1* mutants show significant difference of lesion length in infected rice roots compared with the control Guy11 ($p < 0.01$), and no difference between the different *Δftf1* transformants.

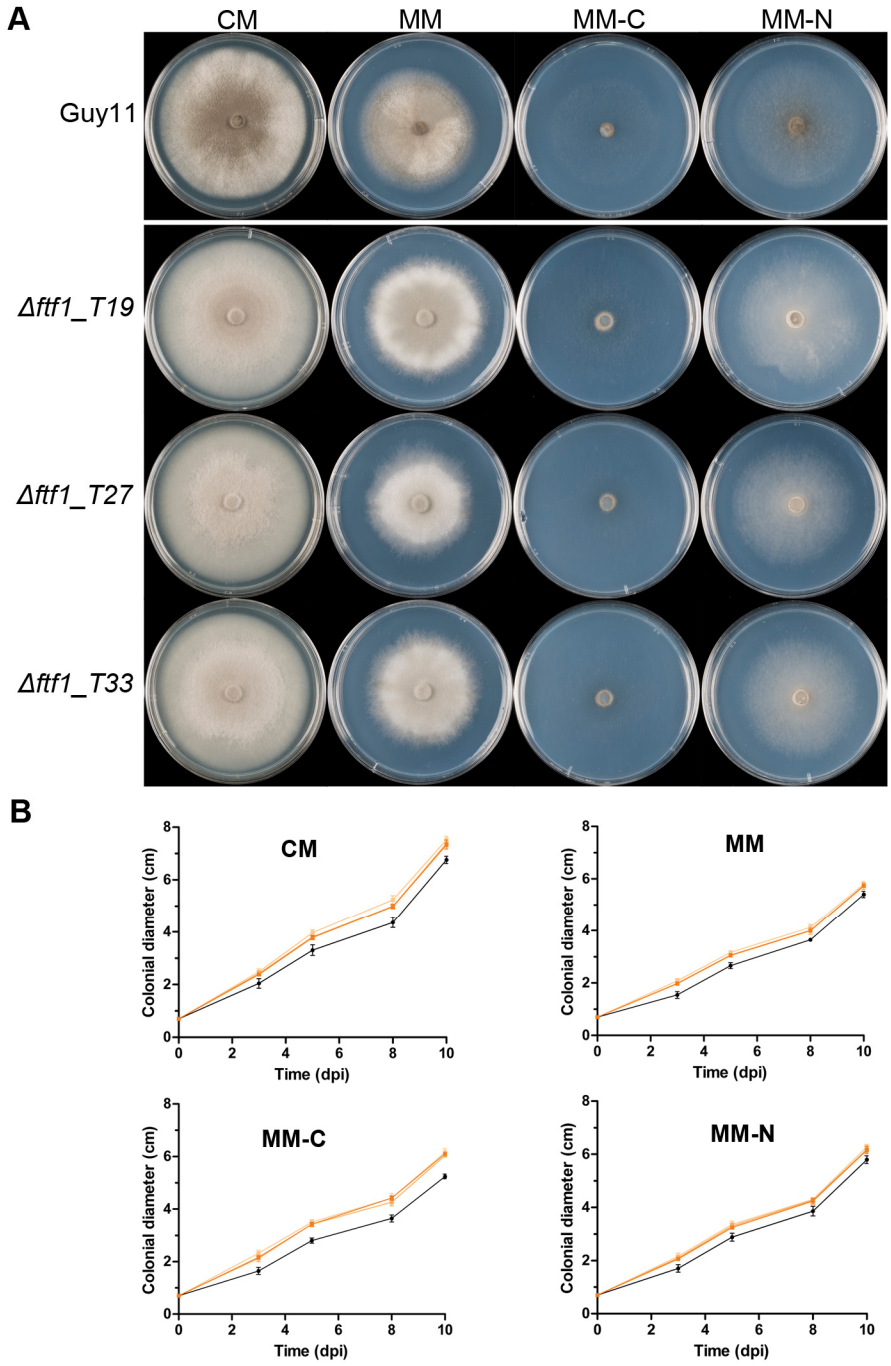

Figure 7.5. The vegetative growth and colony morphology of *Δftf1* mutants.

(A) CM, MM, MM-C and MM-N plates were inoculated with 7 mm plugs of mycelium from Guy11 (Guy11) and the *Δftf1* mutants (transformants T19, T27 and T33 *Δftf1_T19* *Δftf1_T27* *Δftf1_T33*). Plates were incubated at 26ºC and the colony images captured at 10 days after inoculation. **(B)** Diameter of the subsequent colonies was measured at 3, 5, 8 and 10 dpi. Error bars represent the standard deviation of the mean of the three independent replications of the experiment.

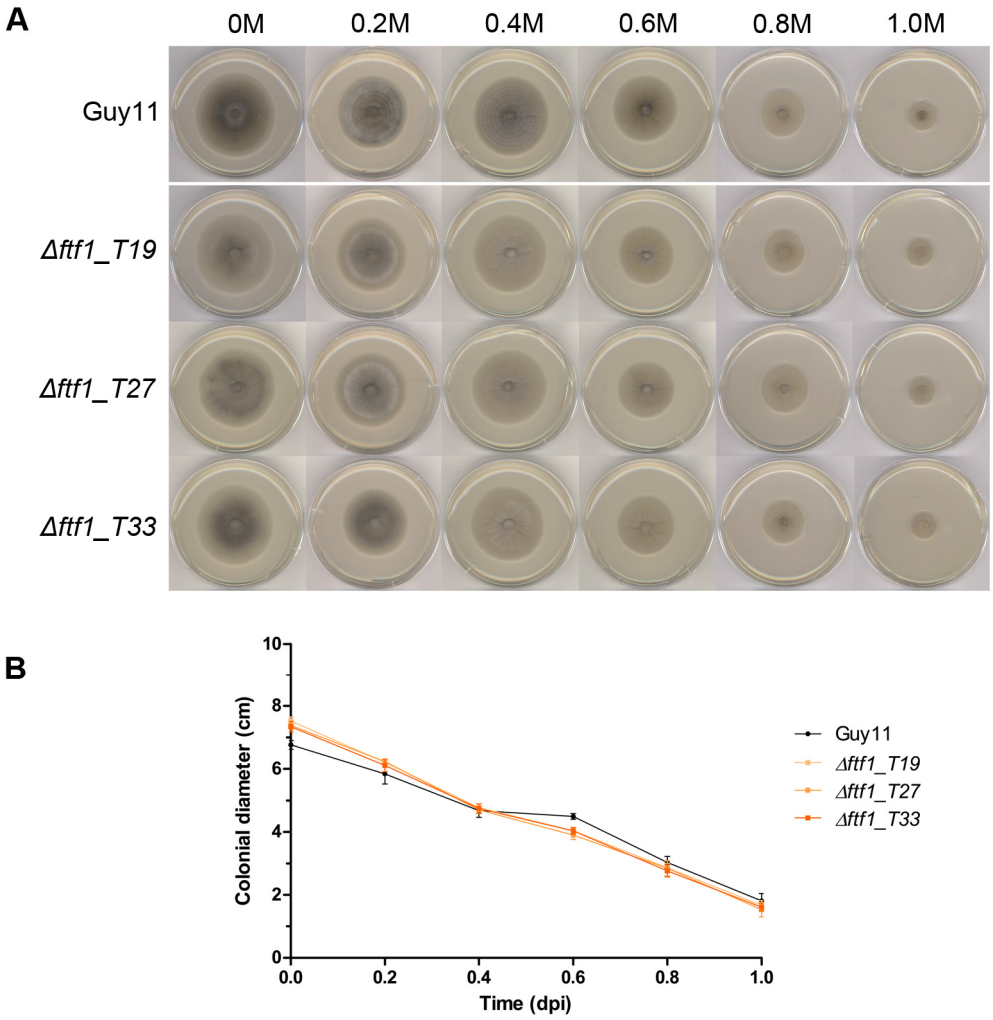

Figure 7.6. The vegetative growth and colony morphology of *Δftf1* mutants under osmotic stress (NaCl).

(A) CM plates with 0M, 0.2M, 0.4M, 0.6M, 0.8M and 1.0M NaCl added to the medium were inoculated with 7 mm plugs of mycelium from Guy11 and the *Δftf1* mutants (transformants T19, T27 and T33). Plates were incubated at 26ºC and the colony images captured at 10 days after inoculation. **(B)** Diameter of the subsequent colonies was measured at 10 dpi. Error bars represent the standard deviation of the mean of the three independent replications of the experiment.

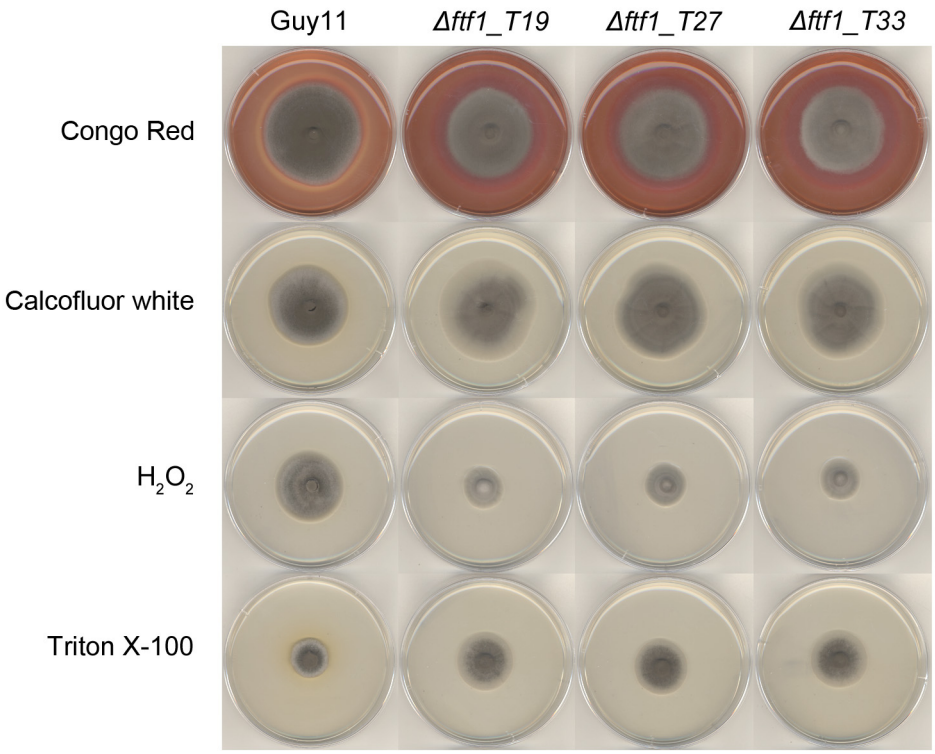

Figure 7.7. The vegetative growth and colony morphology of *Δftf1* mutants in the presence of fungal cell wall inhibitors (CR and CFW), oxidative stress (H_2O_2) and membrane permeabilisant (Triton X-100).

CM plates with 50 µg ml^{-1} Congo Red (CR), 100 µg ml^{-1} Calcofluor white (CFW), 0.1% H_20_2 and 0.1% Triton X-100 added to the medium were inoculated with 5 mm plugs of mycelium from Guy11 and the *Δftf1* mutants (transformants T19, T27 and T33) . Plates were incubated at 26ºC and the colony images captured at 10 dpi.

Table 7.1. Mycelial growth[a] of Guy11 and *Δftf1* mutant strains

	Guy11	***Δftf1_T19***	***Δftf1_T27***	***Δftf1_T33***
CM	6.76 ± 0.13	7.52 ± 0.13[c]	7.38 ± 0.13[c]	7.34 ± 0.16[c]
MM	5.40 ± 0.12	5.80 ± 0.10[c]	5.72 ± 0.13[c]	5.74 ± 0.05[c]
MM-C	5.24 ± 0.09	6.16 ± 0.13[c]	6.04 ± 0.05[c]	6.10 ± 0.07[c]
MM-N	5.80 ± 0.14	6.28 ± 0.08[c]	6.18 ± 0.11[c]	6.16 ± 0.13[c]
50 µg ml^{-1} CR[b]	5.91 ± 0.36	6.54 ± 0.11[c]	6.49 ± 0.07[c]	6.49 ± 0.11[c]
100 µg ml^{-1} CFW[b]	3.99 ± 0.45	5.01 ± 0.21[c]	4.64 ± 0.20[c]	4.59 ± 0.12[c]
0.1% H_2O_2[b]	3.70 ± 0.52	2.41 ± 0.20[c]	2.20 ± 0.27[c]	2.17 ± 0.17[c]
0.1% Triton X-100[b]	1.97 ± 0.35	3.00 ± 0.18[c]	2.84 ± 0.10[c]	3.06 ± 0.14[c]

[a] Growth (mean ± SD cm) was measured as the diameter of the mycelium 10 days after inoculation.
[b] Added to CM.
[c] Means are statistically significantly different from wild-type Guy11 strain, as estimated using one-way ANOVA Dunnett's multiple comparison test ($p < 0.01$).

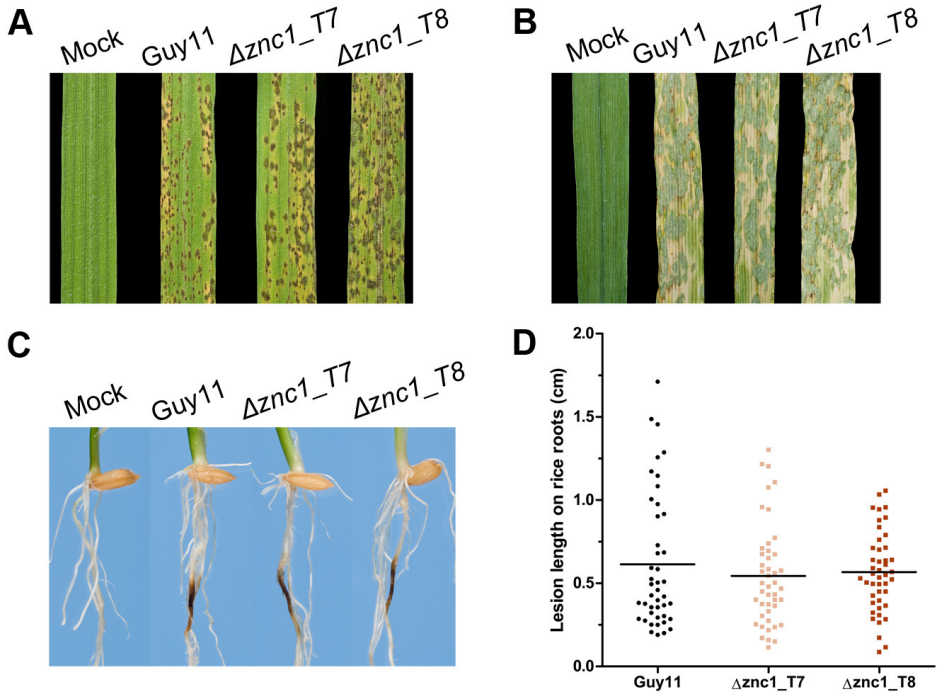

Figure 7.8. The *Δznc1* mutants have wild-type phenotype with regard to leaf and root pathogenicity.

Seedlings of rice cultivar CO-39 **(A)** and barley cultivar Golden Promise **(B)** were inoculated with 0.20% gelatine (mock) and with *M. oryzae* conidial suspensions of identical concentration (10^5 conidia ml^{-1}) of Guy11 and *Δznc1* mutants (transformants T7 and T8). Plants were incubated at 25ºC and 90% humidity. Photographs were taken at 5 dpi. **(C)** Seedlings of rice cultivar CO-39 were inoculated with a plug of agar (mock) and mycelium from Guy11 and *Δznc1* mutants (transformants T7 and T8) and were incubated at 25ºC for 15 dpi. Photographs were taken at 15 dpi. **(D)** Rice blast root lesions were measured at 15 dpi. Horizontal lines indicate the mean. *Δznc1* mutants do not show significant difference of lesion length in infected rice roots compared with the control Guy11, and no difference between them.

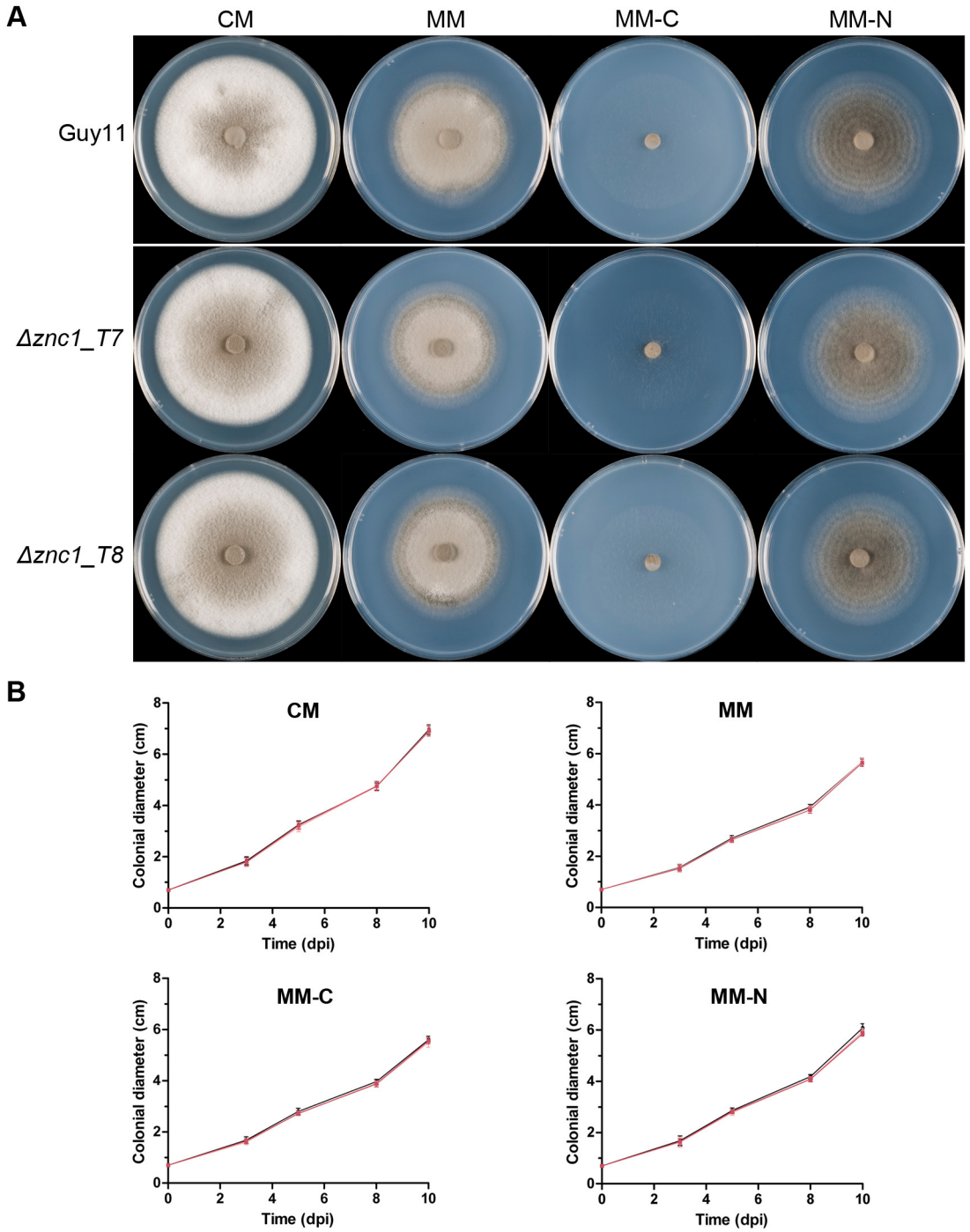

Figure 7.9. The vegetative growth and colony morphology of *Δznc1* mutants.

(A) CM, MM, MM-C and MM-N plates were inoculated with 7 mm plugs of mycelium from Guy11 (Guy11) and the *Δznc1* mutants (transformants T7 and T8 *Δznc1_T8* *Δznc1_T7*). Plates were incubated at 26ºC and the colony images captured at 10 days after inoculation. **(B)** Diameter of the subsequent colonies was measured at 3, 5, 8 and 10 dpi. Error bars represent the standard deviation of the mean of the three independent replications of the experiment.

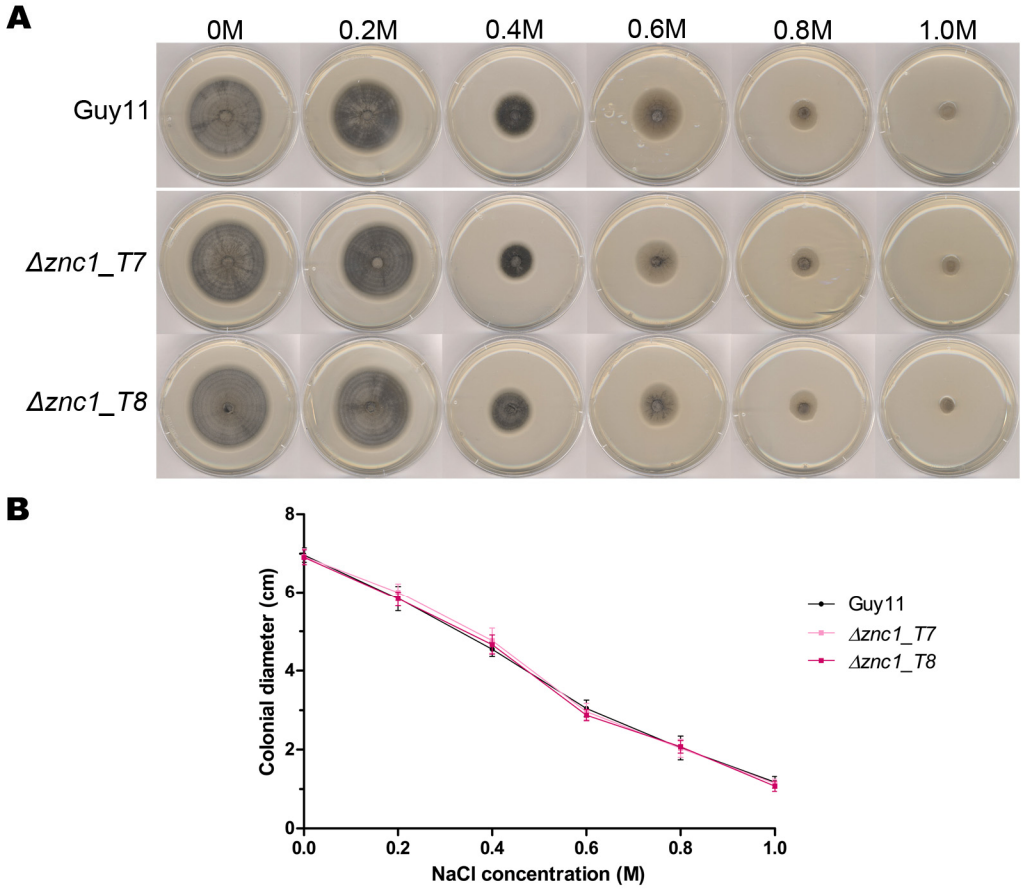

Figure 7.10. The vegetative growth and colony morphology of *Δznc1* mutants under osmotic stress (NaCl).

(A) CM plates with 0M, 0.2M, 0.4M, 0.6M, 0.8M and 1.0M NaCl added to the medium were inoculated with 7 mm plugs of mycelium from Guy11 and the *Δznc1* mutants (transformants T7 and T8). Plates were incubated at 26ºC and the colony images captured at 10 days after inoculation. **(B)** Diameter of the subsequent colonies was measured at 10 dpi. Error bars represent the standard deviation of the mean of the three independent replications of the experiment.

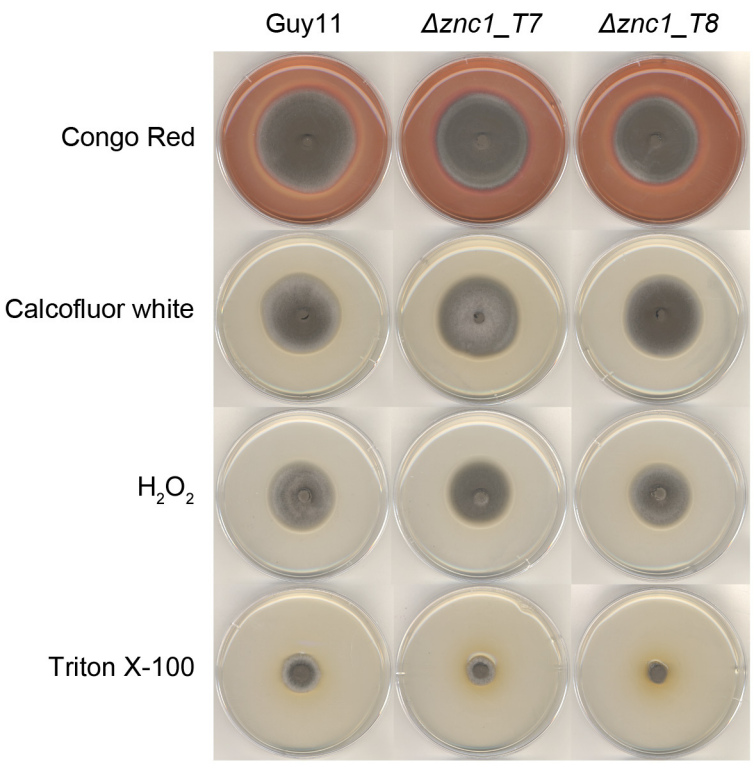

Figure 7.11. The vegetative growth and colony morphology of *Δznc1* mutants in the presence of fungal cell wall inhibitors (CR and CFW), oxidative stress (H_2O_2) and membrane permeabilisant (Triton X-100).

CM plates with 50 µg ml^{-1} Congo Red (CR), 100 µg ml^{-1} Calcofluor white (CFW), 0.1% H_20_2 and 0.1% Triton X-100 added to the medium were inoculated with 5 mm plugs of mycelium from Guy11 and the *Δznc1* mutants (transformants T7 and T8) . Plates were incubated at 26ºC and the colony images captured at 10 dpi.

Table 7.2. Mycelial growth[a] of Guy11 and *Δznc1* mutant strains

	Guy11	***Δznc1_T7***	***Δznc1_T8***
CM	6.96 ± 0.18	6.92 ± 0.20	6.90 ± 0.19
MM	5.68 ± 0.14	5.68 ± 0.16	5.64 ± 0.14
MM-C	5.60 ± 0.14	5.50 ± 0.19	5.56 ± 0.12
MM-N	6.08 ± 0.16	5.94 ± 0.12	5.86 ± 0.10
50 µg ml^{-1} CR[b]	5.91 ± 0.36	6.02 ± 0.16	5.84 ± 0.16
100 µg ml^{-1} CFW[b]	3.99 ± 0.45	4.25 ± 0.37	3.87 ± 0.26
0.1% H_2O_2[b]	3.70 ± 0.52	3.79 ± 0.63	3.85 ± 0.56
0.1% Triton X-100[b]	2.09 ± 0.22	1.45 ± 0.26[c]	1.45 ± 0.15[c]

[a] Growth (mean ± SD cm) was measured as the diameter of the mycelium 10 days after inoculation.
[b] Added to CM.
[c] Means are statistically significantly different from wild-type Guy11 strain, as estimated using one-way ANOVA Dunnett's multiple comparison test ($p < 0.01$).

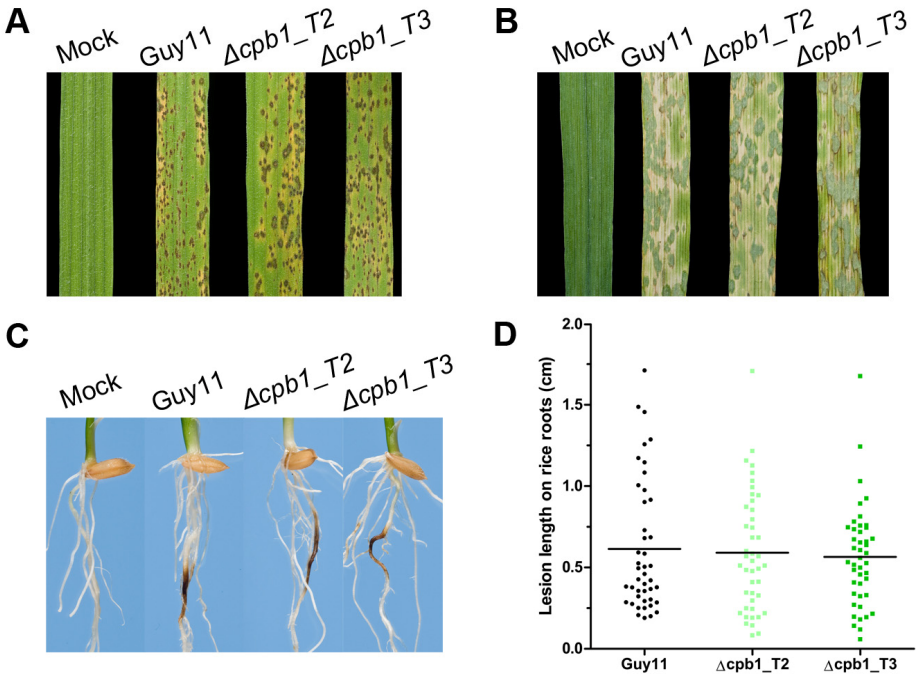

Figure 7.12. The *Δcpb1* mutants have wild-type phenotype with regard to leaf and root pathogenicity.

Seedlings of rice cultivar CO-39 **(A)** and barley cultivar Golden Promise **(B)** were inoculated with 0.20% gelatine (mock) and with *M. oryzae* conidial suspensions of identical concentration (10^5 conidia ml^{-1}) of Guy11 and *Δcpb1* mutants (transformants T2 and T3). Plants were incubated at 25ºC and 90% humidity. Photographs were taken at 5 dpi. **(C)** Seedlings of rice cultivar CO-39 were inoculated with a plug of agar (mock) and mycelium from Guy11 and *Δcpb1* mutants (transformants T2 and T3) and were incubated at 25ºC for 15 dpi. Photographs were taken at 15 dpi. **(D)** Rice blast root lesions were measured at 15 dpi. Horizontal lines indicate the mean. *Δcpb1* mutants do not show significant difference of lesion length in infected rice roots compared with the control Guy11, and no difference between them.

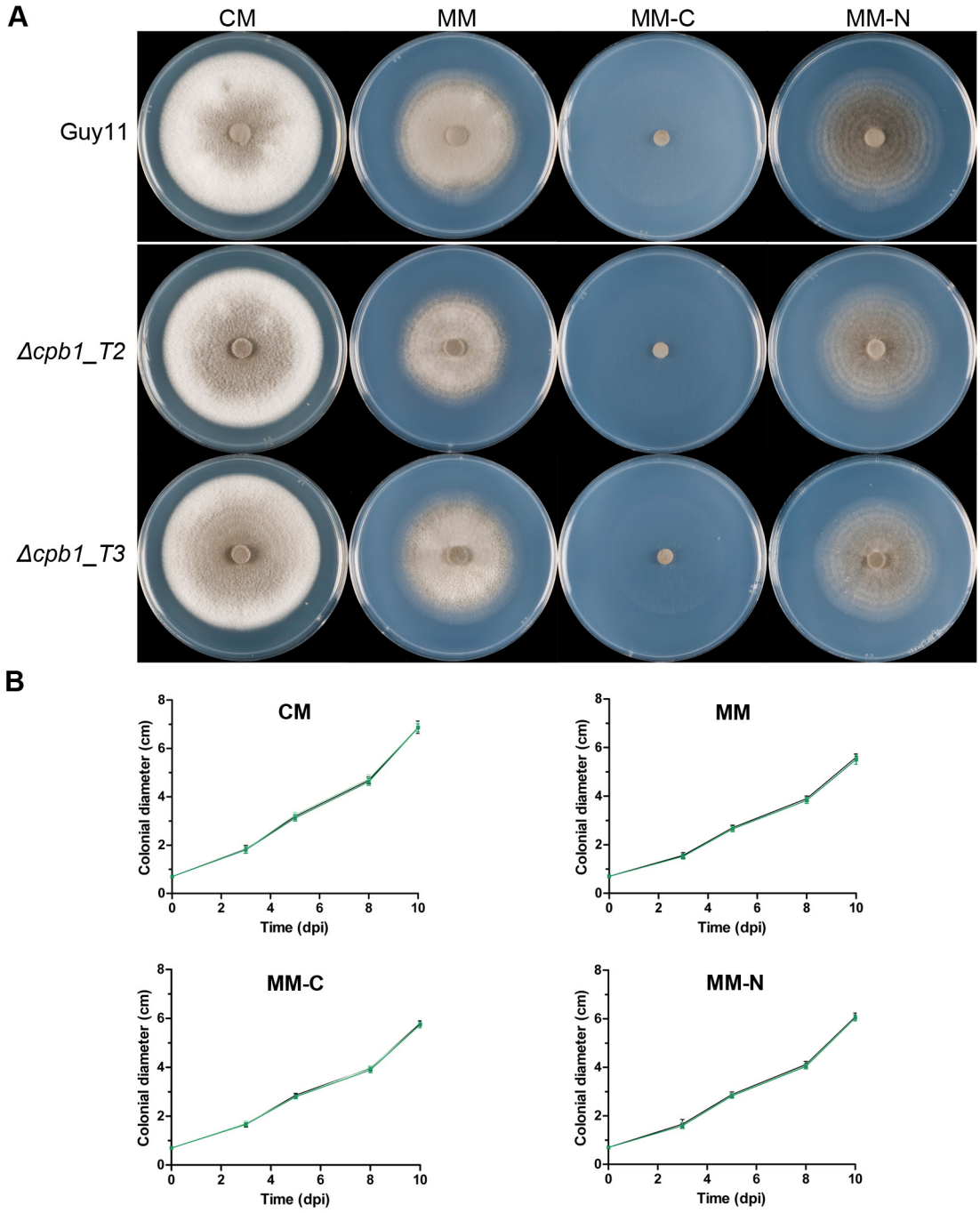

Figure 7.13. The vegetative growth and colony morphology of *Δcpb1* mutants.

(A) CM, MM, MM-C and MM-N plates were inoculated with 7 mm plugs of mycelium from Guy11 (—●— Guy11) and the *Δcpb1* mutants (transformants T2 and T3 —■— *Δcpb1_T2* —■— *Δcpb1_T3*). Plates were incubated at 26ºC and the colony images captured at 10 days after inoculation. **(B)** Diameter of the subsequent colonies was measured at 3, 5, 8 and 10 dpi. Error bars represent the standard deviation of the mean of the three independent replications of the experiment.

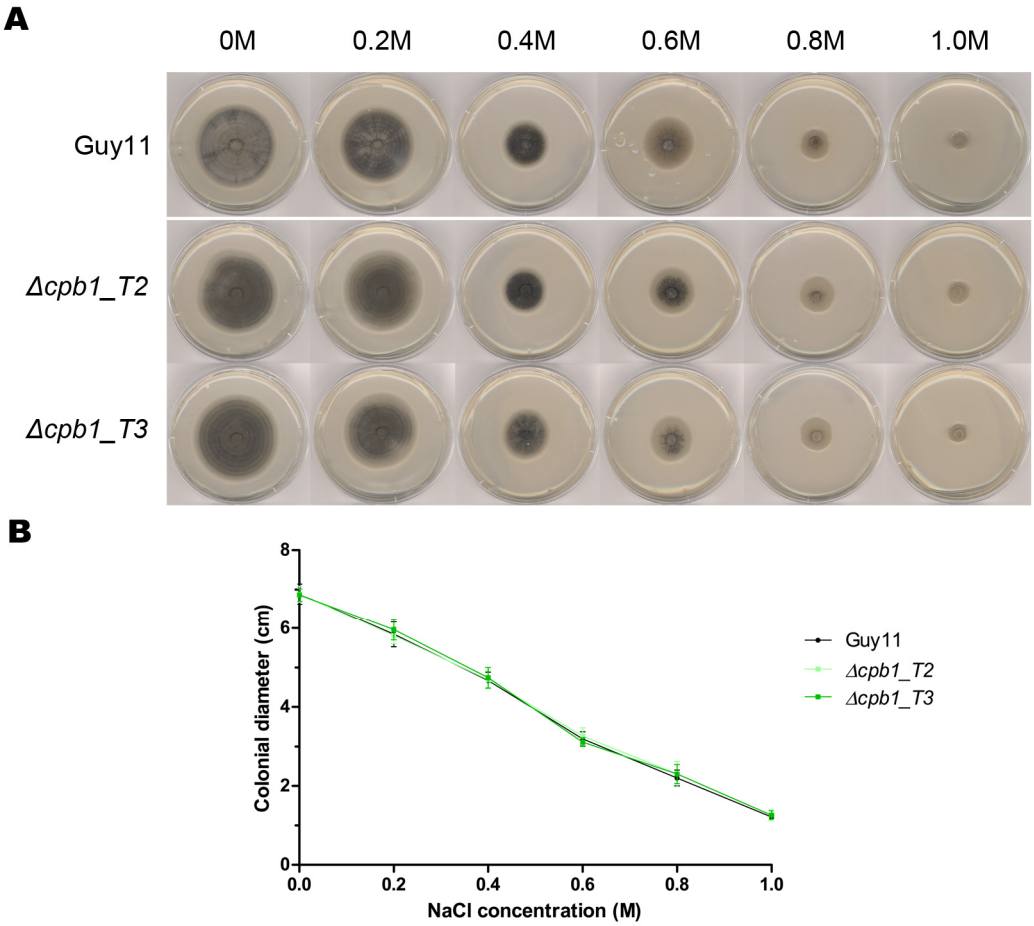

Figure 7.14. The vegetative growth and colony morphology of *Δcpb1* mutants under osmotic stress (NaCl).

(A) CM plates with 0M, 0.2M, 0.4M, 0.6M, 0.8M and 1.0M NaCl added to the medium were inoculated with 7 mm plugs of mycelium from Guy11 and the *Δcpb1* mutants (transformants T2 and T3). Plates were incubated at 26ºC and the colony images captured at 10 days after inoculation. **(B)** Diameter of the subsequent colonies was measured at 10 dpi. Error bars represent the standard deviation of the mean of the three independent replications of the experiment.

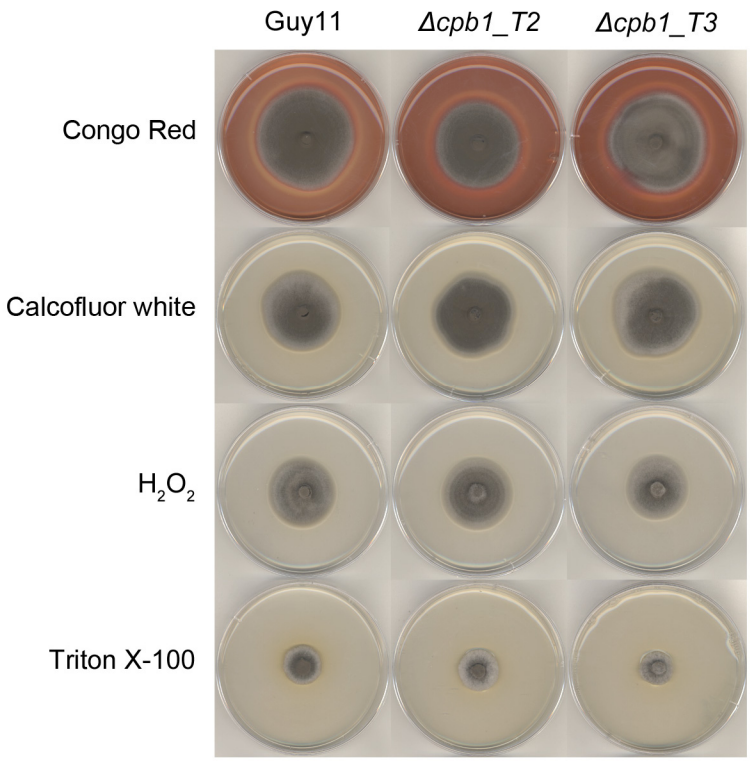

Figure 7.15. The vegetative growth and colony morphology of *Δcpb1* mutants in the presence of fungal cell wall inhibitors (CR and CFW), oxidative stress (H_2O_2) and membrane permeabilisant (Triton X-100).

CM plates with 50 µg ml^{-1} Congo Red (CR), 100 µg ml^{-1} Calcofluor white (CFW), 0.1% H_20_2 and 0.1% Triton X-100 added to the medium were inoculated with 5 mm plugs of mycelium from Guy11 and the *Δcpb1* mutants (transformants T2 and T3) . Plates were incubated at 26ºC and the colony images captured at 10 dpi.

Table 7.3. Mycelial growth[a] in Guy11 and *Δcpb1* mutant strains

	Guy11	***ΔcenpB_T2***	***ΔcenpB_T3***
CM	6.88 ± 0.26	6.88 ± 0.20	6.86 ± 0.16
MM	5.60 ± 0.15	5.50 ± 0.10	5.51 ± 0.20
MM-C	5.80 ± 0.10	5.75 ± 0.09	5.74 ± 0.13
MM-N	6.08 ± 0.16	6.05 ± 0.05	6.04 ± 0.12
50 µg ml^{-1} CR[b]	5.91 ± 0.36	5.86 ± 0.42	6.05 ± 0.17
100 µg ml^{-1} CFW[b]	3.99 ± 0.45	4.05 ± 0.23	4.09 ± 0.31
0.1% H_2O_2[b]	3.70 ± 0.52	3.59 ± 0.29	3.58 ± 0.25
0.1% Triton X-100[b]	2.09 ± 0.22	1.97 ± 0.24	1.99 ± 0.14

[a] Growth (mean ± SD cm) was measured as the diameter of the mycelium 10 days after inoculation.
[b] Added to CM.
[c] Means are statistically significantly different from wild-type Guy11 strain, as estimated using one-way ANOVA Dunnett's multiple comparison test ($p < 0.01$).

7.3.4. Cellular localisation of Ftf1:GFP, Znc1:GFP and Cpb1:GFP during infection-related development and in vegetative hyphae of *M. oryzae*

To determine whether the candidate blast effector proteins, Ftf1, Znc1 and Cpb1, were secreted and translocated *in planta*, fungal transformants were generated to express histone1 fused with red fluorescent protein (H1:RFP) and translational fusions of each putative effector with green fluorescent protein (GFP) at the C-terminus. All effector:GFP constructs were expressed under control of the native promoters. Recently, Khang *et al.* (2010) has shown that pathogen-secreting effectors fused with a fluorescent protein were preferentially accumulated in the BIC and then translocated to the rice cytoplasm. The same localisation pattern might therefore be expected for Ftf1, Znc1 and Cpb1 candidate effector proteins.

The conidia of transformants expressing the GFP fusion proteins (Ftf1:GFP) exhibited fluorescent signals in the nuclei of mycelia, conidia and during appressorium development and were shown to co-localise with H1:RFP (Fig. 7.16). However, no expression could be seen during conidial collapse at 1-appressorial nuclei stage and during invasive growth *in planta* (Fig. 7.16).

Co-localisation of Znc1:GFP and H1:RFP fusion proteins was observed in the nuclei of conidia during infection-related development, but not in mycelia or during invasive growth in rice leaves (Fig. 7.17).

Nuclear localisation of Cpb1:GFP signals was observed in conidia, germ tube germination, appressorium formation and maturation and conidial collapse (Fig. 7.18). No expression of Cpb1 protein was detected in either mycelium or invasive hyphae during leaf sheat assays (Fig. 7.18).

Taken together, the putative effectors identified by bioinformatics did not localise to BICs and there was no evidence that they could be translocated to rice cells. These proteins instead accumulate in the nuclei of *M. oryzae* conidial and hyphal cells.

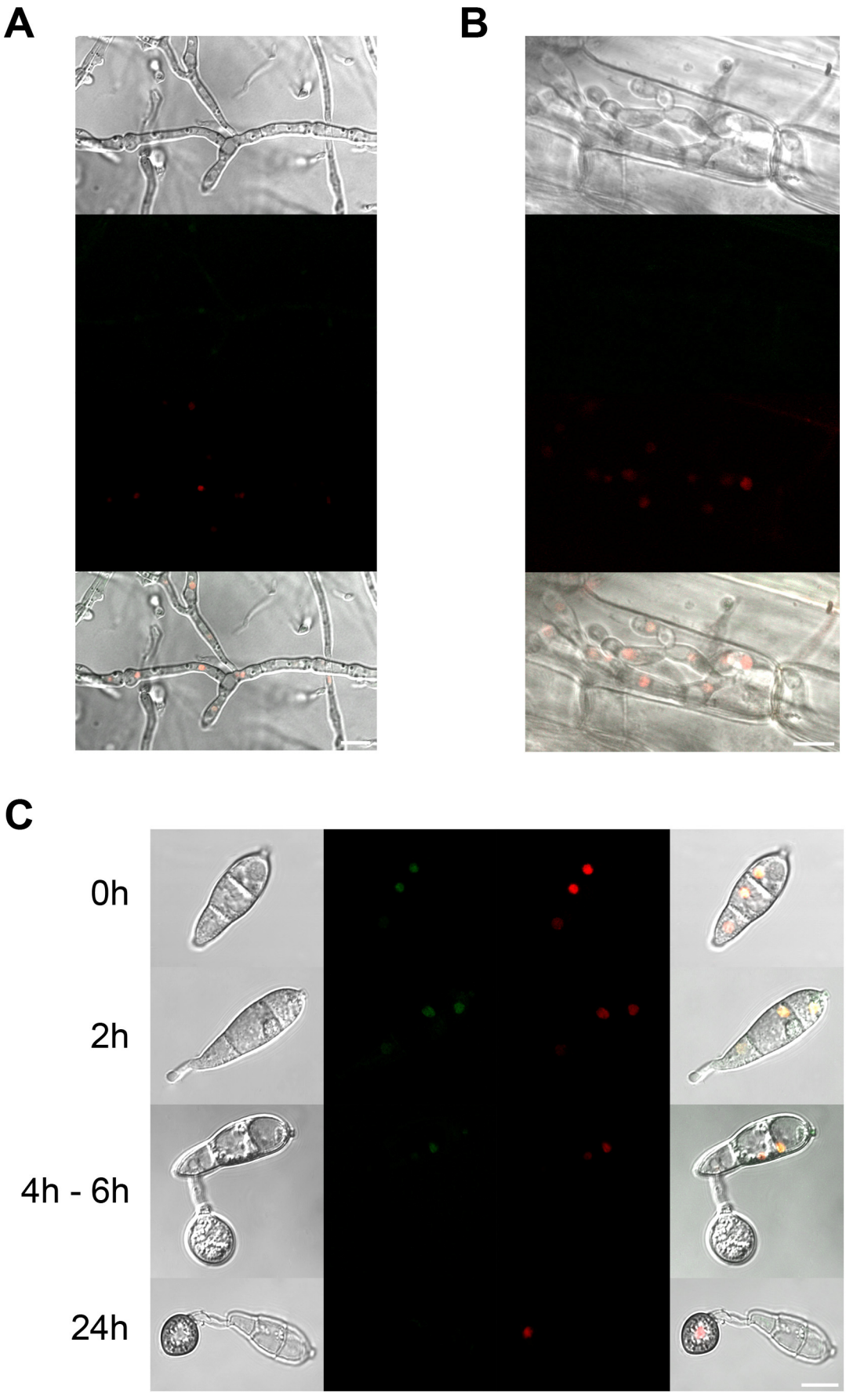
A
B
C
0h
2h
4h - 6h
24h

(previous page)

Figure 7.16. Cellular localisation of *Mo*Ftf1:GFP in vegetative (A) and invasive (B) hyphae and during infection-related development (C) of *M. oryzae*.

(A) A plug of mycelium from a Guy11 transformant expressing H1:RFP and *Mo*Ftf1:GFP was inoculated onto slide covered with CM and incubated at 26ºC. Observations were made 24 hpi by confocal microscopy (Scale bar = 10 µm). **(B)** Rice leaf sheaths were inoculated with conidial suspension (10^5 conidia ml^{-1}) of Guy11 transformant expressing H1:RFP and *Mo*Ftf1:GFP and incubated at 25ºC. Observations were made 24 hpi by confocal microscopy (Scale bar = 10 µm). **(C)** Conidia were harvested from a Guy11 transformant expressing H1:RFP and *Mo*Ftf1:GFP protein fusion, inoculated onto glass coverslips at 26ºC, and observed by confocal microscopy at the times indicated (Scale bar = 10 µm).

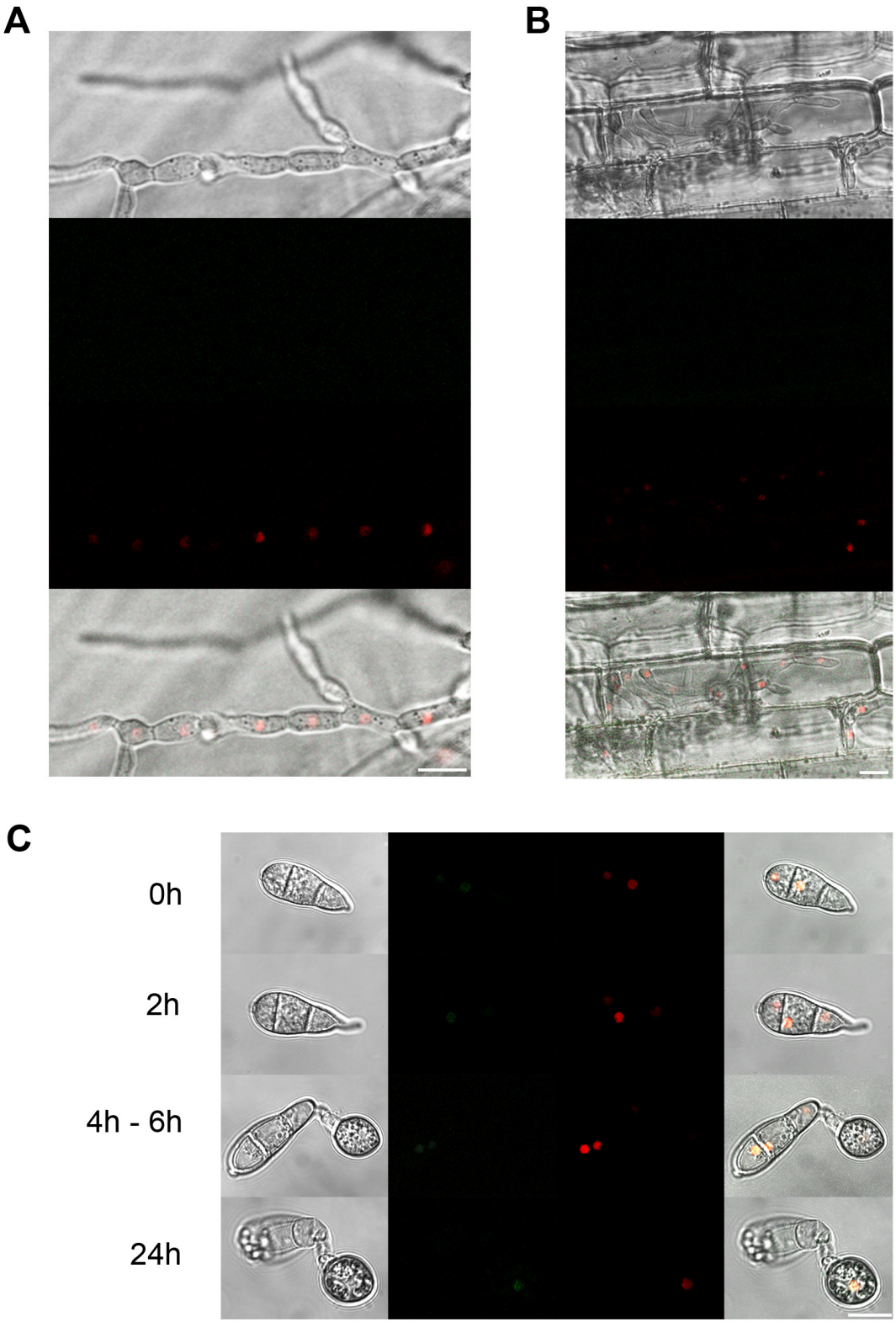
A
B
C
0h
2h
4h - 6h
24h

(previous page)

Figure 7.17. Cellular localisation of MoZnc1:GFP in vegetative (A) and invasive (B) hyphae and during infection-related development (C) of M. oryzae.

(A) A plug of mycelium from a Guy11 transformant expressing H1:RFP and *Mo*Znc1:GFP was inoculated onto slide covered with CM and incubated at 26ºC. Observations were made 24 hpi by confocal microscopy (Scale bar = 10 µm). **(B)** Rice leaf sheaths were inoculated with conidial suspension (10^5 conidia ml^{-1}) of Guy11 transformant expressing H1:RFP and *Mo*Znc1:GFP and incubated at 25ºC. Observations were made 24 hpi by confocal microscopy (Scale bar = 10 µm). **(C)** Conidia were harvested from a Guy11 transformant expressing H1:RFP and *Mo*Znc1:GFP protein fusion, inoculated onto glass coverslips at 26ºC, and observed by confocal microscopy at the times indicated (Scale bar = 10 µm).

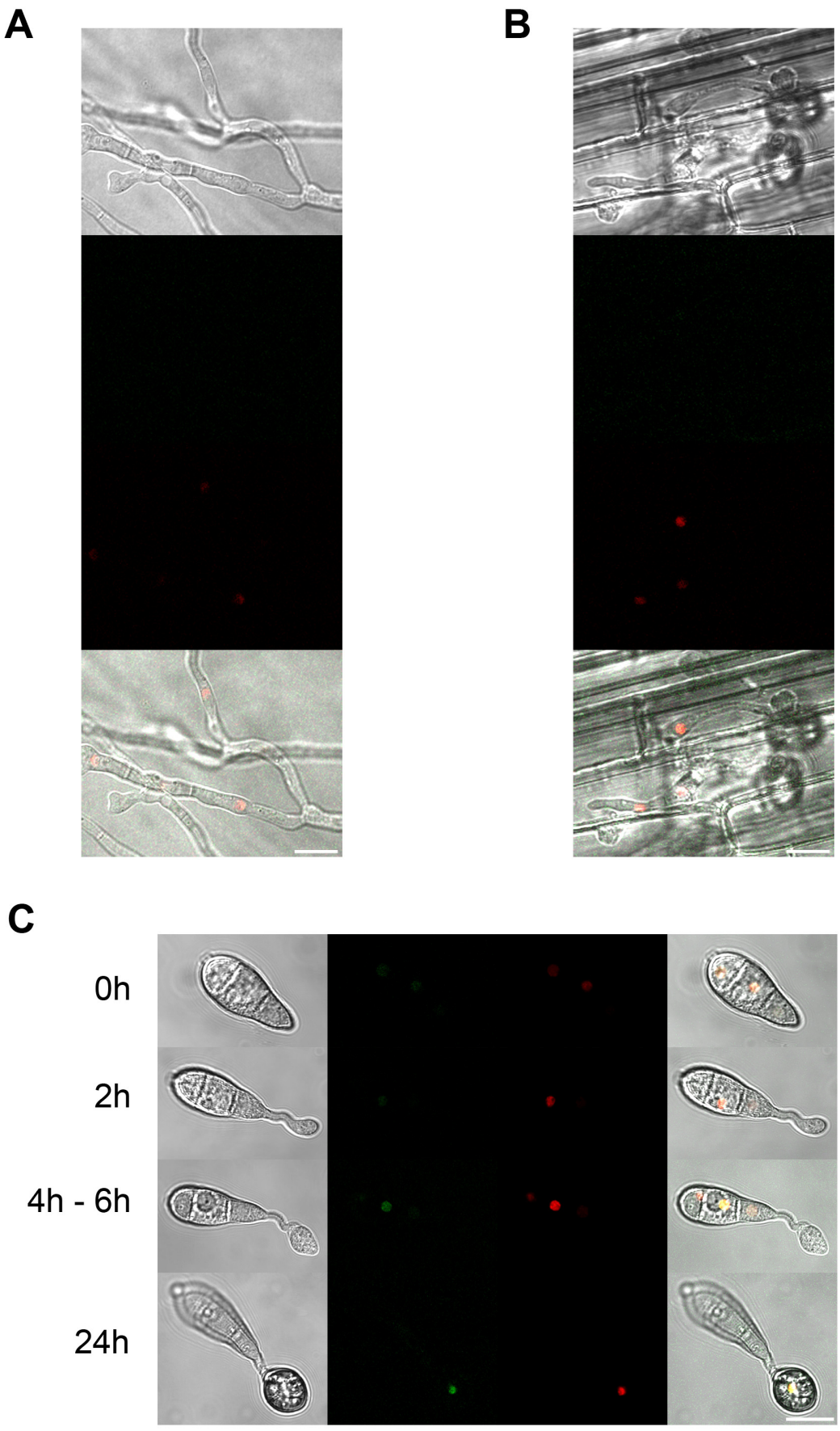
A
B
C
0h
2h
4h - 6h
24h

(previous page)

Figure 7.18. Cellular localisation of *Mo*Cpb1:GFP in vegetative (A) and invasive (B) hyphae and during infection-related development (C) of *M. oryzae*.

(A) A plug of mycelium from a Guy11 transformant expressing H1:RFP and *Mo*Cpb1:GFP was inoculated onto slide covered with CM and incubated at 26ºC. Observations were made 24 hpi by confocal microscopy (Scale bar = 10 µm). **(B)** Rice leaf sheaths were inoculated with conidial suspension (10^5 conidia ml^{-1}) of Guy11 transformant expressing H1:RFP and *Mo*Cpb1:GFP and incubated at 25ºC. Observations were made 24 hpi by confocal microscopy (Scale bar = 10 µm). **(C)** Conidia were harvested from a Guy11 transformant expressing H1:RFP and *Mo*Cpb1:GFP protein fusion, inoculated onto glass coverslips at 26ºC, and observed by confocal microscopy at the times indicated (Scale bar = 10 µm).

7.4. Discussion

The majority of known effectors of filamentous fungi are secreted proteins (Kamoun *et al.*, 2006; Stergiopoulos and de Wit, 2009). In this study, I focused on identifying new *M. oryzae* genes encoding putatively secreted proteins, based on analysis of the published genome sequence of *M. oryzae* strain 70-15 (Dean *et al.*, 2005). The predicted proteome of 70-15 (12,841 proteins; http://www.broadinstitute.org/annotation/fungi/magnaporthe) was screened using a bioinformatics pipeline described in Fig. 7.1 (Chou, 2007), resulting in 1731 putative secreted proteins that were not predicted to contain transmembrane domains. Three putative nuclear-localised secreted effectors, *FTF1* (MGG_03438), *ZNC1* (MGG_04326) and *CPB1* (MGG_13165), were chosen for functional characterisation. Effectors containing putative NLS have been reported to be translocated to plant cell nuclei in several plant pathogenic bacteria. These include the type III effector proteins PopP2 of *Ralstonia solanacearum* (Deslandes *et al.*, 2003) and the AvrBs3 family of *Xanthomonas* spp. (Lahaye and Bonas, 2001; Kay and Bonas, 2009). The AvrBs3 family effectors are also known as TAL (transcription activator-like) effectors because they appear to act as transcription factors binding to double-stranded DNA sequences and are clearly capable of transcriptional activation of plant genes (Yang *et al.*, 2000; Yang *et al.*, 2006; Kay *et al.*, 2007; Römer *et al.*, 2007; Sugio *et al.*, 2007). The type III effectors HsvG and HsvB of *Pantoea agglomerans* have also been shown to target plant cell nuclei, to bind double-stranded DNA, and to activate transcription (Nissan *et al.*, 2006). These studies suggest that phytopathogenic bacteria have evolved effector proteins with eukaryotic motifs to mimic eukaryotic transcription factors. The aster yellows phytoplasma strain Witches' Broom (AY-WB) has been also shown to produce a protein, SAP11, which targets nuclei of plant host cells (Bai *et al.*, 2009). This protein contains an N-terminal signal peptide sequence and a eukaryotic bipartite

NLS and it was suggested that this potential phytoplasma effector may alter plant cell physiology. Recently, Schornack *et al.* (2010) have demonstrated that the oomycete *Phytophthora infestans* secretes several Crinkler (CRN) effector proteins that target the host nucleus. In the case of Crn8, nuclear accumulation of this protein was required to induce plant cell death (Schornack *et al.*, 2010).

In this study, I selected putative *M. oryzae* effectors that were hypothesised to be secreted inside host cells, where they could manipulate various processes in the plant host and contribute to disease development (Chisholm *et al.*, 2006; Desveaux *et al.*, 2006; Hogenhout *et al.*, 2009). I have shown that Ftf1, Znc1 and Cpb1 are unlikely to be secreted blast effector proteins of *M. oryzae*, and are not essential for successful invasion of rice and barley cells (Fig. 7.4, Fig. 7.8 and Fig. 7.12). Although the NLS of Ftf1, Znc1 and Cpb1 proteins was functional inside fungal cells, it was not functional in plant cells. Expression of the proteins was observed in nuclei of vegetative hyphae and conidia, but never during colonisation *in planta* or in highly localised structures (BICs) in IH (Fig. 7.16, Fig. 7.17 and Fig. 7.18). Protein fusions of known *M. oryzae* effectors (Avr-Pita1, Pwl1, Pwl2 and Bas1) with fluorescent proteins have been reported to accumulate in BICs during invasive hypha development and translocated into invaded plant cells during tissue invasion (Khang *et al.*, 2010). BIC development was also coupled to hyphal differentiation from the filamentous penetration hypha into bulbous IH (Heath *et al.*, 1990; Veses and Gow, 2009; Khang *et al.*, 2010). At this stage, the tip BIC moved to sub-apical position relative to the tip of the first IH cell (Khang *et al.*, 2010).

Effector proteins are not considered to be normally required for vegetative growth in filamentous fungi (Sweigard *et al.*, 1995; Böhnert *et al.*, 2004; Bolton *et al.*, 2008; Doehlemann *et al.*, 2009). However, deletion of *FTF1* gene did impair saprophytic development, causing alterations in growth, colonial morphology and stress

resistance responses (Fig 7.5, Fig. 7.6 and Fig. 7.7), reinforcing the idea that Ftf1 is probably not a blast effector protein, but instead fulfil a wider role in growth and development of the fungus. However, *Δznc1* and *Δcpb1* mutants did not show alterations in vegetative growth under nutrient deprivation (Fig.7.9 and Fig. 7.13) and osmotic, cell wall and oxidative stresses (Fig. 7.9, Fig.7.10, Fig. 7.14 and Fig. 7.15).

Overall, the data shown in this chapter demonstrates that the design of the experiment did not lead to identification of strong effector candidates. Prediction of putative effector proteins with signal peptides computationally using *M. oryzae* 70-15 isolate genome sequence did not appear to be appropriate for several reasons. The first is that 70-15 strain shows poor virulence and is derived from a cross between two isolates of *M. oryzae*, one of which is a rice pathogen and the other a weeping lovegrass pathogen (Chao and Ellingboe, 1991). Recently, Yoshida and colleagues (2009) used a similar bioinformatics pipeline to identify genes harbouring polymorphisms associated with AVR phenotypes. However, no association was made between AVR and DNA polymorphisms in the putative secreted protein encoded genes of strain 70-15. They therefore realised that the majority of AVR genes tested in other 22 *M. oryzae* isolates, were absent in the genome sequence of the laboratory strain 70-15. A second reason is that the presence of a signal peptide only indicates that a protein is going to be transported across or integrated into membranes and does not necessarily predict secretion outside the cell (Palade, 1975; Derby and Gleeson, 2007; Rapoport, 2007). The signal peptide is a cleavable segment of 7-12 hydrophobic amino acids that targets proteins to their correct destination, ensuring that their function is maintained (Derby and Gleeson, 2007; Rapoport, 2007). This was the scenario observed with the selected candidate effectors in this study: secreted into the nuclei of fungal cells, but not translocated into the host plant cells.

CHAPTER 8

General Discussion

The fungus *Magnaporthe oryzae* causes rice blast disease, one of the most devastating diseases of all cereals (Valent and Chumley, 1991). This fungus infects rice, the essential staple crop for half of the world's population (Skamnioti and Gurr, 2009). As rice production has expanded through Asia, Africa, Latin and North America, the disease has also spread and it can now be found in over 85 countries worldwide (Khush and Jena, 2009). Annual rice harvest losses have lead to rice shortages in many developing countries in recent years, making effective control of this devastating disease imperative to ensure global food security and economic and social stability (Khush and Jena, 2009). Fortunately, the availability of the genome sequences of both rice (Goff *et al.*, 2002; Yu *et al.*, 2002) and *M. oryzae* (Dean *et al.*, 2005) has made this a model pathosystem for understanding the molecular basis of plant-fungal interactions.

In this study, I sought to identify novel genetic determinants for successful colonisation of plant tissue by *M. oryzae*, using two experimental approaches: 1) by screening a *M. oryzae* random insertional mutagenesis library; and 2) by targeted deletion of putatively secreted *M. oryzae* proteins.

The major outcome of this research project has been the identification of a new *M. oryzae* pathogenicity gene, *TPC1* (*Transcription factor for Polarity Control1*), which was identified as a pathogenicity-defective mutant M1422 generated by random insertional T-DNA mutagenesis. *TPC1* appears to play an important role in vegetative fungal growth and in fungal colonisation *in planta*. Colonies of the M1422 T-DNA mutant were compact and were very reduced in size. This phenotype appeared to be due to a different hyphal branching pattern occurring in the mutant, leading to compact colonies that did not spread to fill the plate culture in the same way as the isogenic wild-type Guy11. The mutant was also severely reduced in

virulence in both leaves and roots and different host species. Conidiogenesis, conidial germination, appressorium formation and conidial collapse were misregulated in the M1422 mutant. Compared with Guy11, the M1422 mutant also sporulated poorly. Strikingly, one- and four-celled conidia were observed to be produced by M1422. Two-celled and abnormally shaped three-celled conidia was also generated. During appressorium development, the M1422 mutant conidia showed multiple phenotypes, including the formation of two germ tubes, two appressoria or one undifferentiated germ tube and an appressorium forming from another conidial cell. M1422 mutant also showed an increased frequency of two cells germinating from conidia. Remarkably, the mutant also had the capacity to form two appressoria from two germinated conidial cells and to germinate a germ tube from the middle cell, phenotypes not observed in Guy11 conidia.

Mislocalisation of fimbrin was detected during germ tube germination, appressorium and appressorium pore formation in the M1422 mutant. Taken together, these phenotypes suggested that *TPC1* is a core polarity protein that is required for the correct development of apical-growing structures such as vegetative and invasive hyphae, germ tubes and penetration pegs. Other fungal species with mutations affecting polarity factors (*e.g. S. cerevisae SEC4*, *U. maydis RRM4*, *C. purpurea RAC* and *CLA4*) have been shown to display similar phenotypes, convoluted colonies, reduction in conidiation, and defects in polarity and pathogenicity (Punt *et al.*, 2001; Becht *et al.*, 2005, 2006; Rolke and Tudzynski, 2008). Interestingly, infection-associated autophagy and glycogen metabolism were also affected and delayed in the M1422 T-DNA mutant. This is consistent with description in the morphogenetic pathway leading to appressorium development and plant infection. Also highlights the importance of developmental transitions to physiological processes in these cells.

This study showed that the establishment of polarity by *M. oryzae* is intimately linked to general developmental processes. To ensure normal patterns of hyphal branching and mycelial organisation, a requirement for polarisation of temporal and spatial regulatory mechanisms was evident. Loss of polarity highlighted the pivotal role that the genetic control of fungal vegetative growth plays in fungal interactions with other organisms, in nutrient acquisition and in exchanging nutrients and signals between different cells of the same colony. Thus, polarised vesicle traffic and differential inheritance of cellular components and fate determinants are necessary during different developmental stages of multicellular organisms (Macara and Mili, 2008). *M. oryzae TPC1* deleted mutant could be used as a role model to dissect polarity establishment process along cytoskeletal elements and morphogenesis and cell fate determination by assimetrically localised RNAs and proteins in filamentous fungi.

The putative transcription factor *TPC1* belongs to the strictly fungal group of $Zn(II)_2Cys_6$ binuclear cluster family transcriptional regulators (MacPherson *et al.*, 2006). Tpc1 was expressed in nuclei of vegetative hyphae and conidia, except during isotropic appressorial growth stage. The Tpc1 expression pattern was therefore concomitant with establishment of polarity axes: vegetative hyphae, germination of the germ tube and penetration peg formation. These results reinforced the idea that Tpc1 acts as a polarity regulator, involved in the re-establishment of polarised growth and traffic of morphogenetic determinants implicated in the generation of positional signals during penetration peg emergence. Other features in Tpc1 are the presence of a putative NLS, putative MAPK docking site and putative phosphorylation and sumoylation sites. Mutagenesis studies revealed that the transcriptional activity of Tpc1 appears to be controlled by a plethora of strategies such as nuclear-cytoplasmic shuffling, DNA binding, phosphorylation and potentially by sumoylation. This complex transcriptional regulation was also observed in other $Zn(II)_2Cys_6$ proteins (Struhl, 1995; Sellick and

Reece, 2005). Cellular mislocalisation of Tpc1 in different mutant backgrounds suggests that the transcription factor plays a crucial role in several signal transduction networks such as the MAPK Pmk1 pathway, the MAPK Mps1 cell wall integrity pathway and infection-associated autophagy. Hence, Tpc1 transcription factor has more than one distinct role and may have overlapping functions, regarding control of gene expression of different subset of genes/ proteins coordinated together or at different times during fungal development. However, in this study no direct interaction studies between Tpc1 and other proteins were carried out. Whole-genome expression studies will therefore be valuable to identify new target genes directly regulated by the *TPC1* transcription factor, as well as novel DNA recognition sites. Techniques such as chromatin immunoprecipitation (ChIP) combined with microarray detection (ChIP-chip) (van Steensel, 2005) or by sequencing directly DNA fragments of interest (ChIP-seq) (Park, 2009) and RNA-seq (Wang *et al.*, 2009) could therefore be applied in future to achieve this objective. Recently, ChIP-chip technology has been described in *M. oryzae* to identify the targets of the *MoCRZ1* transcription factor (Kim *et al.*, 2010). A more convenient and economical system that could also be used is the yeast two-hybrid system (Fields and Song, 1989). Detection of an interaction between “bait”-DNA binding domain fusion and “prey”-activation domain fusion is based on the activation of reporter genes or selection markers (Fields and Song, 1989). It could be applied to large-scale analyses of protein-protein interactions or to confirm specific interactions such as the activation Tpc1 by elements of the Pmk1 MAPK pathway or the interaction by the Atg8.

The comparative analysis of regulatory networks in a diversity of model organisms can be used to identify fundamental principles that underpin cellular processes (Tatusov *et al.*, 1997). To investigate orthologous genes between different species, I analysed the co-occurrence of Tpc1 protein in several fungal genomes. This

provided an indication of whether Tpc1 is conserved among particular fungal species or conversely if this conservation is due to distinct growth habits or lifestyles. Within the *Ascomycota*, Tpc1-like proteins were present in several multicellular fungal species that clustered in groups consistent with their taxonomic classification, and not with lifestyle. The Tpc1-like transcription factor has not been characterised in any other fungal species, so information could not be inferred regarding *Mo*Tpc1 function on gene regulation. The potential orthologue of *Mo*Tpc1 in *N. crassa* genome does not have the putative phosphorylation and sumoylation sites that are present in *Mo*Tpc1. These regulatory changes may have led to gain or loss of gene targets or by remodulating regulatory networks, allowing fine-tuning of the *TPC1* regulatory network. For example, *NcTPC1* KO mutant showed hypersensitivity to high concentration of osmolytes, contrarily to what has been observed with *M. oryzae* M1422 mutant. Perhaps expression divergence occurred between *Magnaporthe* and *Neurospora,* driving *Mo*Tpc1 to acquire the coordination of a novel regulatory network, the *MPS1* pathway. Availability of whole genome sequences from more fungal species (pathogenic and non-pathogenic) is still necessary and may unravel open questions for understanding the evolution and complexity of this fungal specific $Zn(II)_2Cys_6$ family. It would be interesting to analyse if these proteins have conserved protein-DNA and protein-protein interactions among them and transcription factor-binding sites or other regulatory motifs within DNA sequences (Cliften *et al.*, 2001; Kellis *et al.*, 2003). This might then indicate which gene regulation networks are conserved between species.

The majority of known effectors of filamentous fungi are proteins secreted inside host cells, where they could manipulate cellular processes in the host and contribute to disease development (Kamoun, 2006; Hogenhout *et al.*, 2009; Stergiopoulos and de Wit, 2009). Assuming this concept, the secretome of the rice blast fungus was predicted computationally to identify novel effector proteins (Chou, 2007).

Bioinformatics analysis predicted that 1731 putative proteins without transmembrane domains were secreted in the *M. oryzae* strain 70-15 (Chou, 2007). In the second part of this study, I aimed to identify and functionally analyse three putative nuclear-localised *M. oryzae* effectors that contained a DNA-binding domain, termed *FTF1*, *ZNC1* and *CPB1*. Targeted deletion of these genes was attempted in Guy11 isolate by using the split-marker method (Catlett *et al.*, 2002). Unfortunately, these candidate effectors were not essential for successful colonisation of rice and barley cells and were not secreted into the plant host cells. Expression of Ftf1:GFP, Znc1:GFP and Cpb1:GFP was observed inside the nuclei of fungal cells, but never during colonisation *in planta* or in BICs localised in IH. Known blast effectors such as Avr-Pita1, Pwl1, Pwl2 and Bas1 have been shown to accumulate in BICs and translocated into invaded rice cells (Khang *et al.*, 2010). This was not observed for any of the putative effector candidates, suggesting that they are unlikely to serve such a function. The presence of a signal peptide only indicates that a protein is transported across or integrated into membranes and not necessarily translocated outside the cell (Palade, 1975; Derby and Gleeson, 2007; Rapoport, 2007). This was the scenario observed with the candidate effectors analysed in Chapter 7. These proteins were secreted into the nuclei of fungal cells, but not into invaded plant cells. Another important question that can be raised from this study is that although *M. oryzae* possesses a large set of putative secreted proteins, no host-cell targeting motif has yet been identified as has been found in oomycetes with the RXLR motif (Chou, 2007; Soanes *et al.*, 2007; Mosquera *et al.*, 2009). Thus, it will be important to determine whether effector proteins fulfil the same functions in fungi as in oomycete pathogens, or whether the capacity of fungi to use secondary metabolites to modulate host metabolism and plant defence signalling is being underestimated.

Appendix

Primer sequences

Primers for deletion constructs using PCR-fusion method

M13F	5’ CGCCAGGGTTTTCCCAGTCACGAC 3’
M13R	5’ AGCGGATAACAATTTCACACAGGA 3’
HY	5’ GGATGCCTCCGCTCGAAGTA 3’
YG	5’ CGTTGCAAGACCTGCCTGAA 3’
FTF1_F1	5’ GCCTGCTGGTGGACCTTTAAC 3’
FTF1_F2	5’ **GTCGTGACTGGGAAAACCCTGGCG**GCCCATGTCAAAGCCCTCAG 3’
FTF1_F3	5’ **TCCTGTGTGAAATTGTTATCCGCT**GCTCCAGCACTGTTCCTCCA 3’
FTF1_F4	5’ CATGGTCCCTGTCGAATCCTG 3’
ZNC1_F1	5’ CACCCACAAACACCCTCAGC 3’
ZNC1_F2	5’ **GTCGTGACTGGGAAAACCCTGGCG**CCTCGCCTGGACTGCTTGA 3’
ZNC1_F3	5’ **TCCTGTGTGAAATTGTTATCCGCT**CCAGGCAGTTTCGGCTTTT 3’
ZNC1_F4	5’ CTCGACACCTTCCCAGAGCA 3’
CPB1_F1	5’ CGCCAGACAGAGCTAAGCATC 3’
CPB1_F2	5’ **GTCGTGACTGGGAAAACCCTGGCG**CAGGGGTCAAGGAACAGGG 3’
CPB1_F3	5’ **TCCTGTGTGAAATTGTTATCCGCT**CGGAACACACCTGGGCTTG 3’
CPB1_F4	5’ CGTGTGTGCCCCTTGTTCA 3’

Primers for Southern hybridisation probes

Hygromycin Probe

M13F	5’ CGCCAGGGTTTTCCCAGTCACGAC 3’
M13R	5’ AGCGGATAACAATTTCACACAGGA 3’

FTF1 Probe

FTF1_GFP_Fnest	5’ CTCGCCCAGCAAGTATGTGTA 3’
FTF1_GFP_1104_R	5’ CGGAGCCAACGAATTTGACT 3’

ZNC1 Probe

ZNC1_F1	5’ CACCCACAAACACCCTCAGC 3’
ZNC1_F2	5’ **GTCGTGACTGGGAAAACCCTGGCG**CCTCGCCTGGACTGCTTGA 3’

CPB1 Probe

CPB1_outF1	5’ CGAGAGTGCGAAATGGATGC 3’
CPB1_GFP_639_R	5’ GTCCCGGTTTCGTTGTGTGT 3’

Primers for GFP protein fusion constructs

7.GFP_F	5’ ATGGTGAGCAAGGGCGAGGAGCTG 3’
1R.TrpC.EcoRI_nest	5’ ACGAATTCAGTGTACCTGTGCATTCTGGG 3’
FTF1_GFP_F	5’ GAGTACATTGGTGATTAACGAG 3’
FTF1_GFP_Fnest	5’ CTCGCCCAGCAAGTATGTGTA 3’
FTF1_GFP_R	5‘ **CAGCTCCTCGCCCTTGCTCACCAT**GATATTACCAAGCCCCCATGT 3’
ZNC1_GFP_F	5’ GTTATGCTGCTGCCGCCCC 3’
ZNC1_GFP_Fnest	5’ CACACTCCTGACACTTGAATG 3’
ZNC1_GFP_R	5‘ **CAGCTCCTCGCCCTTGCTCACCAT**GGGTGGACCCGTCGGCTG 3’
CPB1_GFP_F	5’ GACGACACCATCCACTCACC 3’
CPB1_GFP_Fnest	5’ CCTTCGCCCGTGTACCCAGC 3’
CPB1_GFP_R	5‘ **CAGCTCCTCGCCCTTGCTCACCAT**GACTGACATGCTGGTGGGCT 3’
TPC1_GFP_F	5’ CCTGCCAACAACCAATCCAC 3’
TPC1_GFP_Fnest	5’ GTCGTGAACTTGATTGTGGGC 3’
TPC1_GFP_R	5‘ **CAGCTCCTCGCCCTTGCTCACCAT**ATTGGCACGAATGACCAACTTG 3’

Primers for sequencing

FTF1_GFP_21_F	5’ CTCGCCCAGCAAGTATGTGT 3’
FTF1_GFP_240_F	5’ GTCGGAGTTGCCTACCTGGA 3’
FTF1_GFP_764_F	5’ AAACGGCTTCTCGGATGGT 3’
FTF1_GFP_1254_F	5‘CAACAAGAGATGCGACGACA 3’
FTF1_GFP_1749_F	5’ GCGAGGAGTGCCTTGTTACC 3’
FTF1_GFP_2246_F	5’ TGGGCAGTGGACAGGTTATG 3’
FTF1_GFP_2737_F	5’ CCATTTCCGTTCGTTCCCTA 3’
FTF1_GFP_3237_F	5’ GGATTTGTTCGGCTTCTTCG 3’
FTF1_GFP_611_R	5’ CCAAAGGCTGCAAGAAAACC 3’
FTF1_GFP_1104_R	5’ CGGAGCCAACGAATTTGACT 3’
FTF1_GFP_1603_R	5’ GGTGGGAAGCCATATCCCTA 3’
FTF1_GFP_2087_R	5’ GGGCCATGGTGGTTAGGATA 3’
FTF1_GFP_2588_R	5’ GCGATGGCGTGATAAAGTGT 3’
FTF1_GFP_3092_R	5’ GGCGCGTCAACCATTCTAGT 3’
ZNC1_GFP_55_F	5’ AACCACGCAAAGCCACTCTC 3’
ZNC1_GFP_393_F	5’ GCTGTTCGTCAGTTGCAGACA 3’
ZNC1_GFP_894_F	5’ TCACACTCGGAAAAATGACCA 3’
ZNC1_GFP_1396_F	5’ AAAAAGAAGCAATCCGCAGAC 3’
ZNC1_GFP_1912_F	5’ GCCTTCGTCGAGAGAACGAT 3’
ZNC1_GFP_2397_F	5’ GGCACGCTGCTACTTCATTG 3’
ZNC1_GFP_2921_F	5’ CGCAGCCAGAACTTCAGCTA 3’

ZNC1_GFP_3411_F	5’ CCCATCAAACATCCAGCAAA 3’
ZNC1_GFP_772_R	5’ GGCAAAGCCAGGTTATGACG 3’
ZNC1_GFP_1278_R	5’ CCCAAGAGTTTCCCCTCTCA 3’
ZNC1_GFP_1776_R	5’ ATGCAGGTTCCTTGTGCTGA 3’
ZNC1_GFP_2249_R	5’ GATCGGAGCACGTTTGTGAG 3’
ZNC1_GFP_2778_R	5’ TGGTCTGAGCGAGATTTCCA 3’
ZNC1_GFP_3267_R	5’ GAAGCTGGACGTGGACGACT 3’
CPB1_GFP_300_F	5’ GGACATGGGGTCATTTTTGG 3’
CPB1_GFP_795_F	5’ CCAAGAGCCGATTTATGACAA 3’
CPB1_GFP_1293_F	5’ ATGCCGCTCCGCTGTCGTTG 3’
CPB1_GFP_1803_F	5’ ACCAGCCACAGTGCTACGAA 3’
CPB1_GFP_2305_F	5’ AGCTACACCCGCTGATCACA 3’
CPB1_GFP_2798_F	5’ GTCGCCTGTAAAACGGATGG 3’
CPB1_GFP_3288_F	5’ AGTCCAGCGACGTTCCACTT 3’
CPB1_GFP_3808_F	5’ AAATGCAGCAGCAACAGCAA 3’
CPB1_GFP_639_R	5’ GTCCCGGTTTCGTTGTGTGT 3’
CPB1_GFP_1135_R	5’ ATGTACCCAACTGGGGCATC 3’
CPB1_GFP_1630_R	5’ CTCGCAACAGATTCCACAGA 3’
CPB1_GFP_2133_R	5’ GCGTGCTCTGGGTGTATGAA 3’
CPB1_GFP_2651_R	5’ TGGTGTGTTTCAATGGGTGA 3’
CPB1_GFP_3132_R	5’ CGGACAGTGGTGATGGTAGC 3’
CPB1_GFP_3632_R	5’ TACGGTAGGGACAGGCGTTC 3’
TPC1_GFP_281_F	5’ CGTCCAACTGGCAAAACAAA 3’
TPC1_GFP_785_F	5’ GGTGGTTGCAAATCCATCG 3’
TPC1_GFP_1285_F	5’ TTTCCGATTCTTTCACGATGAC 3’
TPC1_GFP_1764_F	5’ GATGAGCTTTGGACCCTTCG 3’
TPC1_GFP_2289_F	5’ CAACTGCTTCTCGAGCGATG 3’
TPC1_GFP_2773_F	5’ GACTGGAAGGCCGACTACGA 3’
TPC1_GFP_3261_F	5’ CGAGGGTCAGATTGATGACG 3’
TPC1_GFP_3755_F	5’ TCCAGCCGTGTTAGGTATTTCA 3’
TPC1_GFP_630_R	5’ TTTGGATCTGTCATCCCAAGA 3’
TPC1_GFP_1125_R	5’ ATCACCGTGAAGCCGATTCT 3’
TPC1_GFP_1630_R	5’ GGAACGGTGAGAGCTGGTGT 3’
TPC1_GFP_2119_R	5’ GCGAGAACCCAGTAGGATCG 3’
TPC1_GFP_2618_R	5’ TCACTCGCCTGTTTCCTCTG 3’
TPC1_GFP_3138_R	5’ CGTCTTGAGGATCTCGCTGA 3’
TPC1_GFP_3602_R	5’ GAGATGGCGTGGAAAAGACC 3’
GFP_4290_F	5’ GTGAAGTTCGAGGGCGACAC 3’
GFP_4155_R	5’ CGTAGGTGAAGGTGGTCACG 3’
GFP_4627_R	5’ ACGAACTCCAGCAGGACCAT 3’
GFP_4658_R	5’ GTCCATGCCGTGAGTGATCC 3’

Primers for PCR-site directed mutagenesis constructs

TPC1noNLS_F	5' **GGACCCTTGCG**AATGACAGACTTGGTGGGCT 3'
TPC1noNLS_R	5' **GTCTGTCATT**CGCAAGGGTCCTCTTCTGCC 3'
TPC1noKK_F	5' **GACAGAA**GTTGGCCGCCGCAAGGGT 3'
TPC1noKK_R	5' TTCTGTCTTGCCGTCCTTGCC 3'
TPC1noRR_F	5' **GTCATT**ACGTCAACTGGCAAGGAC 3'
TPC1noRR_R	5' AATGACAGACTTGGTGGGCT 3'
TPC1noSUMO_F	5' GCCGTCCTTGCCAGTTGAC 3'
TPC1noSUMO_R	5' GGACGGC**GC**GACAGAAAAGAAGG 3'
TPC1_T168G_F	5' GTGTTGGAAACCCGTCCCGA 3'
TPC1_T168G_R	5' CCAACAC**G**CGCCCATTGAGT 3'
TPC1_T349G_F	5' CTCGGTCTGTTGATGGTGG 3'
TPC1_T349G_R	5' CAACAGACCGAG**GG**CATCAGCC 3'
TPC1noCYS12_F	5' GC**C**GCGCAGAC**C**AGCACGCAA 3'
TPC1noCYS12_R	5' GCT**G**GTCTGCGC**G**GCAAGTTC 3'
TPC1_GFP_Fnest	5' GTCGTGAACTTGATTGTGGGC 3'
1R.TrpC.EcoRI_nest	5' ACGAATTCAGTGTACCTGTGCATTCTGGG 3'

References

Adachi K and Hamer JE (1998) Divergent cAMP signaling pathways regulate growth and pathogenesis in the rice blast fungus *Magnaporthe grisea. Plant Cell* **10:** 1361-73.

Alfano JR (2009) Roadmap for future research on plant pathogen effectors. *Mol. Plant Pathol.* **10:** 805-13.

Bai YL and Kohlhaw GB (1991) Manipulation of the “zinc cluster” region of transcriptional activator *LEU3* by site-directed mutagenesis. *Nucleic Acids Res.* **19:** 5991-7.

Bai X, Correa VR, Toruño TY, Ammar ED, Kamoun S, Hogenhout SA (2009) AY-WB phytoplasma secretes a protein that targets plant cell nuclei. *Mol. Plant-Microbe Interact.* **22:** 18-30.

Balhadère PV and Talbot NJ (2001) PDE1 encodes a P-type ATPase involved in appressorium-mediated plant infection by the rice blast fungus *Magnaporthe grisea. Plant Cell* **13:** 1987-2004.

Balhadère PV, Foster AJ, Talbot NJ (1999) Identification of pathogenicity mutants of the rice blast fungus *Magnaporthe grisea* by insertional mutagenesis. *Mol. Plant Microbe Interact.* **12:** 129-42.

Ballini E, Morel JB, Droc G, Price A, Courtois B, Notteghem JL, Tharreau D (2008) A genome-wide meta-analysis of rice blast resistance genes and quantitative trait loci provides new insights into partial and complete resistance. *Mol. Plant Microbe Interact.* **21:** 859-68.

Bechinger C, Giebel KF, Schnell M, Leiderer P, Deising HB, Bastmeyer M (1999) Optical measurements of invasive forces exerted by appressoria of a plant pathogenic fungus. *Science* **285:** 1896-9.

Becht P, König J, Feldbrügge M (2006) The RNA-binding protein Rrm4 is essential for polarity in *Ustilago maydis* and shuttles along microtubules. *J. Cell Sci.* **119:** 4964-73.

Becht P, Vollmeister E, Feldbrügge M (2005) A role for RNA-binding proteins implicated in pathogenic development of *Ustilago maydis*. *Eukaryot. Cell* **4:** 121-33.

Beckerman JL and Ebbole DJ (1996) MPG1, a gene encoding a fungal hydrophobin of *Magnaporthe grisea*, is involved in surface recognition. *Mol. Plant Microbe Interact.* **6:** 450-6.

Bendtsen JD, Nielsen H, von Heijne G, Brunak S (2004) Improved prediction of signal peptides: SignalP 3.0. *J. Mol. Biol.* **340:** 783-95.

Bent AF and Mackey D (2007) Elicitors, effectors, and *R* genes: the new paradigm and a lifetime supply of questions. *Annu. Rev. Phytopathol.* **45:** 399-436.

Berbee ML (2001) The phylogeny of plant and animal pathogens in the *Ascomycota*. *Physiol. Mol. Plant Pathol.* **59:** 165-87.

Betts MF, Tucker SL, Galadima N, Meng Y, Patel G, Li L, Donofrio N, Floyd A, Nolin S, Brown D *et al.* (2007) Development of a high throughput transformation system for insertional mutagenesis in *Magnaporthe oryzae*. *Fungal Genet. Biol.* **44:** 1035-49.

Bhambra GK, Wang ZY, Soanes DM, Wakley GE, Talbot NJ (2006) Peroxisomal carnitine transferase is required for elaboration of penetration hyphae during plant infection by *Magnaporthe grisea. Mol. Microbiol*. **61:** 46-60.

Bhattacharjee S, Hiller NL, Liolios K, Win J, Kanneganti TD, Young C, Kamoun S, Haldar K (2006) The malarial host-targeting signal is conserved in the Irish potato famine pathogen. *PLoS Pathog.* **2**, e50, doi:10.1371/journal.ppat.0020050.

Bhattacharyya RP, Reményi A, Yeh BJ, Lim WA (2006) Scaffolds: the role of modular interactions in the evolution and wiring of cell signaling circuits. *Annu. Rev. Biochem.* **75:** 655-80.

Birch PR, Boevink PC, Gilroy EM, Hein I, Pritchard L, Whisson SC (2008) Oomycete RXLR effectors: delivery, functional redundancy and durable disease resistance. *Curr. Opin. Plant Biol.* **11:** 373-9.

Birch PRJ, Rehmany AP, Pritchard L, Kamoun S, Beynon JL (2006) Trafficking arms: oomycete effectors enter host plant cells. *Trends Microbiol.* **14:** 8-11.

Boch J, Scholze H, Schornack S, Landgraf A, Hahn S, Kay S, Lahaye T, Nickstadt A, Bonas U (2009) Breaking the code of DNA binding specificity of TAL-type III effectors. *Science* **326:** 1509-12.

Bogdanove AJ, Schornack S, Lahaye T (2010) TAL effectors: finding plant genes for disease and defense. *Curr. Opin. Plant Biol.* **13:** 394-401.

Bohnert HU, Fudal I, Dioh W, Tharreau D, Notteghem JL, Lebrun MH (2004) A putative polyketide synthase/ peptide synthetase from *Magnaporthe grisea* signals pathogen attack to resistant rice. *Plant Cell* **16:** 2499-513.

Bolton MD, van Esse HP, Vossen JH, de Jonge R, Stergiopoulos I, Stulemeijer IJE, van den Berg GCM, Borrás-Hidalgo O, Dekker HL, de Koster CG *et al.* (2008) The novel *Cladosporium fulvum* lysin motif effector Ecp6 is a virulence factor with orthologues in other fungal species. *Mol. Microbiol.* **69:** 119-36.

Borkovich KA, Alex LA, Yarden O, Freitag M, Turner GE, Read ND, Seiler S, Bell-Pedersen D, Paietta J, Plesofsky N, *et al.* (2004) Lessons from the genome sequence of *Neurospora crassa*: tracing the path from genomic blueprint to multicellular organism. *Microbiol. Molec. Biol. Reviews* **68:** 1-108.

Bourett TM and Howard RJ (1990) *In vitro* development of penetration structures in the rice blast fungus *Magnaporthe grisea. Can. J. Bot*. **68:** 329-42.

Bourett TM and Howard RJ (1992) Actin in penetration pegs of the fungal rice blast pathogen *Magnaporthe grisea*. *Protoplasma* **168:** 20-6.

Brand A and Gow NAR (2009) Mechanisms of hypha orientation of fungi. *Curr. Opin. Microbiol.* **12:** 350-7.

Bricmont PA, Daugherty JR, Cooper TG (1991) The *DAL81* gene product is required for induced expression of two differently regulated nitrogen catabolic genes in *Saccharomyces cerevisiae. Mol. Cell. Biol.* **11:** 1161-6.

Brown DW, Butchko RA, Busman M, Proctor RH (2007) The *Fusarium verticillioides FUM* gene cluster encodes a Zn(II)2Cys6 protein that affects *FUM* gene expression and fumonisin production. *Eukaryot. Cell* **6:** 1210-8.

Bruno KS, Tenjo F, Li L, Hamer JE, Xu JR (2004) Cellular localization and role of kinase activity of PMK1 in *Magnaporthe grisea. Eukaryot. Cell* **3:** 1525-32.

Bryan GT, Wu KS, Farrall L, Jia Y, Hershey HP, McAdams SA, Faulk KN, Donaldson GK, Tarchini R, Valent B (2000) A single amino acid difference distinguishes resistant and susceptible alleles of the rice blast resistance gene Pi-ta. *Plant Cell* **12:** 2033-45.

Burger G, Strauss J, Scazzocchio C, Lang BF (1991) *nirA*, the pathway-specific regulatory gene of nitrate assimilation in *Aspergillus nidulans*, encodes a putative GAL4-type zinc finger protein and contains four introns in highly conserved regions. *Mol. Cell. Biol.* **11:** 5746-55.

Cahuzac B, Cerdan R, Felenbok B, Guittet E (2001) The solution structure of an AlcR-DNA complex sheds light onto the unique tight and monomeric DNA binding of a Zn(2)Cys(6) protein. *Structure* **9:** 827-36.

Caracuel-Rios Z and Talbot NJ (2007) Cellular differentiation and host invasion by the rice blast fungus *Magnaporthe oryzae*. *Curr. Opin. Microbiol.* **10:** 339-45.

Carroll AM, Sweigard JA, Valent B (1994) Improved vectors for selecting resistance to hygromycin. *Fungal Genet. News.* **41:** 22.

Catanzariti AM, Dodds PN, Ellis JG (2007) Avirulence proteins from haustoria-forming pathogens. *FEMS Microbiol. Lett.* **269:** 181-8.

Catanzariti AM, Dodds PN, Lawrence GJ, Ayliffe MA, Ellis JG (2006) Haustorially expressed secreted proteins from flax rust are highly enriched for avirulence elicitors. *Plant Cell* **18:** 243–56.

Catlett NL, Lee BN, Yoder OC, Turgeon BG (2002) Split-marker recombination for efficient targeted deletion of fungal genes. *Fungal Genet. News.* **50:** 9-11.

Chalfie M (1995) Green fluorescent protein. *Photochem. Photobiol.* 62: 651-6.

Chao CCT and Ellingboe AH (1991) Selection for mating competence in *Magnaporthe grisea* pathogenic to rice. *Can. J. Bot.* **69:** 2130-4.

Chauhan RS, Farman ML, Zhang HB, Leong SA (2002) Genetic and physical mapping of a rice blast resistance locus, Pi-CO39(t), that corresponds to the avirulence gene AVR1-CO39 of *Magnaporthe grisea. Mol. Genet. Genomics* **267:** 603-12.

Chen A, Wang PY, Yang YC, Huang YH, Yeh JJ, Chou YH, Cheng JT, Hong YR, Li SS (2006) SUMO regulates the cytoplasm-nuclear transport of its target protein Daxx. *J. Cell. Biochem.* **98:** 895-911.

Chi MH, Park SY, Kim S, Lee YH (2009) A novel pathogenicity gene is required in the rice blast fungus to suppress the basal defenses of the host. *PLoS Pathog.* **5:** e1000401. doi:10.1371/journal.ppat.1000401.

Chida T and Sisler HD (1987) Restoration of appressorial penetration ability by melanin precursors in *Pyricularia oryzae* treated with antipenetrants and in melanin-deficient mutants. *J. Pestic. Sci.* **12**: 49–55.

Chisholm ST, Coaker G, Day B, Staskawicz BJ (2006) Shaping the evolution of the plant immune response. *Cell* **124:** 803-14.

Choi W and Dean RA (1997) The adenylate cyclase gene MAC1 of *Magnaporthe grisea* controls appressorium formation and other aspects of growth and development. *Plant Cell* **9:** 1973-83.

Chou YM (2007) Identification of candidate effector proteins in the rice blast fungus *Magnaporthe grisea* [Master thesis]. [Norwich (UK)]: University of East Anglia.

Chumley FG and Valent B (1990) Genetic analysis of melanin-deficient, non-pathogenic mutants of *Magnaporthe grisea*. *Mol. Plant Microbe Interact.* **3:** 135-43.

Clergeot PH, Gourgues M, Cots J, Laurans F, Latorse MP, Pépin R, Tharreau D, Notteghem JL, Lebrun MH (2001) PLS1, a gene encoding a tetraspanin-like protein, is required for penetration of rice leaf by the fungal pathogen *Magnaporthe grisea*. *Proc. Natl. Acad. Sci. USA* **98:** 6963-8.

Cliften PF, Hillier LW, Fulton L, Graves T, Miner T, Gish WR, Waterston RH, Johnston M (2001) Surveying *Saccharomyces* genomes to identify functional elements by comparative DNA sequence analysis. *Genome Res.* **11:** 1175-86.

Cohen BD, Sertil O, Abramova NE, Davies KJ, Lowry CV (2001) Induction and repression of *DAN1* and the family of anaerobic mannoprotein genes in *Saccharomyces cerevisiae* occurs through a complex array of regulatory sites. *Nucleic Acids Res.* **29:** 799-808.

Cole CN and Hammell CM (1998) Nucleocytoplasmic transport: driving and directing transport. *Curr. Biol.* **8:** 368-72.

Collemare J, Pianfetti M, Houlle AE, Morin D, Camborde L, Gagey MJ, Barbisan C, Fudal I, Lebrun MH, Böhnert HU (2008) *Magnaporthe grisea* avirulence gene *ACE1*

belongs to an infection-specific gene cluster involved in secondary metabolism. *New Phytol.* **179:** 196–208.

Collins TJ (2007) ImageJ for microscopy. *Biotechniques* **43:** 25-30.

Cornelis GR (2006) The type III secretion injectisome. *Nature Rev. Microbiol.* **4:** 811-25.

Cornell MJ, Alam I, Soanes DM, Wong HM, Hedeler C, Paton NW, Rattray M, Hubbard SJ, Talbot NJ, Oliver SG (2007) Comparative genome analysis across a kingdom of eukaryotic organisms: specialization and diversification in the Fungi. *Genome Res.* **17:** 1809-22.

Cubitt AB, Heim R, Adams SR, Boyd AE, Gross LA, Tsien RY (1995) Understanding, improving and using green fluorescent proteins. *Trends Biochem. Sci.* **20**: 448-45.

Cunnac S, Lindeberg M, Collmer A (2009) *Pseudomonas syringae* type III secretion system effectors: repertoires in search of functions. *Curr. Opin. Microbiol.* **12:** 53-60.

Davis MA, Small AJ, Kourambas S, Hynes MJ (1996) The *tamA* gene of *Aspergillus nidulans* contains a putative zinc cluster motif which is not required for gene function. *J. Bacteriol.* **178:** 3406-9.

de Jong JC, McCormack BJ, Smirnoff N, Talbot NJ (1997) Glycerol generates turgor in rice blast. *Nature*. **389:** 244-5.

Dean RA (1997) Signal pathways and appressorium morphogenesis. *Annu. Rev. Phytopathol.* **35:** 211-34.

Dean RA, Talbot NJ, Ebbole DJ, Farman ML, Mitchell TK, Orbach MJ, Thon M, Kulkarni R, Xu JR, Pan H, Read ND, Lee YH, *et al.* (2005) The genome sequence of the rice blast fungus *Magnaporthe grisea*. *Nature* **434:** 980-6.

Defranoux N, Gaisne M, Verdière J (1994) Functional analysis of the zinc cluster domain of the *CYP1* (*HAP1*) complex regulator in heme-sufficient and heme-deficient cells. *Mol. Gen. Genet.* **242:** 699-707.

Deng YZ and Naqvi NI (2010) A vacuolar glucoamylase, Sga1, participates in glycogen autophagy for proper differentiation in *Magnaporthe oryzae*. *Autophagy* **6**

Derby MC and Gleeson PA (2007) New insights into membrane trafficking and protein sorting. *Internat. Rev. Cytol.* **261:** 47-116.

Deslandes L, Olivier J, Peeters N, Feng DX, Khounlotham M, Boucher C, Somssich I, Genin S, Marco Y (2003) Physical interaction between RRS1-R, a protein conferring resistance to bacterial wilt, and PopP2, a type III effector targeted to the plant nucleus. *Proc. Natl. Acad. Sci. USA* **100:** 8024-9.

Desveaux D, Singer AU, Dangl JL (2006) Type III effector proteins: Doppelgangers of bacterial virulence. *Curr. Opin. Plant Biol.* **9:** 376-82.

DeZwaan TM, Carroll AM, Valent B, Sweigard JA (1999) *Magnaporthe grisea* Pth11p is a novel plasma membrane protein that mediates appressorium differentiation in response to inductive substrate cues. *Plant Cell* **11:** 2013-30.

Dixon MS, Jones DA, Keddie JS, Thomas CM, Harrison K, Jones JDG (1996) The tomato Cf-2 disease resistance locus comprises two functional genes encoding leucine-rich repeat proteins. *Cell* **84:** 451-9.

Dixon KP, Xu JR, Smirnoff N, Talbot NJ (1999) Independent signalling pathways regulate cellular turgor during hyperosmotic stress and appressorium mediated plant infection by the rice blast fungus *Magnaporthe grisea. Plant Cell* **11:** 2045-58.

Doehlemann G, van der Linde K, Aßmann D, Schwammbach D, Hof A, Mohanty A, Jackson D, Kahmann R (2009) Pep1, a secreted effector protein of *Ustilago maydis*, is required for successful invasion of plant cells. *PLoS Pathog.* **5:** e1000290. doi:10.1371/journal.ppat.1000290.

Drubin DG (1991) Development of polarity in budding yeast. *Cell* **65:** 1093-6.

Dufresne M and Osbourn AE (2001) Definition of tissue-specific and general requirements for plant infection in a phytopathogenic fungus. *Mol. Plant Microbe Interact.* **14:** 300-7.

Eddy SR (1998) Profile hidden Markov models. *Bioinformatics* **14:** 755-63.

Endo H, Kajiwara S, Tsunoka O, Shishido K (1994) A novel cDNA, *priBc*, encoding a protein with a $Zn(II)_2Cys_6$ zinc cluster DNA-binding motif, derived from the basidiomycete *Lentinus edodes*. *Gene* **139:** 117-21.

Fang EGC and Dean RA (2000) Site-directed mutagenesis of the magB gene affects growth and development in *Magnaporthe grisea*. *Mol. Plant Microbe Interact.* **13:** 1214-27.

Farman ML and Leong SA (1998) Chromosome walking to the AVR1-CO39 avirulence gene of *Magnaporthe grisea*: discrepancy between the physical and genetic maps. *Genetics* **150:** 1049-58.

Farman ML, Eto Y, Nakao T, Tosa Y, Nakayashiki H, Mayama S, Leong SA (2002) Analysis of the structure of the AVR1-CO39 avirulence locus in virulent rice-infecting isolates of *Magnaporthe grisea*. *Mol. Plant Microbe Interact.* **15:** 6-16.

Feinberg AP and Vogelstein BA (1983) A technique for radiolabeling DNA restriction endonuclease fragments to high specific activity. *Ann. Biochem.* **32**: 6-13.

Fields S and Song O (1989) A novel genetic system to detect protein–protein interactions. *Nature* **340:** 245-6.

Finn RD, Mistry J, Tate J, Coggill P, Heger A, Pollington JE, Gavin OL, Gunesekaran P, Ceric G, Forslund K *et al.* (2010) The PFAM protein families database. *Nucleic Acids Res.* **38:** 211-22.

Fischer R, Zekert N, Takeshita N (2008) Polarized growth in fungi – interplay between the cytoskeleton, positional markers and membrane domains. *Mol. Microbiol.* **68:** 813-26.

Flaherty JE and Payne GA (1997) Overexpression of *aflR* leads to upregulation of pathway gene transcription and increased aflatoxin production in *Aspergillus flavus*. *Appl. Environm. Microbiol.* **63:** 3995-4000.

Flor HH (1971) Current status of the gene-for-gene concept. *Annu. Rev. Phytopatol*. **9:** 275-96.

Foster AJ, Jenkinson JM, Talbot NJ (2003) Trehalose synthesis and metabolism are required at different stages of plant infection by *Magnaporthe grisea. EMBO J*. **22:** 225-35.

Fuchs BB and Mylonakis E (2009) Our paths might cross: the role of the fungal cell wall integrity pathway in stress responses and cross talk with other stress response pathways. *Eukaryot. Cell* **8:** 1616-25.

Fudal I, Ross S, Gout L, Blaise F, Kuhn ML, Eckert MR, Cattolico L, Bernard-Samain S, Balesdent MH, Rouxel T (2007) Heterochromatin-like regions as ecological niches for avirulence genes in the *Leptosphaeria maculans* genome: map-based cloning of *AvrLm6. Mol. Plant-Microbe Interact.* **20:** 459-70.

Galagan JE, Calvo SE, Borkovich KA, Selker EU, Read ND, Jaffe D, FitzHugh W, Ma LJ, Smirnov S, Purcell S, *et al.* (2003) The genome sequence of the filamentous fungus *Neurospora crassa*. *Nature* **422:** 859-68.

Gardner KH, Pan T, Narula S, Rivera E, Coleman JE (1991) Structure of the binuclear metal-binding site in the *GAL4* transcription factor. *Biochemistry* **30:** 11292-302.

Gilbert MJ, Thornton CR, Wakley G, Talbot NJ (2006) A P-type ATPase required for rice blast disease and induction of host resistance. *Nature* **440:** 535-9.

Gilbert RD, Johnson AM, Dean RA (1996) Chemical signals responsible for appressorium formation in the rice blast fungus. *Physiol. Mol. Plant Pathol*. **48:** 335-46.

Goff SA, Ricke D, Lan TH, Presting G, Wang R, Dunn M, Glazebrook J, Sessions A, Oeller P, Varma H, Hadley D, Hutchison D, *et al.* (2002) A draft sequence of the rice genome (*Oryza sativa* L. ssp. *japonica*). *Science*. **296:** 92-100.

Guindon S and Gascuel O (2003) A simple, fast, and accurate algorithm to estimate large phylogenies by maximum likelihood. *Syst. Biol.* **52:** 696-704.

Haas BJ, Kamoun S, Zody MC, Jiang RHY, Handsaker RE, Cano LM, Grabherr M, Kodira CD, Raffaele S, Torto-Alalibo T *et al.* (2009) Genome sequence and analysis of the Irish potato famine pathogen *Phytophthora infestans*. *Nature* **461:** 393-8.

Hahn S, Maurer P, Caesar S, Schlenstedt G (2008) Classical NLS proteins from *Saccharomyces cerevisiae*. *J. Mol. Biol.* **379:** 678-94.

Hallstrom TC, Lambert L, Schorling S, Balzi E, Goffeau A, Moye-Rowley WS (2001) Coordinate control of sphingolipid biosynthesis and multidrug resistance in *Saccharomyces cerevisiae*. *J. Biol. Chem.* **276:** 23674-80.

Hamer JE, Howard RJ, Chumbley FG, Valent B (1988) A mechanism for surface attachment in spores of a plant pathogenic fungus. *Science* **239:** 288-90.

Hamer JE, Valent B, Chumley FG (1989) Mutations at the *SMO* locus affect the shape of diverse cell types in the rice blast fungus. *Genetics* **122:** 351–61.

Harris SD (2008) Branching of fungal hyphae: regulation, mechanisms and comparison with other branching systems. *Mycologia* **100:** 823-32.

Harris SD, Read ND, Roberson RW, Shaw B, Seiler S, Plamann M, Momamy M (2005) Polarisome meets spitzenkörper: microscopy, genetics, and genomics converge. *Eukaryot. Cell* **4:** 225-9.

He C and Klionsky DJ (2009) Regulation mechanisms and signalling pathways of autophagy. *Annu. Rev. Genet*. **43:** 67-93.

Heath MC, Howard RJ, Valent B, Chumbley FG (1992) Ultrastructural interactions of one strain of *Magnaporthe grisea* with goosegrass and weeping lovegrass. *Can. J. Bot*. **70:** 779-87.

Heath MC, Valent B, Howard RJ, Chumbley FG (1990) Interactions of two strains of *Magnaporthe grisea* with rice, goosegrass, and weeping lovegrass. *Can. J. Bot.* **68:** 1627-37.

Heim R, Cubitt AB, Tsien RY (1995) Improved green fluorescence. *Nature* **373**: 663-4.

Hemler ME (2005) Tetraspanin functions and associated microdomains. *Nat. Rev. Mol. Cell Biol.* **6:** 801-11.

Henson JM, Butler MJ, Day AW (1999) The dark side of the mycelium: melanins of phytopathogenic fungi. *Annu. Rev. Phytopatol*. **37:** 447-71.

Hepler PK, Vidali L, Cheung AY (2001) Polarized cell growth in higher plants. *Annu. Rev. Cell Dev. Biol.* **17:**159-87.

Hiller NL, Bhattacharjee S, van Ooij C, Liolios K, Harrison T, Lopez-Estraño C, Haldar K (2004) A host-targeting signal in virulence proteins reveals a secretome in malarial infection. *Science* **306:** 1934-7.

Ho SN, Hunt HD, Horton RM, Pullen JK, Pease LR (1989) Site-directed mutagenesis by overlap extension using the polymerase chain reaction. *Gene* **77:** 51-9.

Hogenhout SA, Van der Hoorn RA, Terauchi R, Kamoun S (2009) Emerging concepts in effector biology of plant-associated organisms. *Mol. Plant-Microbe Interact.* **22:** 115–22.

Horton P, Park KJ, Obayashi T, Fujita N, Harada H, Adams-Collier CJ, Nakai K (2007) WoLF PSORT: protein localization predictor. *Nucleic Acids Res*. doi:10.1093/nar/gkm259.

Houterman PM, Speijer D, Dekker HL, de Koster CG, Cornelissen BJC, Rep M (2007) The mixed xylem sap proteome of *Fusarium oxysporum*-infected tomato plants. *Molec. Plant Pathol.* **8:** 215-21.

Howard RJ and Valent B (1996) Breaking and entering: host penetration by the fungal rice blast pathogen *Magnaporthe grisea. Ann. Rev. Microbiol*. **50:** 491-512.

Howard RJ, Ferrari MA, Roach DH, Money NP (1991) Penetration of hard substrates by a fungus employing enormous turgor pressures. *Proc. Natl. Acad. Sci. USA* **88:** 11281-4.

Hutchison CA, Phillips S, Edgell MH, Gillam S, Jahnke P, Smith M (1978) Mutagenesis at a specific position in a DNA sequence. *J. Biol. Chem.* **253:** 6551-60.

Jackson JC and Lopes JM (1996) The yeast *UME6* gene is required for both negative and positive transcriptional regulation of phospholipids biosynthetic gene expression. *Nuclei Acids Res.* **24:** 1322-9.

Jelitto TC, Page HA, Read ND (1994) Role of external signals in regulating the pre-penetration phase of infection by the rice blast fungus, *Magnaporthe grisea. Planta* **194:** 471-7.

Jeon J, Park SY, Chi MH, Choi J, Park J, Rho HS, Kim S, Goh J, Yoo S, Choi J *et al.* (2007) Genome-wide functional analysis of pathogenicity genes in the rice blast fungus. *Nature Genet.* **39:** 561-5.

Jia Y, McAdams SA, Bryan GT, Hershey HP, Valent B (2000) Direct interaction of resistance gene and avirulence gene products confers rice blast resistance. *EMBO J*. **19:** 4004-14.

Jiang RHY, Tripathy S, Govers F, Tyler BM (2008) RXLR effector reservoir in two *Phytophthora* species is dominated by a single rapidly evolving superfamily with more than 700 members. *Proc. Natl. Acad. Sci. USA* **105:** 4874-9.

Johnston M (1987) A model fungal gene regulatory mechanism: the *GAL* genes of *Saccharomyces cerevisiae*. *Microbiol. Reviews* **51:** 458-76.

Johnston M and Dover J (1987) Mutations that inactivate a yeast transcriptional regulatory protein cluster in an evolutionary conserved DNA binding domain. *Proc. Natl. Acad. Sci.* **84:** 2401-5.

Jones JDG and Dangl JL (2006) The plant immune system. *Nature* **444:** 323-9.

Joosten MHAJ, Cozijnsen TJ, de Wit PJGM (1994) Host resistance to a fungal tomato pathogen lost by a single base-pair change in an avirulence gene. *Nature* **367:** 384-6.

Kale SD, Gu B, Capelluto DG, Dou D, Feldman E, Rumore A, Arredondo FD, Hanlon R, Fudal I, Rouxel T, Lawrence CB, Shan W, Tyler BM (2010) External lipid PI3P

mediates entry of eukaryotic pathogen effectors into plant and animal host cells. *Cell* **142:** 284-95.

Kall L, Krogh A, Sonnhammer ELL (2004) A combined transmembrane topology and signal peptide prediction method. *J. Mol. Biol.* **338:** 1027-36.

Kamoun S (2006) A catalogue of the effector secretome of plant pathogenic oomycetes. *Annu. Rev. Phytopathol.* **44:** 41-60.

Kang S, Sweigard JA, Valent B (1995) The PWL host specificity gene family in the blast fungus *Magnaporthe grisea*. *Mol. Plant Microbe Interact.* **6:** 939-48.

Kankanala P, Czymmek K, Valent B (2007) Roles for rice membrane dynamics and plasmodesmata during biotrophic invasion by the blast fungus. *Plant Cell* **19:** 706-24.

Kankanala P, Mosquera G, Khang CH, Valdovinos-Ponce G, Valent B (2009) Cellular and molecular analyses of biotrophic invasion in rice blast disease *in:* Wang GL, Valent B (Eds), *Advances in genetics, genomics and control of the rice blast disease*. DOI10.1007/978-1-4020-9500-9 7, pp. 83-92.

Kay S and Bonas U (2009) How *Xanthomonas* type III effectors manipulate the host plant. *Curr. Opin. Microbiol.* **12:** 37-43.

Kay S, Hahn S, Marois E, Hause G, Bonas U (2007) A bacterial effector acts as a plant transcription factor and induces a cell size regulator. *Science* **318:** 648-51.

Kellis M, Patterson N, Endrizzi M, Birren B, Lander ES (2003) Sequencing and comparison of yeast species to identify genes and regulatory elements. *Nature* **423:** 241–254.

Kerscher O, Felberbaum R, Hochstrasser M (2006) Modification of proteins by ubiquitin and ubiquitin-like proteins. *Annu. Rev. Cell Dev. Biol*. **22:**159-80.

Kershaw MJ and Talbot NJ (2009) Genome-wide functional analysis reveals that infection-associated fungal autophagy is necessary for rice blast disease. *Proc. Natl. Acad. Sci. USA* **106:** 15967-72.

Kershaw MJ, Thornton CR, Wakley GE, Talbot NJ (2005) Four conserved intramolecular disulphide linkages are required for secretion and cell wall localization of a hydrophobin during fungal morphogenesis. *Mol. Microbiol*. **56:** 117-25.

Kershaw MJ, Wakley G, Talbot NJ (1998) Complementation of the Mpg1 mutant phenotype in *Magnaporthe grisea* reveals functional relationships between fungal hydrophobins. *EMBO J.* **17:** 3838-49.

Khang CH, Berruyer R, Giraldo MC, Kankanala P, Par SY, Czymmek K, Kang S, Valent B (2010) Translocation of *Magnaporthe oryzae* effectors into rice cells and their subsequent cell-to-cell movement. *Plant Cell* **22:** 1388–1403.

Khush GS and Jena KK (2009) Current status and future prospects for research on blast resistance in rice (*Oryza sativa* L.) *in:* Wang GL, Valent B (Eds), *Advances in genetics, genomics and control of the rice blast disease*. DOI10.1007/978-1-4020-9500-9 7, pp. 1-12.

Kim JH, Polish J, Johnston M (2003) Specificity and regulation of DNA binding by the yeast glucose transporter gene repressor Rgt1. *Mol. Cell. Biol.* **23:** 5208-16.

Kim S, Ahn IP, Rho HS, Lee YH (2005) *MHP1*, a *Magnaporthe grisea* hydrophobin gene, is required for fungal development and plant colonization. *Mol. Microbiol.* **57:** 1224-37.

Kim S, Hu J, Oh Y, Park J, Choi J, Lee YH, Dean RA, Mitchell TK (2010) Combining ChIP-chip and expression profiling to model the *MoCRZ1* mediated circuit for Ca^{2+}/Calcineurin signaling in the rice blast fungus. *PLoS Pathog*. **6:** e1000909. doi:10.1371/journal.ppat.1000909.

Klar AJ and Halvorson HO (1974) Studies on the positive regulatory gene, *GAL4*, in regulation of galactose catabolic enzymes in *Saccharomyces cerevisiae. Mol. Gen. Genet.* **135:** 203-13.

Koga H (1994) Hypersensitive death, autofluorescence, and ultrastructural changes in the cells of leaf sheaths of susceptible and resistant near-isogenic lines of rice (Pi-z^t) in relation to penetration and growth of *Pyricularia oryzae. Can. J. Bot*. **72:** 1463-77.

Koga H (1994) Hypersensitive death, autofluorescence, and ultrastructural changes in cells of leaf sheaths of susceptible and resistant near-isogenic lines of rice (*Pi-z*^{t}) in relation to penetration and growth of *Pyricularia oryzae*. *Can. J. Bot.* **72:** 1463-77.

Koga H and Nakayachi O (2004) Morphological studies on attachment of spores of *Magnaporthe grisea* to the leaf surface of rice. *J. Gen. Plant Pathol.* **70:** 11-5.

Koga H, Dohi K, Nakayachi O, Mori M (2004) A novel inoculation method of *Magnaporthe grisea* for cytological observation of the infection process using intact leaf sheaths of rice plants. *Physiol. Mol. Plant Pathol.* **64:** 67-72.

Kulkarni RD and Dean RA (2004) Identification of proteins that interact with two regulators of appressorium development, adenylate cyclase and cAMP-dependent of protein kinase A, in the rice blast fungus *Magnaporthe grisea*. *Mol. Gen. Genomics* **270:** 497-508.

Kulkarni RD, Kelkar HS, Dean RA (2003) An eight-cysteine-containing CFEM domain unique to a group of fungal membrane proteins. *Trends Biochem. Sci*. **28:** 118-21.

Kulkarni RD, Thon MR, Pan H, Dean RA (2005) Novel G-protein-coupled receptor-like proteins in the plant pathogenic fungus *Magnaporthe grisea*. *Genome Biol.* **6:** R24.

Lahaye T and Bonas U (2001) Molecular secrets of bacterial type III effector proteins. *Trends Plant Sci.* **6:** 479-85.

Laity JH, Lee BM, Wright PE (2001) Zinc finger proteins: new insights into structural and functional diversity. *Curr. Opin. Struct. Biol.* **11:** 39-46.

Lau GW and Hamer JE (1998) *Acropetal*: a genetic locus required for conidiophore architecture and pathogenicity in the rice blast fungus. *Fungal Genet. Biol.* **24:** 228–39.

LaugéR, Goodwin PH, de Wit PJGM, Joosten MHAJ (2000) Specific HR-associated recognition of secreted proteins from *Cladosporium fulvum* occurs in both host and non-host plants. *Plant J.* **23:** 735-45.

Laughon A and Gesteland RF (1982) Isolation and preliminary characterization of the *GAL4* gene, a positive regulator of transcription in yeast. *Proc. Natl. Acad. Sci. USA* **79:** 6827-31.

Lee YH and Dean RA (1993) cAMP regulates infection structure formation in the plant pathogenic fungus *Magnaporthe grisea*. *Plant Cell* **5:** 693-700.

Lee YH and Dean RA (1994) Hydrophobicity of contact surface induces appressorium formation in *Magnaporthe grisea*. *FEMS Microbiol. Lett*. **115:** 71-6.

Li L, Xue C, Bruno K, Nishimura, Xu JR (2004) Two PAK kinase genes, *CHM1* and *MST20*, have distinct functions in *Magnaporthe grisea*. *Mol. Plant Microbe Interact.* **17:** 547-56.

Li Y, Yan X, Wang H, Liang S, Ma WB, Fang MY, Talbot NJ, Wang ZY (2010) *Mo*Ric8 is a novel component of G-protein signaling during plant infection by the rice blast fungus *Magnaporthe oryzae*. *Mol. Plant Microbe Interact.* **23:** 317-331.

Liu H, Suresh A, Willard FS, Siderovski DP, Lu S, Naqvi NI (1997) Rgs1 regulates multiple Gα subunits in *Magnaporthe* pathogenesis, asexual growth and thigmotropism. *EMBO J.* **26:** 690-700.

Liu JL, Wang XJ, Mitchell T, Hu YJ, Liu XL, Dai LY, Wang GL (2010) Recent progress and understanding of the molecular mechanisms of the rice-*Magnaporthe oryzae* interaction. *Mol. Plant Pathol.* **11:** 419-27.

Liu S and Dean RA (1997) G protein α subunit genes control growth, development, and pathogenicity of *Magnaporthe grisea*. *Mol. Plant Microbe Interact.* **10:** 1075-86.

Liu XH, Lu JP, Zhang L, Dong B, Min H, Lin FC (2007) Involvement of a *Magnaporthe grisea* serine/threonine kinase gene, *MgATG1*, in appressorium turgor and pathogenesis. *Eukaryot. Cell* **6:** 997–1005.

Lodish H, Berk A, Zipursky SL, Matsudaira P, Baltimore D, Darnell J (2000) Molecular Cell Biology, p. 427-34; *In* Freeman WH and Company (ed.), New York, USA.

Lucau-Danila A, Delaveau T, Lelandais G, Devaux F, Jacq C (2003) Competitive promoter occupancy by two yeast paralogous transcription factors controlling the multidrug resistance phenomenon. *J. Biol. Chem.* **278:** 52641-50.

MacPherson S, Larochelle M, Turcotte B (2006) A fungal family of transcriptional regulators: the zinc cluster proteins. *Microbiol. Molec. Biol. Reviews* **70:** 583-604.

Mamane Y, Hellauer K, Rochon MH, Turcotte B (1998) A linker region of the yeast zinc cluster protein Leu3p specifies binding to everted repeat DNA. *J. Biol. Chem.* **273:** 18556-61.

Mamnun YM, Pandjaitan R, Mahe Y, Delahodde A, Kuchler K (2002) The yeast zinc finger regulators Pdr1p and Pdr3p control pleiotropic drug resistance (PDR) as homo-and heterodimers *in vivo*. *Mol. Microbiol.* **46:** 1429-40.

Marmorstein R, Carey M, Ptashne M, Harrison SC (1992) DNA recognition by *GAL4*: structure of a protein-DNA complex. *Nature* **356:** 408-14.

Matsudaira P (1994) The fimbrin and alpha-actinin footprint on actin. *J. Cell Biol.* **126:** 285-7.

Mead DA, Pey NK, Herrnstadt C, Marcil RA, Smith LM (1991) A universal method for the direct cloning of PCR amplified nucleic acid. *Biotechnol.* **9**: 657-63.

Mendgen K and Hahn M (2002) Plant infection and the establishment of fungal biotrophy. *Trends Plant Sci.* **7:** 352-6.

Mendgen K, Schneider A, Sterk M, Fink W (1988) The differentiation of infection structures as a result of recognition events between biotrophic parasites and their hosts. *J. Phytopathol*. **123:** 259-72.

Mitchell TK and Dean RA (1995) The cAMP-dependent protein kinase catalytic subunit is required for appressorium formation and pathogenesis by the rice blast pathogen *Magnaporthe grisea. Plant Cell* **7:** 1869-78.

Miura K and Hasegawa PM (2010) Sumoylation and other ubiquitin-like post-translational modifications in plants. *Trends Cell Biol.* **20:** 223-32.

Momany M (2002) Polarity in filamentous fungi: establishment, maintenance and new axes. *Curr. Opin. Microbiol.* **5:** 580-5.

Mosquera G, Giraldo MC, Khang CH, Coughlan S, Valent B (2009) Interaction transcriptome analysis identifies *Magnaporthe oryzae* BAS1-4 as biotrophy-associated secreted proteins in rice blast disease. *Plant Cell* **21:** 1273–90.

Mullins ED, Chen X, Romaine P, Raina R, Geiser DM, Kang S (2001) *Agrobacterium*-mediated transformation of *Fusarium oxysporum*: an efficient tool for insertional mutagenesis and gene transfer. *Phytopathology* **91:** 173-80.

Nakatogawa H, Suzuki K, Kamada Y, Ohsumi Y (2009) Dynamics and diversity in autophagy mechanisms: lessons from yeast. *Nat. Rev. Mol. Cell Biol.* **10:** 458-67.

Nakielny S and Dreyfuss G (1999) Transport of proteins and RNAs in and out of the nucleus. *Cell* **99:** 677-90.

Nikolaev I, Cochet MF, Felenbok B (2003) Nuclear import of zinc binuclear cluster proteins proceeds through multiple, overlapping transport pathways. *Eukaryot. Cell* **2:** 209-21.

Nishimura M, Park G, Xu JR (2003) The G-beta subunit MGB1 is involved in regulating multiple steps of infection-related morphogenesis in *Magnaporthe grisea. Mol. Microbiol.* **50:** 231-43.

Nissan G, Manulis-Sasson S, Weinthal D, Mor H, Sessa G, Barash I (2006) The type III effectors HsvG and HsvB of gall-forming *Pantoea agglomerans* determine host specificity and function as transcriptional activators. *Mol. Microbiol.* **61:** 1118-31.

Nolan T, Hands RE, Bustin SA (2006) Quantification of mRNA using real-time RT-PCR. *Nat. Protoc.* **1:** 1559-82.

Oh SK, Young C, Lee M, Oliva R, Bozkurt TO, Cano LM, Win J, Bos JIB, Liu HY, van Damme M *et al.* (2009) In planta expression screens of *Phytophthora infestans* RXLR effectors reveal diverse phenotypes, including activation of the *Solanum bulbocastanum* disease resistance protein Rpi-blb2W. *Plant Cell* **21:** 2928-47.

Ohuchi T, Seki M, Enomoto T (2008) Nuclear localization of Rad52 is pre-requisite for its sumoylation. *Biochem. Biophys. Res. Commun.* **372:** 126-30.

Orbach MJ, Farrall L, Sweigard JA, Chumbley FG, Valent B (2000) A telomeric avirulence gene determines efficacy for the rice blast resistance gene Pi-ta. *Plant Cell* **12:** 2019-32.

Palade G (1975) Intracellular aspects of the process of protein synthesis. *Science* **189:** 347-58.

Pan T and Coleman JE (1990) *GAL4* transcription factor is not a “zinc finger” but forms a $Zn(II)_2Cys_6$ binuclear cluster. *Proc. Natl. Acad. Sci. USA* **87:** 2077-81.

Pan T and Coleman JE (1991) Sequential assignments of the 1H NMR resonances of $Zn(II)_2$ and $113Cd(II)_2$ derivatives of the DNA-binding domain of the *GAL4* transcription factor reveal a novel structure motif for specific DNA recognition. *Biochemistry* **30:** 4212-22.

Park G, Bruno KS, Staiger CJ, Talbot NJ, Xu JR (2004) Independent mechanisms mediate turgor generation and penetration peg formation during plant infection in the rice blast fungus. *Mol. Microbiol*. **53:** 1695-707.

Park G, Xue C, Zhao X, Kim Y, Orbach M, Xu JR (2006) Multiple upstream signals converge on the adaptor protein Mst50 in *Magnaporthe grisea. Plant Cell* **18:** 2822-35.

Park G, Xue C, Zheng L, Lam S, Xu JR (2002) MST12 regulates infectious growth but not appressorium formation in the rice blast fungus *Magnaporthe grisea*. *Mol. Plant Microbe Interact.* **15:** 183-92.

Park PJ (2009) ChIP–seq: advantages and challenges of a maturing technology. *Nat. Rev. Genet.* **10:** 669-80.

Parlange F, Daverdin G, Fudal I, Kuhn ML, Balesdent MH, Blaise F, Grezes-Besset B, Rouxel T (2009) *Leptosphaeria maculans* avirulence gene *AvrLm4-7* confers a dual recognition specificity by the *Rlm4* and *Rlm7* resistance genes of oilseed rape, and circumvents *Rlm4*-mediated recognition through a single amino acid change. *Mol. Microbiol.* **71:** 851-63.

Parsons LM, Davis MA, Hynes MJ (1992) Identification of functional regions of the positively acting regulatory gene *amdR* from *Aspergillus nidulans. Mol. Microbiol.* **6:** 2999-3007.

Peng YL and Shishiyama J (1989) Timing of a cellular reaction in rice cultivars associated with differing degrees of resistance to *Pyricularia oryzae*. *Can. J. Bot.* **67:** 2704-10.

Pfeifer K, Kim KS, Kogan S, Guarente L (1989) Functional dissection and sequence of yeast *HAP1* activator. *Cell* **56:** 291-301.

Prasher DC, Eckenrode VK, Ward WW, Prendergast FG, Cormier MJ (1992) Primary structure of *the Aequorea victoria* green-fluorescent protein. Gene **111:** 229-33.

Punt PJ, Seiboth B, Weenink XO, van Zeijl C, Lenders M, Konetschny C, Ram AFJ, Montijn R, Kubicek CP, van den Hondel CAMJJ (2001) Identification and characterization of a family of secretion-related small GTPase-encoding genes from the filamentous fungus *Aspergillus niger*: a putative *SEC4* homologue is not essential for growth. *Mol. Microbiol.* **42:** 513-25.

Qi M and Elion EA (2005) MAP kinase pathways. *J. Cell Sci.* **118:** 3569–72.

Quinn J (2008) Differences in stress responses between model and pathogenic fungi, in: Avery SV, Stratford M, van West P (Eds), *Stress in yeasts and filamentous fungi*. pp: 67-85.

Ram AF, Wolters A, Ten Hoopen R, Klis FM (1994) A new approach for isolating cell wall mutants in *Saccharomyces cerevisiae* by screening for hypersensitivity to calcofluor white. *Yeast* **10:** 1019–30.

Ramos-Pamplona M and Naqvi NI (2006) Host invasion during rice-blast disease requires carnitine-dependent transport of peroxisomal acetyl-CoA. *Mol. Microbiol*. **61:** 61-75.

Rapoport TA (2007) Protein translocation across the eukaryotic endoplasmic reticulum and bacterial plasma membranes. *Nature* **450:** 663-9.

Reece RJ and Patshne M (1993) Determinants of binding-site specificity among yeast C6 zinc cluster proteins. *Science* **261:** 909-11.

Reiser V, Ruis H, Ammerer G (1999) Kinase activity-dependent nuclear export opposes stress-induced nuclear accumulation and retention of Hog1 mitogen-activated protein kinase in the budding yeast *Saccharomyces cerevisiae*. *Mol. Biol. Cell* **10**: 1147-61.

Rep M, van der Does HC, Meijer M, van Wijk R, Houterman PM, Dekker HL, de Koster CG, Cornelissen BJ (2004) A small, cysteine-rich protein secreted by *Fusarium oxysporum* during colonization of xylem vessels is required for I-3-mediated resistance in tomato. *Mol. Microbiol.* **53:** 1373-83.

Rho HS, Kang S, Lee YH (2001) *Agrobacterium tumefaciens*-mediated transformation of the plant pathogenic fungus *Magnaporthe grisea*. *Mol. Cells* **12:** 407-11.

Ridout CJ, Skamnioti P, Porritt O, Sacristan S, Jones JDG, Brown JKM (2006) Multiple avirulence paralogues in cereal powdery mildew fungi may contribute to parasite fitness and defeat of plant resistance. *Plant Cell* **18:** 2402–14.

Rohde JR, Trinh J, Sadowski I (2000) Multiple signals regulate *GAL* transcription in yeast. *Mol. Cell. Biol*. **20:** 3880-6.

Rohel EA, Payne AC, Fraaije BA, Hollomon DW (2001) Exploring infection of wheat and carbohydrate metabolism in *Mycosphaerella graminicola* transformants with differentially regulated green fluorescent protein expression. *Mol. Plant-Microbe Interact.* **14**: 156-63.

Rolke Y and Tudzynski P (2008) The small GTPase Rac and the p21-activated kinase Cla4 in *Claviceps purpurea*: interaction and impact on polarity, development and pathogenicity. *Mol. Microbiol.* **68:** 405-23.

Römer P, Hahn S, Jordan T, Strauß T, Bonas U, Lahaye T (2007) Plant pathogen recognition mediated by promoter activation of the pepper bs3 resistance gene. *Science* **318:** 645-8.

Sadowski I, Costa C, Dhanawansa R (1996) Phosphorylation of Gal4p at a single C-terminal residue is necessary for galactose-inducible transcription. *Mol. Cell. Biol*. **16:** 4879-87.

Sambrook J, Fritsch EF, Maniatis T (1989) Molecular cloning – *a laboratory manual, second edition*. Cold Spring Harbour Laboratory press, New York, USA.

Saunders DG, Aves SJ, Talbot NJ (2010) Cell-cycle mediated regulation of plant infection by the rice blast fungus. *Plant Cell* **22:** 497-507.

Schaeffer HJ and Webber MJ (1999) Mitogen-activated protein kinases: specific messages from ubiquitous messengers. *Mol. Cell. Biol.* **19:** 2435-44.

Schjerling P and Holmberg S (1996) Comparative amino acid sequence analysis of the C6 zinc cluster family of transcriptional regulators. *Nucleic Acids Res.* **24:** 4599-607.

Schmelzer E (2002) Cell polarization, a crucial process in fungal defence. *Trends Plant Sci.* **7:** 411-5.

Schornack S, van Damme M, Bozkurt TO, Cano LM, Smoker M, Thines M, Gaulin, Kamoun S, Huitema E (2010) Ancient class of translocated oomycete effectors targets the host nucleus. *Proc. Natl. Acad. Sci. USA* doi/10.1073/pnas.1008491107.

Schuster-Böckler B, Schultz J, Rahmann S (2004) HMM logos for visualization of protein families. *BMC Bioinformatics* **5:** 7.

Sellick CA and Reece RJ (2005) Eukaryotic transcription factors as direct nutrient sensors. *Trends Biochem. Sci.* **30:** 405-12.

Sesma A, Osbourn AE (2004) The rice blast pathogen undergoes developmental processes typical of root-infecting fungi. *Nature* **431:** 582-6.

Shaner NC, Steinbach PA, Tsien RY (2005) A guide to choosing fluorescent proteins. *Nat. Methods* **2:** 905-9.

Shi Z and Leung H (1995) Genetic analysis of sporulation in the rice blast fungus *Magnaporthe grisea. Mol. Plant-Microbe Interact.* **7:** 113–20.

Skamnioti P and Gurr SJ (2007) *Magnaporthe grisea* cutinase2 mediates appressorium differentiation and host penetration and is required for full virulence. *Plant Cell* **19:** 2674-89.

Skamnioti P and Gurr SJ (2009) Against the grain: safeguarding rice from rice blast disease. *Trends Biotechnol.* **27:** 141-50.

Smith DA, Morgan BA, Quinn J (2010) Stress signalling to fungal stress-activated protein kinase pathways. *FEMS Microbiol. Lett.* **306:** 1-8.

Soanes DM, Richards TA, Talbot NJ (2007) Insights from sequencing fungal and oomycete genomes: what can we learn about plant disease and the evolution of pathogenicity? *Plant Cell* **19:** 3318-26.

Southern EM (1975) Detection of specific sequences among DNA fragments separated by gel electrophoresis. *J.Molec. Biol.* **98**: 503.

Spellig T, Bottin A, Kahmann R (1996) Green fluorescent protein (GFP) as a new vital marker in the phytopathogenic fungus *Ustilago maydis*. *Mol. Gen. Genet.* **252**: 503-9.

Stein A, Pache RA, Bernado P, Pons M, Aloy P (2009) Dynamic interactions of proteins in complex networks: a more structured view. *FEBS J.* **276:** 5390-405.

Stergiopoulos I and de Wit PJGM (2009) Fungal effector proteins. *Annu. Rev. Phytopathol*. **47:** 233–63.

Storici F and Resnick MA (2003) *Delitto perfetto* targeted mutagenesis in yeast with oligonucleotides. *Genet. Eng.* **25:** 189-207.

Strich R, Surosky RT, Steber C, Dubois E, Messenguy F, Esposito RE (1994) *UME6* is a key regulator of nitrogen repression and meiotic development. *Genes Dev.* **8:** 796-810.

Struhl K (1995) Yeast transcriptional regulatory mechanisms. *Annu. Rev. Genet.* **29:** 651-74.

Sugio, A, Yang B, Zhu T, White FF (2007) Two type III effector genes of *Xanthomonas oryzae* pv. *oryzae* control the induction of the host genes *OsTFIIAγ1* and *OsTFX1* during bacterial blight of rice. *Proc. Natl. Acad. Sci. USA* **104:** 10720-5.

Suzuki M, Gerstein M, Yagi N (1994) Stereochemical basis of DNA recognition by Zn fingers. *Nucleic Acids Res.* **22:** 3397-405.

Sweigard JA, Carrol AM, Kang S, Farral L, Chumbley FG, Valent B (1995) Identification, cloning, and characterization of PWL2, a gene for host species specificity in the rice blast fungus. *Plant Cell* **7:** 1221-33.

Sweigard JA, Chumbley FG, Valent B (1992) Disruption of a *Magnaporthe grisea* cutinase gene. *Mol. Gen. Genet.* **232:** 183-90.

Sweigard JA, Chumley FG, Carroll A, Farrall L, Valent B (1997) A series of vectors for fungal transformation. *Fungal Genet. Newslett.* **44**: 52-3.

Takahashi M, Ashizawa T, Hirayae K, Moriwaki J, Sone T, Sonoda R, Noguchi MT, Nagashima S, Ishikawa K, Arai M (2010) One of two major paralogs of AVR-Pita1 is functional in Japanese rice blast isolates. *Phytopathology* **100:** 612-8.

Talbot NJ (1995) Having a blast: exploring the pathogenicity *of Magnaporthe grisea. Trends Microbiol.* **3:** 9-16.

Talbot NJ (2003) On the trail of a cereal killer: exploring the biology of *Magnaporthe grisea*. *Annu. Rev. Microbiol.* **57:** 177-202.

Talbot NJ and Kershaw MJ (2009) The emerging role of autophagy in plant pathogen attack and host defence. *Curr. Opin. Plant Biol.* **12:** 444-50.

Talbot NJ, Ebbole DJ, Hamer JE (1993) Identification and characterization of MPG1, a gene involved in pathogenicity from the rice blast fungus *Magnaporthe grisea. Plant Cell* **5:** 1575-90.

Talbot NJ, Kershaw MJ, Wakley GE, de Vries OMH, Wessels JGH, Hamer JE (1996) MPG1 encodes a fungal hydrophobin involved in surface interactions during infection-related development of *Magnaporthe grisea. Plant Cell* **8:** 985-99.

Talbot NJ, McCafferty HRK, Ma M, Moore K, Hamer JE (1997) Nitrogen starvation of the rice blast fungus *Magnaporthe grisea* may act as an environmental cue for disease symptom expression. *Physiol. Mol. Plant Pathol*. **50:** 179-95.

Tatusov RL, Koonin EV, Lipman DJ (1997) A genomic perspective on protein families. *Science* **278:** 631-7.

Thines E, Weber RWS, Talbot NJ (2000) MAP kinase and protein kinase A-dependent mobilization of triacylglycerol and glycogen during appressorium turgor generation by *Magnaporthe grisea. Plant Cell* **12:** 1703-18.

Thompson DA and Regev A (2009) Fungal regulatory evolution: *cis* and *trans* in the balance. *FEBS Lett.* **583:** 3959-65.

Tirosh I, Reikhav S, Levy AA, Barkai N (2009) A yeast hybrid provides insight into the evolution of gene expression regulation. *Science* **324:** 659-62.

Tirosh I, Weinberger A, Carmi M, Barkai N (2006) A genetic signature of interspecies variations in gene expression. *Nat. Genet.* **38:** 830-4.

Todd RB and Andrianopoulos A (1991) Evolution of a fungal regulatory gene familiy: the $Zn(II)_2Cys_6$ binuclear cluster DNA binding motif. *Fungal Genet. Biol.* **21:** 388-405.

Todd RB, Murphy RL, Martin HM, Sharp JA, Davis MA, Katz ME, Hynes MJ (1997) The acetate regulatory gene *facB* of *Aspergillus nidulans* encodes a $Zn(II)_2Cys_6$ transcriptional activator. *Mol. Gen. Genet.* **254:** 495-504.

Tosa Y, Osue J, Eto Y, Oh HS, Nakayashiki H, Mayama S, Leong SA (2005) Evolution of an avirulence gene, AVR1-CO39, concomitant with the evolution and differentiation of *Magnaporthe oryzae*. *Mol. Plant Microbe Interact.* **18:** 1148-60.

Tsuji G, Kenmochi Y, Takano Y, Sweigard J, Farrall L, Furusawa I, Horino O, Kubo Y (2000) Novel fungal transcriptional activators, Cmr1p of *Colletotrichum lagenarium* and Pig1p of *Magnaporthe grisea*, contain Cys_2His_2 zinc finger and $Zn(II)_2Cys_6$ binuclear cluster DNA-binding motifs and regulate transcription of melanin biosynthesis genes in a developmentally specific manner. *Mol. Microbiol*. **38:** 940-54.

Tuch BB, Li H, Johnsonn AD (2008) Evolution of eukaryotic transcription circuits. *Science* **319:** 1797-9.

Tucker SL, Besi M, Galhano R, Franceschetti M, Goetz S, Lenhert S, Osbourn A, Sesma A (2010) Common genetic pathways regulate organ-specific infection-related development in the rice blast fungus. *Plant Cell* **22:** 953-72.

Turcotte B, Akache B, MacPherson S (2004) The zinc cluster proteins: a yeast family of transcriptional regulators, p. 233-49; *In* Pandalai SG (ed.), Recent developments in nucleic acid research, vol. 1. Transworld Research Network, Trivandrum, Kerala, India.

Tyler BM, Tripathy S, Zhang X, Dehal P, Jiang RHY, Aerts A, Arredondo FD, Baxter L, Bensasson D, Beynon JL *et al.* (2006) *Phytophthora* genome sequences uncover evolutionary origins and mechanisms of pathogenesis. *Science* **313:** 1261-6.

Tyson JR and Stirling CJ (2000) LHS1 and SIL1 provide a luminal function that is essential for protein translocation into the endoplasmic reticulum. *EMBO J.* **19:** 6440-52.

Uchiyama T and Okuyama K (1990) Participation of *Oryza sativa* leaf wax in appressorium formation by *Pyricularia oryzae*. *Phytochemistry* **29:** 91-2.

Upadhyay S and Shaw BD (2008) The role of actin, fimbrin and endocytosis in growth of hyphae in *Aspergillus nidulans*. *Mol. Microbiol.* **68**: 690-705.

Valent B and Chumley FG (1991) Molecular genetic analysis of the rice blast fungus, *Magnaporthe grisea*. *Annu. Rev. Phytopathol.* **29:** 443-67.

Valent B and Khang CH (2010) Recent advances in rice blast effector research. *Curr. Opin. Plant Biol.* **13:** 1-8.

Valent B, Farrall L, Chumley FG (1991) *Magnaporthe grisea* genes for pathogenicity and virulence identified through a series of backcrosses. *Genetics* **127:** 87-101.

van den Ackerveken GFJM, van Kan JA, Joosten MHAJ, Muisers JM, Verbakel HM, de Wit PJGM (1993) Characterization of two putative pathogenicity genes of the fungal tomato pathogen *Cladosporium fulvum. Mol. Plant-Microbe Interact.* **6:** 210-5.

van Steensel (2005) Mapping of genetic and epigenetic regulatory networks using microarrays. *Nat. Genet.* **37:** S18.

Veneault-Fourrey C, Barooah M, Egan M, Wakley G, Talbot NJ (2006*a*) Autophagic fungal cell death is necessary for infection by the rice blast fungus. *Science* **312:** 580-3.

Veneault-Fourrey C, Lambou K, Lebrun MH (2006*b*) Fungal Pls1 tetraspanins as key factors of penetration into host plants: a role in re-establishing polarized growth in the appressorium. *FEMS Microbiol*. **256:** 179-84.

Veses V and Gow NAR (2009) Pseudohypha budding patterns of *Candida albicans. Med. Mycol.* **47:** 268-75.

Vethantham V, Rao N, Manley JL (2008) Sumoylation regulates multiple aspects of mammalian poly(A) polymerase function. *Genes Dev.* **22:** 499-511.

Villalba F, Collemare J, Landraud P, Lambou K, Brozek V, Cirer B, Morin D, Bruel C, Beffa R, Lebrun MH (2008) Improved gene targeting in *Magnaporthe grisea* by inactivation of *MgKU80* required for non-homologous end joining. *Fungal Genet. Biol.* **45:** 68–75.

Vleeshouwers VGAA, Rietman H, Krenek P, Champouret N, Young C, Oh SK, Wang M, Bouwmeester K, Vosman B, Visser RGF *et al.* (2008) Effector genomics accelerates discovery and functional profiling of potato disease resistance and *Phytophthora infestans* avirulence genes. *PLoS ONE* **3:** e2875.

Wang RC and Levine B (2010) Autophagy in cellular growth control. *FEBS Lett*. **584:** 1417–26.

Wang Z, Gerstein M, Snyder M (2009) RNA-Seq: a revolutionary tool for transcriptomics. *Nat. Rev. Genet.* **10:** 57-63.

Wang ZY, Soanes DM, Kershaw MJ, Talbot NJ (2007) Functional analysis of lipid metabolism in *Magnaporthe grisea* reveals a requirement for peroxisomal fatty acid β-oxidation during appressorium-mediated plant infection. *Mol. Plant Microbe Interact.* **5:** 475-91.

Ward WW and Bokman SH (1982) Reversible denaturation of *Aequorea* green-fluorescent protein: physical separation and characterization of the renatured protein. *Biochemistry* **21**: 4535-40.

Whisson SC, Boevink PC, Moleleki L, Avrova AO, Morales JG, Gilroy EM, Armstrong MR, Grouffaud S, van West P, Chapman S *et al.* (2007) A translocation signal for delivery of oomycete effector proteins into host plant cells. *Nature* **450:** 115-8.

Wilson RA and Talbot NJ (2009) Under pressure: investigating the biology of plant infection by *Magnaporthe oryzae*. *Nature Rev. Microbiol.* **7:** 185-95.

Wilson RA, Jenkinson JM, Gibson RP, Littlechild JA, Wang ZY, Talbot NJ (2007) Tps1 regulates the pentose phosphate pathway, nitrogen metabolism and fungal virulence. EMBO J doi:10.1038/sj.emboj.7601795.

Win J, Morgan W, Bos J, Krasileva KV, Cano LM, Chaparro-Garcia A, Ammar R, Staskawicz BJ, Kamoun S (2007) Adaptive evolution has targeted the C-terminal domain of the RXLR effectors of plant pathogenic oomycetes. *Plant Cell* **19:** 2349-69.

Wood PJ and Fulcher RG (1983) Dye interactions. A basis for specific detection and histochemistry of polysaccharides. *J. Histochem. Cytochem.* **31:** 823-6.

Xiao JZ, Ohshima A, Kamakura T, Ishiyama T, Yamaguchi I (1994*a*) Extracellular glycoprotein(s) associated with cellular differentiation in *Magnaporthe grisea. Mol. Plant Microbe Interact.* **7:** 639-44.

Xiao JZ, Watanabe T, Kamakura T, Ohshima A, Yamaguchi I (1994*b*) Studies on cellular differentiation of *Magnaporthe grisea*. Physicochemical aspects of substratum surfaces in relation to appressorium formation. *Physiol. Mol. Plant Pathol*. **44:** 227-36.

Xu JR (2000) MAP kinases in fungal pathogens. *Fungal Genet. Biol*. **31:** 137-52.

Xu JR and Hamer JE (1996) MAP kinase and cAMP signalling regulate infection structure formation and pathogenic growth in the rice blast fungus *Magnaporthe grisea. Genes Dev.* **10:** 2696-706.

Xu JR, Staiger CJ, Hamer JE (1998) Inactivation of the mitogen-activated protein kinase Mps1 from the rice blast fungus prevents penetration of host cells but allows activation of plant defence responses. *Proc. Natl. Acad. Sci. USA* **95:** 12713-8.

Xu JR, Urban M, Sweigard JA, Hamer JE (1997) The CPKA gene of *Magnaporthe grisea* is essential for appressorial penetration. *Mol. Plant Microbe Interact.* **10:** 187-94.

Xu JR, Zhao X, Dean R (2007) From genes to genomes: a new paradigm for studying fungal pathogenesis in *Magnaporthe oryzae. Adv. Genetics* **57:** 175-218.

Xue C, Park G, Choi W, Zheng L, Dean RA, Xu JR (2002) Two novel fungal virulence genes specifically expressed in appressoria of the rice blast fungus. *Plant Cell* **14:** 2107-19.

Yang B, Sugio A, White FF (2006) Os8N3 is a host disease-susceptibility gene for bacterial blight of rice. *Proc. Natl. Acad. Sci. USA* **103:** 10503-8.

Yang B, Zhu W, Johnson LB, White FF (2000) The virulence factor AvrXa7 of *Xanthomonas oryzae* pv. *oryzae* is a type III secretion pathway-dependent nuclear-localized double-stranded DNA-binding protein. *Proc. Natl. Acad. Sci. USA* **97:** 9807-12.

Yi M, Chi MH, Khang CH, Park SY, Kang S, Valent B, Lee YH (2009) The ER chaperone LHS1 is involved in asexual development and rice infection by the blast fungus *Magnaporthe oryzae. Plant Cell* **21:** 681–95.

Yoshida K, Saitoh H, Fujisawa S, Kanzaki H, Matsumura H, Yoshida K, Tosa Y, Chuma I, Takano Y, Win J *et al.* (2009) Association genetics reveals three novel avirulence genes from the rice blast fungal pathogen *Magnaporthe oryzae*. *Plant Cell* **21:** 1573–91.

Yu J, Hu S, Wang J, Wong GKS, Li S, Liu B, Deng Y, Dai l, Zhou Y, Zhang X, Cao M, Liu J, *et al.* (2002) A draft sequence of the rice genome (*Oryza sativa* L. ssp. *indica*). *Science* **296:** 79-92.

Yuan GF, Fu YH, Marzluf GA (1991) *nit-4*, a pathway-specific regulatory gene of *Neurospora crassa*, encodes a protein with a putative binuclear zinc DNA-binding domain. *Mol. Cell. Biol.* **11:** 5735-45.

Zhao X and Xu JR (2007) A highly MAPK-docking site in Mst7 is essential for Pmk1 activation in *Magnaporthe grisea. Mol. Microbiol*. **63:** 881-94.

Zhao XH, Kim Y, Park G, Xu JR (2005) A mitogen-activated protein kinase cascade regulating infection-related morphogenesis in *Magnaporthe grisea. Plant Cell* **17:** 1317-29.

Zhou Z, Li G, Lin C, He C (2009) Conidiophore *stalk-less1* encodes a putative zinc-finger protein involved in the early stage of conidiation and mycelial infection in *Magnaporthe oryzae*. *Mol. Plant Microbe Interact.* **22:** 402-10.